UNIVERSITÀ DEGLI STUDI DI MODENA E REGGIO EMILIA
DIPARTIMENTO DI INGEGNERIA ENZO FERRARI
CORSO DI STUDIO: INGEGNERIA INDUSTRIALE E DEL TERRITORIO

RACE TO ROAD:
INVESTIGATIONS ON KNOCK FROM FORMULA 1 TO HIGH PERFORMANCE ROAD CARS

Tesi di Ricerca di:
Dáire James Corrigan

Relatore:
Prof. Stefano Fontanesi
Alessandro D'Adamo

Coordinatore:
Prof. Alberto Muscio

2022 - XXXIV Cycle

Abstract

MOTORSPORT is almost as old as the motor vehicle itself. Since the beginning it has been used as a proving ground for new technology and as a means of marketing for automotive brands. As time has gone by however, road and race cars would appear to have diverged. In the years leading up to 2014, there was a concerted effort to make Formula 1 more road relevant. Formula 1 effectively became a competition to minimize specific fuel consumption. These engines are now among the most efficient spark ignition units on the planet, hence evaluating what technologies could potentially be transferred to other applications has obvious appeal. Largely this high efficiency is due to effective knock mitigation permitting operation at very high compression ratios.

Knock is a topic that has been studied almost since the birth of the automobile. There is consequently a rich vein of literature available. A detailed literature survey is therefore presented, covering a century of activity in the field.

Despite all the existing contributions in the literature on knock, a gap is identified between typical experimental results interpretation and complex first principles Computational Fluid Dynamics (CFD) models. A simple acoustic model of engine combustion chambers is proposed and constructed in CFD. This is benchmarked against historic literature and modern engine data. It is shown to help understand what occurs between autoignition events and cylinder pressure measurements.

Fuel has historically been a key area of knock research. Formula 1 features tailored fuels for each engine manufacturer. A similar fuel development work-flow is demonstrated to produce a reliable surrogate version of a full boiling range, high octane commercial gasoline.

Prechamber ignition systems are a current Formula 1 technology that are effective in knock mitigation. Their application to passenger cars is studied. This is shown to be

more problematic due to emissions constraints. A new prechamber concept engine, designed to alleviate this issue, is introduced and experimental results are shown.

Prechambers produce additional high frequency signal content on cylinder pressure data. This can render knock borderline interpretation more difficult. It is fundamental to accurately characterize this for a fair comparison of prechambers to conventional ignition systems. A detailed study of knocking data for both combustion systems is described.

Lastly, whilst most engine research and calibration focuses on stationary measurements, knock is shown to be a phenomenon with a significant transient component. Methodologies from Formula 1 to characterize and harness this phenomenon are reapplied to road car development, to good effect.

Through the activity presented, it is shown that despite the apparent divergence in road and race car technology, much of the learning in the realm of knock taken from a racing environment can be harnessed for modern passenger cars. New approaches developed in the course of this study, which can aid in understanding and characterization of knock for both powertrain types, are also demonstrated.

In what some consider the last days of the internal combustion engine, it is shown that there is still much potential left to explore.

Abstract (Italiano)

Gli sport automobilistici nascono di pari passo ai veicoli stessi e sin dall'inizio sono stati un terreno di prova ideale per le nuove tecnologie e contemporaneamente un modo per le case automobilistiche stesse di promuoversi. Col passare del tempo tuttavia, macchine da corsa e macchine stradali sembra abbiano intrapreso direzioni divergenti. Negli anni che portano al 2014, è stato fatto un ingente sforzo per rendere la Formula 1 più rilevante verso la tecnologia stradale. La Formula 1 di fatto è divenuta una competizione per minimizzare il consumo specifico di carburante tanto che oggigiorno i motori Formula 1 sono tra i più efficienti al mondo. Risulta pertanto evidentemente interessante valutare quali tecnologie potrebbero essere trasferite ad altre applicazioni. In gran parte questa cospicua efficienza è dovuta alla mitigazione della detonazione, che consente di operare con rapporti di compressione molto alti.

La detonazione è un argomento studiato praticamente dagli albori dell'automobile, di conseguenza esiste una ricca letteratura che ne tratta ampiamente. Qui di seguito presentiamo un approfondimento di tale letteratura che copre un secolo di attività nel settore.

Nonostante tutti i contributi esistenti, è stata identificata una lacuna tra l'interpretazione dei tipici risultati sperimentali e i complessi modelli "di principi primi" di combustione e fluidodinamica. Si propone un semplice modello acustico delle camere di combustione del motore reso in CFD. Confrontando dati storici e moderni, si mostra come questo aiuti alla comprensione di cosa succede tra l'autoaccensione e le misurazioni della pressione dei cilindri.

Il combustibile è stato storicamente un'area chiave nelle ricerche legate alla detonazione. La Formula 1 è caratterizzata dalla possibilità di utilizzare carburanti messi a punto su misura per ogni costruttore di motori. Si è provato come un simile flusso di lavoro per lo sviluppo del carburante produca una versione surrogata affidabile di un benzina

commerciale ad alto valore di ottano.

I sistemi con combustione a precamera sono correntemente una tecnologia Formula 1 effettiva sulla mitigazione della detonazione. Viene studiata la loro applicazione alle macchine stradali. Si dimostra come ciò sia più problematico a causa dei vincoli sulle emissioni. Un nuovo motore con precamera, disegnato per alleggerire questo problema, viene introdotto e ne vengono mostrati i risultati sperimentali.

La precamera genera maggiori segnali ad alta frequenza sulle tracce di pressione nel cilindro. Questo può rendere più difficile l'interpretazione delle detonazioni incipienti. È fondamentale pertanto caratterizzarlo accuratamente per un corretto confronto tra la precamera e i sistemi di accensione convenzionali. Viene descritto uno studio dettagliato dei dati della detonazione per entrambi i sistemi.

Infine, mentre la maggior parte della ricerca e calibrazione sui motori si concentra su punti stazionari, la detonazione si dimostra essere un fenomeno con una significativa componente transitoria. Per caratterizzare e sfruttare al meglio questo fenomeno, sono riapplicate con successo le metodologie della Formula 1 allo sviluppo delle macchine stradali.

Attraverso l'attività presentata, si mostra come, nonostante l'apparente divergenza tra la tecnologia stradale e quella di gara, molte delle cose apprese sulla detonazione proprio grazie alle corse possono essere sfruttate nell'ambito dei moderni veicoli per passeggeri. Sono anche proposte nuove tecniche che possono aiutare nello sviluppo di entrambi i gruppi propulsori.

In quello che alcuni considerano come il canto del cigno dei motori a combustione interna, si dimostra come ci sia ancora molto potenziale da esplorare.

Reports of my death have been greatly exaggerated...

Mark Twain

Acknowledgements

THE author is immensely grateful to the large number of people who have supported him over the years, both personally and professionally.

Firstly, a huge thanks to my parents, Eamon and Margaret Corrigan, for having always believed in me, supported me and having given me everything I needed to succeed. In this last period especially, this has necessarily been at a distance. Hopefully things will get back to normal soon.

From my time at Queen's University Belfast, I am very grateful for the support in particular of Dr. Robert Kee, who among other things ignited an enthusiasm in me for report writing. Thanks also to Dr. Geoffrey McCullough, who supported me in extending my final year project activity beyond simulation into the world of dyno testing and indication.

Among my former colleagues at Mercedes-Benz HighPerformanceEngines, thanks to Nico Ramsperger, for support and enthusiasm in particular on indication topics during my graduate role. Thanks also to Andy Fairley, whose drive, enthusiasm and professionalism was inspirational.

From my time at Ferrari Gestione Sportiva, Dr. David Salters and Dr. Luca Marmorini stand out. They created a great working environment for research of the 2014 engine regulations. I have never learned so much so quickly.

From my most recent period at Ferrari, I have also learned a great deal and continue to do so. Special thanks in particular to Massimo Medda, Massimo Barichello, Dr. Stefano Paltrinieri and of course Vittorio Dini, with whom I had the pleasure to collaborate also in Formula 1.

I am very grateful for the support of my supervisor during my PhD - Prof. Stefano Fontanesi. Once again someone whose enthusiasm was infectious and whose assistance was instrumental. A big thanks also to Dr. Sebastiano Breda for expert help with CFD calculations.

The biggest thanks of all must go to my family however, and in particular my wife Elena. Completing a PhD with a (often more than) full time job and two young children has not been easy. There is no way it would have been possible without your support. Of course thanks also to our wonderful girls, Éila and Kiva, who have not seen as much of their father during this PhD as would otherwise have been possible.

And finally, I am hugely grateful to all the engineers I have learned from through the literature but have never had the fortune of meeting. The world of internal combustion engine research has benefited from a massive number of contributions from many great minds over the years. Long may it continue to do so!

Contents

CHAPTER 1

Introduction

1.1 Abstract

The motor car, depending on how it is defined, is now well into its second century. It was not long after the first examples hit the road that people began to race them. This was both for sporting reasons and also as a means of publicity for automotive brands.

Racing became increasingly serious in the early 20th century and power outputs already reached 600 CV in the 1930s. The first race of the FIA Formula 1 Drivers' World Championship took place in 1950 and Ferrari was among the entries. Soon after, Ferrari began to produce and sell high performance cars for use on the road. Ferrari has produced high performance road and race cars ever since.

As automotive technology has evolved, passenger car and racing applications would appear to have increasingly diverged. In fact, many of the objectives of road cars and racing cars differ, as do the development constraints - for example passenger cars must comply with emissions legislation. Despite these differences, maximizing full load powertrain performance is key for both.

Engine performance is firstly limited by the amount of fuel the engine can burn. This is in turn linked to the maximum air mass-flow the engine can ingest. There is a second fundamental limit on performance which also limits efficiency however - the expansion ratio of the engine. This is linked to the compression ratio and is constrained by knock.

1.2 Motoring and Motorsport: An Abridged History

1.2.1 Early Motorcars and Motorsport

The first production automobile is generally considered to be the Benz Patent-Motorwagen. The patent was granted on the 29th of January 1886 to Benz & Co. of Mannheim, Germany [1]. A sketch from the patent document is shown in Figure 1.1. The vehicle featured a 954 CC[1] four-stroke single-cylinder engine producing just 500 W of power.

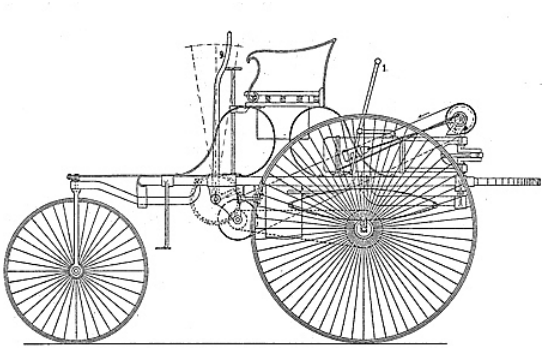

Figure 1.1: Benz Patent-Motorwagen [1]

It was not long after that the first organized motor race between multiple competitors with internal combustion engined vehicles took place. This was the Paris-Rouen. It was organized in July 22 1894 by the Parisian magazine "*Le Petit Journal*". 25 automobiles took part in the race. The race distance was 127km. The first car across the line was steam powered and so was disqualified. The first internal combustion engined car to finish was a Peugeot Type 5 with a time of 10 hours and 18 minutes corresponding to an average speed of just 12.3 kph. It featured a 565 CC two cylinder engine with 2 CV[2] output [2]. An example of this model is shown in Figure 1.2.

Figure 1.2: Peugeot Type 5 built from 1893-1896 [2]

Racing initially was carried out on public roads, but purpose built venues began to appear already in the early 1900s. Brooklands in England was completed in 1907, the Indianapolis Motor Speedway in the United States of America in 1909, and the Autodromo Nazionale Monza in Italy in 1922. Races at these venues were already considered to be Grand Prix events. In the 1920s the competition was mainly between French and Italian cars whilst in the 1930s, the German teams of Mercedes and Auto Union dominated. Already at this point power outputs of cars such as the Mercedes-Benz W 125, as shown in Figure 1.3, had risen to 600 CV [3].

[1] Cubic Centimeter

[2] Cavalli Vapore, 1 CV = 735.5 W

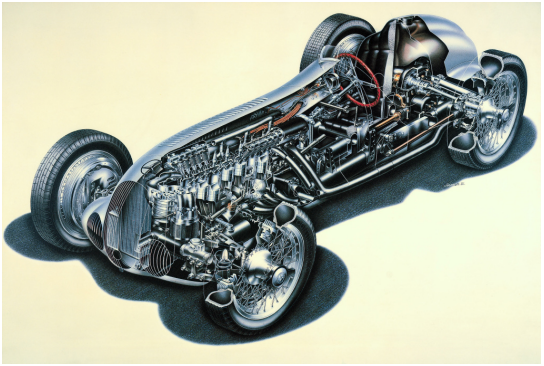

Figure 1.3: Mercedes-Benz W 125 from 1937 [3]

1.2.2 Formula 1

International racing events had already been taking place for some time when the first constructors' World Championship was organized in 1925. This consisted of just four races. A European drivers' championship was introduced in 1931. Racing was interrupted by the Second World War, but in 1946, the *Fédération Internationale de l'Automobile* (FIA) was formed and the first Formula 1 regulations were described. It was not until 1950 that the first Drivers' World Championship Formula 1 race was held at Silverstone in England. 14 teams took part that year in a Championship of seven races. It was won by Alfa Romeo with the 158, an example of which is shown in Figure 1.4. It was in actual fact a car which had its origins in a 1938 design.

Figure 1.4: Alfa Romeo 158 - Model which Won the First Formula 1 World Championship [4]

1.2.3 Ferrari

Ferrari's first car was the 125 S, as shown in Figure 1.5. The concept was conceived in 1945 with the express aim of beating Alfa Romeo. Enzo Ferrari had been firstly a driver and later the race team boss of Alfa Romeo in the years leading up to the Second World War. The 125 S was so named for its cylinder swept volume of 125 CC. It featured a V12 engine which developed 120 CV at 6800 rpm [5]. The car was fired up for the first time on the 12th of March 1947 and had its race debut two months later in Piacenza. It was leading the race when its fuel pump failed. The first race victory came just nine days later in the Rome Grand Prix.

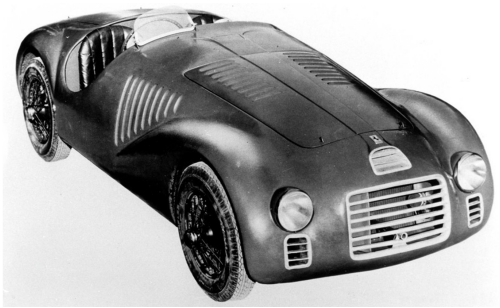

Figure 1.5: Ferrari 125 - The first Ferrari Car [5]

The 125 S was a racing car but in 1948 the 166 MM *('Mille Miglia')* was revealed. This came in both race and road versions. An example of a road going version is shown in Figure 1.6. The racing version would go on to win the 24 hours of Le Mans in 1949.

Figure 1.6: Ferrari 166 MM - The first Ferrari Road Car [5]

Ferrari took part in what is considered to be the inaugural season of Formula 1 in 1950 with the 125 F1, as shown in Figure 1.7. This featured a volumetric supercharger to increase the engine performance. The car was first driven at the Monaco Grand Prix by Alberto Ascari and finished in second place. The car was considered under-powered in comparison to the Alfa Romeo 158. Ferrari introduced three new cars in this same season with progressively larger V12 normally aspirated engines: the 275, the 340 and finally the 375.

The 375 would bring the team its inaugural Formula 1 victory the following year at the 1951 British Grand Prix, as shown in Figure 1.8. The car would go on to win four races that season, with Ascari finishing second in the championship. Alberto Ascari would win the Formula 1 World Championship the following year.

Ferrari is the only team to have taken part in every single season of the Formula 1 World Championship. To date it has won 15 Drivers' Championships, 16 Constructors'

Figure 1.7: Ferrari 125 F1 - The first Ferrari F1 Car [5]

Figure 1.8: 1951 Ferrari 375 - Multiple Race Winner in the 1951 Formula 1 Season [5]

Championships and a total of 237 races. It has competed in over 1000 races.

The company remains famous for its luxury sports cars and in 2020 was ranked as the World's Most Powerful Brand by Brand Finance [6]. In 2019 the company announced the SF90 Stradale road car as shown in Figure 1.9 - sharing its name with the 2019 F1 entrant the SF90, shown in Figure 1.10. This is the company's first Plug-in Hybrid Electric Vehicle (PHEV), featuring a combined power output of 1000 CV from a 780 CV V8 Internal Combustion Engine (ICE) of 3990 CC swept volume and three electric motors. As in the inaugural 1950 season, in 2019 both road and racing Ferraris shared their name.

1.3 Objectives of Road and Race Powertrain Development

The objectives of road and race engine development are not the same. A Formula 1 race engine spends well over 50% of its time in full load, whilst a road car engine will spend almost all its time in part load conditions. A road car engine needs to satisfy emissions and noise legislation, whilst a Formula 1 engine does not. Cost is a key factor for a road car engine, even for a luxury sports car, whilst it is less of a concern for a racing prototype.

The primary objective in racing car development is to minimize laptime. The main powertrain parameter with an impact on laptime is the power output. From 1989 to 2013 in Formula 1, maximizing power output generally meant maximizing engine air massflow. The air/fuel ratio was a calibration parameter and engines tended to run somewhat rich of stoichiometric. Everything changed when the V6 hybrid regulations were introduced for the 2014 season [7]. These fixed a maximum fuel massflow limit of 100 kg/h. This meant that the power output would depend purely on BSFC, as shown in Equation 1.1, where $\dot{m}_{fuel}$ is the fuel massflow.

$$BSFC = \frac{\dot{m}_{fuel}}{Power} \tag{1.1}$$

Figure 1.9: 2019 Ferrari SF90 Stradale [5]

Figure 1.10: 2019 Ferrari SF90 Formula 1 Car [5]

BSFC is not a single parameter for a powertrain however - it depends primarily on engine speed and load. For a Formula 1 engine, it is the BSFC at the fuel massflow limit which impacts the maximum power output and hence this is of primary importance. For a road car engine, normally the part load efficiency will be targeted; particularly the average BFSC on fuel-consumption measurement cycles such as the WLTC.[3]

The aim of Ferrari road cars is not only to be fast on a race track but also to be fun to drive. In terms of powertrain objectives, this translates to fast transient response. The goal is that the engine torque builds very rapidly following a step increase in torque demand by the driver. A large turbocharger, which would give high airflow and hence high power output, will generally also have high inertia and hence slow transient response. Full load performance and transient response must therefore be balanced against each other to produce an optimum overall product.

A racing driver will generally request a gradually increasing torque profile on corner exit in order to not overwhelm the grip of the tyres. This can be seen in Figure 1.11. This means whilst for a road car the objective can be said to maximize transient response, for a race car it is enough that the powertrain can satisfy a certain gradient of increasing torque demand and it is not necessary to do more than this.

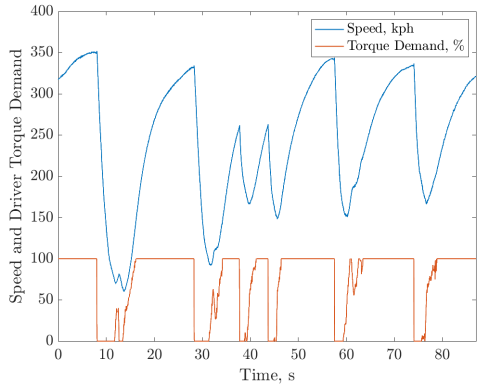

Figure 1.11: Driver Relative Torque Demand in a Formula 1 Vehicle (Alonso Monza Qualifying Lap, 2014)

These objectives are summarized in Figure 1.12. It can be seen that the main common point of interest between Ferrari road cars and Formula 1 race cars is full load performance. Factors which limit full load performance will be considered in the subsequent chapters, as will the possibility for transfer of Formula 1 technology and know-how to improving this aspect of road car engines.

[3] Worldwide harmonized Light duty driving Test Cycle [8].

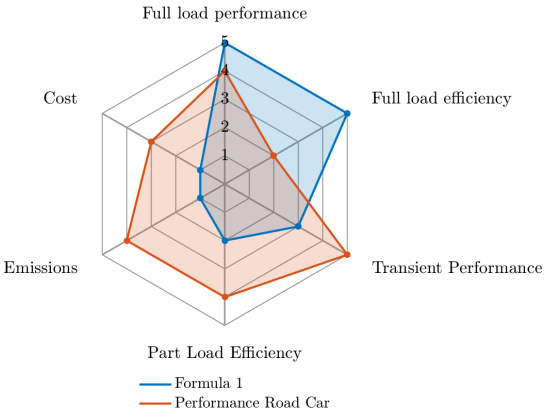

Figure 1.12: Comparison of Some Ferrari Road Car and Formula 1 Race Car Powertrain Objectives (based on the Author's Experience)

1.4 Emissions Legislation

Emissions legislation is a major driver of powertrain design for modern road cars. This was not always the case. In the early days of the automobile, environmental impact was not such a key concern. There were few cars on the road and negative health concerns of tailpipe emissions had not yet been raised. This changed in the 1920s. Tetra Ethyl Lead (TEL) was introduced as an additive to gasoline. It allowed the compression ratio of the engine to be increased and hence improved fuel efficiency. Eleven people involved in the manufacture of TEL died between 1923 and 1925 however, due to acute lead poisoning [9]. Lead had been known to be hazardous to human health since Roman times. Whilst precautions could be taken in the additive's manufacture, concerns were also raised about the long term effects of trace quantities of lead from vehicle exhaust fumes. Research programs were conducted to investigate this supported both by animal testing [10] and cohort studies [11]. Significant evidence of negative health impacts of use of leaded fuel were not found in this period, hence TEL would continue to be used for many years.

In the 1950s, the first Clean Air Act was enacted in the USA [12] but this first version had little impact. It just said the Surgeon General should co-ordinate research. The third Clean Air Act [13] of 1965 however, required the establishment of standards to reduce air pollution from motor vehicle emissions in order to protect health and welfare of the public. Oxides of nitrogen (NO_x), aldehydes and evaporative hydrocarbon emissions were the main concerns. Vehicles would be tested to demonstrate compliance. Around the same time, concerns about TEL were once again raised. This time based on the high amount of lead contamination then present in the human environment in comparison to historic levels [14]. It would subsequently be shown

that leaded fuel indeed was resulting in negative health consequences, in particular for urban populations [15]. Unleaded fuel was reintroduced to the US market in 1974, as leaded fuel was incompatible with catalytic converters. These were required for updated emissions legislation [16]. Leaded gasoline was not finally removed from the world market until July of 2021 with the last sales in Algeria [17].

Unfortunately, leaded gasoline has not been the only emissions scandal to have hit the automotive industry. In 2015, Volkswagen was found to have fitted emissions "defeat devices" to their diesel cars [18]. These allowed the vehicles to identify when they were under laboratory test conditions and to use alternative calibrations when this was not the case. This resulted in much higher NO_x emissions in real world use than permitted by legislative limits. This scandal was followed by a significant drop in sales of diesel cars and has probably accelerated the uptake of electrified vehicles. Emissions legislation in many markets now features Real Driving Emissions (RDE) testing. Here vehicles are tested on the road with Portable Emissions Measurement Systems (PEMS) devices to ensure compliance not only in laboratory conditions.

An official proposal for future European emissions legislation is expected in 2022. This is known as "Euro 7". It is anticipated to feature drastically reduced limits [19] and to necessitate actively heated after-treatment systems. With every reduction in emissions limits, manufacturers must still seek to offer products that consumers want to buy that can also be offered for a reasonable price. Meeting stringent emissions legislation is particularly challenging for high performance vehicles.

1.5 Basic Internal Combustion Engine Theory

Full load performance was identified in Figure 1.12 as being a common priority both for high performance road cars and competition vehicles. The power output of an engine will depend on the mass flow rate of fuel which it burns, $\dot{m}_{fuel}$, the fuel energy, often characterized by its Lower Heating Value (LHV), the efficiency of conversion from chemical energy to heat, η_{comb}, and the efficiency of conversion from heat to work, η_{th}, as shown in Equation 1.2.

$$Power = \dot{m}_{fuel}.LHV.\eta_{comb}.\eta_{th} \tag{1.2}$$

The fuel mass flow rate will depend on the air mass flow rate and the relative air/fuel ratio λ. η_{comb} depends strongly on λ, as shown in Figure 1.13. It can be seen that it is not very sensitive from conditions of stoichiometry in the lean direction ($\lambda \geq 1$), but reduces significantly moving rich of stoichiometry ($\lambda < 1$). The power output is maximum at slightly rich conditions, typically around $\lambda = 0.9$, where the additional fuelflow in comparison to stoichiometry more than offsets the reduction in η_{comb}.

The fuel energy depends on the blend of molecules it contains. Figure 1.14 shows LHV values of different classes of hydrocarbon as a function of RON[4]. Commercial gasoline is formed of a mixture of such compounds and has an LHV of around 43.5 MJ/kg [20] and a RON of 95. Note that alcohols, which can conveniently be produced from bio-feedstocks, have high RON but low LHV values.

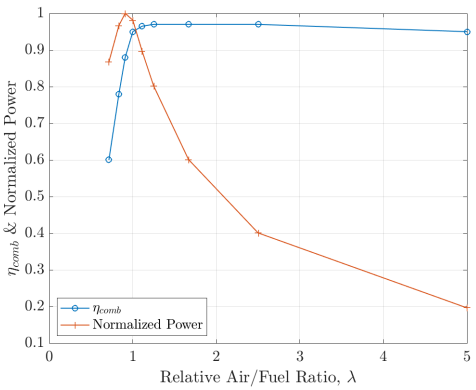

Figure 1.13: Empirical Dependency of η_{comb} and Normalized Power on λ, data from [21]

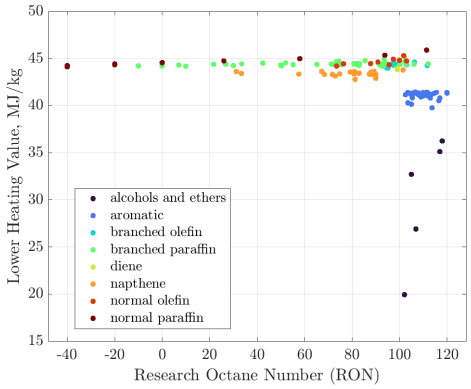

Figure 1.14: Lower Heating Value and Research Octane Number of some Hydrocarbon Molecules

Assuming λ is constant, a high power output requires a high air mass flow rate. This can be achieved through high volumetric efficiency, high engine speed, forced induction and large engine swept volume. A first approximation of η_{th} on the other hand, is the ideal air-standard

[4]Research Octane Number, a measure of fuel knock resistance

cycle efficiency. Some basic efficiency sensitivities from air standard cycles will therefore be described.

1.5.1 Ideal Otto Cycle

The basic thermodynamic cycle used in Spark Ignition (SI) internal combustion engines is the Otto cycle. This is named after the German engineer Nicolaus August Otto who built the first prototype of such an engine in 1876 and patented his invention in the US a year later [22]. The cycle comprises four processes:

- 1-2 Adiabatic Compression
- 2-3 Isochoric heat addition
- 3-4 Adiabatic expansion
- 4-1 Isochoric heat rejection

The cycle is frequently depicted using axes of system pressure and volume, as shown in Figure 1.15. On such a *"pV"* diagram, the work output of the cycle is the area enclosed by the pressure/volume plot.

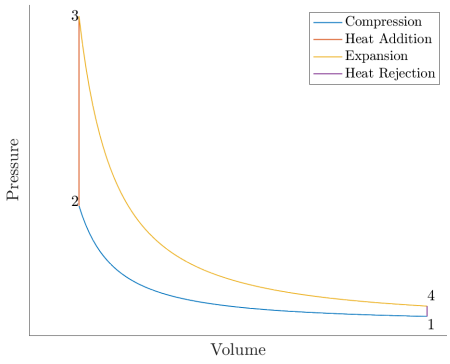

Figure 1.15: Ideal Air-Standard Otto Cycle

The cycle output is more formally expressed as shown in Equation 1.3, where W is the work output, p is the system pressure and V is the system volume.

$$W = \oint pdV \tag{1.3}$$

The thermal efficiency η_{th}, from the First Law of Thermodynamics, is the work output per unit heat input as shown in Equation 1.4, where Q_{in} is the heat input.

$$\eta_{th} = \frac{W}{Q_{in}} \tag{1.4}$$

An alternative equation, based on the fact that the First Law of Thermodynamics states that heat and work are equivalent, is shown in Equation 1.5, where Q_{out} is the heat rejected during the cycle.

$$\eta_{th} = \frac{Q_{in} - Q_{out}}{Q_{in}} = 1 - \frac{Q_{in}}{Q_{out}} \tag{1.5}$$

It can furthermore be shown that for the ideal air-standard Otto cycle, the efficiency η_{Otto} is a function of the ratio of maximum to minimum cycle volume - the expansion ratio. For the standard Otto cycle, this is equal to the so-called Compression Ratio (CR). Equation 1.6 shows the dependence of the ideal Otto cycle efficiency on this parameter. Here, $\gamma = \frac{C_p}{C_v}$ is the trapped charge ratio of the specific heat at constant pressure to that at constant volume.

$$\eta_{Otto} = 1 - \frac{1}{CR^{\gamma-1}} \tag{1.6}$$

It is clear from Equation 1.6 that to improve cycle efficiency what is required is a high compression ratio and a high value of γ. The sensitivity of cycle efficiency to these two parameters is shown in Figure 1.16.

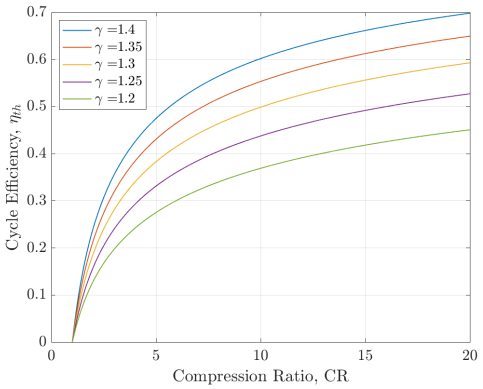

Figure 1.16: Sensitivity of Air-Standard Otto Cycle to CR and γ

A value of γ of 1.4 corresponds to air at standard atmospheric temperature and pressure. As temperature increases, such as takes place in an internal combustion engine due to compression and combustion processes, γ decreases. γ also depends on the chemical composition of the gas in the engine. This is changing as oxygen and fuel molecules combine during combustion to produce water vapor and carbon dioxide. The average molecular weight of products and reactants is rather similar however [23]. Figure 1.17 shows how γ depends on temperature, pressure and equivalence ratio, $\phi = \frac{1}{\lambda}$.

The γ value can be managed to an extent through running the engine lean and/or with dilution. Most SI engines however, run with stoichiometric air/fuel ratios to enable use of effective and relatively inexpensive Three Way Catalyst (TWC) after-treatment systems. These only function in a narrow window around stoichiometry, as shown in Figure 1.18.

Exhaust Gas Recirculation (EGR) is an alternative dilution strategy that is compatible with TWC after-treatment. The improvement in γ for a given dilution factor is more modest than for lean combustion

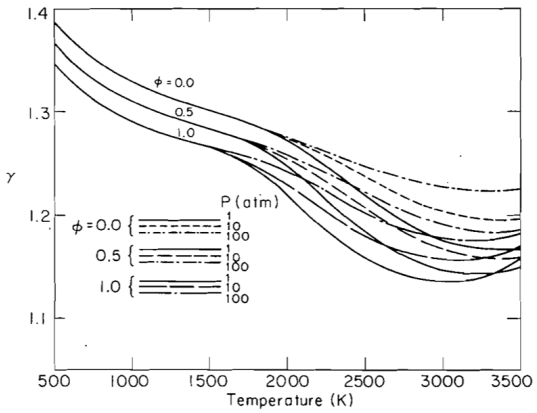

Figure 1.17: Variation of γ for Hydrocarbon-air Combustion Products with Pressure, Temperature and Equivalence Ratio ($\phi = \frac{1}{\lambda}$), from [24]

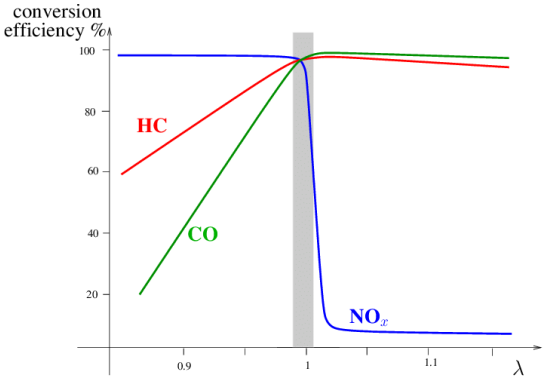

Figure 1.18: Three Way Catalyst Conversion Efficiency Dependency on Relative Air/Fuel Ratio, λ, from [25]

however [26]. In practice, in an SI ICE, the value of γ is generally between 1.3 and 1.4 during compression and between 1.2 and 1.3 during expansion.

The CR is a design parameter for the engine and from consideration of air-standard cycles it seems clear that for efficiency it should be maximized. As the compression ratio increases however, so too does the end of compression temperature and the maximum cycle pressure, as shown in Figure 1.19. The theoretical maximum pressure with a compression ratio of 20:1 is almost three times higher than for a compression ratio of 8:1. The end of compression temperature is almost 50% higher. Maximum cycle temperatures also increase, although to a lesser extent. There are therefore practical limitations on what compression ratio can be run:

- **Mechanical constraints:** as the compression ratio is increased, for a given heat input, the maximum cycle pressure increases significantly as shown in Figure 1.19. To withstand this pressure, stronger and hence heavier engine components are required increasing overall engine weight. This will also increase friction due to larger dynamic forces.
- **Geometrical constraints:** a very high compression ratio implies a very small minimum or "clearance" volume. This gives less freedom to design the combustion chamber to promote fast flame-front propagation - which is generally improved by minimizing flame travel distances and chamber surface area to volume ratio. The combustion chamber form may therefore become unfavorable for promoting fast and complete combustion. This is particularly the case for high performance, high volumetric efficiency engines, where bore to stroke ratios and included valve angles tend to be high and significant valve overlap is run. The piston geometry will therefore likely be largely dictated by the valve pockets.
- **Thermal constraints:** a high compression ratio means a high peak pressure and thus also high peak temperature. This may damage components and may also result in increased emissions of NO_x[5]. This may be the limiting factor for the compression ratio of a compression-ignition engine, although NO_x can be managed to an extent through dilution, which lowers peak temperatures, and after-treatment systems.
- **Combustion constraints:** in an engine which compresses not only air but a mixture of air and fuel (the so called "premixed strategy", as is prevalent in SI engines) the high pressures and temperatures resulting from a high compression

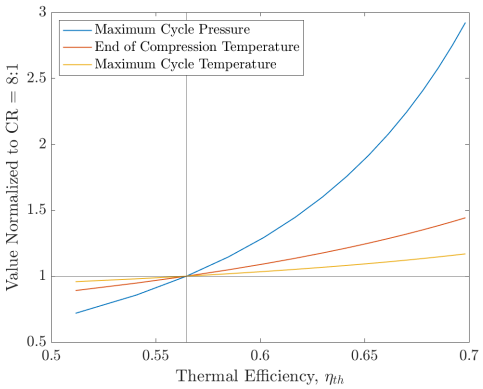

Figure 1.19: Impact of CR on some key Otto Cycle Parameters

[5]These are a major constituent of diesel exhaust emissions and in fact the Volkswagen scandal was because NO_x emissions were much higher in real world use than for laboratory testing [18]

ratio may result in some or all the air/fuel mixture auto-igniting before it is consumed in a controlled manner by flame-front propagation. This is commonly known as "knock" and can be highly damaging to engine components. This is the primary reason why spark-ignited engines have lower compression ratios than their compression-ignited equivalents. As it is the primary constraint on turbo-charged spark-ignition engine output, it will be examined in some detail in this work.

1.5.2 Practical Four-Stroke Cycle

In theory it would be possible to construct a device which runs on the Otto cycle without mass transfer across the system boundaries. This would require infinitely powerful heat exchangers however, for isochoric heat addition and heat rejection, or a method of holding the engine stationary at maximum and minimum volume. In practice, in an internal combustion engine, the heat addition is through combustion of a mixture of air and fuel and the heat rejection is performed by expelling hot gases from the combustion chamber to the atmosphere. Fresh charge must then be drawn into the combustion chamber in order to return to the starting point and begin the compression phase. With a four-stroke engine, these gas exchange phases represent two of the four strokes:

- Intake
- Compression
- Expansion
- Exhaust

A more realistic Otto cycle therefore comprises six events:

- 1-2 Adiabatic Compression
- 2-3 Isochoric heat addition
- 3-4 Adiabatic expansion
- 4-5 Isochoric heat rejection
- 5-6 Isobaric Exhaust Outflow
- 6-1 Isobaric Intake Inflow

These additional strokes can be shown on the pV diagram as seen in Figure 1.20.

In Figure 1.20 the intake and exhaust strokes are shown as taking place at constant and equivalent pressure, which implies zero work. In reality, work is required to draw charge into the engine and to expel it in order to recommence the process. This is known as "pumping work" and generally results in a reduction in useful work output from the cycle[6]. This is particularly the case with modern road car engines with extensive exhaust emission after-treatment systems - these result in a significant pressure increase in the exhaust line in comparison to atmospheric conditions.

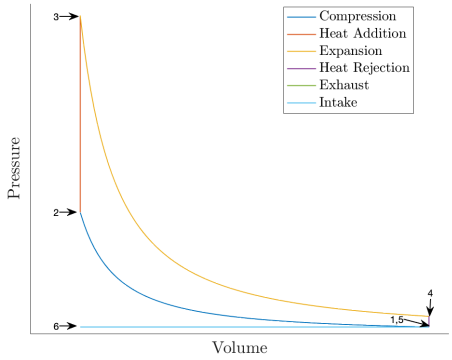

Figure 1.20: Ideal Air-Standard Otto Cycle with Intake and Exhaust Strokes

The most common four-stroke engine configuration consists of a piston, connecting rod and crank mechanism, although over the years alternatives have been tried. This is the only configuration permitted by the current Formula 1 regulations and is also the configuration used by almost all road cars on sale today or in the recent past, including all Ferrari road cars.

1.5.3 Ideal Miller Cycle

A number of alternative thermodynamic cycles exist for internal combustion engines, perhaps the most famous being the Diesel cycle. Another cycle, which is enjoying significant interest in recent years is the Miller cycle. This was originally proposed to limit cycle temperatures for diesel locomotive engines [27]. It features supercharging and intercooling. Most significantly, in this cycle the intake process is interrupted before maximum volume. This is known as an Early Intake Valve Closing (EIVC) strategy. There follows an adiabatic expansion before the compression stroke begins. The process is illustrated in Figure 1.21, taking inspiration from the illustration shown by Miller in his original paper.

The Miller cycle effectively has a lower compression ratio than the Otto cycle equivalent for a given expansion ratio. This means that the Miller cycle is more efficient. The end of compression and peak temperatures are also lower which means that the risk of knock is reduced and less NO_x should be formed.

[6] A boosted engine with high component efficiencies and low exhaust pressure may have zero or even positive pumping work

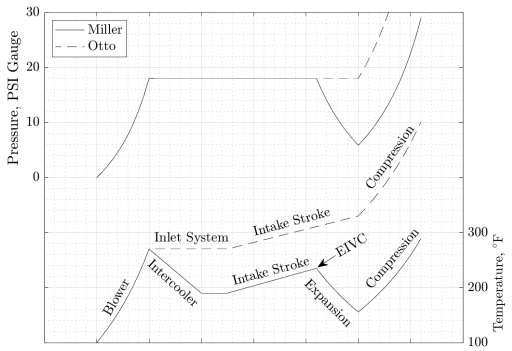

Figure 1.21: Miller Cycle Explanation, based on [27]

The Miller cycle also has disadvantages however:

- The fact that the intake stroke is interrupted before reaching maximum cylinder volume means that a lower mass of air is ingested by the engine for a given intake pressure. Assuming stoichiometric combustion, this implies less fuel can be burned, hence less heat released and so a lower work output. For this reason, the Miller cycle also features forced induction to mitigate the effect of the lower inherent volumetric efficiency.

- In a conventional engine with a piston, crank and intake and exhaust valves, the motion of charge as air enters the combustion chamber during the intake stroke generates significant turbulence later in the cycle. This can help with mixing of fuel and air and to accelerate burn rates. Interrupting air intake early, as is the case with the Miller cycle, results in lower turbulence hence poorer mixing and slower combustion.

- Volumetric efficiency of an engine is improved if valve lift is increased. The limiting factor is generally valve acceleration, particularly for high speed engines. Shortening the intake valve open duration means that the valve lift must be decreased for a given valve acceleration limit. This further decreases the volumetric efficiency of a practical Miller engine

Despite the above disadvantages, where an adequate boosting system is available and full load efficiency is of interest, the Miller cycle may be the most appropriate choice. It is hence currently used in Formula 1 engines and is increasing in popularity for road car applications. This will be discussed in more detail in a subsequent chapter.

1.6 Practical Performance Limitations for High Performance Engines

A Normally Aspirated (NA) engine will generally be airflow limited. This means that the main design effort for a high performance application will be to maximize engine speed and volumetric efficiency for a given swept volume. This was the main development driver in Formula 1 from 1989 until the 2014 regulations were introduced [28]. For a turbocharged SI engine, such as is now used in Formula 1, and is common in most high performance road car applications, achieving target airflow is not so challenging. The engine will most likely be knock-limited however. Technologies for improving turbocharged engine performance therefore generally focus on knock mitigation.

Knock can be thought of as a race between the flame-front propagation and oxidation reactions in the air/fuel mixture in regions of the combustion chamber where the flame has not yet arrived [21]. These so-called end-gas reactions occur mores swiftly at elevated temperatures and pressures. They are therefore most problematic for boosted engines with high compression ratios. The reaction rate may be orders of magnitude higher than that of flame-front propagation and can quickly lead to pressure and temperature conditions within the chamber that can destroy an engine. The compression ratio is typically lower for boosted engines to compensate, but this reduces efficiency (and for a given fuelflow rate and combustion phasing, power).

As knock is probably the main limitation on turbocharged SI engine performance, and is also perhaps the most important limitation on SI engine efficiency, it was decided to perform a literature review on the subject. Knock has been studied for some time, hence the literature is very extensive. It was thought a worthwhile exercise to begin with historical papers and follow the research through to the present day. This will be described in the next chapter.

1.7 The Author

The author of this thesis is fortunate to have worked in Formula 1 engine development for ten years[7] before having moved to road car development in 2017. This gives the benefit of an "outsider" perspective. An objective of Ferrari has always been to bring Formula 1 technology and know-how to its customers. It is hoped that the present work follows that historic trend and that avenues

[7] for Mercedes from 2007-2011 and for Ferrari from 2011-2017

to improve road car technology and methodology taking inspiration from racing approaches will be identified in the course of the research undertaken.

CHAPTER 2

Historic Literature on Knock

2.1 Abstract

Knock is one of the main limitations on increasing spark ignition engine efficiency. This has been known for at least one hundred years and it is still the case today. Knock occurs when conditions ahead of the flame-front in a spark ignition engine result in one or more autoignition events in the end-gas. The autoignition reaction rate is typically much higher than that of flame-front propagation. This may lead to the creation of pressure waves in the combustion chamber and hence an undesirable noise that gives knock its name. The resulting increased mechanical and thermal loading on engine components may eventually lead to engine failure. Reducing the compression ratio lowers end-gas temperatures and pressures, reducing end-gas reactivity and hence mitigating knock. This has a detrimental effect on engine efficiency however.

Automotive companies must significantly reduce their fleet CO_2 values in the coming years to meet targets resulting from the 2015 Paris Agreement. One path towards meeting these is through partial or full electrification of the powertrain. The vast majority of automobiles in the near future will still feature a gasoline fueled spark ignition engine however, hence improvements in combustion engine efficiency remain fundamental.

As knock has been a key limitation for so long, there is a huge amount of literature on the subject. A number of reviews of knock have already been published, including in recent years. These generally concentrate on current understanding and status. The present work in contrast, aims to track the progress of research on knock from the 1920s right through to the present day. It is hoped that this can be a useful reference for new and existing researchers of the subject, and give further weight to occasionally neglected historical activity, which can still provide important insights today.

2.2 Introduction

In December 2015, an international treaty was agreed as part of the United Nations Framework Convention on Climate Change. This is now known as the Paris Agreement [29]. Its goal was to limit the increase in global average temperatures to within a maximum of 2° C, and ideally to within 1.5° C, of pre-industrial levels. In order to respect this, all signatories must reduce greenhouse gas emissions significantly. The European Union (EU) set targets for its automotive manufacturers to reduce CO_2 emissions as shown in Figure 2.1 [30]. It can be seen that the 2030 target is just 50% of the 2015 status. Electrification of the fleet is expected to play a major role in achieving these targets. 2020 was a record year for Electrically Chargeable Vehicle (ECV[1]) sales in the EU, as shown in Figure 2.1, but the total market share was just 10% [31]. Around half of these were plug-in hybrids, which also feature a combustion engine. Diesel engines do not suffer from end-gas knock, as combustion primarily occurs in locally rich regions in an otherwise very lean chamber. They tend to have higher oxides of nitrogen (NO_x) and particulate matter emissions as a result and hence require more expensive after-treatment systems than typical homogeneous charge stoichiometric Spark Ignition (SI) engines. Whilst in 2015 diesel engined vehicle sales made up 52% of the European market, following the 2015 Volkswagen "Dieselgate" emissions scandal [18] equivalent sales had reduced to just 28% by 2020. Alternative fuels such as Liquefied Petroleum Gas (LPG), Natural Gas (NG) and 85% ethanol blends (E85) accounted for less than 2% of sales. Vehicles with gasoline fueled SI engines therefore dominated the market in 2020 and are expected to continue to do so in the near future. If CO_2 targets are to be met, significant gains in SI engine efficiency are therefore required.

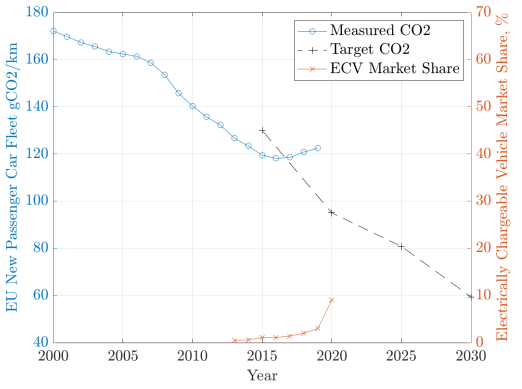

Figure 2.1: EU Fleet CO_2/km Target and Achieved Values for New Passenger Cars [30] and Electrically Chargeable Vehicle Sales [31]

SI engines operate on the Otto cycle. The thermal efficiency of this cycle is a function of the Expansion Ratio (ER) as is well known. For the basic Otto cycle, the Compression Ratio (CR) is equal to the expansion ratio. Compression ratio should therefore be maximized in order to minimize CO_2 output. The primary limitation on how high compression ratio can be raised is knock.

2.2.1 Knock Description

"Knock" was the name given by early engine researchers to a certain abnormal combustion noise made by an In-

[1]ECVs are defined as Battery Electric Vehicles (BEV), Fuel-cell Electric Vehicles (FCEV), Plug-in Hybrid Vehicles (PHEV) and Range Extender Vehicles (EREV)

ternal Combustion Engine (ICE). It was a sharp, metallic sound that could easily be discerned by the human ear. Sir Dugald Clerk [32] in a 1921 paper referred back to the problem in the 1870s. Knock has therefore been a recognized issue since at least around the time of Otto's famous 1876 patent for a compressed charge four-cycle engine. It was noted that knock occurred shortly after ignition timing and so was a distinct phenomenon to preignition. H.R. Ricardo [33] in 1922 said that knock was what limited the compression ratio of an engine and hence its performance and efficiency. Ricardo also described the phenomenon of knock as being caused by a spontaneous ignition of the unburnt charge, ahead of the flame-front.

A number of theories of the origin and nature of knock have been proposed in the meantime, but the basics of current understanding are not far removed from Ricardo's description. The theory has however, been significantly refined as will become clear in the main body of this work. A brief summary of the phenomenon in any case will now be given. Knock in an SI engine occurs when a region of the unburnt charge ignites ahead of an advancing flame-front. The autoignition almost always begins at one or a number of localized regions known as hot-spots or exothermic centers. Once a localized autoignition event takes place, what happens next depends on the size of this exothermic center and the reactivity gradient around it. A pressure wave is frequently, but not always, generated. For moderate knocking, this propagates at sonic velocity across the chamber and is then reflected by the chamber boundary. Standing waves result which produce audible vibrations at key frequencies dictated by the acoustic modes of the combustion chamber volume. These cause vibrations in the engine structure that give rise to the characteristic sound. It is also possible that the initial pressure wave becomes coupled with local autoignition chemistry and thus generates a reaction front traveling at well above sonic velocities. This results in very strong pressure wave behavior and hence is likely to cause engine damage. This phenomenon is sometimes referred to as "super-knock" and is an example of Developing Detonation (DD).

Knock in the present paper refers to end-gas autoignition. This definition separates it from Low Speed Pre-Ignition (LSPI), which is generally thought to be driven by solid particles detached from the combustion chamber walls or liquid droplets of oil/fuel mixture separated from the liner or the piston rings. These may go on to form relatively large exothermic centers, which can cause strong autoignition events that cannot be controlled by retardation of spark timing. This problem is most likely to occur at low speed and high load in modern Gasoline Direct Injection (GDI) engines and is a large field of research in itself. The current paper will not comment upon LSPI in detail, as it is somewhat distinct from what may be called "conventional knock" behavior, which is the main focus of the current work. Controlled Auto-Ignition (CAI) engines will be referred to, but only where there are important links to current SI knock understanding - for example pressure wave behavior following autoignition or Spark Assisted Compression Ignition (SACI) combustion systems.

2.2.2 Recent Knock Literature Reviews

The current paper is far from the first literature review on the subject of knock and indeed a number of high quality reviews have been published in recent years. These will now be commented upon and the motivation for a new review paper explained.

In 1998 Towers and Hoekstra [34] of the University of Central Florida published their paper titled *"Engine Knock, A Renewed Concern in Motorsports - A Literature Review"*. The background was the proposed introduction of unleaded fuel in Winston Cup NASCAR racing. A wide ranging review was performed including basic theory, damage mechanisms and design considerations. Although some historic works were commented upon, in particular the visualization activity of Miller in the 1930s, almost two thirds of the 46 papers cited were from only the preceding two decades.

In 2012 Zhen *et al.* [35] of Tianjin University published their work *"The engine knock analysis - an overview"*. The knocking phenomenon was described as were detection, quantification and visualization techniques. Simulation and chemical kinetics models were also discussed as were methods of knock suppression. 70 papers were reviewed but once again the majority of these were from the preceding twenty years - over 90%.

A large scale literature review on knock titled *"Knocking combustion in spark-ignition engines"* was published as recently as 2017 by Wang and Liu of Tsinghua University and Reitz of the University of Wisconsin-Madison [36]. Both conventional knock and super-knock resulting from oil droplets and solid particles were discussed in detail, as were analysis methods, suppression and control strategies and future research directions. Over 300 works were cited, but once more over 90% of these were from the two decades preceding publication.

Also in 2017, Gautam Kalghatgi [37] published his review *"Knock onset, knock intensity, super-knock and preignition in spark ignition engines"*. Of the articles published, a large majority were from the preceding 20 years. In this case three quarters of the total of 60.

A paper from 2015 entitled *"A Literature Review of Abnormal Ignition by Fuel and Lubricant Derivatives"* by

Chapman and Costanzo [38] did make a concerted effort to study historical work; making comparisons of abnormal combustion observed in earlier periods with that seen with modern engines. Less than a third of citations were from the twenty years leading up to publication with the majority concentrated on older activity. This work focused on pre-ignition rather than knock however and more specifically pre-ignition sensitivity to oil and fuel derivatives.

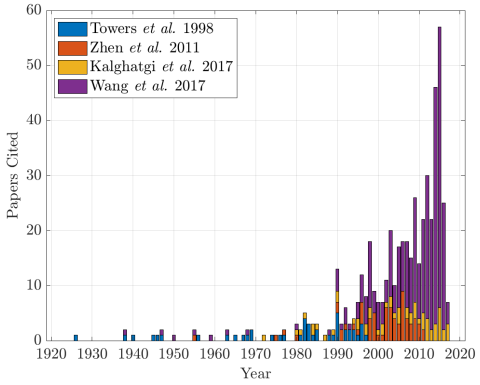

Figure 2.2: Number of Works Cited from Each Year by Some Recent Literature Reviews on Knock

The above comments on existing knock review papers should not be seen as a criticism of the approach taken by the relevant authors, as each work has made a significant contribution to our understanding of the subject. However, the period from 1920 to 1990 has not been covered in great detail in these papers (with the exception of the work by Chapman *et al.* on pre-ignition) despite the importance of the early period in explaining how we have arrived at our modern understanding and approach. This is shown in Figure 2.2. The current paper therefore seeks to fill this gap in the literature, through describing the contributions that have been made in each decade from the 1920s up until the present day. This is intended to be complementary to existing recent surveys of knock.

2.2.3 Paper Structure

The paper aims to take the reader from a starting point one hundred years ago through to the present day, commenting on significant works over the decades. The conclusion section will summarize our current understanding based on this accumulated learning with particular emphasis on knock mitigation techniques. Suggestions are also made for future research activity.

2.2.4 Paper Selection

It is relatively easy to survey the relevant literature in the early period but the volume of work has increased significantly in the last years. The first database of literature investigated was that of the Society of Automotive Engineers (SAE). Papers from the early decades were found by searching for "knock" or "detonation" in the SAE database, either in the title or full text. As the years progressed, a more selective approach had to be taken in order to render realistic completion of the review within the available time. In the more recent years, papers were primarily identified from having "knock" in the title and since 2007 from having achieved journal publication. Other key works in journals including *"Combustion and Flame"*, *"Proceedings of the Royal Society"* and *"Proceedings of the Combustion Institute"*, together with relevant textbooks, have also been referred to. In order to give a broader overview, related engine development, scientific progress, societal and regulatory changes have also been commented upon.

Despite the significant effort made, undoubtedly important works have been overlooked for which the authors apologize in advance. It is hoped that enough activity has been covered to give a general overview of the research progress over the decades and to point the reader towards sources where more detailed information can be found.

2.3 The 1920s: Fuel Shortages, New Experimental Methods and Tetra-Ethyl Lead

A number of detailed studies on knock were already published in the 1920s. The driving interest was a shortage of high quality fuels following the First World War in comparison to a greatly increasing number of vehicles on the road, as described by Kettering [39]. Knock was already a well known issue to these engineers, with Sir Dugald Clerk [32] (a pioneer of early two-stroke engines) referring back to the problem in the 1870s. Knock was an issue because of its unpleasant noise and the possibility of engine failure. The ignition timing was typically adjusted by the driver to avoid the knocking sound. Motorists were therefore highly aware of the phenomenon and the impact of variable fuel quality. Gasoline was produced at the time through fractional distillation of crude oils and shale oils with boiling temperatures in the range 50-200° C. The knock resistance of the fuel was heavily dependent on the source of the crude oil. Certain oilfields, such as Pennsylvania, produced oil high in paraffins (alkanes). Oil from Borneo on the other hand, was high in aromatics [40]. Clerk also cited some methods of managing knock that have enjoyed a resurgence in recent years: cooled Exhaust Gas

Circulation (EGR) and water injection. Horning [41] of the Waukesha Motor Company noted the knock mitigation effects of fuel enrichment and the importance of charge and component temperature reduction. In particular, avoiding hot spots in the combustion chamber from the valves and spark plug, maintaining piston temperatures low and having an effective water jacket. Note that heating of the inlet manifold was typically required at the time to achieve adequate vaporization of the available fuels, with obvious deleterious impact on the compression ratio which could be tolerated.

Knock was also discussed in some detail in a seminal paper by the esteemed engineer Harry R. Ricardo in 1922, where he stated that it was the main limit on spark-ignited engine performance and efficiency [33]. Ricardo also suggested that the fundamental cause of knock originated from an autoignition event in the end-gas. This theory had actually originally come from his Professor at Cambridge University, Hopkinson, as Ricardo himself would later describe. The influence of temperature, pressure, turbulence, mixture strength and fuel type were all considered. A Rapid Compression Machine (RCM) was constructed, together with his colleagues Tizard and Pye, in order to more properly understand the underlying dependencies. It was found that for a given fuel and equivalence ratio, whether autoignition occurred depended on a critical temperature being reached in the machine. Both rich and lean mixtures were shown to be beneficial for knock in an engine, as shown in Figure 2.3. For homogenous gasoline mixtures, enleanment was only possible in a narrow range, due presumably to combustion instability. Hydrogen as a fuel was shown to permit further enleanment and knock benefits. A stratified charge engine making use of a prechamber was also built. This extended the lean limit with gasoline and was shown to be advantageous from a knocking point of view. Over Head Valve (OHV) and "L-head" (side valve) engines were compared. OHV engines gave superior knock resistance and better volumetric efficiency. The importance of minimizing the distance from the spark plug to the furthest extreme of the combustion chamber was stressed. Compression ratios studied in the work ranged from 4.0 to 7.5 using a variable compression ratio engine to rate different fuel types[2]. Alcohols and aromatics were most resistant to autoignition whilst parafins were the worst, although there was considerable variability within the same hydrocarbon family. The knock limit was detected by the human ear only, but this was judged to be very repeatable. The indicated thermal efficiency with aromatic free gasoline was around 30%.

Alternative methods of recognizing knock were already available and indeed, cylinder pressure curves during knocking were presented in this period by a number of researchers including Kettering [39], Dickinson [43] and Midgely [44]. These came from optical indicating devices where a beam of light is focused by a mirror onto photographic film. An issue with such systems was separating vibration effects of the instrument from pressure oscillations due to knock. Natural frequencies of the instruments were between 1200 and 1700 Hz [45] - too low to measure typical knock driven pressure oscillations. An alternative system was a string galvanometer constructed by Professor Augustus Trowbridge [46] of Princeton University, which recorded rate of change of cylinder pressure on photographic film. Ion current measurements were developed, by MacKenzie and Honaman [47] at the Bureau of Standards. This enabled flame-speed measurement in an internal combustion engine for the first time, by making use of multiple spark plugs. Flame velocities from 1 to 4 m/s were observed. Knocking cycles were seen to feature rapid combustion. Clark [48], an applied chemist at the Massachusetts Institute of Technology, applied ultraviolet spectroscopy using a crank-angle synchronous shutter to an engine running on different fuels in knocking and non-knocking conditions. Greater spectral content in the ultraviolet range was seen for knocking cycles in the early stages of combustion.

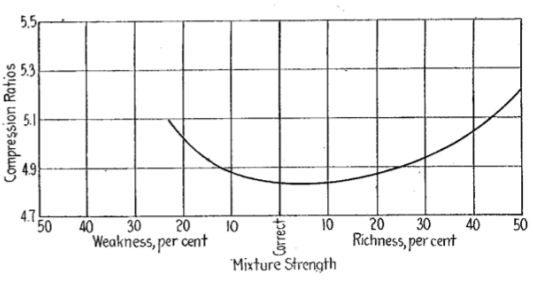

Figure 2.3: Knock Limited Compression Ratio Variation with Mixture Strength for Aromatic Free Gasoline as Measured by Ricardo, from Ricardo [33]

A method which would later become a standard was the so-called "Dickinson Bouncing Pin". H.C. Dickinson also worked at the Bureau of Standards, Washington. The pin rested on a small piston, which was exposed to combustion chamber pressure. During knocking combustion, the pin would jump clear of the piston as high as $1\frac{1}{2}$ inches. Midgely [44], working at General Motors Research Corporation on fuels research, added an integration device to this instrument by having the jumping of the pin close a circuit that performed electrolysis on dilute sulphuric acid mixture. The resulting gas was collected and the flow rate used to indicate the severity of the knock. The instrument is shown in Figure 2.4. A review of the range of methods of knock determination and fuel rating in use at the time was given by H.K. Cummings [49] of the Bureau of Standards in 1927. The

[2]The most popular car of the period, the Ford Model-T, featured a side-valve four cylinder engine of 3.98:1 compression ratio [42]

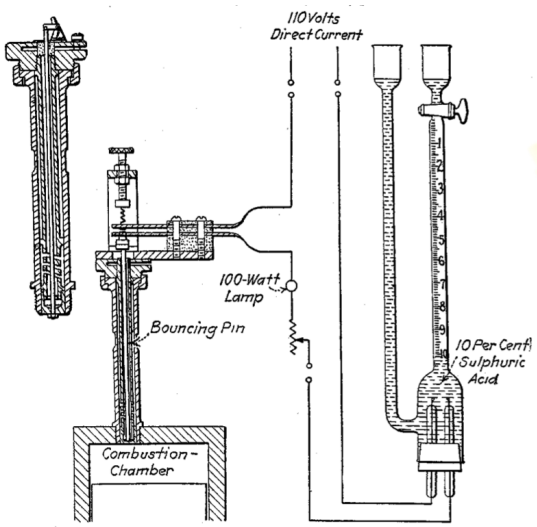

Figure 2.4: Dickinson / Midgely Bouncing Pin Knock Indicator, from Cummings [49]

bouncing pin was said to be the most common device in use. In 1928, a new electrical indicator was described by Martin and Caris [45] of General Motors. This enabled registering of single cycles on photographic film at frequencies of several kilohertz. It was based on the pressure in the engine varying the resistance of two carbon pile rheostats and could be connected to a cathode-ray oscilloscope. The frequency bandwidth was said to be high but was not quantified. Another electrical instrument, a condenser based device created by Obata and Yosida of Tokyo Imperial University, could measure up to 12000 Hz and so was capable of measuring knocking pressure oscillations.

Midgely [50] published not only on experimental methodology but also theoretical analysis of knock physics and chemistry. He is regarded as being one of the key figures behind the introduction of Tetra-Ethyl Lead (TEL) [51]. His colleague, C.F. Kettering, published on similar themes, discussing the molecular structure of various hydrocarbons, their knock propensity and distillation characteristics [39]. TEL allowed for remarkable improvements in knock behavior when added in small quantities to gasoline. It was manufactured by the Ethyl Gasoline Corporation, which was formed by General Motors and Standard Oil of New Jersey. Treat rates of 3 cubic-centimeters (CC) per gallon were typical. This enabled a significant increase in compression ratio and hence fuel efficiency for a given fuel cost. Health risks were noted at an early stage however. Eleven people involved in the manufacture of TEL died between 1923 and 1925 due to acute lead poisoning, as documented by Hamilton *et al.* [9] in the Journal of the American Medical Association in 1925.[3] This was likely through skin contact. Sale was banned and new precautions were taken in manufacturing facilities to reduce exposure risk. A second potential issue was chronic lead poisoning through inhalation of exhaust fumes over extended periods from engines operating on fuel containing TEL. General Motors Research Corporation requested and paid for an investigation into this by the United States Bureau of Mines in 1923. An interim update on this work was given in 1924 by Sayers *et al.* [53] and did not demonstrate a link between inhalation and lead poisoning. The report was criticized in terms of its methodology and conclusions by, among others, Hamilton *et al.*, who suggested further investigations should be performed and in the meantime to suspend use of TEL in gasoline. Testing continued until 1925 although the final report was not published until 1927 by Sayers *et al* [10]. The Surgeon General organized an independent study in the meantime [52]. The resulting report in 1926 by Leake *et al.* [11] found insufficient evidence for prohibiting use of TEL. However, longer term independent study was recommended. TEL returned to the market and it would be many years before the issue would once again return to the public consciousness.

TEL was a commercially successful product as it improved the antiknock resistance of fuels and such fuels were sought after by consumers. An objective rating scale of knock resistance of commercial gasolines was required. This was the task of the Cooperative Fuels Research (CFR) group. It was Edgar Graham [54] of the Ethyl Gasoline Corporation who suggested the use of iso-octane (2,2,4 trimethyl pentane) and n-heptane as the scale against which all other gasolines could be compared. It was stated that commercial fuels of the time behaved similarly in knocking terms to a mixture of 40-60% iso-octane in n-heptane. Iso-octane / n-heptane mixtures are now known as Primary Reference Fuels (PRF), with a following number which corresponds to the percentage iso-octane content. Thermal cracking was becoming more popular as a refinery process meaning more olefinic hydrocarbons (alkenes) were being used in gasoline [40].

At the end of the decade, Robert N. Janeway [55], a consulting engineer in Detroit, stated that it was generally accepted that knock was primarily driven by maximum unburnt gas temperature. He also derived mathematical relationships between flame-front propagation, inflamed volume and cylinder pressure.

[3] Alice Hamilton was recognized as being a leading expert on lead poisoning and industrial toxicology [52] and was also the first woman appointed to the faculty of Harvard University

2.4 The 1930s: The RON and MON Methods, Flame-front Visualisation and Knock Frequencies

In the early 1930s, work continued to refine a standardised method of rating the knock resistance of fuel, led by the CFR (Cooperative Fuels Research) group. There was general agreement that a knock-prone and a knock-resistant hydrocarbon should form the basis of the scale. Normal heptane had already been suggested by Ricardo as being an adequately knock-prone reference. There was some discussion however, on what should be the knock-resistant fuel. Some laboratories, such as that of the Asiatic Petroleum Co. in London, continued for a time with the suggestion of Ricardo in using benzene [56][4]. Iso-octane, as suggested by Graham [54], was preferred by Campbell, Lovell and Boyd of General Motors, primarily as it had similar physical properties to n-heptane. This meant they mixed well and hence there was little risk of the components separating in the intake system of an engine. Campbell *et al.* [57] tested a number of candidate pure hydrocarbons mixed with n-heptane in a variable compression ratio OHV $3\frac{1}{4}$" bore engine at 600 rpm with no inlet heating. This low engine speed was used both because it made knock easier to hear, and also it increased knock propensity. Testing was performed with spark timing for maximum power (according to tabulated values against compression ratio) and with mixture ratio for maximum performance. The results are shown in Figure 2.5. The authors noted that perhaps iso-octane was not adequately knock-resistant to cover all potential future fuels. Despite this concern, the laboratories converged on an n-heptane / iso-octane scale. This was said to give greater variation in knock intensity and more consistency than the main alternative considered, benzene, as documented by Barton *et al.* [58]. This scale is still in use to this day.

Work was carried out in parallel on the development of a dedicated CFR knock rating engine to facilitate quick and accurate testing, as described by Kegerreis [59]. Investigations were performed and recommendations made for water jacket temperature by Graham [60] and for carburettor setting and ignition timing by Campbell *et al.* [61] at General Motors. The Air Fuel Ratio (AFR) was to be swept for maximum knock[5]. The compression ratio would be adjusted in testing, as had been suggested by Ricardo, to obtain a target amount of knock as judged by the bouncing pin. It was initially recommended that the theoretical best ignition timing for each compression ratio be used. It was shown by Huf [62] of the Atlantic Refining Co. that the exact knock intensity at which

[4]Ricardo also experimented with toluene in his own laboratories

[5]it was found that most fuels had a maximum knocking tendency at an air fuel ratio of 13-14:1

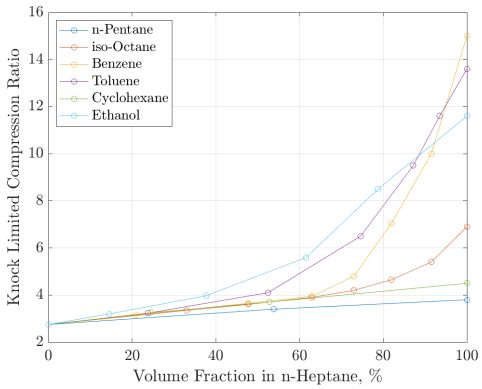

Figure 2.5: Knock Limited Compression Ratio of Various Hydrocarbons in n-Heptane Mixtures, as measured by Campbell *et al.* [57]

fuels were rated was not critical, providing that it was consistent over the duration of the test activity and that the reference and test fuels had a similar knock propensity. This work would form the basis of what is still known as the Research Octane Number (RON) test procedure and this was approved by the American Society for Testing and Materials (ASTM) in 1931. Some details are shown in Table 2.1 from the 1932 CFR Committee report [63]. Note that in the approved version the spark timing was fixed at 13° CA (Crank Angle) Before Top Dead Center (BTDC) rather than being variable with compression ratio as suggested by Campbell *et al.* An electronic knockmeter was used with the bouncing pin indicator - taking the place of the earlier electrolysis device. This procedure, with some minor modifications, is now known as ASTM-D2699 [64].

Table 2.1: 1931 CFR Research Method Test Conditions, from the 1932 CFR Committee Report [63]

Engine Type	Waukesha CFR OHV
Bore / Stroke	3.25 " / 4.5"
Compression Ratio	4-18:1
Piston	Cast Iron
Engine Speed	600 rpm
Intake Air Temperature	52° C
Coolant Temperature	100° C
Spark Advance	13 ° BTDC
Carburettor Adjustment	Maximum Knock
Knock Feedback	Bouncing Pin with Knockmeter

The problem of fuel rating appeared to have been solved. It was noticed however, that the ranking of fuels in road testing did not fully agree with the results of the RON test. A large scale study was again co-ordinated by the Cooperative Fuels Research group as described by Veal *et al.* [65] in 1933. 14 companies, from both fuel and automotive backgrounds, took part. Testing took place

at Uniontown. 15 different vehicles were used with reported compression ratios from 4.9-7.0. 15 fuels were tested in a blind manner. Testing took place over a range of vehicle speeds with the knocking tendency tending to die out as the car accelerated. Charts were therefore produced of knock intensity, judged aurally, against vehicle speed. It was decided however, that the maximum knock would be taken as the criterion against which to judge a reference fuel, irrespective of the speed at which it occurred. Over 2500 test runs were performed. It was noted that different engines had different so called "sensitivities" to different fuels. The same fuels were then tested on the CFR engine using the RON procedure. Modifications were implemented both to the engine and to the procedure, with a view to improving correlation with the road-test results. A shrouded intake valve was introduced in order to create swirl, with the aim of producing more consistent knock measurements. An improved vapor condenser was also installed. The water jacket circulation pump was removed to increase wall temperatures. The test speed was moved to 900 rpm and an air/fuel mixture temperature of 300 °F was stipulated (149° C). The key changes are summarized in Table 2.2.

This would form the basis of the CFR Motor method. This gave the Motor Octane Number (MON) of a fuel. Correlation was much improved with road test results of the period. This procedure is now known as ASTM-D2700 [66].

Table 2.2: 1933 CFR Motor Method Modifications from Research Method, from Veal *et al.* [65]

Engine Speed	900 rpm
Air/Fuel Mixture Temperature	149° C
Spark Advance	Variable with Compression Ratio

A follow up report by the CFR group was published in 1935, once again by Veal [67]. Good, though not perfect, correlation was again demonstrated between MON values and on-road measurements on a wide range of cars and fuels. The concept of fuel sensitivity "S" was defined as RON - MON. A car-dependent index known as the "Engine Severity Factor" attempted to weigh how close the road rating corresponded to MON and RON values, as shown in Equation 2.1. This can be seen as a forerunner of the modern "K-factor" approach.

$$\text{Severity Factor} = \frac{\text{RON} - \text{Road Rating}}{\text{RON} - \text{MON}} \tag{2.1}$$

A further review of road knock tests was published in 1938, this time by Boyd [68] of General Motors. This featured around three times the number of cars in comparison to the prior study and 38 fuels covering both summer and winter grades. The MON test was again shown to be closest to the road test results. Statistical analysis of this dataset was also performed by Campbell *et al.* [69] at GM (General Motors) focusing on the probability of error in road and lab octane tests. It was shown that the variability in road testing was three to six times higher than for CFR engine tests.

At around the same time, work was also being performed by Beale and Stansfield [70] at the Anglo-Iranian Oil Company on an alternative method of knock feedback on the CFR engine. This was based on block vibrations measured using an electromagnetic pickup. The signal was rectified and amplified and then displayed on a knockmeter with adjustable damping. No details of the frequency bandwidth of the instrument were given. This was known as the Sunbury Knock Indicator and became an alternative to the bouncing pin method for CFR testing. It was relatively new in 1939 when the CFR group performed an international review of the precision of laboratory knock testing. The lead author was Brooks [71] of the National Bureau of Standards. It was not found to improve precision in comparison to the bouncing pin, although it was noted that this may have been simply for the immaturity of the technique. In general, the standard deviation of octane measurements between around 100 laboratories was less than 0.5 by the end of the decade.

Optical techniques to track flame-front propagation were being applied in this period by Marvin [72] of the National Bureau of Standards. Multiple small windows were made in an L-head engine and stroboscopic techniques allowed tracking of typical flame-front position at a given crank angle over a number of cycles. The technique recalls somewhat the fiber-optic method, which is commonly used today. Different fuels and knock conditions were compared and optical filters were used to study infrared emissions in bandwidths for carbon particles, CO_2 and H_2O. Flames were seen far from the spark plug at an earlier point in the cycle when knock occurred. Radiation also peaked at earlier crank angles.

Perhaps the most famous researchers on flame-front measurements at this time were Rassweiler and Withrow [73] at General Motors. In 1935, they published on gas temperature measurements in an internal combustion engine, for both knocking and non-knocking conditions, using the sodium line reversal method. As well as observing higher temperatures during knocking combustion, they also noted an increased heat transfer rate, which was attributed to higher turbulence caused by pressure oscillations. Sudden increases in luminosity were observed at the moment of knock. Pressure waves traveling in the combustion chamber following knock were also mentioned. In 1936 Withrow and Rassweiler [74] used a quartz plate on an L-head engine to have a complete view of the combustion chamber. A camera was used which could take 5000 pictures per second. The propagation of the flame-front could be clearly tracked. High luminosity from incandescent carbon - a result of burning decomposed lubricating oil - was noted. A fast sampling valve was also used to confirm the chemistry in unburnt, burning and burnt zones.

The knocking cycles photographed, demonstrated the presence of an autoignition event far away from the advancing flame-front (rather than a sudden acceleration of the flame-front, an alternative theory of knock at the time) as shown in Figure 2.6. The autoignition was correlated to pre-flame reactions, confirmed by absorption spectra taken in this zone prior to knock. The knock initiation location was seen to vary, which was taken as evidence that it was not driven by surface hot-spots in the combustion chamber.

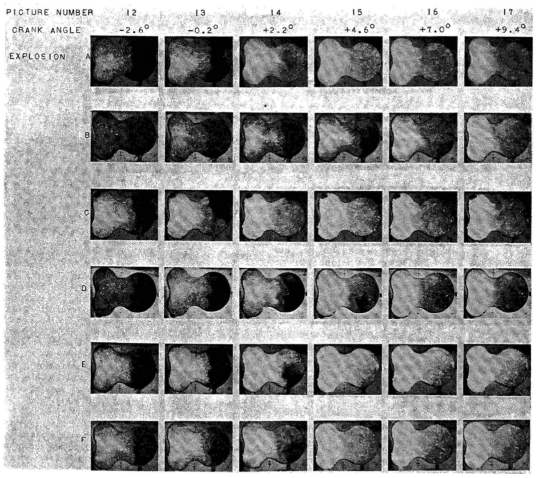

Figure 2.6: High Speed Images of Six Knocking Combustion Cycles at 900 rpm, from Withrow and Rassweiler [74]

Rassweiler's and Withrow's [75] most famous work however, was correlating flame-front propagation with pressure indication in 1938. The transparent L-head engine was again employed. Plaster casts of the combustion chamber at various piston positions were made. Photographs of the inflamed area as viewed through the transparent window were projected onto the casts as shown in Figure 2.7. The casts were then separated into "burnt" and "unburnt" regions and weighed. Single cycles, where the ignition was cut, were used to generate data of unburnt pressure versus total volume. It was found that there was a polytropic relationship between these values. The volume inflamed, based on the photographs and plaster casts, could be corrected to the original volume of this charge at ignition timing, through the polytropic relationship. Given that at ignition timing charge density is assumed to be spatially uniform, the volume fraction equals the mass fraction. This approach can be applied for each photograph in order to convert from volume fraction to Mass Fraction Burned (MFB). Of course what is desirable is the possibility to obtain these data without optical access. A method was derived based on separating pressure differences due to piston movement, which can be calculated assuming a polytropic process, from those due to combustion. The pressure rises due to combustion at a given volume were furthermore adjusted to the pressure rise which would have occurred at the initial combustion chamber volume at ignition timing. The result of the analysis is shown in Equation 2.2.

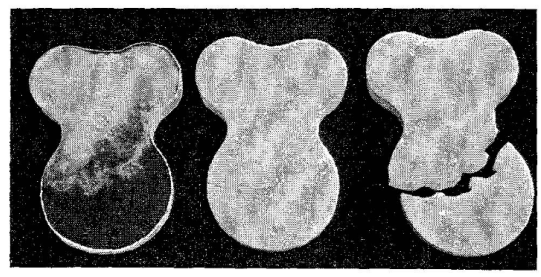

Figure 2.7: Plaster Casts with Flame Area Projections Used by Rassweiler and Withrow to Determine Flame Volume [75]

$$MFB = \frac{P_t^{\frac{1}{n}} V_t - P_{ti}^{\frac{1}{n}} V_{ti}}{P_{tf}^{\frac{1}{n}} V_{tf} - P_{ti}^{\frac{1}{n}} V_{ti}} \tag{2.2}$$

Where $P =$ combustion chamber pressure

$V =$ combustion chamber volume

$ti =$ state at ignition timing

$t =$ any time between start and end of combustion

$tf =$ state at end of combustion

and $n =$ polytropic coefficient

Equation 2.2 is still employed in combustion analysis to this day. A summary paper of work at the General Motors laboratory was published by Boyd [76] in 1939. This was notable for showing the identical frequency of pressure oscillations in the combustion chamber and acoustic measurements just outside the engine. Pre-flame reactions in knocking cycles were also evidenced by differences in emission spectra and UV absorption in comparison to non-knocking combustion. Formaldehyde (HCHO) was seen to form ahead of the flame-front for knocking cycles.

Advances were also being made in indication technology enabling characteristic frequencies of knock in cylinder pressure traces and sound recordings to be identified. MacCoull [77] used a condenser microphone together with an electronic instrument which could perform frequency analysis and high pass filtering. Knock on the CFR OHV engine was shown to take place between 6 and 7 kHz whilst on an L-head engine a lower peak at 3500 Hz was also observed, as shown in Figure 2.8. This is likely because L-head combustion chambers have a length of approximately twice their bore diameter, as exemplified in Figure 2.7.

Draper [78] used a moving coil indicator connected through a vacuum-tube amplifier to an oscillograph to measure pressure oscillations during knocking in a

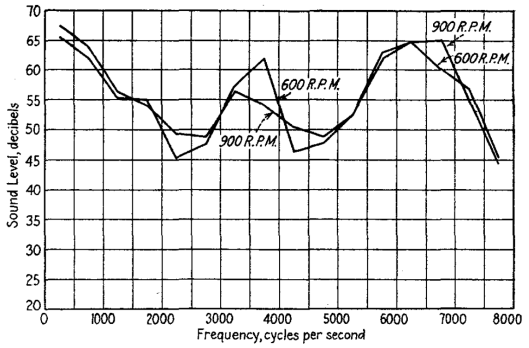

Figure 2.8: Characteristic Acoustic Frequencies of Knocking L-head Engine as measured by MacCoull [77]

CFR engine in 1935. He also noted that frequencies of around 6500 Hz were dominant in a frequently cited NACA (National Advisory Committee for Aeronautics) paper. Draper explained why this frequency was present, through deriving the fundamental frequencies of oscillation of a plain ended cylinder. 6500 Hz was characteristic of the transverse acoustic mode (with a single nodal plane) of the cylinder at the expected gas conditions. The fired engine measurements were complemented by stationary recordings in the same engine where a small explosive charge was set off. It was shown that theoretically many modes could potentially be excited. In general, pressure measurement equipment of the day only had a bandwidth of around 10 kHz and hence only content at 6500 Hz was confirmed. Draper [79] published a follow up paper with the Institute of Aeronautical Sciences in 1938 with a more extensive theoretical analysis where modal frequencies up to 50 kHz were calculated. In this new work, an electromagnetic indicator with a resonant frequency of 95 kHz was coupled to an amplifier-oscillograph system with an extended bandwidth - greater than 20 kHz. The predominant frequency observed was still around 6500 Hz. Draper noted that other frequencies were present, but that a higher film speed would have been required to isolate them.

Other significant activity for NACA was taking place at the time by Rothrock and Spencer [80] at Langley Field. They took schlieren photographs of the combustion chamber of a NACA research engine, initially at 1,000 frames per second. The engine was of a fuel injection type and indeed diffusion combustion, resulting from the injector sac volume, could be seen on the photographs. A similar phenomenon is frequently observed with modern GDI engines. Knock was apparent as a sudden increase in light intensity. A slight pressure rise was noted immediately prior to the knock event. Experiments were also performed charging a 2 μF condenser to 30 kV and then discharging it through a 0.004 inch copper wire in the combustion chamber. Although this produced a shock wave, it did not cause knock. This was to investigate one of the theories at the time that shock waves traveling through the combustion chamber were the cause of initial autoignition. This phenomenon is harnessed in shock-tube reactors to produce autoignition. It can also occur in engines if developing detonation takes place following an initial autognition event. This would form a key avenue of research in later decades.

The octane value required to prevent knocking in automotive applications at this time was around 70 [67]. Gasoline octane had improved through introduction of new refinery techniques such as polymerization and alkylation. Polymerization combines light olefins to give heavier olefins that can be used in gasoline. These tend to have high RON but low MON. Alkylation produces iso-octane by catalytically reacting light olefins with isobutane [40]. For military aeroplane engines, an octane value of 87 was targeted at the beginning of the decade. This required use of aromatics and tetra-ethyl lead as described by Heron [81], a research engineer for the Air Corps at Wright Field. Close to the outbreak of WWII, values of over 100 were becoming common for aviation fuels as noted by Du Bois and Cronstedt [82] of the Aviation Manufacturing Corp. The CFR group studied dedicated octane rating measurements for aviation gasoline. The objective, as described by Nutt [83] in 1933, was to develop a standard of knock rating for all types of aviation fuels that would be applicable to all engines. Veal [84] reported on status in 1936. Testing had been performed on four multi-cylinder aero-engines, three of which were supercharged, made by Wright, Pratt & Whitney and Lycoming. Testing was by sweeping the fuel flow from "full-rich" to "minimum-allowable" at fixed throttle position. Cylinder temperatures, fuel flow and power output were recorded and each test fuel was bracketed with reference fuels. The point where cylinder temperature increased as fuel flow was reduced was used to define knocking behavior. The correlation with the Motor Octane method depended on the class of hydrocarbons in the base fuel. Further testing was reported in 1938 by Cummings [85]. The peak cylinder pressure was found to give a much better feedback on the knock limited minimum fuelflow in comparison to the cylinder head temperature, as used in previous tests. Test fuels were bracketed by mixtures of technical iso-octane (Reference fuel S-1) and low-knock resistance Michigan Gasoline (Reference fuel M-1), rather than pure iso-octane and n-heptane, for cost reasons. TEL was used to extend the octane scale beyond 100 based on Indicated Mean Effective Pressure (IMEP) increases on a modified supercharged CFR engine as shown in Figure 2.9. A new laboratory method was suggested in 1939 by Stansfield and Taylor [86]. The CFR engine modifications included fitting an aluminum piston, improving engine volumetric efficiency through valve and carburetor modifications and the use of a supercharger. Limitations of the bouncing-pin device were noted, where fast combustion with high pressure

rise rates could result in false detection of knock. The rate of change of pressure was therefore shown on an oscilloscope and a knock index was developed based on the maximum rate of pressure rise of the first knocking oscillation each cycle, observed over a minute of operation. Peak-knock air/fuel ratio was also identified using this method rather than the bouncing pin. The volumetric fuelflow was then increased by 25%, 35% and 45% from this value. Compression ratio was adjusted at each air/fuel ratio to give constant knocking for the reference fuel based on the oscilloscope method. This same compression ratio for each air/fuel ratio was used also for the test fuels. The ratio of the knock signal for test and reference fuels against enrichment was then calculated. Different tendencies for different fuels were noted. The 45% rich setting was said to be representative of takeoff conditions. This combined activity would lead to the definition of the *"Supercharge Rating of Spark-Ignition Aviation Gasoline"* - now described by ASTM D909 [87]. Some key details of the current standard are shown in Table 2.3. The procedure produces a knock-limited IMEP curve of the fuel over a range of fuel-air ratios from 0.08 to 0.12 with a fixed compression ratio. The manifold pressure is firstly adjusted to produce "standard knock"[6] at a fuel-air ratio of 0.08. The mixture is then progressively enriched and manifold pressure increased to return to the same knock level. The IMEP of the test fuel is compared to the IMEP of the reference bracketing fuels at the best mixture IMEP of the lower bracketing reference. Interpolation of these IMEP values gives the fuel rating. The rating scale for octane values above 100 was indeed based on addition of TEL. A performance number was defined as shown in Figure 2.10.

Table 2.3: Current Standard Test Method for Supercharge Rating of Spark-Ignition Aviation Gasoline (ASTM D909-18e01) [87]

Engine Type	CFR F-4
Bore / Stroke	3.25" / 4.5"
Engine Speed	1800 rpm
Piston	Aluminum
Intake Air Temp. (Surge Tank)	107° C
Supercharger Pressure	Variable
Coolant Temperature	191° C
Spark Advance	45° CA BTDC
Compression Ratio	7:1
Fuel System	Manifold Injection 82-99 bar
Fuel-Air Ratio	0.08 - 0.12
Knock Feedback	Determined by Ear

Together with advances in combustion measurement techniques and improved octane fuel availability, engine technology was also evolving. Dillstrom and Torbjorn [88] of the Hesselman Motor Corporation published on use of fuel injection on a spark-ignition engine to permit a higher compression ratio in 1934. End of compression stroke injection was used and swirl employed to have adequate homogenization in full load conditions. A stratified approach was employed at part load. A deep bowl was used in the piston to

[6]Despite the interesting studies on use of an oscilloscope for knock feedback, "standard knock" is still defined as trace or light knock as determined by ear in the modern procedure

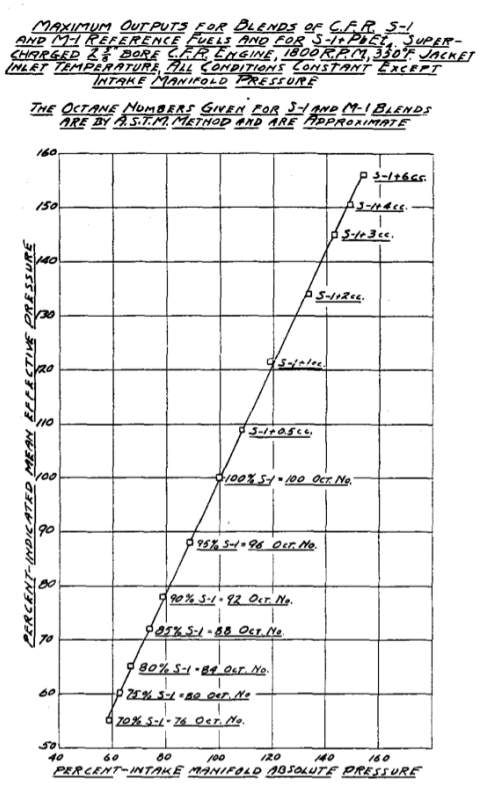

Figure 2.9: Relative Indicated Mean Effective Pressure for Reference Fuels used in CFR Aviation Testing, from Cummings [85]

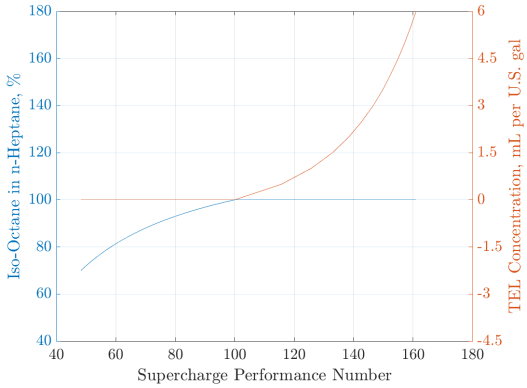

Figure 2.10: Supercharge Performance Number Dependency on Iso-Octane in n-Heptane and TEL Concentration as Definited by ASTM D909 [87]

avoid fuel spray contacting the liner. A second goal of the fuel injection system was to reduce fuel volatility requirements. Compression ratios from 6:1 to 10:1 were discussed. For aviation applications, towards the end of the decade, availability of fuels with octane values in excess of 100 permitted increases in compression ratio and supercharging as described by Du Bois *et al.* [82]. A paper by Tsien [89] at the Massachusetts Institute of Technology (MIT) discussed the limits of high output piston engines of the day for aircraft applications. Typical engines at the time had a Brake Mean Effective Pressure (BMEP) of around 14 bar and piston speeds of around 14 m/s. A research engine is cited as having reached 40 bar BMEP with peak cylinder pressures of 107 bar at 2.6 bar absolute inlet pressure. This engine made use of water injection. High performance aviation piston engine technology had developed during the Schneider Trophy era of 1913-1931. Engines were now being further developed for war. Extensive details of these engines have recently been revealed by Douglas [90]. These engines will be commented upon further in the next section.

2.5 The 1940s: High Performance Aircraft Piston Engines, New Refinery Techniques, On Board Knock Measurement and High Speed Photography

Considerable fuel and engine development took place in the late 1930s and early 1940s in a bid to extract more performance from military aeroplane engines for use in World War II. A number of new refinery techniques had become available, including catalytic cracking and alkylation as described by Risk [91] of Ethyl Corporation. This enabled more knock resistant fuel components to be introduced and iso-octane to be manufactured at scale more cheaply. Catalytic reforming was also used, which improves octane numbers by producing aromatics from naphthenes (cycloalkanes) [40]. More complex branched molecules were studied, sacrificing volatility for aircraft applications in the quest for increased knock resistance, as noted by Barnard [92] of the Standard Oil Company of Indiana. The octane rating of aviation gasoline had increased to 100 by 1940, according to Hives *et al.* of Rolls-Royce [93]. By the beginning of the same decade, the MON values of premium motor gasoline were 80, up from around 70 in 1930, as pointed out by Humber of Ethyl [94].

The ASTM Motor Octane Number was the most commonly used standard for automotive octane rating at the time, according to Risk [91]. Confidence in how well it represented knocking tendencies on-road began to decrease in this period however, including that of the CFR group [95]. They began studying the effects of engine speed and ignition testing on typical cars of the day. It was found that some fuels performed better at low speed and others at high speed, but the so called "Uniontown" road-rating method only gave a single value per acceleration run. The "Borderline" knock test method was therefore adopted by the CFR group in 1940. With this approach, a borderline ignition timing curve against engine speed is determined for the given fuel from multiple acceleration tests where the ignition angle is progressively adjusted. The Knock-Limited Spark Advance (KLSA) was generally non-linear with engine speed whilst the distributor spark advance characteristic for vehicles at the time could not match this. This is shown in Figure 8.1. Significantly, L-head engines (an older design) were found to knock more at high speed and less at low speed in comparison to more modern "valve-in-head" (OHV) types [91].

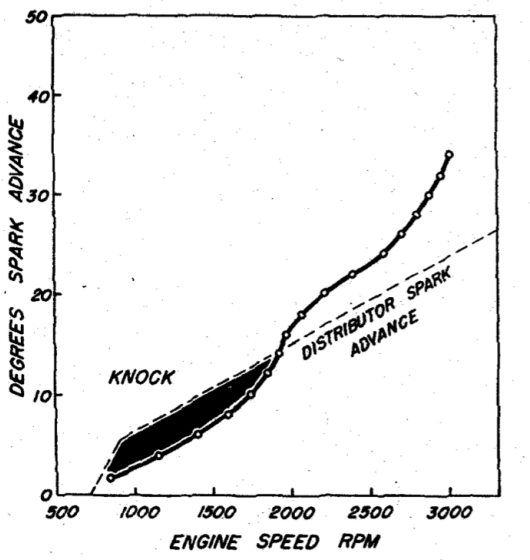

Figure 2.11: "Borderline" Ignition Timing showing Knock Region in Comparison to Distributor Advance Curve, from Risk [91]

Rothrock [96] at NACA proposed a more complex approach to fuel rating where curves of limiting end-gas density against temperature were plotted through varying boost, compression ratio and inlet temperature. A number of suggestions were made for how to measure knock at Octane values greater than 100, as told by Brooks [97] of the CFR group, although there was no clear agreement. Use of TEL additive was proposed as was the use of triptane as a new reference knock resistant base hydrocarbon. The lack of a reference for octane values greater than 100 was increasingly problematic with the advent of synthetic fuels and increased sensitivity, commented upon respectively by Heron [98] and Gay [99], both of Ethyl Corporation.

Piston engine technology was being pushed forward by the military for aviation applications. This included use of two stage boosting with air-to-water charge cooling, four-valve cylinder heads and sodium cooled valves at Rolls-Royce, as described by Hives *et al.* [93]. Drogemueller *et al.* [100] of Pratt & Whitney commented on the knock benefits of charge cooling, water injection and low exhaust backpressure - an advantage of mechanical supercharging over turbocharging leading to lower in-cylinder residuals. Rowe [101] of Wright Aeronautical Corporation presented results of water injection on a Wright Cyclone 9 and a CFR engine after the war in 1946. Pure water gave the strongest engine cooling whilst water/methanol mixture gave highest knock-limited power output. Water/ethanol was less effective. Obert [102] of Northwestern University published on water injection in 1948. The fact that water slows combustion was noted. In testing on a CFR engine at 900 rpm and intake temperature of 143° C, it was estimated that less than 50% of injected water had evaporated by the end of compression. 50% water in fuel reduced the volumetric efficiency of the engine by 2%. Much activity of course did not make it into the academic literature during the war. Some of this has been recently revealed by Douglas [90]. German engines such as the Daimler-Benz 601 featured GDI at 90 bar pressure. BMW introduced a mechanical engine management system on the 800 engine, whose successor, the 801, powered the FW 190 fighter in 1941. The Jumo 211 featured water-cooled exhaust valve guides and variable inlet guide vanes (referred to as a "swirl throttle") on the compressor. Developments of much of this technology are still in use today, including in Formula 1.

One of the most significant contributions made to modern spark-ignition engine knock mitigation came, perhaps surprisingly, from the diesel engine locomotive industry in this period. In 1947, R.H. Miller [27] proposed a new cycle which nowadays bears his name. Miller was a Chief Engineer at Nordberg and the suggested application of the cycle was for diesel engines. The concept is illustrated in Figure 2.12 and features a boosting system, an intercooler to bring temperatures down to an intermediate level, then Early Intake Valve Closing (EIVC) and subsequent expansion in the remainder of the intake stroke to further cool the trapped charge. The objective was to lower mean cycle temperature to allow higher load for locomotive diesel engines. It was also mentioned that it could be used to increase the geometric compression ratio of a spark ignition engine and indeed this is frequently applied today.

The period was also notable for significant advances in knock instrumentation, again driven by military aircraft requirements. One instrument was the MIT Sperry Indicator which came from activity carried out by Draper [103, 104]. This measured vibrations originating from knock in the range 5000-10000 Hz. These were

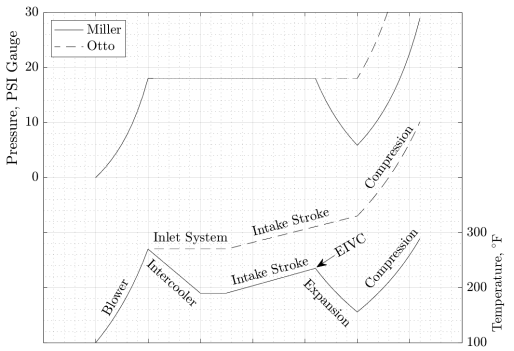

Figure 2.12: Original Miller cycle concept explanation, based on [27]. Impact on charge pressure and temperature is shown as the charge makes its way through the engine. Comparison between a standard Otto cycle with a blower and a new proposal with intercooler and in-cylinder expansion for charge temperature reduction.

amplified by a device with automatic gain control and caused a light to flash in the cockpit of the aircraft when knock was detected. A closed loop system was also introduced which controlled air fuel ratio to maintain the engine at borderline knock both in takeoff (rich) and cruise (lean) conditions. This was but one of a number of devices available, based on the review by Bogen [105] of Universal Oil Products. They generally operated on similar principles and with various methods of handling other high frequency noise sources apart from knock. It is perhaps no surprise that these devices were applied to automotive activity shortly after the war, as described by Goffe and Wheeler [106] of Sperry Gyroscope. At this stage, integration devices had also been introduced to allow a stable knock measurement over a number of cycles.

Fundamental engine combustion research was still taking place, as summarised by Fiock [107] of the Bureau of Standards, with significant activity undertaken by NACA and General Motors at the time. NACA notably carried out high speed photography of combustion and knock. The first study, published in 1941 by A.M Rothrock, R.C. Spencer and C.D. Miller, was with a frame rate of 40,000 photographs per second [108]. As in their previous work, schlieren techniques were applied. Thermal gradients in the end-gas shortly before knock onset were seen, suggesting exothermic reactions were already taking place. The knock event itself was found to take place over just 0.0005 seconds. This corresponded to two frames of their camera. A follow on study was published in 1943 by the same group, this time authored by Miller and Olsen [109]. The simple autoignition theory of knock described by Ricardo was

called into question and an experimental campaign performed to test if autoignition always preceded pressure oscillations, as measured by a piezoelectric transducer. On knocking cycles, a blurring of a region of the schlieren image was observed in the end-gas which corresponded to the start of knock as judged by the pressure transducer. It was determined to be a reaction covering just 25 μs - much faster than the slow autoignition events recorded by Withrow and Rassweiler a decade earlier. Mottling of the schlieren images was observed in the end-gas before the blur appeared. This was considered by the researchers to be a form of combustion, but not that of a thin flame. They were possibly observing evidence of pre-flame reactions, but these would not be studied in detail until the following decade. A new experimental apparatus was developed by NACA in order to cover the time scales of the initial knock event. This device could take photographs at 200,000 frames per second. A report was published in 1946 by Miller *et al.* with 20 ultra high speed photographs of a single knock event [110]. It was seen that the initial knocking reaction traveled through the charge at around twice the speed of sound. A follow up work was published by the same group in 1948 [111]. This time a much greater body of data allowed firmer conclusions to be drawn. A new experimental approach allowed much clearer visualization of the end-gas. Three different fuels were tested with different knocking tendencies. Both homogenous autoignition and so called "pin-point" autoignition were observed. The pin-point type was hypothesized to perhaps originate from particles, but was seen in any case to respond to the fuel knock resistance. The pin-point type autoignition did not always result in significant pressure rise rates or knock. The homogenous type on the other hand generally resulted in high pressure rise rates and knocking combustion. A reaction front that moved at around twice the expected acoustic velocity was observed and was surmised to be a type of detonation wave, although it was thought this was of an unstable type and did not last for very long. This is now described as Developing Detonation. Knock was revealing itself to be a more complex phenomenon than had been supposed just some years earlier.

At around the same time, a very large scale fuel study was taking place organised by the American Petroleum Institute. This was known as American Petroleum Research Project 45. 225 pure hydrocarbons were tested in 29 different operating conditions in an engine. Some highlights were presented by Lovell [112] of GM. This generated a wealth of data for the future on the relationship between fuel molecular structure and knock tendency. An example is shown in Figure 2.13.

Although general tendencies for different types of hydrocarbon were found, the knocking tendencies were seen to overlap between classes, as had also been noted by Ricardo in more limited studies in the 1920s [33]. It was shown that it was necessary to evaluate pure components over a range of conditions, or at least RON and MON, instead of just a single test point. An important hydrocarbon which was used during WWII was triptane (trimethyl butane). Kettering [113] of General Motors told the story of this highly knock resistant fuel which was first tested in an engine at GM in 1926. It allowed a 50% power output over iso-octane in supercharged engines. A special plant was constructed to produce triptane in quantity for the war effort in 1943. This hydrocarbon would still find many applications today, in particular for modern Formula 1 boosted engines. It is no longer commercially available in large quantities however.

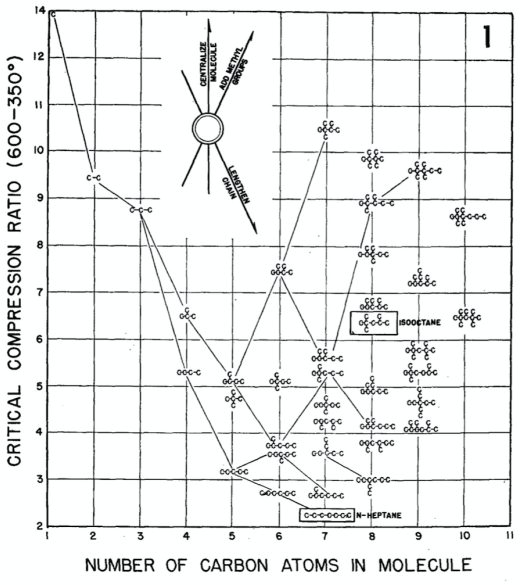

Figure 2.13: Relationship between Critical Compression Ratio and Molecular Structure for Paraffinic Hydrocarbons, from Lovell [112]

2.6 The 1950s: The beginnings of a Chemical Kinetics Approach and New Combustion Problems

In the early part of the 1950s, a new approach to knock investigations emerged. This was to use a motored engine with conditions tailored to approach that of fired engine end-gas. Retailliau *et al.* [114] at Esso Laboratories ran a CFR engine in motored conditions with PRF 75 as the fuel. The exhaust gas was collected and condensed and distillation was performed to identify which hydrocarbons were present. Half of the original fuel had undergone reactions. Subsequent testing was performed on this blend and also pure iso-octane and pure benzene. A temperature plug in the engine

indicated heat release during motoring above a certain compression ratio for the paraffinic fuels but not for benzene. Fired engine testing indicated a correlation between these so-called "pre-reactions" and knock onset. TEL appeared to reduce the extent of pre-reactions in paraffinic fuel. Pastell [115] at Du Pont reported on similar activity on a CFR engine at their laboratory[7]. Here, the pre-reaction work was identified on pressure/volume diagrams. This was then characterized against mixture temperature, compression ratio and manifold pressure. An example is shown in Figure 2.14. Here a region is clearly visible where increasing temperature does not increase pre-reaction heat release. This is non-Arrhenius behavior. The reactions occurring were noted to be of the cool-flame type and could also be observed using a photo-multiplier tube sensitive in the range 200-700 nm. Photo-multiplier tubes were also used to characterize such reactions in a fired engine by Cornelius and Caplan [116] of GM. A narrower band device with peak sensitivity around 400 nm was used as cool flames were expected to be in the range 340-450 nm. Pre-reaction heat release was again evaluated using cylinder pressure measurements. Peak reaction rates were found to be before Top Dead Center (TDC) on PRF 80 suggesting the existence of a Negative Temperature Coefficient (NTC) region. This NTC region was said to be that of cool-flame reactions and indeed a pale blue luminescence could be seen for fuels exhibiting this behavior. A number of hydrocarbons were tested with cool-flame behavior correlating with presence of normal paraffins as expected. However, the companion hydrocarbon in a two-component mixture with normal paraffins also had an impact. It was noted that cyclopentane/n-heptane reduced pre-reaction heat release for a given octane number relative to iso-octane/n-heptane blends. Many years later cyclopentane would be discovered to be very effective in improving knock behavior when blended with iso-octane and aromatics [117]. The National Bureau of Standards investigated the nature of the cool flame radiation using a spectroscope together with a photomultiplier tube in 1952 as described by Levedahl and Broida [118]. A CFR engine was run over a range of compression ratios to achieve either only pre-reactions or full autoignition with n-heptane fuel. Full autoignition was characterized by two peaks of emission intensity against time. The first peak, of lower intensity, was the cool flame reaction. The second peak was the hot flame. Between the two peaks emission intensity reduced. The spectrum of the cool flame reactions was stated to be that of formaldehyde fluorescence. An interesting research activity also took place at Ethyl Corporation where a fueled, motored CFR engine was used to generate partially reacted products which were then sent to the intake of a fired engine. This was described by Mason and Hesselberg [119] in 1954. It was found that the knock limit of the fired engine depended on the compression ratio of the motored engine and hence the extent of the pre-flame reactions. The highest compression ratios in the motored engine actually gave an improved knock rating in the fired engine, despite higher motored exhaust temperatures. A significant work by Sturgis [120], again of Du Pont, showed that radicals of hydrogen had perhaps the key role in the knock reaction chain: when running an engine on carbon monoxide, the knocking tendency greatly reduced as humidity was lowered and hence the engine was starved of hydrogen containing molecules. In general, there was intense activity to understand the reaction chain resulting in knock and also the mechanism of antiknock substances. This field is known as chemical kinetics and is still a very important part of knock research today. The underlying theory is based on the concept of chain reactions. This was developed by Semenov [121] of the Institute of Chemical Physics of the USSR and Hinshelwood of Oxford University in the 1930s. They would share the Nobel prize in Chemistry in 1956 for their contribution to understanding chemical reactions.

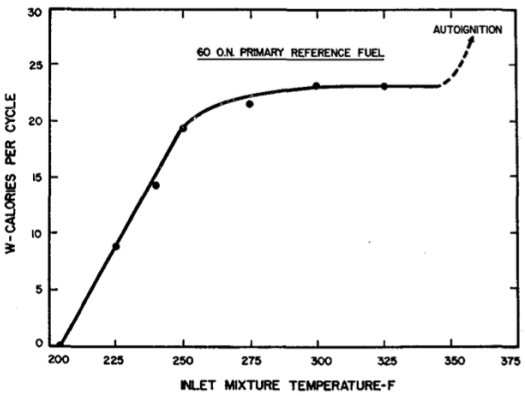

Figure 2.14: Relationship between Pre-reaction Heat Release and Inlet Mixture Temperature, from Pastell [115]

The motored engine approach was an alternative to the RCM technique which was being used at MIT. The MIT apparatus was described in detail by Taylor *et al.* in 1950 [122]. The machine featured optical access to the combustion chamber. Various sensitivities were presented for a range of fuels including n-heptane, iso-octane and benzene. It was not clear at the time how to compare data from such a machine with those of a running engine. A significant step forward was made in 1955 by Livengood and Wu [123] with their seminal paper *"Correlation of Autoignition Phenomena in Internal Combustion Engines and Rapid Compression*

[7] In the discussion of this paper Learny and Livengood of MIT mentioned that the CFR engine could operate in a stable manner on a low-octane fuel without a spark and remarked that this cycle could be interesting for the future. They were describing what would later be known as Homogeneous Charge Compression Ignition (HCCI).

Machines". Equation 2.3 was presented.

$$\frac{d(x)}{dt} = \phi_1(p, T, t), \phi_2(F, \text{composition, etc.}) \tag{2.3}$$

where (x) = concentration of pertinent reaction products
t = time
p = absolute pressure
T = absolute temperature
ϕ_1, ϕ_2 = empirical functions
F = Fuel air ratio

Equation 2.3 implies a fixed relationship between rate of reaction and instantaneous state. It was assumed that there was a critical concentration of reactants, x_c, which would result in a sudden transition to a very rapid completion of combustion. The time required to reach x_c is known as the ignition delay, τ. Applying the concept of a critical concentration correlated with the ignition delay time, as shown in Equation 2.4 and Equation 2.5:

$$\frac{d}{dt}\left[\frac{(x)}{(x_c)}\right] = \phi\left(\frac{t}{\tau}\right) \tag{2.4}$$

$$\therefore \frac{(x)}{(x_c)} = \int_{t=0}^{t=t_c} \phi(t/\tau)dt = 1 \tag{2.5}$$

Assuming the reaction rate does not change with time for a fixed state, we arrive at the final famous Livengood-Wu integral as shown in Equation 2.6:

$$\frac{(x)}{(x_c)} = \int_{t=0}^{t=t_c} \frac{1}{\tau}dt = 1 \tag{2.6}$$

In order to apply Equation 2.6 to experimental data from an engine, the state/time history of the process must be known. The equation was shown to give good agreement between motored engine, fired engine and RCM results. Some doubts were already raised in the paper that perhaps two separate integrations might be necessary to cover two-stage reactions. It was also noted that photographic records of the RCM devices available at the time, showed evidence of inhomogeneity of the reactions and even flame-front propagation. Doubts were also raised by the authors concerning what would happen with mixtures of different hydrocarbons. Despite this, the Livengood-Wu approach is still used, with some refinements, to the present day. The work at MIT was sponsored by the Ethyl Corporation. A summary of some of the learning gained in this machine and its applicability to internal combustion engines was given by Rifkin and Walcutt [124] of Ethyl Corp. in 1957. Notably, the dependence of the autoignition reaction rate on thermal gradients in the combustion chamber was commented upon, with small gradients hypothesized to result in autoignition of a large volume of unburnt charge in a small time - a volumetric ignition. It was thought that this could explain the appearance of supersonic reaction fronts in the optical measurements of Miller *et al.* from the previous decade. Miller himself attributed the supersonic reaction front to detonation waves. It is now known that both regimes are possible in a knocking engine and that this depends, among other things, on the thermal gradients around an exothermic center.

Whilst numerous researchers were studying the impact of time on compressed reactants, the importance of flame propagation on knock was also being investigated, by Diggs [125] at Du Pont. He modified a CFR head to include 17 spark plugs which could be fired in any combination. The combustion duration was reduced to 60% of the standard value, which give an improvement in octane requirement of nine points at 900rpm. The modified cylinder head is shown in Figure 2.15.

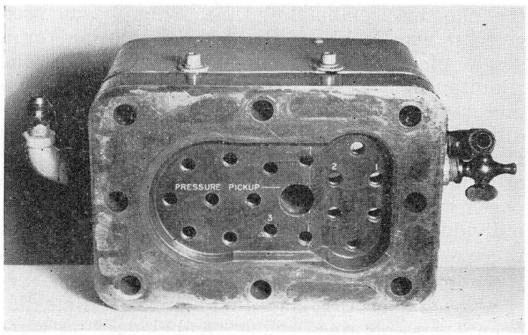

Figure 2.15: Modified Cylinder Head with 17 Spark Plug Locations, from Diggs [125]

A new practical combustion problem also reared its head: "rumble". This was described in a paper by Meagher *et al.* [126] of Du Pont in 1955. This seemed to be brought about by the fact that compression ratios had increased by almost three points and octane numbers by nine units since the post-war period, according to Perry *et al.* [127] of Socony Mobil Oil. Indeed, compression ratios were around 10:1 at this time and fuels with a RON value of 102-108 were being used in research settings by Hostetler *et al.* [128] at Standard Oil Ohio and Wiese [129] at GM. Rumble caused a low frequency noise, distinct from knocking. It was believed to come from multiple ignition points resulting from hot combustion chamber deposits. It was found to correlate with surface ignition, and ion-current measurements were commonly used to diagnose it. A new crank angle time recorder was also produced by Warren and Hinkamp [130] of Ethyl which could keep track of cyclic variation in such events. Rumble was found to be worse with high aromatic content [128] and could be reduced by use of additives and fuels with better tail-end[8] volatility [129].

[8]The "tail-end" refers to the highest boiling point components of a gasoline mixture, which will be the last to evaporate in the engine. The most volatile components are referred to as the "front-end"

Some interesting historical papers were also published in this period. One was by Ricardo [131] and covered his early period including when he was an undergraduate under Hopkinson at Cambridge University in 1905. Hopkinson was possibly the first to suggest that knock was an explosion in the end-gas. Ricardo proposed the concept of "highest useful compression ratio" and his early research work significantly informed the future CFR method of fuel testing. Pope [132] of Waukesha also published a historical paper some years later, where he explained the background to what would go on to become the CFR engine. This was originally intended for testing at just 600rpm, but improvements led to the 1948 version which could run up to 4500rpm. The Midgely/Dickinson Bouncing Pin indicator was used until 1954, when it was replaced by a new device. This was again based on a mechanical pin but which now made contact with a magneto-restrictive pickup. It was in any case tuned to agree with audible knock.

2.7 The 1960s: Octane Rating Discussions and Computer Analysis

In the 1960s, there were renewed investigations on the representativeness of the RON and MON tests. Buerstetta *et al.* [133] of Ethyl Corp. and Esso Research and Engineering Co. described testing with four cars and a matrix of 51 fuels to investigate the impact of a range of key parameters. Uniontown and Borderline road methods were compared to RON, MON and fuel composition information. A number of formulae were suggested to weigh RON and MON values to match the in-vehicle response. A common approach then applied is shown in Equation 2.7. The Coefficient of Determination (R^2), value using Equation 2.7 was just 0.61. Adding a term of aromatics content, improved the R^2 value to 0.84. Adding further terms for TEL and sulfur content improved the correlation to an R^2 value of 0.96.

$$\text{Road Octane Number} = a.RON + b.MON + c \tag{2.7}$$

Bartholomew [134] in 1961 described how engines, fuels and vehicles had changed since the creation of the RON and MON tests. Engine cooling systems had improved, volumetric efficiency had increased giving better performance at higher speeds and, in the US (United States), automatic transmissions with high stall speeds had increased the engine speed of most relevance to knock. Compression ratios had more than doubled. Fuels had higher aromatic content than in the past and were of higher sensitivity. He commented that it was remarkable that the then 30 year old RON and MON tests were still in use. Road testing was performed with a GM V8 engine at compression ratios from 8.5:1 to 12:1 on a range of fuels. A new laboratory test procedure was then created on the CFR engine with high speed crankcase and Removable Dome Head (RDH) combustion chamber, thought to be more representative of production engines of the time. A low speed test point was rather similar to the standard RON condition. A 2400rpm test point was also performed, again with low intake temperature. This was shown to give good correlation to results in-vehicle at 3500 rpm. Knock was detected by ear. The paper was intended to stimulate discussion to update the RON and MON tests for modern vehicles.

Brewster [135] of Ethyl gave a broad overview of combustion and fuel problems experienced in this period - not only knock but also preignition, rumble, excessive pressure rise rates[9], deposit issues and more. Gerard [136] of Socony Mobil Oil published on an alternative octane formula which took into account mixture segregation in the intake manifold. This was said to be critical at low speeds and was confirmed by comparison of carburetor to fuel injection systems. A Distribution Octane Number (DON) was referred to. This was a modified RON test where fuel segregation in the intake system was provoked.

The number of cars on the road was increasing, particularly outside of the US. Whilst US consumers sought high performance and chose cars with automatic transmissions, in most other markets fuel economy was more important and cars were sold mostly with manual transmissions [137]. Manual transmissions meant higher torque could be requested from the engine at low speeds than their automatic counterparts and hence knock was more problematic in this operating region. Automatic transmissions of the era had high anti-stall speeds. Maximum compression ratios in most markets were around 11:1 and premium gasoline was generally sold with a RON value of circa 98 in 1967. This was a significant increase in comparison to the start of the decade and was mostly due to the use of catalytic reforming as a refinery technique.

Fundamental research continued in the laboratory giving greater insight on what the RON and MON tests were really measuring. Gluckstein *et al.* [138] at Ethyl performed measurements of end-gas temperature in a modified CFR engine using an approach pioneered by MIT, based on the speed of sound in the unburnt medium. It was shown that end-gas temperatures were significantly hotter for a MON-like test in comparison to RON-like conditions on iso-octane, whilst pressure conditions were relatively similar. Measured temperature histories for these two test conditions are shown in Figure 2.16. End-gas temperatures were evaluated using an alternative technique by Johnson [139] at the U.S. Army Tank Automotive Center, in collaboration with Myers and Uyehara at the University of Wisconsin. Here an

[9] around 5 bar/°CA (Crank Angle) was the limit given - similar guideline values are still used today.

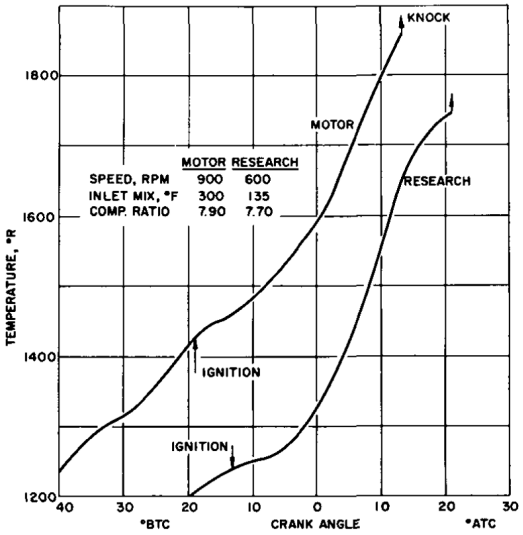

Figure 2.16: End-Gas Temperature Measurements in a Significantly Modified CFR Engine with Iso-Octane Fuel and RON and MON-Like Test Conditions, from Gluckstein *et al.* [138]

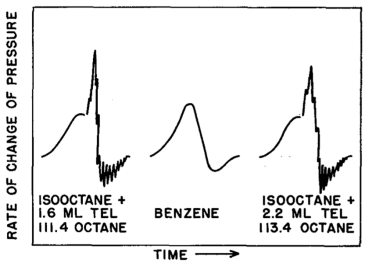

(a) Unfiltered Signal of Knockmeter

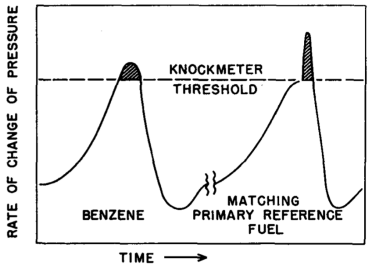

(b) Filtered Signal of Knockmeter

Figure 2.17: Erroneous Knocking Determination for Benzene in Comparison to its Bracketing Primary Reference Fuels (PRF), from Hoffman [140]

infrared pyrometer was employed. Measurements were complemented by calculations on an IBM computer running FORTRAN code. This was used to calculate net rate of energy release from chemical reactions, based on Semenov's approach to reaction kinetics. The authors stated that as much as 10% of the energy of the fuel was released in pre-combustion reactions and hence neglecting these could lead to large errors.

The RON and MON tests used the Model 501 knock meter at this stage, which had taken the place of the "bouncing pin". These meters apply a Low-Pass Filter (LPF) to the data from the pickup with a cutoff frequency of approximately 2500 Hz. This means they are not sensitive to the typical frequencies excited by knocking combustion in the CFR engine. The meter was shown by Hoffman [140] of Du Pont to respond to maximum rate of pressure change and this could lead to false knock detection for benzene, as illustrated in Figure 2.17. This issue had already been noted for the predecessor bouncing-pin indicator in 1939 [86]. A Kistler piezoelectric sensor was mounted in the location of the knock meter pickup and characteristic resonant frequencies were measured for a range of fuels. It was confirmed that these were in the range 6000-7600 Hz. A knock index was defined where a High Pass Filter (HPF) was used on rate of change of pressure data. A threshold was defined based on background noise intensity and a counter system used to track threshold excursions over 1000 cycles. Knocking cycles were found to be randomly distributed. Investigations were carried out on a range of fuels, using this system as the feedback instead of the knock meter, for updated RON and MON ratings. The disadvantage of this approach was that it took longer than the standard method.

Taylor [141] at MIT studied the impact of engine size on knocking tendencies in 1962, citing previous activity in the German literature in 1939. He found that smaller cylinder sizes significantly improved the knock limit, both for matched piston speed and matched crankshaft angular velocity.

There was much debate at the time on the true nature of knock. Miller at NACA had claimed to have seen detonation waves during his activity in the previous decade, whilst other researchers thought that this was impossible. Curry [142] presented data in 1963 from an array of ion current sensors in a split-head CFR engine. He said that this showed evidence of flame-front acceleration to 10-20 times the normal velocity. Strictly speaking, the experimental evidence suggested much faster reaction rates in the end-gas and an apparent reaction front in the same direction as the flame-front. The approximately 10 mm spatial resolution and the fact that key zones of the OHV head could not be instrumented meant that strong assumptions were made to suggest a continuous combustion phenomenon and hence that the flame-front had accelerated. An alternative explanation could have been autoignition occurring ahead of the flame-front. The paper was also notable for description of an Analogue to Digital Converter (ADC) applied to the pressure signals to allow digital storage of experi-

mental data on a magnetic tape unit. This could then be accessed by a computer and data plots from many cycles produced. Haskell [143], at Shell's Wood River Research Laboratory, measured knocking wave-front transit times, using two piezoelectric sensors and an oscilloscope triggered by an ion current sensor. He observed only sonic velocities and hence no detonation waves (which have supersonic propagation velocities) were detected. An optical window was also used with a photomultiplier to give a second measurement of the moment of autoignition at 8.5 mm distance from the ion probe. This showed a similar timing to the ion signal and hence a volumetric explosion was implied, which suggests small temperature gradients in the end-gas. The authors were confident that their work showed that autoignition was the "true" mechanism of knock, rather than flame-front acceleration into developing detonation. Curry contested their claim. Haskell's colleague Graiff [144] published on the antiknock effect of TEL the following year. He used a fueled motored engine to study how TEL decomposed in an engine. Sweeping the compression ratio, various oxides of lead were obtained as confirmed by X-ray diffraction. There was a dependency of the oxide type on the fuel type used and this was correlated with pre-flame reactions. For paraffinic fuels, pseudocubic oxide was formed, whilst for benzine and toluene, only orthorhombic yellow oxide was observed. This could explain the different octane gains on different fuel types with addition of TEL. TEL and the related compound Tetra Methyl Lead (TML) was once again coming under scrutiny as a potential health issue. Patterson [14] in the Journal *"Archives of Environmental Health"* in 1965 analyzed the amount of lead in human bodies in the USA in that period in comparison to natural levels. The level was estimated to be 100 times higher than that of pre-industrial times. It was stated that lead alkyls (such as TEL) were the primary source of lead absorbed by the respiratory system in urban environments. Other sources with different pathways into the human body included lead piping, food can solder and paints.

Air pollution was an increasingly public concern. Although the first version of the Clean Air Act had been passed in 1955 [12], this merely suggested that the Surgeon General should be involved in co-ordinating research. The 1963 Clean Air Act [145] gave the primary responsibility on reducing pollution to individual States but said that efforts should be made to reduce vehicle exhaust emissions. The 1965 Motor Vehicle Air Pollution Control Act [13] required the establishment of standards to reduce air pollution from motor vehicle emissions in order to protect health and welfare of the public. Oxides of nitrogen, aldehydes and evaporative hydrocarbon emissions were the main concerns. Vehicles would be tested to demonstrate compliance. Funding was made available to realize these objectives.

Fundamental research on reactions was carried out by Burwell [146] of the United Aircraft Corporation using a steady flow reaction tube with iso-octane air mixtures. Ignition timing was mapped for a range of temperatures and pressures, although only up to twice atmospheric pressure. 10% of available oxygen was observed to have been consumed before autoignition and only 50% of the iso-octane remained at this point. A mass spectrometer was used to measure chemical species along the reaction tube. Propylene, ethylene, methane, hydrogen, carbon monoxide and carbon dioxide were observed. The first half of the preignition period was dominated by pyrolysis and then peroxidation reactions. Jost and Martinengo [147] of Göttingen University detailed studies on an RCM of n-octane and iso-octane air mixtures. They discussed the history of the RCM method, which they traced back to Nernst in 1906, along with contributions by Ricardo's collaborators Tizard and Pye. The researchers at Göttingen used the rupture of a diaphragm at predetermined stage of the reaction to rapidly expand and hence freeze the chemistry for further analysis using gas and paper chromatography. This allowed for evaluation of species concentration against reaction time on a millisecond time scale, as shown in Figure 2.18. Two stage reaction was seen for iso-octane

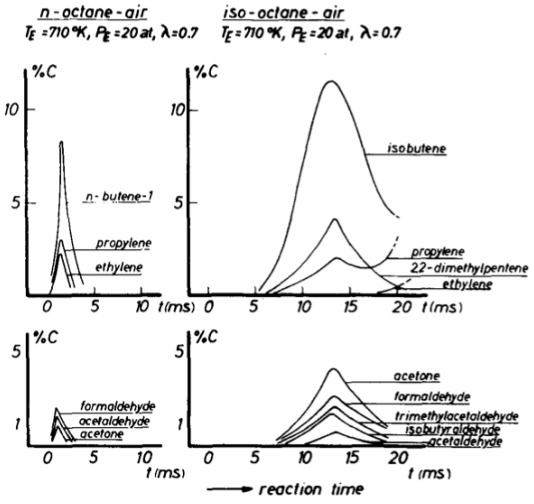

Figure 2.18: Species Concentration against Reaction Time for n-Octane and iso-Octane Air Mixtures, from Jost *et al.* [147]

but not n-octane. Quader [148] at General Motors performed UV (Ultra Violet) absorbance measurements in the end-gas of a CFR engine in collaboration with Myers and Uyehara of the University of Wisconsin. Wavelengths from 250-500 nm were investigated with the highest absorbance seen at 260 nm. This was particularly the case for knocking cycles. It was not clear at the time which species was absorbing at this wavelength. The absorption was strongly correlated with end-gas temperature and fuel type. No correlation was seen between preflame reactions and flame-front

velocity - contradicting the accelerating flame-front theory of knock, which as mentioned above still had some proponents at the time.

2.8 The 1970s: Oil Shortages, Emissions Control and Unleaded Fuels

In 1970 the US Environmental Protection Agency (EPA) was founded. On the 31st of December of the same year, the Clean Air Act was significantly amended [149]. The EPA would set national standards of air quality and its Administrator could bring civil action against those who did not comply. States would need to submit to the EPA plans of how they would achieve these standards. Vehicle emissions limits would be for Full Useful Life (FUL). Light duty vehicle carbon monoxide (CO) and hydrocarbon (HC) emissions limits would be reduced by 90% from 1970 to 1975. This would result in the introduction of two-way oxidation catalysts. Oxides of nitrogen (NO_x) would need to be reduced by 90% of measured 1971 levels by 1976. Periodic inspection of motor vehicles for emissions compliance was implemented. The best emissions control technology that was technically and economically feasible should be applied. There was also a section on fuel additives which gave the Administrator of the EPA power to regulate such substances and to require manufacturers to conduct tests to demonstrate their safety in accordance with procedures of the EPA. However, a substance could only be regulated or banned after a cost benefit analysis was performed taking into account both scientific and economic data.

In the 1970s, the connection between leaded fuels, atmospheric lead and health problems in the population was the object of detailed study. A series of reports from the newly formed Environmental Protection Agency document this. In 1971 an EPA report by Engel *et al.* [16] of the Air Pollution Control Office stated that 97% of airborne lead was due to combustion of leaded gasoline in vehicles. Atmospheric lead was correlated with traffic density and hence was a greater issue in urban areas. It was also noted that lead alkyl additives were incompatible with catalytic converter systems, which would shortly be introduced, and that this required the reintroduction of unleaded fuel from 1974 onwards. In 1972, the EPA published *"Health Hazards of Lead"* [150] and recommended that lead emissions from vehicles would need to reduce by at least 60% to achieve an air quality target of 2 $\mu g/m^3$. In 1972 the EPA also published their official position on the matter of health effects of airborne lead [15]. Lead from exhaust emissions could enter the human body both through the respiratory tract and through ingestion of lead contaminated dust. There was a correlation between neurological impairment in children and lead exposure. High lead concentrations were also found in the umbilical cord blood of pregnant women. It was stated that *"Lead in the air as well as in street dirt and household dust are preventable exposures which can be readily decreased by regulating the use of lead as a gasoline additive."* The previously suggested limit of 2 $\mu g/m^3$ was said to be too high and in fact a limit of 1.5 $\mu g/m^3$ was proposed in 1977 [151]. An EPA report in 1975 by Angle *et al.* [152] showed evidence of a link between blood lead levels in urban children and how close they lived to traffic. By 1979, numerous further studies had taken place suggesting a link between increased lead absorption and neurological problems in young childern, as documented by Dage [153] of the EPA.

By the late 1970s, new regulations meant that unleaded gasoline accounted for a third of US sales and this value was increasing, as shown in Figure 2.19, based on data from Dage. The proposed limit on average lead content for 1979 was 0.59 g/gal. As well as the introduction of unleaded gasoline, lead was also reduced in both regular and premium fuel types. The net result was a reduction in octane values of leaded gasoline, as documented by Shelton *et al.* [154] of the US Department Of Energy (DOE). The sales percentages from EPA data and the octane values compiled by the DOE, together with an assumed RON value of 91 for unleaded fuel in this period [155], have been combined in Figure 2.20. It can be seen that the average RON value reduced from 96.4 in 1970 to 93.1 in 1978. The average compression ratio of new cars sold in the US was also documented by Shelton *et al.* This reduced from around 9.4 in 1970 to 8.2 already by 1974 - manufacturers were designing their cars to tolerate the reduction in market octane values and in particular vehicles with catalytic converters would need to run on unleaded fuel with an EPA mandated minimum RON of 91 [155]. Lower compression ratios also lower peak temperatures in the combustion chamber and hence NO_x emissions. Oxygenated components such as alcohols and ethers would eventually be used to improve the knock resistance of unleaded gasoline [40].

Investigations were carried out to optimize engine out emissions. Duke [156] of Pennsylvania State University showed that knock could reduce unburnt hydrocarbon (HC) emissions, due to reduced quenching on the cylinder walls. Advancing the engine into knock increased NO_x emissions however. EGR was applied to reduce NO_x. 10% EGR reduced NO_x emissions by 50% and 20% EGR by 75%. There was an upper limit though, dictated by combustion instability. With moderate levels of EGR (10-15%), the reduction in end-gas reactivity outweighed the slower flame-front propagation and hence the compression ratio could be raised and BSFC (Brake Specific Fuel Consumption) improved, as described by Hodges [157] of Rensselaer Polytechnic Institute. EGR in combination with lean air-fuel ratios was also being investigated, by Morgan [158] of Mobil Research and Development, but led to HC increases. Secondary air

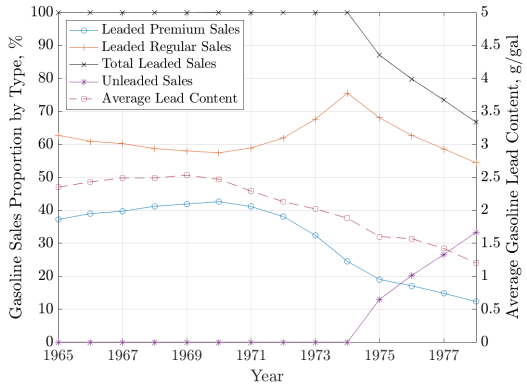

Figure 2.19: Leaded and Unleaded Gasoline US Market Share, Average Lead Content and Proposed Limit for 1979, data from Dage [153].

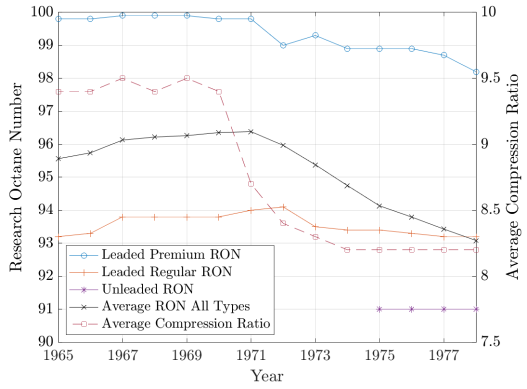

Figure 2.20: Octane Number Trends for US Gasolines and Compression Ratio of US New Car Sales, based on data from Shelton *et al.* [154] and Dage [153].

introduction into the exhaust system was found to be effective in reducing HC emissions, but only for stoichiometric or rich mixtures.

Oil shortages in the 1970s, due to the 1973 oil embargo of the USA and allies by the Organization of Arab Petroleum Exporting Countries (OAPEC), meant a new push to increase engine efficiency. Alternative fuels such as methanol were also investigated, by Gething [159] of Pennsylvania State University, to reduce the dependence on oil. The idea at the time was to produce the methanol from coal however, rather than from biological sources. A number of manufacturers including Ford, General Motors, Honda and Volkswagen were also working on lean burn prechamber engines, as detailed in a large scale review by Roessler and Muraszew [160] for the EPA in 1975. Such engines gave lower CO emission and a reduction in NO_x, along with potentially better fuel consumption, but similar hydrocarbon emissions to a more conventional SI engine. Prechamber engines were not completely new: Honda's Compound Vortex Controlled Combustion (CVCC) prechamber engine [161] had been in production in Japan since late 1973 and a Fairbanks opposed-piston heavy-duty stationary gas engine since 1952 [10]. Detonation-like noise was observed for some prechamber concepts independently of fuel octane number. Some, but not all concepts, had a lower octane requirement - the Gussak active prechamber concept with a rich prechamber and lean main chamber permitted a compression ratio increase of 0.8 and could be run at an air fuel ratio of 30:1. The primary motivation at the time for most manufacturers however, was to run lean for low pumping losses and with a view to meeting 1977 Federal emissions standards without a three-way catalytic converter. It was thought that this would not be feasible if the NO_x limit were further reduced. There was a lot of variety with some systems featuring separate valves for the prechamber whilst others would be known today as passive systems, such as the Ford Torch Ignition engine. The majority of the described engines did not make it to market, largely as lean running was incompatible with three-way exhaust gas catalysts, which would become ubiquitous.

Research activity was also ongoing on better understanding the influence of turbulence in more conventional SI engines, again with the objective of improving combustion efficiency and emissions. Turbulence had been identified as key in accelerating flame-front propagation in the early days of the Otto engine by Clerk [32] but the quantitative relationship between turbulence and flame speed in internal combustion engines was still not well understood at this stage. Blizard and Keck [162] of MIT made an important contribution to modeling of turbulent flame speed in engines in 1974. This was based on a characteristic turbulent eddy burn-up time $\tau = l_e/u_l$ where l_e is the eddy radius and u_l is the laminar flame-speed. The rate of combustion depends on the eddy entrainment speed u_e, which itself was assumed to correlate with inlet gas speed, l_e. Inlet gas speed was assumed to be a function of intake valve lift and compression ratio. The model was calibrated and compared against experimental data on a single-cylinder engine with good results. Lancaster [163] of GM measured turbulence in a motored CFR engine with both shrouded and non-shrouded intake valves in 1976. Measurements of turbulence intensity u' were made using a DISA 55F81 tri-axial hot-wire anemometer with 10 μm elements. Data were analyzed from the engine shortly before end of compression TDC. Turbulence intensity was defined as the Root Mean Square (RMS) of velocity fluctuation about a mean value. In a companion paper by Lancaster *et al.* [164], fired measurements were described. Gas was sampled through an electromagnetic valve prior to combustion and pressure was measured with an AVL

[10] Ricardo had already made a prechamber engine in 1918 [33]

piezoelectric transducer and a Kistler charge amplifier. Spherical flame-front propagation was assumed in the fired engine, to calculate turbulent flame-speed from heat release analysis. Turbulent flame-speed was then compared to expected laminar flame-speed under these conditions giving a Flame Speed Ratio (FSR). This was found to be linearly correlated with turbulence intensity from motored engine measurements over a range of test conditions and both intake valve types, as shown in Figure 2.21. Nagayama *et al.* [165] published on the effect of swirl and squish the following year. Swirl generated by the cylinder head was measured with a paddle wheel in a flow rig and in a motored engine using a spark discharge and ion sensing technique. Squish was calculated based on bowl diameter and squish height. Swirl ratios were 0.7 and 1.4 for two different intake ports whilst maximum squish velocities at 2400 rpm were estimated as 4 m/s and 15 m/s for two different combustion chambers. Both swirl and squish improved the lean misfire limits and the combined effect was better still, as shown in Figure 2.22. The motivation was to extend the dilution limit to improve fuel economy and engine out emissions.

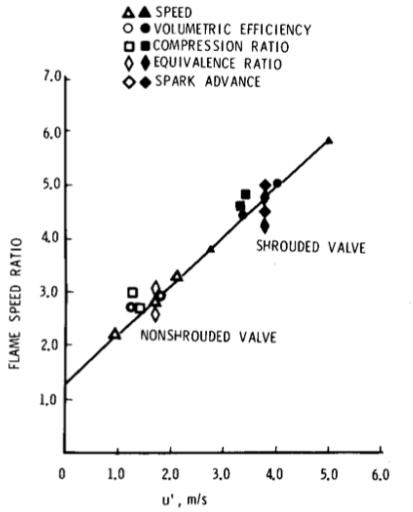

Figure 2.21: Ratio of Turbulent to Laminar Flame Speed as Determined by Lancaster *et al.* on a CFR engine and Correlation with Motored Turbulence Intensity u', from Lancaster *et al.* [164]

Electronic data acquisition systems were becoming more common, which permitted efficient evaluation of statistical phenomena. Allwood *et al.* [166] at Shell compared flame-front propagation, characterized by ion sensors, against cylinder pressure measurements on a statistical basis using a multichannel electronic gating and counting system. Cyclic dispersion was compared for different fuels, residual gas content and air-fuel ratios. It was seen that there was a tendency for knocking cycles for a given operating point to be those with faster burn rates.

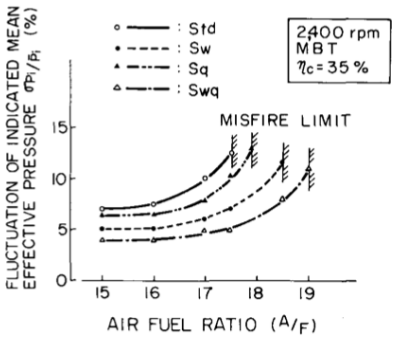

Figure 2.22: Extension of Lean Misfire Limit with Swirl and Squish Charge Motions, from Nagayama *et al.* [165]. Std = Low Swirl and Squish, Sw = Increased Swirl, Sq = Increased Squish, Swq = Increased Swirl and Squish

This implies that reducing cyclic variability would improve the knock limit - as KLSA is dictated by the faster burning cycles in the dataset rather than the mean cycle. Barton *et al.* [167] at Pennsylvania State University used an electronic system to target a given percentage of knocking cycles above a threshold. The feedback signal was based on a Band Pass Filtered (BPF) rate of pressure rise measurement. The threshold was based on the RMS value of non-knocking cycles. Chiampo *et al.* [168] of FIAT also investigated correlation between flame-front arrival time from ion sensors and knocking cylinder pressure measurements on a FIAT 125 engine and noted similar results to Allwood. An alternative "kinetic knock index" was proposed by Ferraro [169] of the Polytechnic of Turin based on wave energy rather than the more typical amplitude or integral methods in use at the time, and indeed still today.

A greater number of papers in the SAE literature were being written in Europe. Here, leaded fuel had not yet been removed from the market, although this was expected to take place in the future. Engines were therefore being prepared for RON 91 unleaded gasoline. It was noted by Arrigoni *et al.* [170] of Snamprogetti, that the vast majority of literature to that date was on research engines, such as the CFR, rather than on production engines. Testing was therefore performed on the road, to characterize knocking tendencies against engine speed, as had been done in the past. It was noted once again that high speed knock was correlated with MON and low speed knock with RON, as had been observed in the prior decade. Engine damage was also studied in a disciplined manner with erosion seen on the head and piston. A later study by Cornetti *et al.* [171] at FIAT cited further failure modes such as ring sticking, head gasket failure and piston holing. 100 hour knock damage accumulation tests were performed with temperature measurements in the combustion chamber. Temperatures were seen to rise

with engine speed and so less knock intensity was required to cause the same damage at higher speeds. Ring sticking was the primary failure mode, driven by material transfer from the eroded piston.

Knock measurement was moving out of the laboratory and into production cars by the late 1970s[11]. Piezoelectric cylinder pressure sensors, typically manufactured by Kistler, connected to a charge amplifier had become the standard knock research tool. For on-road measurements or engine durability runs, accelerometers were popular according to Arrigoni *et al.* [172]. Microphones and load washers under the spark plug were also considered by Randall *et al.* [173] of Systems Control Inc., similar to an approach demonstrated by Kondo *et al.* [174] of Gakushuin University in 1975. A knock control system based on spark retard was described by Kraus *et al.* [175] of Exxon Research and Development in 1978 and in the same year Buick introduced a closed loop knock control system on its 1978 downsized turbocharged V6 engine, as detailed by Wallace [176]. A BPF accelerometer signal would retard the ignition angle in response to knock and then gradually return to the base settings. The base ignition management was through centrifugal and vacuum advance and the electronics of the knock control system were analog rather than digital.

In terms of fundamental understanding, two papers stand out from the end of the decade. The first was by Douaud and Eyzat [177] at the Institut Français du Pétrole (IFP). They pointed out that RCM data allowed good understanding of fuel knock tendencies, and the datasets thus generated could be applied to engines, but that it was rather difficult to implement such a methodology. They proposed a formula for the ignition delay with three unknowns. These unknowns could be obtained from engine testing at three conditions, although four were preferred to allow for error checking. They proposed a modified RON and MON test, together with the standard versions to generate these data for each fuel. One of these constants was found to correlate with the octane number. This paper is famous and very frequently cited. The mathematical approach is as follows in Equations 2.8, 2.9, 2.10 and 2.11

$$\frac{d\alpha}{dt} = \alpha A' p^n e^{\frac{B}{T}} \tag{2.8}$$

Where:

$$\begin{aligned} p &= \text{pressure} \\ T &= \text{temperature} \\ \alpha &= \text{concentration} \\ A' &= \text{constant} \\ n &= \text{pressure coefficient} \\ B &= \text{temperature coefficient} \end{aligned}$$

[11] Although there had been some isolated examples in the late 1940s it had not become a common technique

For constant pressure and temperature:

$$\tau = t_c - t_0 = Ap^{-n} e^{\frac{B}{T}} \tag{2.9}$$

Where $\tau = t_c - t_0$ is usually referred to as the ignition delay. Assuming that the critical concentration α_c is independent of pressure and temperature:

$$1 = \int_{t_0}^{t_c} \frac{dt}{Ap^{-n}(t) e^{\frac{B}{T(t)}}} \tag{2.10}$$

There are therefore three unknowns A, n and B to be determined experimentally from engine data. For primary reference fuels with octane values "OCTN" between 80 and 100, with units of kg/cm^2 for pressure and Kelvin for temperature, Douaud and Eyzat determined:

$$\begin{aligned} A &= 0.01869 \left(\frac{\text{OCTN}}{100} \right)^{3.4017} \\ n &= 1.7 \\ B &= 3800 \end{aligned} \tag{2.11}$$

Assuming a constant pressure of 22 kgf/cm^2 (21.6 bar), the predicted ignition delay response is as shown in Figure 2.23.

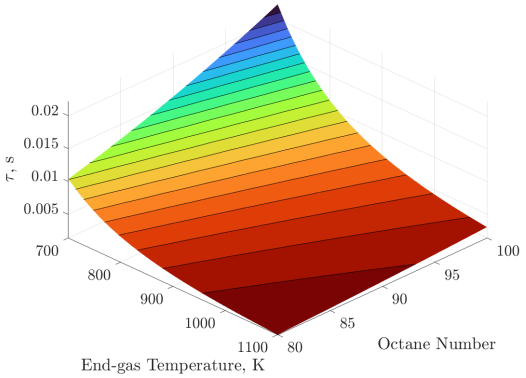

Figure 2.23: Ignition Delay Time τ as a function of PRF Octane Number and End-gas Temperature with a Pressure of 22 kgf/cm^2, as Predicted by Douaud & Eyzat Approach [177]. It can be seen that higher Octane Numbers are Correlated with longer Ignition Delay Times

It should be underlined however, that Equation 2.8 assumes a single stage reaction. Such a simplification had also been employed by Livengood and Wu [123] in 1955. This is generally not the case for paraffinic hydrocarbons, which undergo a two stage reaction. In 1975 Haltead, Kirsch, Prothero and Quinn of Shell published *"A mathematical model for hydrocarbon autoignition at high pressures"* [178]. This was based on a degenerate branched chain mechanism. The oxidation of a paraffinic fuel was described by eleven

Table 2.4: "Shell" Reaction Model of Alkane Oxidation by Halstead *et al.* [178]

Primary Initiation	$RH + O_2 \rightarrow 2R\cdot$	1
Main propagation	$R\cdot + O_2 \rightarrow RO_2\cdot$	2
	$RO_2\cdot \rightarrow \text{products} + OH\cdot$	3a
	$RO_2\cdot \rightarrow Q + OH\cdot$	3b
	$OH\cdot + RH \rightarrow R\cdot + H_2O$	4
Propagation forming degenerate branching agent	$RO_2\cdot + RH \rightarrow RO_2H + R\cdot$	5
	$RO_2\cdot + Q \rightarrow RO_2H + R\cdot$	6
	$RO_2\cdot + RH \rightarrow H_2O_2 + \text{products} + R\cdot$	7
Branching	$RO_2H \rightarrow 2R\cdot + \text{products}$	8
Decomposition	$H_2O_2 \rightarrow 2OH\cdot$	9
Termination	$R\cdot + R\cdot \rightarrow \text{inert products}$	10
	$R\cdot + O_2 \rightarrow \text{inert products}$	11

reactions as shown in Table 2.4. The rate coefficients for each reaction were assumed to follow Arrhenius-like behavior. The model initiates with partial oxidation of the fuel "RH" resulting in chain propagating radicals "R·" and combustion products. A number of further radical and reactive species are generated in the following steps, including an intermediate species "Q" produced by cool-flame chemistry, before reaction terminates leaving only inert products. The model was compared with RCM data of iso-octane and was capable of reproducing similar two-stage ignition and NTC behavior. This model was applied by Kirsch and Quinn [179] at Shell in 1977. The chemical kinetics model was coupled to an engine simulation model of a CFR engine. PRF 90 and a Toluene Reference Fuel (TRF) also with RON of 90 were compared in the model at both RON and MON test conditions. The model prediction of knock and the relative behavior of the fuels between the test conditions was consistent with experimental data. The model suggested that temperature was the dominant cause of TRF fuels rating lower than PRF on the MON test if they have matched RON values. The approach of linking engine and chemical kinetics simulations has become standard practice today. The model became known as the "Shell model" and would be used frequently in the coming decades.

2.9 1980s: Electronic Ignition Control, Computerized Analysis and Japanese Research

Closed loop ignition control systems to protect production engines against knock had come to the market in the late 1970s [176] and would become ubiquitous during the 1980s. Whilst the original Buick system was based on analogue electronics and coupled to mechanical ignition timing adjustment, microprocessors would become standard during the 1980s allowing greater precision and control. The most common control response to detected knock was reduction of ignition advance, as described by Boccadoro *et al.* [180] of Renault and Decker *et al.* [181] of Bosch[12]. Management of boost pressure was proposed as an alternative by Gillbrand [182] at Saab and this system would also increase the boost pressure when lower than expected knock was observed. This gave a performance increase, especially in transient maneuvers. An accelerometer was typically used as the feedback device, with the raw signal being bandpass filtered to highlight signal energy associated with the expected combustion chamber acoustic modes, as detailed by Nakamura *et al.* [183] of Toyota. Priede *et al.* [184] of the University of Cape Town explained how cylinder pressure oscillations transformed into structure borne resonances in 1989 and studied experimentally the resonance modes of combustion chamber castings using a vibration generator and a local microphone. Alternatives to accelerometers were again considered: ion current sensing using the spark plug electrodes was proposed by Collings *et al.* [185] at Cambridge University and Sawamoto *et al.* [186] of Nissan again suggested use of a piezoelectric ring fitted under the spark plug. Amann of General Motors published two detailed reviews of combustion analysis techniques in 1985 which are still frequently cited. The first of these [187] was a historical review of combustion analysis methods covering 100 years of progress. The second [188] covered the history of cylinder pressure measurement and gave guidelines on the information which can be obtained from such an analysis, including knock. As knock had effectively become closed loop in production vehicles, their octane appetite could be compared by evaluating acceleration times on a range of different fuels. McNally *et al.* [189] observed in a 1989 Co-ordinating Research Council (CRC) report that over a range of 15 cars, the normally aspirated models did not improve with a RON value higher than 87 whilst turbocharged models benefited from RON values as high as 100. Sutton *et al.* [190] stated that from 1945-1980 compression ratios had increased significantly. Fuels had also changed radically with higher RON and sensitivity due to the implementation of catalytic cracking as a refinery technique. Despite this, typical vehicles at higher engine speeds still seemed to respond to MON values. It was expected that future engines would run lean and it was shown that this engine type would have a knocking tendency more aligned with RON test conditions.

Computerized analysis in research labs meant it was much more convenient to perform statistical analysis on combustion data than in the past and hence a number of statistical investigations were reported. By [191], of the Northern Research and Engineering Co., together with

[12] As has already been mentioned, World War II aircraft also had closed loop control for knock but the control parameter was air fuel ratio.

Kempinski and Rife at MIT, published a large study on the CFR engine in 1981. The impact of fuels, compression ratio, equivalence ratio, ignition timing, EGR, inlet pressure and inlet temperature were all studied experimentally and results were compared to literature models. Leppard [192] at General Motors noted that the distribution of knock intensity characterized by the Maximum Amplitude Pressure Oscillation (MAPO) was not normal and skewness and kurtosis were described. In this same study it was demonstrated that individual cylinders could have different octane requirements by up to four octane units. Chun and Heywood [193] at MIT also noted the statistical non-normality of knocking intensity with more cycles being observed at lower values. It was Iwata *et al.* [194] at Nippondenso in Japan who described the distribution as log-normal. This is still commonly stated today, although Iwata *et al.* actually wrote that both knocking and non-knocking cycles follow separate log-normal distributions of knock intensity. At borderline conditions, there exists a mixture of both and hence two superimposed log-normal distributions are required to adequately describe the data. This was made clear using a diagram on logarithmic normal probability paper as shown in Figure 2.24. In such a diagram, one axis is the logarithmic intensity and the other describes the Gaussian cumulative population. Such an analysis approach would appear to allow the number of knocking cycles in a dataset to be estimated without the need to manually select a threshold - a very useful feature.

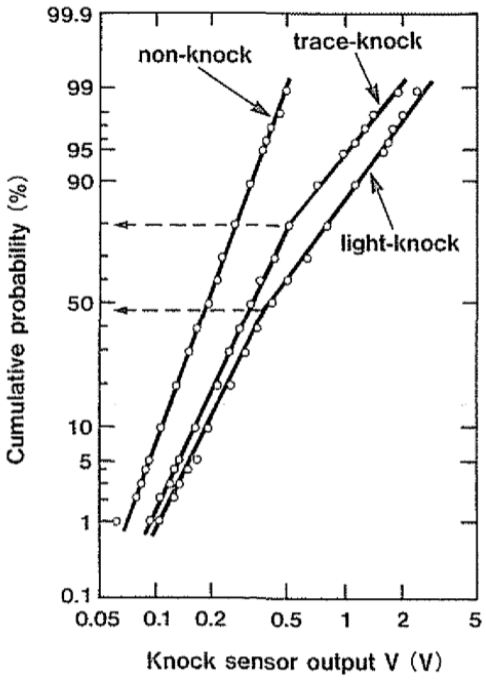

Figure 2.24: Lognormal Analysis by Iwata *et al.* Showing Separate Distributions for Knocking and Non-Knocking Cycles in the Same Dataset [194]

The use of computerized analysis also meant it was possible to consider a wide range of different algorithms to describe knocking intensity on individual cycles. The Maximum Amplitude of Pressure Oscillation was common [192, 193, 195–197] and indeed still is today. Integrating the pressure oscillations was an alternative [188] as was the related technique of signal energy quantification used by Spicher and Kollmeier [198]. These methods relied on high-frequency acquisition and were also somewhat vulnerable to non knock-related high-frequency noise sources. An alternative technique was proposed by Checkel and Dale [199] at the University of Alberta, based on the third derivative of the pressure trace. This did not require high sample rate data, as it was based on the idea that when knock occurs there is normally an abrupt increase followed by an abrupt decrease on the pressure curve[13]. This occurs before pressure oscillations are observed in the chamber. An example is shown in Figure 2.25. An index based on the second derivative of cylinder pressure was suggested by Hiromitsu Ando *et al.* [200] at Mitsubishi.

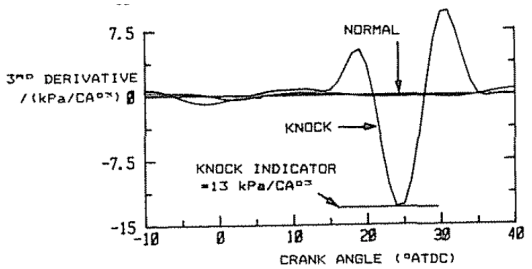

Figure 2.25: Third Derivative of Cylinder Pressure used by Checkel and Dale as a Knock Index [199]

It was also becoming more straightforward to calculate rate of heat release from pressure data. Harrington [201] of AMOCO (AMerican Oil Company) in 1982 showed plots of $\log pV^v$, which have a similar appearance to cumulative mass fraction burned plots, in a paper on the effects of both liquid and vapor phase water introduced in the intake system of a CFR engine. Slower combustion and increased HC emissions were noted with water introduction. Klimstra [202] of N.V. Nederlandse Gasunie applied Wiebe fits to mass fraction burned data from cycles slightly retarded from the knock limit. He then used this profile to estimate the quantity of mixture remaining at the moment of autoignition for knocking cycles. The calculated isochoric pressure rise due to this mixture's ignition was used as a knock index. This assumes that knock intensity depends only on unburnt gas quantity at the moment of autoignition, which would only be the case for a homogeneous end-gas thermal explosion.

[13] This may be what causes the bouncing-pin to lose contact with its piston and hence bounce

The effects of knock on heat flux and engine damage were also investigated. Lee and Schaefer [195] at Volkswagen reported on a study where fast response thermocouples on the cylinder head flame face showed that knocking cycles could have three times the heat losses of non-knocking cycles. Damage testing was performed which showed erosion on the aluminum piston surface. Applying a 20 μm iron coating to the piston surface was enough to protect it.

Whilst the prior decade had seen significant research on knock being reported in Europe, in the 1980s there were a large number of high quality studies originating in Japan. Some of these were on control topics with key contributions being the dual log-normal distribution already commented upon and a knock control ignition advancing (not only retarding) strategy, described by Ando *et al.* [200] of Mitsubishi. Here it was noted that up to 12° of ignition advance could be applied when combustion chambers were cool. The fundamental mechanisms of knock were also studied in Japan at the time. Iwashita and Saito [203] of Toyota described a high speed camera and digitization system that permitted statistical analysis of flame-front propagation. Hayashi *et al.* [204], also of Toyota, used a Rapid Compression and Expansion Machine (RCEM) with transparent access and high speed laser shadowgraph photography at 100,000 frames per second to study end-gas autoignition. The RCEM also featured a spark plug. This allowed fully premixed measurements to be made with very little flow or turbulence. It was shown that very strong autoignition events resulted in supersonic wave propagation (1600 m/s with a reference acoustic velocity of 1100 m/s). Only this incident wave exhibited this supersonic velocity, with the first reflected wave already traveling at normal acoustic speeds. Nakagawa *et al.* [196] of Nissan applied a similar technique in a fired engine with part optical access to study autoignition locations at 30,000 frames per second. Cylinder pressure data were also acquired. Multiple autoignition locations were seen, often close to the cylinder wall. Autoignition events just ahead of the flame-front were also observed. It was confirmed that autoignition could occur without producing knocking cylinder pressure oscillations. His collaborator and co-author Takagi [205] was the lead of a study published in 1988, again using the laser shadowgraph technique, this time focusing on knocking heat release quantities. With heavy knock, up to 40% of the charge was consumed by autoignition, which was 90% of the remaining charge in the cylinder at the time. A squish piston was found to reduce knocking tendency for a given spark timing due to faster combustion and increased end-gas cooling. In this study it was also observed that a reflected pressure wave caused further autoignition events. In 1985 Hiroshi Sakai *et al.* [206] of the University of Tokyo published on an experimental supercharged Miller engine where effective EIVC was achieved through use of a rotary valve in the intake system, together with a conventional poppet valve in the cylinder head. This was almost forty years after the concept had first been proposed [27]. It was found that by advancing the effective intake valve closing, the end of compression temperature could be reduced by over 100 K. The system was shown to effectively mitigate knock and a 15% power increase was achieved in boosted conditions, together with improved BSFC and lower exhaust gas temperatures.

Fundamental research was also taking place in Germany. An impressive study was described by Schäpertöns and Lee [207] of Volkswagen, where the Shell model of autoignition was coupled to a two-dimensional Computation Fluid Dynamics (CFD) simulation of a combustion chamber. The model was capable of simulating both the autoignition location and the ensuing pressure waves. This allowed, among other things, to show the sensitivity of pressure transducer location in the chamber.

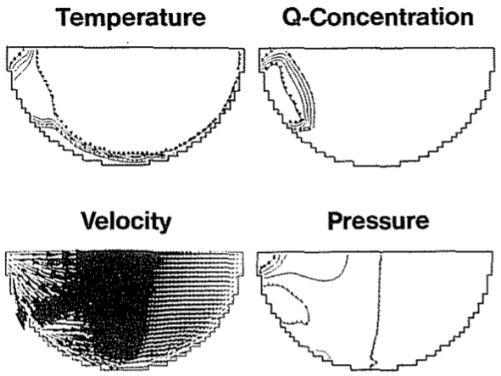

Figure 2.26: 2D CFD Calculations with Integrated Shell Kinetics Model by Schäpertöns and Lee of Volkswagen in 1985 [207]. The Simulation shows a Hotspot on the Left Wall at Knock Onset

Spicher and Kollmeier [198] at Aachen Technical University in 1986, reported on a study where 51 optical fiber bundles were installed in a two valve Rotax engine. Photomultiplier tubes were used to amplify the light in the range 250-650 nm. They observed supersonic wave velocities for strong autoignition events. Autoignition locations were distributed around the end-gas with considerable variability. Interestingly, knock damage was observed in a different location to the preferred autoignition region. In the US, the same Shell model implemented at Volkswagen in 2D CFD was used by Najt [197] of General Motors in a zero dimensional model. Here the combustion chamber was described by three zones: burned region, main unburned region and crevice. The model was compared to experimental data for both PRF 70 and PRF 90 fuels with good correlation observed. Lower octane PRF gave greater exothermic heat release from cool-flame chemistry.

When Kirsch *et al.* first applied the Shell model to combustion engine modeling, they assumed homogeneous temperatures in the end-gas. If the end-gas reactivity were truly homogeneous, autoignition would occur in the entire unburnt region simultaneously. In reality in practical systems, such as internal combustion engines, reactivity gradients in the mixture exist. Zeldovich [208] of the Institute of Chemical Physics in Moscow explained in 1980 how such gradients can result in distinct reaction front "Spontaneous Propagation" (SP) velocities u_{sp} and pressures p [14]. This depends on the nature of the reactivity gradients in the unburnt mixture. The four different possibilities are shown in Table 2.5. For Type 1, associated with small reactivity gradients (for example small temperature and species concentration gradients), the behavior is that of a thermal explosion. The reaction front velocity u_{sp} is above that of a classical detonation wave u_J, which means that the chemistry and the gas-dynamics of the system cannot become coupled. Zeldovich referred to this as a weak detonation. The pressure rise is larger than that associated with constant volume combustion p_v, but no shock-wave behavior is present. Type 2 is potentially the most damaging. The reaction front velocity is less than or equal to the Jouget velocity u_J. The chemical kinetics and gas dynamics are interacting and the reaction is feeding energy into a shock-wave. The pressure can approach that of a classical Chapman-Jouget detonation. Type 3 could be described as a benign autoignition. The reactivity gradient is large enough that when one element ignites, the surrounding medium has time to expand and hence equalize the pressure. This occurs for propagation velocities significantly less than the acoustic velocity but higher than that of flame-front propagation. The pressure wave generated by the autoignition detaches before it can interact with the next element which has yet to begin to auto-ignite. Type 4 is when reactivity gradients are so large that the next element ignites due to flame-front propagation before it has a chance to auto-ignite. Autoignition will therefore not occur.

Table 2.5: Zeldovich Spontaneous Propagation Reaction Front Classification [208]

Reactivity Gradient	Propagation Velocity	Front Pressure
Small	$u_{sp} > u_J$	$p_v < p < p_J$
Intermediate	$u_{sp} \leq u_J$	$p \cong p_J$
Large	$u_f < u_{sp} << a < u_J$	$p \approx 0$
Very Large	$u_{sp} = u_F$	$p \approx 0$

The vast majority of activity was to understand knock and operate conventional engines close to its limit. Oppenheim [209], of the University of California, Berkeley, proposed that knock could be seen as a positive phenomenon if it were to be harnessed in a controlled manner. He performed a detailed literature review going back to the 1880s and then went on to describe measurements in optically accessible shock tubes to study the autoignition mechanism. He stated that a number of exothermic centers per unit mass are generally present, but their distribution is unknown. The temperature distribution however, decides the character of the combustion. Autoignitions were characterized as strong or weak. As a means of eliminating knock, combustion by *"a great multitude of miniscule, properly distributed in time, micro explosions"* was proposed. This is effectively a Homogeneous Charge Compression Ignition (HCCI) or Controlled Auto Ignition (CAI) engine, although that terminology was not used. Oppenheim [210] also published *"Dynamic Features of Combustion"* in this period, describing the different combustion modes from flame propagation through to detonation. Examples of Deflagration to Detonation Transition (DDT) in constant cross section tubular combustion bombs were shown. Here combustion begins at the closed end of the tube and the burnt gases behind the flame-front cause it to accelerate. Pressure waves coalesce forming shock waves which interact with the walls thereby generating turbulence. Further pressure waves are created and eventually this positive feedback mechanism can accelerate the turbulent flame-front until detonation occurs. This known phenomenon in tubular bombs was what led some researchers to suggest knock in an ICE resulted from flame-front acceleration into detonation, notably Curry [142]. Maly and Ziegler [211] of the University of Stuttgart published a modeling study on this in 1982. A mechanism whereby a positive feedback mechanism of flame-front turbulence in an ICE was proposed and was said to explain some historical observations. Note that for DDT to occur, turbulent flame-front propagation needs to reach the Chapman-Jouget detonation velocity, which is significantly higher than the acoustic velocity in the unburnt medium. This is more than an order of magnitude higher than typical turbulent flame velocities in an ICE and hence a very strong positive feedback would be required. Cuttler [212] of Jaguar, together with Girgis of Coventry Polytechnic, described three types of combustion that could theoretically result in knock-like noise: explosion (homogenous autoignition), detonation (supersonic reaction front) and deflagration (subsonic flame-front propagation through rapid entrainment) in 1988. Note that subsonic sequential autoignition is also possible. Optical measurements were carried out using a transparent "Bowditch" piston engine. On a disk type combustion chamber, end-gas autoignition was observed. For a compact bowl in piston chamber on the other hand, rapid combustion in the squish region was hypothesized to be due to rapid entrainment and caused pressure rise rates of 8 bar/°CA. Pressure oscillations for this condition were rather weak. The window diameter was 60 mm with a bore diameter of 80 mm and the frame rate of the camera was only 8000 frames per second, hence the optical setup was not ideal for drawing firm conclusions. Reverse squish

[14] Zeldovich had been publishing on detonation since the 1940s, primarily in the Russian literature.

effects can accelerate a flame-front into the squish zone as the piston descends however, and this phenomenon, like knock, is also sensitive to ignition timing.

Swirl and squish had been used to improve turbulent flame speed for many years and had been quantitatively studied in the 1970s. In the 1980s, investigations on an alternative charge motion took place. In 1983, Witze *et al.* [213] of Sandia National Laboratories and the University of Michigan Ann Arbor described experimental measurements of flow and turbulence in an optically accessible engine with an inlet valve in the side of the combustion chamber. Laser Doppler Velocimetry (LDV) was used to measure both mean and turbulent flow velocities. A shroud could be rotated on the intake valve generating different bulk fluid motions. It was discovered that directing inlet flow towards the piston, a tumble motion was created in the charge. This large scale motion was destroyed late in compression, which resulted in a peak in turbulence intensity at the center of the chamber at around 30° CA before firing TDC. Results were compared to a zero dimensional turbulence model and fired engine data. The 0-D (zero dimensional) model could not directly replicate the peak in turbulence during late-compression. In 1985, Gosman *et al.* [214] of Imperial College of Science and Technology again described flow and turbulence measurements using laser Doppler techniques. A transparent model engine was used with a single inlet valve in the head, once more with a shrouded section. A tumble motion was again produced, but this time experimental results were compared to 3D CFD code [15]. A turbulence peak around firing TDC resulting from the tumble motion was once again observed and it was commented that this would likely be beneficial in improving early combustion rates. Kent *et al.* [215] of Ford published on comparisons between swirl and tumble charge motions and their effect on burn rates on four valve pent-roof engines in 1989. Charge motion of the engines were estimated in a flow rig with moving piston and optical access, which used water as the test fluid rather than air. Reynolds numbers were matched to give dynamic similarity to the target low-speed engine condition. A tumble ratio of 1.4 was found to give similar 0-90% burn duration to swirl ratios of a similar magnitude. It was suggested that a combined swirl and tumble charge motion may make sense - tumble results in a turbulence peak at around ignition timing whereas swirl survives later into the cycle and can improve burn rates at a later stage. Tumble was relatively easy to create with four-valve pent-roof heads, which were becoming more popular due to their improved volumetric efficiency and hence power output. Of course four-valve heads were not a new technology. They were widely used in WWII aircraft piston engines, as has already been described, and in racing applications.

In 1988, Heywood published his book *"Internal Combustion Engine Fundamentals"* [21]. Knock was described as a "race between the advancing flame-front and the precombustion reactions in the unburned end-gas". Autoignition and accelerating flame-front theories of knock were both mentioned, although it was thought that autoignition theory was better supported by evidence and hence the most widely accepted. The importance of cyclic variability was highlighted, as fast burning cycles have the highest knocking tendency and so are those which limit the compression ratio. MAPO was suggested to be the most appropriate method of pressure sensor knock feedback. The road octane rating of vehicles at the time was said to be well aligned with an average of RON and MON values, the Anti-Knock Index (AKI). This textbook would become one of the key references for University students of Internal Combustion Engines around the world and remains so to this day.

The 1980s was a period when high output turbocharged engines dominated Formula 1. Otobo *et al.* [216] of Honda published on their V6 1.5 liter turbocharged engines in the last year of the relevant regulations - 1989. The 1987 RA167E engine produced 1010 CV [16] at 4 bar absolute manifold pressure with a relatively low compression ratio of 7.4:1. A boost pressure limit of 2.5 bar for the 1988 season permitted an increase in compression ratio to 9.4:1. Power output was 685 CV and peak cylinder pressure 167 bar. IMEP was 38 bar. The maximum octane value of the fuel by regulation was a RON of 102. A study was performed using iso-octane, n-heptane and toluene to perform a toluene sweep from 25% up to 84% at constant RON. It was possible to improve knock limited spark advance by more than 10°. As toluene was added, the MON dropped from 94 to 90 and hence it could be interpreted that this engine had a negative "K-factor" as will be explained in a subsequent section.

2.10 The 1990s: Chemical Kinetics, Exothermic Centers and Time Frequency Analysis

In 1990, Maly and König of Daimler-Benz together with Klein of Princeton and Peters [217] of RWTH (Rheinisch-Westfälische Technische Hochschule) Aachen University, published a very detailed study on the impact of shock waves in an L-shaped combustion chamber, intended to represent the piston top-land crevice zone. The experiments were at atmospheric pressure but used an ethylene/oxygen mixture. The device is shown in Figure 2.27. The initial section

[15] Gosman would later become one of the key figures behind STAR-CD 3D-CFD software - one of the most popular CFD packages used in engine development in the 1990s and still today.

[16] 1 CV = 0.7355 kW

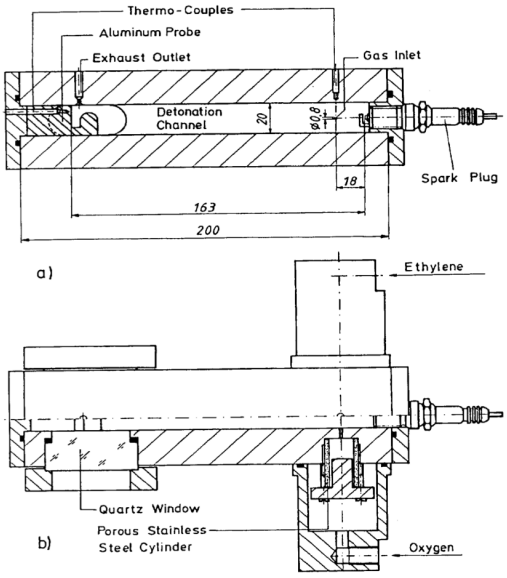

Figure 2.27: Bomb Used to Study Detonation Waves Entering Piston Crevice Area by Maly *et al.* [217]

resembles a tubular bomb. A spark plug was sufficient to generate the incident shock wave. The initial shock traveled at up to 2000 m/s whereas the reflections were at around one third of this speed. However, the reflected shocks gave higher pressures and temperatures than the incident wavefront. Duration runs were carried out on this bomb and erosion damage was seen which resembled that typically observed on the piston of a knocking engine. One of the co-authors, König, published two other key works the same year in collaboration firstly with Sheppard [218] of the University of Leeds and secondly with Maly, Sheppard, Bradley and Lau [219]. Here the importance of temperature gradients around exothermic centers was discussed based on the theory of Zeldovich. Developing detonation was promoted through the introduction of metal particles in the engine in an effort to generate appropriate exothermic centers and gradients. Maly also co-authored a paper with Herweg [220] in this period on flame kernel modeling in SI engines. The model accounted for electrical parameters of the ignition system, heat loss to the electrodes, mixture properties and turbulence. It was shown to correlate well with optical measurements of flame kernel growth taken in a specially adapted engine. Understanding properly early flame kernel growth is key for extending the dilution limit of engines, which also improves the knock limit. Later in the decade, Pan [221] of the University of Leeds, published on computer code which could reproduce the three autoignition modes of Zeldovich. In 1991, Spicher [222] now of FEV (Forschungsgesellschaft für Energietechnik und Verbrennungsmotoren) together with Kröger and Ganser of the Technical University of Aachen, published schlieren photography at 200,000 frames per second together with optical fiber measurements at 500 kHz. Here supersonic reaction fronts were seen. Almost homogeneous autoignition was also observed. The highest knocking intensities were correlated with the fastest reaction front propagation and were thought to likely be developing detonations. It was highlighted in this work that accelerating flame-fronts were never observed and hence the autoignition theory of knock appeared to be the correct one. It was also remarked that it was not obvious why in the 50 films examined autoignition never began next to the advancing flame-front, given that this region could be expected to be the hottest and hence most reactive.

Chemical kinetics calculations were coming of age in engine development and more complex models were being published. Westbrook [223] and Pitz of Lawrence Livermore National Laboratory (LLNL), together with Leppard of GM, applied a mechanism with 500 species and 2500 elementary reactions to CFR engine data. Analysis of the reaction mechanism showed the importance of the production of OH radicals from isomerization reactions on octane values. A detailed model was also used by Ronney *et al.* [224] of Princeton University, again together with LLNL, where the knock-limited intake temperature for a range of different fuels with enleanment was compared. Those which featured an NTC region benefited the most from enleanment. It was suggested that this was due to reduced alkylperoxy radical isomerization with greater presence of oxygen, based on the reaction mechanisms. A much simpler model was used by Brussovansky *et al.* [225] at MIT with just 17 species and 19 reactions. This work also studied the effects of heat transfer. A similar kinetics model was used by Nakano *et al.* [226] of Toyota. Simpler models had the advantage of shorter calculation times, particularly if implemented in multi-dimensional CFD. The Shell model was integrated in 3D CFD code at Loughborough University by Blunsdon and Dent [227]. This model was capable of simulating knock and the resulting pressure waves. The expected acoustic modes of the combustion chamber were excited in the model.

Chemical kinetics models require accurate descriptions of temperature in the end-gas to produce reliable results. They are generally calibrated using rapid compression machines and shock tubes, where conditions are better known and more conveniently measured than in an engine. Researchers in the 1990s applied Coherent Antistokes Raman Spectroscopy (CARS) techniques to measure end-gas temperature in a running engine. These are based on the overlaying of two laser beams of different wavelengths to excite nitrogen molecules. The resulting spectrum corresponds to the temperature. This can be calibrated in a simple bomb. CARS gives a point measurement based on where the beams are focused. Kalghatgi *et al.* [228] of Shell applied CARS

on a Ricardo E6 engine for a range of different fuels and compared measured temperatures to those predicted by polytropic compression. For all fuels except propane, which doesn't exhibit cool flame chemistry, measured temperatures indicated low temperature heat release was taking place. Knocking cycles were also seen to exhibit higher end-gas temperatures shortly before autoignition. Nakano *et al.* [226] of Toyota compared CARS measurements with chemical kinetics calculations. Direct sampling of residual gases was also performed. The calibrated engine model which resulted was then used to see the relative impact of faster burn rates on knock limited torque - rapid combustion was confirmed to be an advantage for a given temperature during late compression and trade-offs between these two parameters were presented. An alternative approach to chemical kinetics modeling is to measure chemical activity directly. Direct measurements of OH, CH and C_2 radicals, using absorption and emission spectroscopy on a running engine, were performed by Shoji and Saima of Nihon University together with Shiino of Mazda [229]. The engine was run with PRF 50 fuel and a compression ratio of just 6.4:1 at a speed of 1800rpm. The level of activity in the blue flame interval, characterized by dips in CH and C_2 absorption, correlated to subsequent autoignition intensity. An example is shown in Figure 2.28. Golombok *et al.* [230]

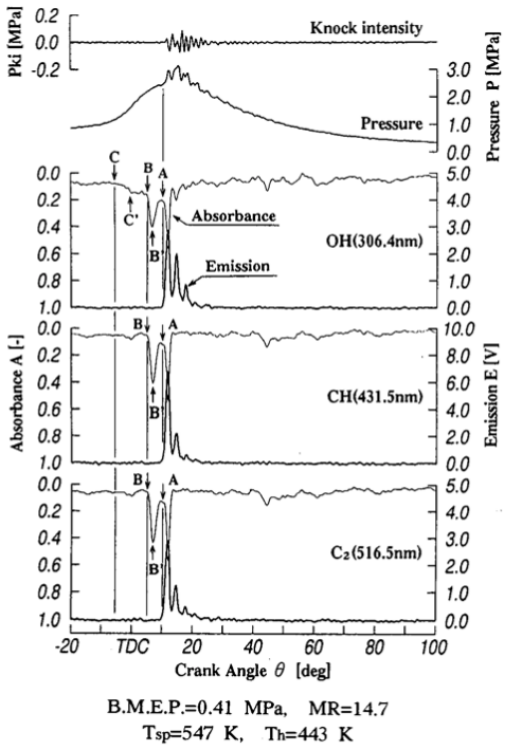

Figure 2.28: Absorption and Emission Spectroscopy Measurements in a Knocking Engine by Shoji et al. [229]

of Shell, published on the differences in knocking heat release rate between paraffinic (such as iso-octane and n-heptane) and aromatic fuels. Maximum heat release rate for aromatics when knocking was seen to be much lower than for PRF blends - coherent with empirical knowledge that aromatics knock "more quietly". This may be due to the lack of an NTC region encouraging more progressive sequential autoignition. The benefits of N-methyl aniline (NMA) as a knock suppressor were also demonstrated and the mechanism was shown to be through modification of only the low temperature chemistry.

More complex techniques were also being applied to interpret knocking cylinder pressure signals. Kaneyasu *et al* [231] of Hitachi used the Signal to Noise Ratio (SNR) in multiple frequency bands to separate knocking from non-knocking cycles. Samimy *et al.* [232] of Ohio State University applied the Wigner-Ville Distribution to create time-frequency plots of knocking data. The same technique was also applied by Scholl *et al.* [233] of Ford. Burgdorf *et al.* [234] of Chalmers University of Technology applied Wavelet Transforms (WT). They took advantage of their flexible time-frequency windows and reduced computation intensity in comparison to windowed FFT (Fast Fourier Transform) analysis. They were also able to show multiple autoignition events in the same cycle using this approach. Burgdorf and Denbratt [235] would also compare eight different pressure-based knock detection methods in a separate publication, but no method was thought to have a significant advantage over the conventional MAPO approach. The same authors [236] also published the following year on knock statistics including giving advice on minimum population sizes. More than 1000 cycles were required to meet their criterion for a pent-roof geometry. That same year, Burgdorf and Chomniak [237] presented a study seeking to understand why sometimes pressure oscillations increase after the initial knock event, even for low amplitude knock. A micro shock tube was used to fire into the end-gas of a combustion chamber. At idle-like conditions this gave a knock-like signal but no autoignition. The flame-front was seen to act as a sort of low pass filter. It was hypothesized that shock waves may reflect in crevice zones and eject crevice gases into the main charge and thereby ignite them.

Some new optical measurements were also being performed. Stiebels *et al.* [238], of the Lehrstuhl für Technische Thermodynamik of RWTH Aachen University, used two intensified CCD (Charge Coupled Device) cameras, 15 μs out of phase, triggered by autoignition. This allowed autoignition location and reaction spatial velocity to be studied. Velocities ranged from subsonic to sonic. As seen by other researchers, autoignition frequently originated close to the wall. This was believed to be due to NTC behavior. Once again it was observed that autoignition did not always produce knocking cylinder pressure oscillations (three pressure

transducers were used simultaneously to measure these). A representative image from this work is shown in Figure 2.29.

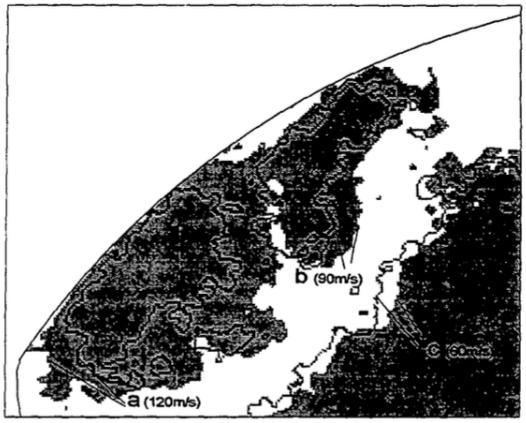

Figure 2.29: Two Superimposed Images of Autoignition Region in an Engine Endgas with 15μs Time Difference used by Stiebels *et al.* to Calculate Autoignition Front Velocity [238]

Knock location could also be calculated from cylinder pressure data if there were at least three transducers opportunely arranged in the combustion chamber. This was demonstrated by Liiva *et al.* [239] of Texaco. Four transducers were used on a CFR engine, mounted on a spacer plate between the head and the cylinder. This allowed checking of errors between groups of three sensors. The knock location generally agreed to within 6 mm between the groups. Such a calculation assumes that the incident knock wavefront travels spherically at reference acoustic velocities. In engine development environments, combustion and knock calculations from cylinder pressure data could now be performed in real-time and hence used for automatic mapping and calibration, as demonstrated by Gschweitl [240] *et al.* of AVL (Anstalt für Verbrennungskraftmaschinen List).

Cooled EGR was being investigated as a replacement for enrichment fueling to avoid knock and/or high temperatures. Grandin *et al.* [241] of the Royal Institute of Technology in Stockholm and Saab Automobile tested cooled EGR in the range 0-21% on a four cylinder 2.3 liter turbocharged engine. The highest load was achieved with 13% EGR but combustion stability was poor. 10% EGR gave the same maximum load as 10% enrichment at fixed boost pressure. Another approach to reduce knock, suggested by Ueda *et al.* [242] of Toyota, was to increase squish effects on a pent roof engine through use of a slanted squish area. A 5° gain in knock limited ignition timing was found. Goto [243], together with collaborators at Mazda and the Kanesaka Technical Institute, described a downsized V6 supercharged engine with a Late Intake Valve Closing (LIVC) strategy. This had the expansion ratio of a Normally Aspirated (NA) engine and the effective compression ratio of a turbocharged engine. A Lysholm compressor was used to avoid turbo lag. The 2.3 L supercharged Miller engine had equivalent performance to a 3.3 L NA but with 13% improved cycle fuel consumption. The following year, Hitomi [244] and researchers at Mazda presented analysis of the Miller cycle as an effective approach to improve CO_2 emissions. LIVC was thought to be superior to EIVC, as less heat transfer to the charge in the cylinder was expected. The boost pressure characteristic against engine speed was also more favorable. Despite this, one year later Ueda [245] of the University of Tokyo, together with colleagues and collaborators at Mazda, published on an effective EIVC engine where a rotary valve in the intake system was applied, such as had been studied by the same University a decade before. This time the engine in question was naturally aspirated and intended to take the place of a diesel engine. The expansion ratio was increased from 8.4:1 to 11:1. Problems with long burn durations at low load were observed, although it was suggested that these could be reduced through use of a high energy ignition system.

Gasoline Direct Injection engines were also reintroduced to the automotive market in the late 1990s. GDI had been used on fighter aircraft in WWII and subsequently in 1954 on the Mercedes-Benz 300SL but most production cars in the 1990s used Port Fuel Injection (PFI) systems. Mitsubishi's GDI engine went on sale in Japan in 1996 and that of Toyota one year later. Iwamoto *et al.* [246] of Mitsubishi described their concept in 1997. Electronic control of the injection timing meant these modern concepts could adopt different strategies over the engine speed and load range. Late injection timing at low speed and load permitted lean stratified operation, with an ignitable air/fuel ratio still guaranteed at the spark plug. At high speed and load, early injection timing produced an homogeneous mixture. The Mitsubishi engine featured an unusual reverse tumble intake port which produced a tumble ratio of 1.8. The injector was mounted underneath this. The piston featured an offset spherical bowl and high squish on the exhaust side. Injection pressure was rather low by current standards (50 bar), both to reduce fuel pump work and for reliability concerns. Air fuel ratios greater than 30:1 could be run in the stratified mode together with EGR. Maximum EGR quantities were as high as 40%, despite a coil energy of just 60 mJ and a narrow-gap plug. EGR was used to reduce engine-out NO_x emissions but the exhaust after-treatment also included a NO_x abatement system. Use of homogeneous GDI in full load gave a 5% improvement in volumetric efficiency and an estimated reduction in end of compression temperature of 30 K. Harada *et al.* [247] described the Toyota Direct Injection gasoline engine in the same year. In contrast to the Mitsubishi system, a swirl control valve was used to generate charge motion in the piston bowl. Low speed and load was again partnered with a late injection strategy whilst high speed and load was with early injection. The transition zone used two injec-

tions per cycle. Injection pressure was 120 bar. Like the Mitsubishi engine, a combination of enleanment and up to 35% EGR was used and a NO_x after-treatment system was required. Claimed fuel consumption reductions for these two engine types were in the range 20-30%.

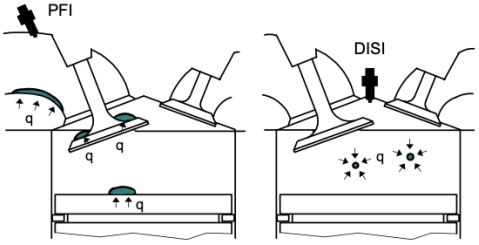

Figure 2.30: Potential of Improved Charge Cooling with a Direct Injection Spark Ignition (DISI) System in Comparison to Port Fuel Injection, from Yang *et al.* [248]

Not all engine manufacturers were convinced that stratified lean systems would comply with future emissions limits. Anderson *et al.* [249] of Ford published research activity on a GDI engine designed for homogeneous operation in 1996. The engine featured an open combustion chamber. Both the injector and the spark plug were mounted centrally. This compromised the valve sizes and hence a high volumetric efficiency, low tumble intake port was applied to compensate. Comparisons between PFI and GDI injection on the same research engine at full load and knock limited conditions were presented. GDI fueling allowed a 10% increase in WOT IMEP. Around 2% of this was from improved volumetric efficiency whilst the rest was from knock mitigation. The knock limit improved as injection time was retarded, up until the point where combustion became unstable due to inadequate mixing time. Volumetric efficiency peaked at earlier injection timings where the intake valve was still open. The knock limit improvement was attributed to the more effective charge cooling of direct injection - the vaporization of the fuel cools the air directly, rather than cooling the intake port and valve, as in a PFI system. This is shown schematically in Figure 2.30 from Yang *et al.* [248] of the same research group in 1998. In this publication, a split injection strategy was used to achieve a better trade-off between volumetric efficiency and knock. GDI systems are ubiquitous now and generally modern GDI engines run at stoichiometric conditions to fulfill significantly more stringent emissions limits with the use of a three-way catalytic converter and without lean after-treatment systems. They take advantage of the knock mitigation effect of direct injection to run higher compression ratios than their PFI predecessors.

Direct injection of gasoline was also seen as a potential enabling technology for Controlled Auto Ignition. A collaborative venture between Daimler-Benz, IFP, Ford and Peugeot to study Controlled Auto Ignition was described by Willand *et al.* [250] of Daimler-Benz in the same period. It was thought that negative valve overlap could be applied to promote autoignition and stratified charge, through direct injection strategies, used to control it.

2.11 The 2000s: Optical Measurements in Engine Development and Developing Detonation Theory

In the early 2000s, optical measurements began to come out of the research lab and into the standard engine development environment. Spicher [198] had already published on optical fibers in a cylinder head in 1986. His collaborators Töpfer *et al.* [251] described installation of optical fibers into a spark plug in 2000, as shown in Figure 2.31. This was used on a production Mitsubishi GDI engine. A similar approach was taken by Philipp *et al.* [252] of AVL in their work published the following year. These systems meant that optical measurements could be conveniently applied even on production engines, with no modifications required. They could be used for autoignition location determination, early flame-front propagation measurement and to identify diffusive combustion.

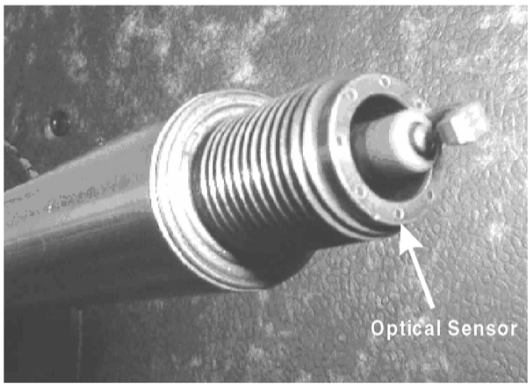

Figure 2.31: Spark Plug with Optical Fibers Used by Töpfer *et al.* for Knock Location Determination on a Production GDI Engine [251]

Fundamental research on knock continued in the lab, with a number of interesting studies being published by Swedish universities, in a collaborative research project. Westin *et al.* [253] of the Royal Institute of Technology applied direct sampling on a 2.3 liter four cylinder turbocharged engine and tested the effect of residuals concentration on KLSA. A 2% increase in residuals corresponded to a 5° retard requirement. This was at least partly temperature driven, and indeed the effect on

charge temperatures was estimated as 30 K, although it was remarked that the NO concentration of the residual gases may also have a significant effect. Stenlåås *et al.* [254] of Lund University of Technology, investigated the impact of NO by adding it to the intake system on the same engine type used by Westin. In this study, NO was found to worsen the KLSA with 400 ppm corresponding to almost 4° of retard. Burluka *et al.* [255] of the University of Leeds found that the effects of NO depended on the fuel used: with pure iso-octane the knock limit actually improved as NO was added. For unleaded gasoline it worsened. Both Westin and Stenlåås had used unleaded gasoline in their activities. A series of investigations took place at Swedish universities on a modified Volvo cylinder head, with a horseshoe shaped combustion chamber and dual side-spark locations to allow optical access to the end-gas. CARS was applied, by Grandin *et al.* [256] of Chalmers University of Technology, together with thin film resistance temperature measurement, to measure heat flux for knocking and non-knocking cycles. Peak heat flux was three times higher when knock occurred - a similar value had been found by Lee *et al.* in the 1980s. The thermal boundary layer was also measured and found to be just 0.5 mm thick. The experimental setup is shown in Figure 2.32. In the same year, the same authors [257], together with researchers at Lund University, also published on heat release in the end-gas with PRF 75 fuel for a range of air-fuel ratios and EGR concentrations. Significant end-gas heating was found for all conditions due to pre-flame reactions - temperatures were typically 50 K hotter than that predicted by isentropic compression. A 60 species, 232 reaction chemical kinetics model was also used in the study. Two zone combustion models were popular, as they were computationally efficient and chemical kinetics calculations could be implemented in them without necessitating excessively high calculation times. A simple two-zone model assumes homogeneous end-gas however, which is rarely the case in reality, and exothermic centers had been highlighted as key in the previous decades. Gogan *et al.* [258] of Lund University combined a two zone model with stochastic particles based on a probability density function. Particles gradually move from the unburned to the burned zone in this approach and random variations of temperature and mass can be described. Turbulence mixing governs how the original variations converge to the mean bulk conditions over time. This methodology gave more realistic autoignition pressure peaks than simple two zone models. An alternative was presented by Sjöberg *et al.* [259] of Sandia in 2005. They applied a five zone approach to model HCCI combustion. One zone was dedicated to the crevice region and others could be used to describe temperature stratification.

More lean burn engines were coming to market and hence understanding cyclic variability was crucial. Aleiferis *et al.* [260] of Imperial College of Science, Technology and Medicine, in collaboration with Honda,

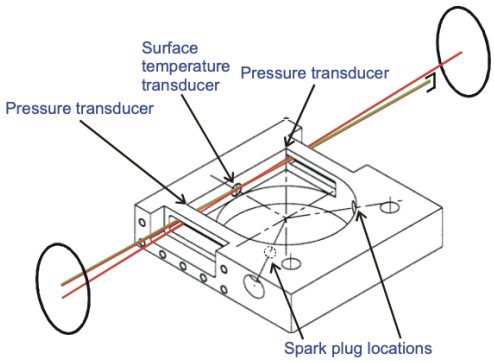

Figure 2.32: Modified Volvo Cylinder Head with Horseshoe Combustion Chamber and Twin Side Spark Plugs used by Grandin and a Series of Researchers in Sweden. CARS Beams Shown [256]

published on the subject in 2000. Particular emphasis was placed on early flame kernel growth. Optical measurements of flame kernel volume were found to be strongly correlated with burn rates later in the cycle. Cross-flow spark plug ground electrode orientations were found to perform best and sensitivity to ignition energy and spark duration was also demonstrated. Extended spark durations were thought to be particularly effective if air fuel ratios varied strongly with crank angle near the spark plug location at ignition timing.

Gasoline Direct Injection engines were increasingly popular, as summarized in a book by Zhao *et al.* [261] in 2002. Already at this stage production and near-production systems existed at Nissan, Renault, Adam Opel, Audi, FIAT, Ford, Honda, Isuzu, Mazda, Mercedes-Benz, PSA, SAAB, Subaru and Volkswagen. Whilst the first DI engines to market in the 1990s ran at part load in stratified lean conditions, some manufacturers were now using the technology with engines which only ran at stoichiometric air-fuel ratio. This meant a conventional three-way catalyst was the only aftertreatment required to meet emissions limits. The knock mitigation benefits of direct injection were of increased importance when it became popular to combine GDI with turbocharging and downsizing later in the decade. One example of this is the Ford EcoBoost engine, described by Yi *et al.* [262] in 2009. A turbocharged direct injection 3.5 L engine took the place of a normally aspirated PFI engine of 5.4 L capacity. The combustion system was optimized through a combination of CFD, optical measurements and conventional dynamometer testing, as illustrated in Figure 2.33. CFD was now well established in engine development environments and allowed a wide range of potential hardware designs to be screened in software. This meant a reduced number of prototype parts needed to be produced and is now the standard approach of most engine manufacturers. The

engine ran in an homogeneous mode for all operating conditions except for cold-start and catalyst heating. A dedicated stratified injection strategy was used to improve stability during catalyst warm-up. This is particularly challenging for turbo-charged engines, as some of the exhaust enthalpy required for catalyst light-off is lost in warming up of the turbocharger. A modified piston crown was also implemented to improve stability in this operating point. Careful work on optimizing the combustion system for knock allowed a compression ratio of 10:1 to be used, despite the downsizing. A fuel economy improvement of 12% was achieved on the FTP 75 drive cycle, for similar power and torque to the larger engine.

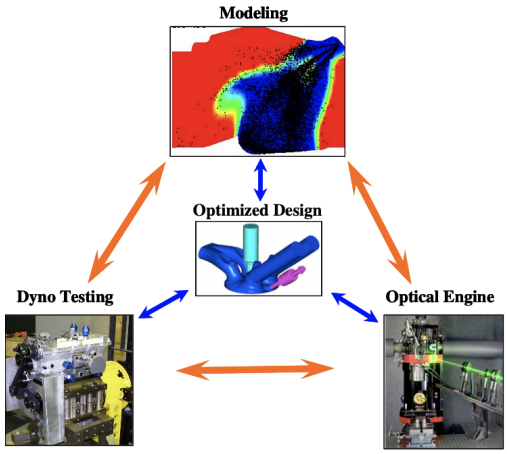

Figure 2.33: Integrated Combustion System Development Methodology Combining CFD, Optical Engine and Dyno Testing, as Applied at Ford in EcoBoost Engine Development, from Yi *et al.* [262]

Research continued on alternative combustion concepts, some of these with direct relevance to conventional SI knock. A significant paper on CAI engines was published by Bradley and Morley [263] of the University of Leeds and Shell in 2002 together with Gu and Emerson of CLRC Daresbury Laboratory. Hot spots inevitably exist in the end-gas of both CAI and SI engines. There tends to be a reaction gradient around them and Zeldovich [208] had shown in 1980 that if an autoignition front develops, its velocity relative to acoustic and Chapman-Jouget detonation velocities is key in determining if a developing detonation occurs. A resonance parameter was defined as $\xi = \frac{a}{u_a}$, where a is the acoustic velocity and u_a is the autoignition front velocity. The authors showed that a second term is also required to ascertain if developing detonation can occur in practical systems: $\varepsilon = \frac{r_0/a}{\tau_e}$, where r_0 is the hot spot radius and τ_e is the excitation time (time from 5% to maximum chemical power). When ξ and ε are plotted against each other, developing detonations only occur in a given range, as shown in Figure 2.34. The hot spot size is key, with very small hot spots not resulting in developing detonation. In the same year Eng [264] published an analysis on the differences between pressure waves resulting from HCCI combustion and knock. It was shown that HCCI combustion generally leads to high signal energy at around 5-6 kHz - in this sense similarly to knocking combustion. For HCCI however, around 90% of the energy from 4-22 kHz is for this mode whilst for knocking combustion it is just 65%. It was suggested that objectionable engine noise from knock was a result of more effective transmission of these higher frequencies through the block structure and hence to the ambient air. A formula for Ringing Intensity of HCCI combustion was derived based on wave intensity I. Wave intensity is described by Equation 2.12 and has units of W/m^2. It was assumed that pressure pulsation amplitude Δp should scale with maximum pressure rise rate $\frac{dp}{dt}$. The Ringing Intensity was then as shown in Equation 2.13 [264]. β was a constant to be tuned with experimental data and was found to have a value of 0.05 for the described experiment. This formula was frequently cited by HCCI researchers in the coming years.

$$I = \frac{1}{2\gamma}\frac{\Delta p^2}{p}\sqrt{\gamma RT} \tag{2.12}$$

$$\text{Ringing Intensity} \approx \frac{1}{2\gamma}\frac{\left(\beta \frac{dp}{dt}_{max}\right)^2}{p_{max}}\sqrt{\gamma RT_{max}} \tag{2.13}$$

Bradley and Kalghatgi [265] published a further work in 2009 linking pressure oscillations Δp to the rate of autoignition driven combustion. This was based on the rate of an autoignition hotspot expansion in comparison to local acoustic velocity. For non detonative autoignition in engines, the resulting pressure oscillation behavior is approximated by Equation 7.2 where p is the undisturbed cylinder pressure.

$$\frac{\Delta p_{max}}{p} \approx \xi^{-2} \tag{2.14}$$

A new CAI control mode for four-stroke applications was also researched - Spark Assisted Compression Ignition (SACI). Two notable papers were published on the topic in 2005. Hyvönen [266] of Fiat-GM Powertrain Sweden, together with Haraldsson and Johansson of Lund Institute of Technology, performed testing on a Saab variable compression ratio five-cylinder engine with PFI fueling. Compression ratio could be controlled from 10-30:1 and an inlet air heater was also present. Cylinder pressure analysis showed an initial heat release primarily from spark ignition before a transition to autoignition, as shown in Figure 2.35. Ringing on the pressure trace can be seen and hence this is effectively similar to a knocking cycle in a conventional spark ignition engine, although the transition to autoignition may occur at much lower mass fraction burned percentages - around 36% for the example shown. The amount of heat release

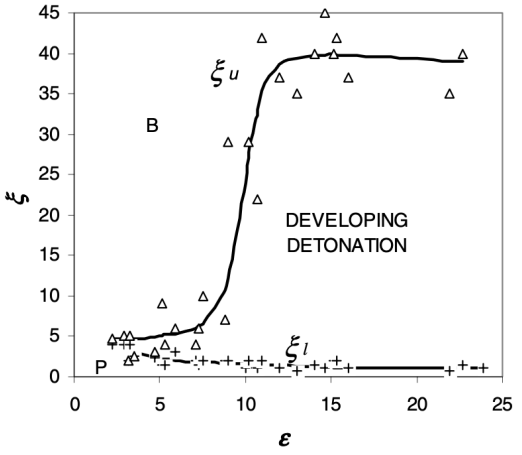

Figure 2.34: Diagram Proposed by Bradley *et al.* to Explain Conditions Necessary for Developing Detonation in an Engine. $\xi = \frac{a}{u_a}$ is the Resonance Parameter. $\varepsilon = \frac{r_0/a}{\tau_e}$ defines the Hotspot Reactivity and depends on the Hotspot Dimensions [263]

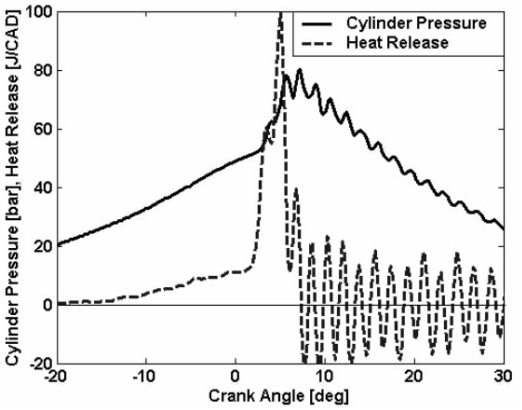

Figure 2.35: Spark Assisted HCCI Pressure Trace and Heat Release Analysis, from Hyvönen *et al* [266]

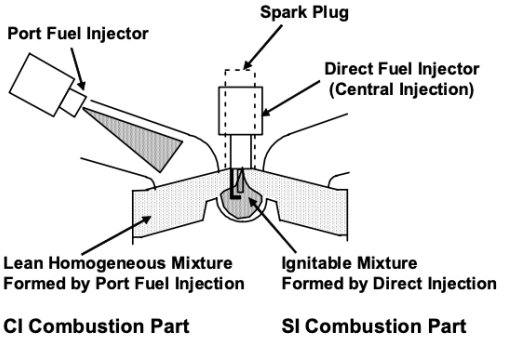

Figure 2.36: Nissan Spark Assisted Gasoline Compression Ignition Research Engine, from Urushihara *et al.* [267]

from flame-front propagation was just 5% at high compression ratios with a relative air fuel ratio $\lambda > 2$. The spark assisted mode was seen as a means of transferring in a controlled manner from extremely lean HCCI with high compression ratios to stoichiometric conventional SI at low compression ratios. Urushihara *et al.* [267] of Nissan published their study on spark assisted gasoline compression ignition engine the same year. Here, the compression ratio was fixed at 15:1. The engine featured PFI fueling to create an overall lean homogeneous mixture and a direct injector was used to produce a locally rich cloud near the spark plug. A small bowl was created in the piston for the same reason. The concept is shown in Figure 2.36. The pressure rise from flame-front propagation was said to function similarly to increasing the compression ratio. Variable valve overlap to control internal residuals allowed use of spark assisted compression ignition from IMEP values of around 3.5-6.5 bar without knocking. Airflow was fixed at WOT conditions and PFI fueling was used to adjust load. Knocking limited the richest air-fuel ratio and hence the load which could be achieved. At still lower loads, pure HCCI was run.

Fundamental knocking research also continued in Japan. Suzuki *et al.* [268], of Nihon University, used light emission spectroscopy to study HCHO (formaldehyde - cool flames, 395 nm) and HCO (formyl radical - blue flames, 330 nm) in the end-gas region of a single-cylinder engine. Ion current sensors were also utilized. It was found that the duration of HCHO formation before knock was sensitive to combustion chamber temperature for PRF 30 and PRF 60, but not for pure n-heptane. The duration of HCO light emission decreased for all blends as combustion chamber wall temperature increased. Hirooka *et al.* [269] of Toyota studied the impact of turbulence on burn rates and knock using direct injection of high pressure air and of hydrogen. Various patterns of high pressure air could increase turbulence near the spark plug or in the periphery of the combustion chamber. Combustion duration could be halved. Best results were found when accelerating the late part of combustion, with a 13° improvement in KLSA. Note that turbulence generated by tumble tends to primarily accelerate the early phase of combustion. Fast burn rates also led to combustion noise however, between 800 and 2000 Hz. Although the gain in performance was as much as 10%, when compressor work to generate the high pressure air was factored in, the overall efficiency gain dropped to 4%. The hydrogen study documented by Shinagawa *et al.* [270] gave similar burn rates to that of the compressed air research, and again it was possible to improve conditions close to the plug or in the end-gas. At similar burn rates to the high

pressure air injection study, the knock limit was further improved. Chemical kinetics calculations suggested this was due to consumption of the hydroxyl radical by hydrogen.

A great number of papers were published on signal processing techniques. Part of the reason was to improve the SNR of production accelerometers, but noise was also an issue for cylinder pressure transducers. Zhong [271] of the Industrial Technology Center of Okayama Prefecture and Tomota of Okayama University used wavelet transforms with multiple voices per octave to identify knock in noisy signals. Wavelet pattern matching was applied to compare actual and reference signals. Carstens-Behrens [272] of Ruhr University Bochum, together with collaborators at Bosch, performed time-frequency analysis using the Wigner-Ville transform and compared this to Finite Element Method (FEM) acoustic mode calculations of a pent-roof combustion chamber for various piston heights, as shown in Figure 2.37. Noubari and Dumont [273] of the University of Tehran and the University of British Columbia, employed wavelet methods to reduce both white and colored noise in accelerometer signals. The entropy of the de-noised accelerometer signal could be used to quantify knock: knocking cycles showed lower entropy. Borg *et al.* [274], of Hitachi America and Oakland University, Michigan, also used Wavelet Transforms. Correlation was studied between accelerometers and pressure transducers. Best correlation in this study was found between 4 and 8 kHz. Borg *et al.* [275] characterized autoignition using heat release analysis in the same year. Maximum heat release rate of knocking as opposed to non-knocking cycles were compared. Worret *et al.* [276], of the University of Karlsruhe, reviewed a number of pressure-based knock algorithms and also proposed a variant based on Rate Of Heat Release (ROHR) three years prior to this. One of the issues in using ROHR as a knock index, is that the data become very noisy when knock occurs. Corti *et al.* [277] of the University of Bologna suggested to use a combination of three Wiebe functions to fit the data, with one being dedicated for the knocking heat release. Hettinger *et al.* [278] of Bosch suggested dealing with the problem by fitting a single Wiebe function only up to the moment of knock onset and then comparing this to the measured heat release post-knock. In general, noise on pressure transducer and accelerometer signals becomes more problematic at higher engine speeds and loads. Cavina *et al.* [279] of the University of Bologna proposed methods to deal with this and examined the susceptibility of different indices to windowing and filtering effects. Naber *et al.* [280] of Michigan Technological University and Motorola compared time frequency spectrograms of cylinder pressure and accelerometer signals as shown in Figure 2.38. They also considered the knock intensity from both sensors to be well fitted by a single log-normal distribution[17].

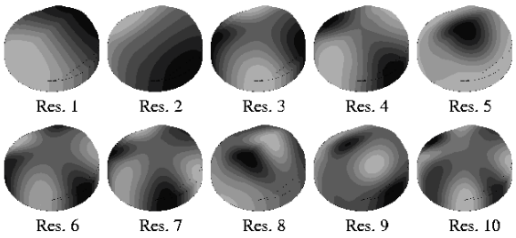

Figure 2.37: First Ten Acoustic Modes for Pent-roof Combustion Chamber as Calculated by Carstens-Behrens *et al.* [272]

Cylinder pressure transducers and accelerometers were the standard tools, but Mittal *et al.* [281] of MIT found that a microphone could also identify knocking peaks at around 6 kHz in their study. Higher amplitudes were seen on the cylinder pressure signal in the 15-22 kHz range, but the microphone signal was bandpass filtered from 6-12 kHz to correspond to audible knock. Abhijit and Naber [282], of Michigan Technological University, compared cylinder pressure and ion current signals using a range of techniques. It was stressed that both are local measurements and hence for single cycles the correlation may be poor. It was also noted that only two peaks were visible on an FFT of the ion-current signal whilst four could be seen for the pressure transducer. Correlation was best between the highest frequency common peak. This was partly because at high speed, noise extended above 6 kHz on the ion current signal. Although cyclic correlation was poor, statistically the two sensors responded in a coherent manner to changing spark advance. Knock statistics were also studied by Zhu *et al.* [283] of Visteon. A stochastic knock controller was proposed, based on a non-linearly

[17]The dual log-normal work of Iwata *et al.* [194] was not referenced)

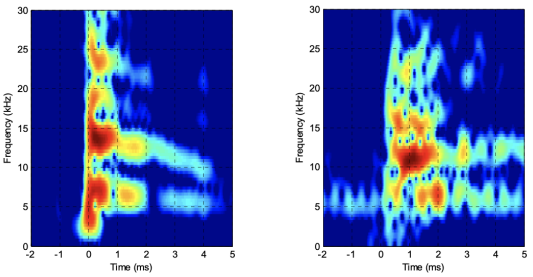

(a) Cylinder Pressure Transducer **(b)** Accelerometer

Figure 2.38: Comparison of Cylinder Pressure Transducer and Accelerometer Time Frequency Data by Naber *et al.* [280]

modified Gaussian Probability Density Function (PDF). This was updated cyclically by an online buffer. It allowed a more stable ignition control than for conventional "count-up/down" knock controllers and hence a lower COV (Coefficient Of Variation) of IMEP.

Knock localization could be performed with optical techniques, but a number of researchers developed the multiple pressure sensor method also. One of the main issues is to reliably estimate the time difference between the signals, to allow triangulation of the incident knock wave source. Castagné *et al.* [284] of IFP and Metravib RDS used an inter-correlation calculation rather than relying on the simple wave arrival time. For 5 mm geometric accuracy, the time difference needed to be precise to within 5 μs. It was seen that piezoelectric pressure sensors were reliable in bench testing to within 1 μs. The methodology was tested also in CFD to check the influence of engine geometry and inhomogenous acoustic speeds and was found to still be valid. Both four standard Kistler 6052 piezoelectric sensors and an instrumented head gasket with twelve pressure sensitive elements were tried. Rothe *et al.* [285] of the University of Karlsruhe used data from five cylinder pressure transducers to ascertain the location of autoignition and combined this with flame-front measurements from 17 optical fibers. Knock was seen to occur in regions of the end-gas where the flame-front arrives late. Hettinger *et al.* [278] of Bosch, used six sensors, one of which was in the spark plug. Modal analysis with FEM was used to identify knocking frequencies and the pressure distribution in the chamber. The effect on accuracy of considering acoustic velocity stratification was quantified and found to be non-negligible. Knock was also seen in this study to primarily occur in the last region where the flame-front arrived, as measured by OH visualization.

In 2001 Kalghatgi [286, 287] of Shell published two papers on how RON and MON values could be used, together with a "K-factor", to match road octane requirements of modern vehicles. The first paper dealt with testing on a single cylinder engine with a pent roof head and two different compression ratios. A fuel matrix of thirteen blends with decorrelated RON and sensitivity (S) was used. It was found that KLSA was weakly correlated with MON, quite well correlated with RON, and strongly correlated with a new octane index as shown in Equation 2.15. The K-factor was found to become less negative as engine speed increased but more negative as octane requirement increased. Acceleration testing on 23 European and Japanese cars with knock control systems, over a range of fuels, showed that most cars had a negative K-factor and hence responded best to fuels with high RON and low MON. Mittal and Heywood [288] of MIT applied the K-factor concept in analysis of historical data from 70 years of Coordinating Research Council (CRC) vehicle octane sensitivity studies. Whilst in 1951 only 10% of vehicles exhibited a negative K-factor, by 1991 this had increased to 50%. It was suggested and demonstrated by 1-D (one-dimensional) simulations that modern engines with higher volumetric efficiency, faster burn rates and better cooling meant that conditions in the combustion chamber were at higher pressures and lower temperatures than for older vehicles. This meant that the relevant temperature regime had moved away from MON towards RON. For boosted direct injection engines, the calculations suggested a negative K-factor as described by Kalghatgi or "beyond RON" conditions.

$$OI = RON - KS \tag{2.15}$$

Milpied [289] of IFP together with collaborators from Renault, Ademe, Total, and PSA attempted to separate the effects of latent heat of vaporization from RON and MON by exchanging Ethyl Tert-Butyl Ether (ETBE) for ethanol in a fuel matrix at matched RON. It was estimated that 30-60% of the knock-limited load gain benefit of ethanol blends at matched RON was from their increased latent heat of vaporization, which reduces charge temperatures. These studies were performed on a downsized boosted single-cylinder engine with direct injection. Nakama [290] of Sukuki together with Kusaka and Daisho of Waseda University, showed that splash blends of ethanol in a ternary mixture of iso-octane, n-heptane and toluene gave significant knock benefits: 20% of ethanol allowed a 5-10° KLSA improvement on a 0.33 liter engine with compression ratios ranging from 9:1 to 15:1. An alternative approach to knock mitigation with conventional gasoline was through addition of fuel reformate (CO and H_2). This was being studied by Topinka *et al.* [291] at MIT with 15% simulated reformate giving an 8° improvement in KLSA on a single cylinder pent-roof engine.

Swarts *et al.* [292] at the University of Cape Town and Sasol Technology investigated what the RON and MON tests actually measured by instrumenting a CFR engine with a cylinder pressure transducer and an exhaust gas oxygen sensor. Testing was performed in RON like conditions but with a fixed relative air-fuel ratio $\lambda = 0.9$. It was noted that changes in the burn rate could be seen on pressure and MFB curves before knocking oscillations were observed. It was suggested that the standard knock meter responds to these burn rate variations. This problem had also been noted in the 1960s by Hoffman [140].

Chemical kinetics were frequently employed in simulation environments. Some employed simple techniques, such as that used by Elmqvist *et al.* [293] of Fiat-GM Powertrain, the Royal Institute of Technology and Shell. Their approach was based on Livengood-Wu / Douaud-Eyzat methods to enable a closed loop controller on knock in a 1D simulation environment. Noda *et al.* [294] of Nissan used a reduced mechanism from LLNL, with 99 species and 462 reactions, to study the cause of knock at the beginning of vehicle accelerations. This was found to be due to a spike in temperatures in the intake system. The mechanism was for PRF fuels

and it was stated that a chemical kinetic model for real gasoline was not available. Yates *et al.* [295] of the University of Cape Town and Sasol Advanced Fuels Laboratory fitted chemical kinetics calculations with thousands of reactions using a three stage Arrhenius model. The total ignition delay is expressed as shown in Equation 2.16.

$$\tau_{overall} = \left[(\tau_1 + \tau_2)^{-1} + (\tau_3)^{-1}\right]^{-1} \quad (2.16)$$

Figure 2.39 compares the ignition delay map for iso-octane based on the fit terms of Yates *et al.* to that which results from Douaud and Eyzat's CFR based approach using the same fuel. The single-Arrhenius fit of Douaud and Eyzat of course cannot describe the NTC region, which is clear in the correlation of Yates *et al.* In the high temperature region, the models give more similar results. For example, using a temperature of 1010 K and a pressure of 22 kgf/cm^2 (a reference point from Douaud and Eyzat's original paper), their formula gives 2.9 ms whilst that of Yates *et al.* results in 1.6 ms. Commercial gasolines tend to have a smaller NTC region than iso-octane but care should in any case be taken in describing their characteristics by a single Arrhenius fit. Of course, many more data points would be required to fit three Arrhenius functions to engine data in comparison to the Douaud and Eyzat approach. Fitting to engine data also requires significant assumptions to be made regarding end-gas temperature and homogeneity. Two papers were published by Milan Polytechnic on detailed kinetic models in this period. The first, by Mehl *et al.* [296] was with 250 species and 5000 reactions. This was implemented in a two-zone model but it was possible to account for temperature stratification in the crevices. The model was correlated against data of critical compression ratios in PRF testing on CFR engines. A successive activity described by D'Errico *et al.* [297] used a quasi-dimensional approach with 300 species and 6000 reactions. A transparent piston engine was tested with UV optical measurements for OH and HCO. HCO was shown to precede OH and was a result of formaldehyde decomposition. A simpler kinetic scheme with 32 species and 55 reactions was used by Bozza *et al.* [298] at the University of Naples "Federico II", again in a quasi-dimensional model. Here cyclic variability was introduced through random variations of flame kernal duration and radius, air fuel ratio, residuals concentration and intensity. Quasi-dimensional simulation of combustion was also performed by Hattrell *et al.* [299] at the University of Leeds and Mahle Powertrain. This was used to evaluate burn rates for various knock reduction strategies. Whilst 30% enleanment and 15% EGR gave similar BSFC benefits, the combustion stability was poorer for the lean case. It was calculated that lean running results in a lower Damköhler number than use of EGR and hence greater risk of local quenching and poor combustion stability. Liang *et al.* [300] at the University of Wisconsin-Madison used the so-called "G-equation" model in KIVA-3 3D CFD code to model turbulent

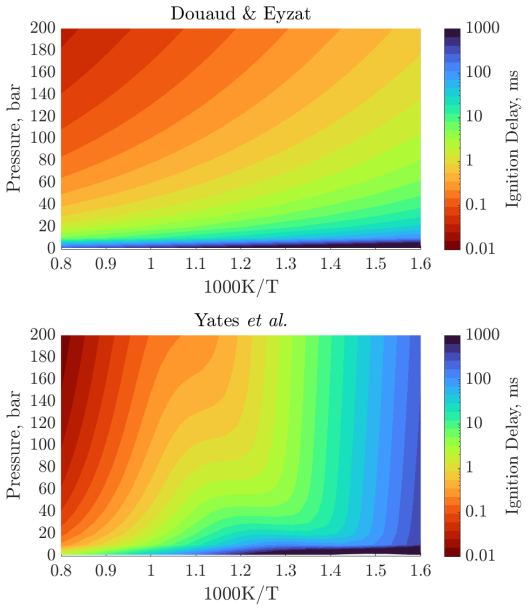

Figure 2.39: Stoichiometric Ignition Delay for Iso-Octane based on Triple-Arrhenius Approach of Yates *et al* [295] Compared with Douaud and Eyzat [177] Single-Arrhenius Method Recalculated from CFR Data at Maximum Knock Air Fuel Ratio

combustion, combined with a chemical kinetics mechanism in CHEMKIN software for iso-octane with 22 species and 42 reactions. This was benchmarked against experimental activity on a 12:1 compression ratio GDI SI engine with excellent agreement observed. Eckert *et al.* [301] of the same research group had published on knock simulation using the Shell kinetics model, again in KIVA-3, some years earlier. A "discrete particle ignition kernel" model was used. Good agreement was found in comparison to engine data and pressure oscillations were also reproduced. Corti and Forte [302], of the University of Bologna, also used KIVA-3 but with the alternative Extended Coherent Flamelet Model (ECFM) for turbulent flame-front propagation and a simpler kinetic approach based on the Shell mechanism. Experimental activity on the same FIAT 1.2 liter engine then showed that knocking cycles could be identified based on their net heat release, which was lower due to the increase in heat transfer due to knock.

Coupled 3D simulations were also being applied to water jacket optimization in an effort to improve knock limits. Kleeman *et al.* [303] at IFP and Renault used FLUENT for water jacket simulation coupled with KIVA-II combustion modeling using the Douaud knock model. The influence of local cooling on knock could therefore be investigated. It was noted that cooling of the exhaust valves did not result in a change in autoignition location

in comparison to cooling of the liner - knock remained under the exhaust valves in both cases. In the same year, Shih *et al.* [304] of Honda R&D performed simulations of the water jacket of a V6 engine using STAR-CD software. An experimental approach with thermocouples and knock limit measurements was used to confirm the simulated improvements in knock from increased cooling of the central cylinder of each bank.

There was renewed activity on prechamber engines in a number of countries. Couet *et al.* [305] of the University of Orleans presented the so-called APIR concept meaning "Self-ignition Triggered by Radical Injection". A rich prechamber was used together with small holes, which caused quenching of the reaction products and hence seeded radicals into the main combustion chamber. This resulted in distributed ignition sites in the main chamber, far from the prechamber itself, as evidenced by combined laser sheet tomography and direct visualization. Kettner *et al.* [306] at the University of Karlsruhe with Kuhnert and Latsch of Multitorch published on a passive prechamber spark plug where rich mixture was introduced from a small bowl in the piston into the prechamber late in the compression stroke. This was known as the BPI concept. Full load combustion phasing could be improved by 5° CA in comparison to the same engine with a conventional spark plug. Kuhnert and Latsch [307] also published a paper, together with Getzlaff and colleagues at IAV (Ingenieurgesellschaft Auto und Verkehr), on a prechamber with pilot injection. A single stroke engine with optical access was used together with a filtered ICCD (Intensified Charge Coupled Device) camera to capture OH radiation. It should be noted that prechambers were already common on large gas engines, as documented by Kawabata and Mori [308] of Tokyo Gas Company and Winter *et al.* [309] of Graz University of Technology. Prechamber research was also undertaken at the University of Melbourne by Toulson, Watson and Attard [310]. A fueled prechamber was added to a CFR engine in the side of the chamber (the normal spark plug location). Various fuels were compared both for the prechamber and the main chamber. Chemical kinetics calculations were integrated in 3D CFD and compared to optical results. Main chamber and prechamber lambda were also varied. Best results were obtained with a rich prechamber mixture and H_2 as the prechamber fuel. It was possible to run to a relative air fuel ratio as lean as $\lambda = 5$. Interest in prechambers for both lean limit and knock limit extension would increase in the following decade.

2.12 2010s: Aggressive CO_2 Targets, Electrification and Downsizing

The number of publications on knock has increased significantly in the last ten years. This is largely driven by greater pressure on manufacturers to reduce fleet average CO_2 emissions. Whilst for a period diesel was seen as an appropriate means to achieve this, at least in Europe, the Volkswagen diesel emissions scandal of 2015 [18] led to a crash of the diesel engined car market and hence manufacturers having to make significant improvements in gasoline powered vehicle CO_2 in order to meet their targets. Downsizing enables reduction of pumping losses and friction on emissions drive cycles by increasing engine load for a given vehicle power requirement. This higher load increases the risk of knocking however, particularly at high output.

Cooled EGR was widely studied once again. It gives efficiency gains through lower peak cylinder temperatures and hence lower heat losses and dissociation, an increase in specific heat ratio and a knock limit improvement. It also reduces flame speeds however, and so the quantity of EGR which can be tolerated is limited by combustion stability. Hoepke *et al.* [311] of MIT proposed a modification of the Douaud and Eyzat ignition delay expression to account for EGR and to calculate an equivalence of EGR and Octane number. 10% of EGR was found to have a similar effect to a 3% improvement in octane. Alger *et al.* [312], at Southwest Research Institute, evaluated EGR and octane interactions with fuels of RON 91 up to RON 109. As much as 30% of EGR could be tolerated on an engine with tumble ratio of 1.5 and fine electrode spark plugs with a large gap. A somewhat higher sensitivity was found in comparison to the MIT work. 1% of EGR was equivalent to a 0.5-0.75 improvement in octane number. EGR from stoichiometric combustion is largely composed of CO_2, N_2 and H_2O, but will also contain traces of other substances, in particular if taken from upstream of a catalytic converter. Of these, NO is of particular interest as it may worsen the knock limit as had already been shown in the previous decade. Investigations on its effect continued at the University of Leeds where Roberts *et al.* [313] compared synthetic EGR with and without NO for PRF, TRF (Toluene Reference Fuel) and full boiling range blends. The results implied that NO was detrimental to knock for fuels with little NTC region, but could give an improvement on PRF 90. Of course, EGR does not necessarily have to come from stoichiometric combustion and researchers at Southwest Research Institute demonstrated a "Direct-EGR" engine, where one cylinder ran rich and exhausted to the inlet manifold of the other three cylinders of a four cylinder engine. This meant that the EGR was high in CO and H_2 and therefore the normal issues of reduced flame speed and poor combustion stability were

mitigated. Every 10% of enrichment in the EGR producing cylinder gave an octane improvement of 1.8 units. The EGR cylinder began to run into rich stability issues however at equivalence ratios $\phi > 1.3$ as described by Algers *et al.* [314]. Szybist *et al.* [315] of Oak Ridge National Laboratory commented that turbocharged engines were increasingly popular in the US with the market having increased from 3% in 2006 to 25% in 2016. The effectiveness of EGR at high load (up to 19 bar IMEP) was studied and it was found that at high pressures and low temperatures, EGR did not significantly improve ignition delay time. In 2019, Sjöberg *et al.* [316] of Sandia National Laboratories performed a further investigation on the effect of NO in EGR gas. Skip firing was used to clean the test engine of residual NO and then synthetic EGR and bottled NO was added in a range of concentrations on different fuel types. The NO response curve in terms of knock limited combustion phasing was confirmed to be significantly different for different fuel types. Whilst for alkylate fuel (low Sensitivity) knock strongly worsened in the range 0-40 ppm, then the effect gradually diminished, for all other fuels NO had a smaller detrimental effect up to 500 ppm. With aromatic fuel, the effect was slight. Interestingly, a correlation was found between peak pressure of the preceding cycle and NO concentration in residuals - this gives a prior-cycle effect in terms of knock, even though the cyclic variation in knock is normally considered to be random. Cooled EGR was used together with twin stage boosting, a high tumble intake port and direct injection on the heavily downsized "Ultra Boost" engine. This was a collaboration between Jaguar Land Rover, GE Precision Engineering, Lotus Engineering, Shell Global Solutions, CD-adapco, the University of Bath, Imperial College London and the University of Leeds as described by Turner *et al.* [317]. The target was to replace a 5.0 liter V8 engine with a 2.0 liter unit achieving the same torque curve but with a reduction in drive cycle fuel consumption of 35%. The engine had a compression ratio of 9:1, but could run at over 32 bar BMEP at 3500 rpm in stoichiometric conditions, even without EGR, with RON 97 E5 gasoline. EGR and enrichment were used at higher speeds. The engine featured both PFI Port Fuel Injection and GDI fuelling systems and testing showed that the knock limit improved as a the proportion of fuel injected directly into the cylinder increased, as shown in Figure 2.40.

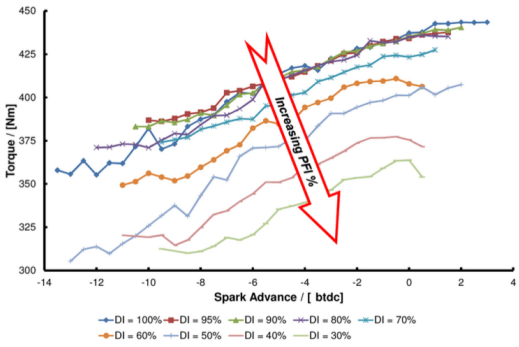

Figure 2.40: Knock Implications of PFI and GDI Fuelling Strategies at 2000 rpm on "Ultra Boost" Project Engine [317]

Dilution has a detrimental impact on combustion speed and stability as it reduces laminar flame speed. One of the main ways of compensating for this is with increased turbulence. The intake port design is key in achieving this. It had already been demonstrated in the 1980s that high tumble ports resulted in improved turbulence and higher flame speeds. A high tumble port may also generate strong secondary motions however, such as cross tumble, omega tumble and swirl. Cyclic variability in the flow structures may have a detrimental impact on combustion stability and knock. This was examined using high speed Particle Image Velocimetry (PIV) by Adomeit *et al.* [318] of FEV in 2011. Testing was performed on a motored engine rig with a transparent liner. Peak tumble ratios from 2.4 to 5.8 were investigated. A solid state Nd:YLF laser and a high speed CMOS (Complementary Metal Oxide Semiconductor) camera allowed a frame rate of 6000 Hz at a resolution of 1024 x 992 pixels. Imaging was in both the tumble and cross-tumble planes. It was found that ports which gave higher tumble intensities also gave higher cyclic variability in the cross-tumble plane. This would also likely lead to higher cyclic variability in combustion. The optimum port design is therefore a trade-off. Flow measurements in engines had generally been either point based (such as hot wire anemometry) or planar (such as PIV) up until this point. Baum *et al.* [319] of the Technical University of Darmstadt, together with LaVision, published on tomographic PIV in 2012. This allowed the 3D flow field in an engine to be interrogated directly for the first time. The technique required the use of four CCD cameras simultaneously. The measurement volume in the region of the tumble plane and had dimensions of 47 x 35 x 4 mm. Such tools can be used to calibrate 3D CFD models of charge motion, which can then be used to screen intake port geometries in a software environment. One of the main inlet port trade-offs studied in CFD is the relationship between tumble and volumetric efficiency. Tumble is normally generated by biasing more flow over the upper edge of the valve and less over the lower side. This is generally achieved by having a large included angle between the intake valve axis and that of the inlet port and/or through shrouding of the lower part of the intake valve. This reduces the effective valve curtain area and hence is detrimental to filling efficiency. This is particularly important for normally aspirated engines where volumetric efficiency cannot be compensated with increased manifold pressure. The optimization of the tumble/flow trade-off was described by Yoshihara *et al.* [320] of Toyota in 2016. Both the inlet port to

inlet valve angle and the inlet port to exhaust valve angle were found to be important in order to generate efficient tumble. Tumble efficiency was defined as energy transformed into generating tumble normalized by extra pumping work due to intake flow restriction. Stroke to bore ratio is also a key design decision to be made when designing a new engine and was shown to be a tradeoff by Itabashi *et al.* [321] of Toyota in 2017. Low stroke to bore ratios mean large valves can be fitted which improves volumetric efficiency and hence specific output for a given manifold pressure. Mean piston speed is reduced which helps limit friction. Large stroke to bore ratios on the other hand, mean small flame travel distances and high mean piston velocities (driving turbulence) and hence fast combustion. EGR tolerance, knock and thermal efficiency are therefore improved. The tradeoff in intake port design is shown in Figure 2.41 and that of stroke to bore ratio is shown in Figure 2.42. The optimized normally aspirated engine achieved a maximum thermal efficiency of 40% with a compression ratio of 13:1 and 61 kW/L specific output.

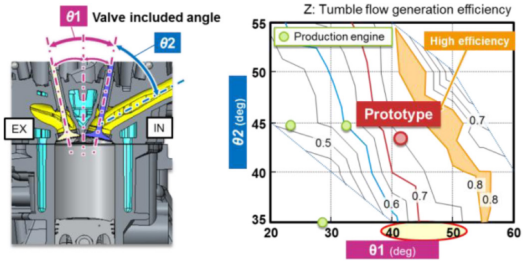

Figure 2.41: Tumble Efficiency Sensitivity to Exhaust Valve/Inlet Valve Included Angle θ_1 and Inlet Port/Inlet Valve Included Angle θ_2 from Itabashi *et al* [321]

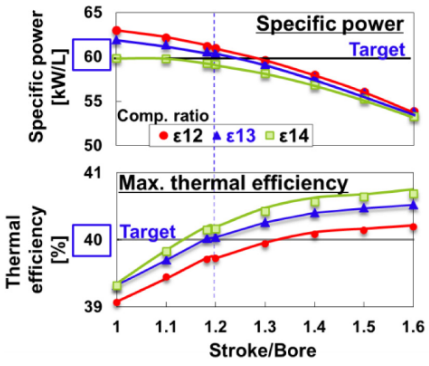

Figure 2.42: Stroke to Bore Ratio Tradeoffs, from Itabashi *et al* [321]

Whilst tumble can help improve early burn rates in dilute mixtures, the ignition system may also require development. High tumble ports can promote significant residual charge motion at ignition timing. This may result in

(a) Short-Circuiting of Discharge Path

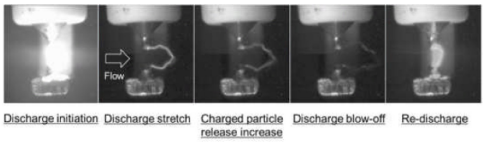

(b) Blow-off of Discharge

Figure 2.43: Blow-off and Short-Circuiting of Spark Ignition Discharges in a High Velocity Flowfield, from Hayashi *et al.* [323]

excessive velocities across the spark plug. It is generally desirable to mount the spark plug ground electrode in a cross-flow orientation in comparison to the residual flow. This promotes the extension of the discharge channel out of the plug gap, which therefore increases the discharge channel surface area and reduces the heat losses to the electrodes. Suzuki *et al.* [322] in 2016 described how flow velocities in excess of 30 m/s could lead to misfire however. The discharge channel is overly extended leading to a short circuiting or blow-off behavior. This may mean inadequate time for the discharge channel to produce a self-sustaining flame kernel in the surrounding mixture. Small flame kernels with low laminar flame speeds also may not survive in highly turbulent environments. Suzuki was the coauthor of a subsequent paper on the theme by Hayashi *et al.* [323] of Denso and Toyota the following year. Here discharge current sensitivites were further examined. Examples of blow-off and short-circuiting were shown with optical analysis as can be seen in Figure 2.43 [323]. Restriking can be reduced and the flame kernel encouraged to grow by maintaining adequate discharge current for an extended period. A conventional ignition coil produces a descending discharge current profile following breakdown. A constant current profile, realized by closed loop control, allowed blow-offs to be suppressed and the lean limit to be extended by 15% at lower energy expenditure than for a conventional high energy system. Whilst large spark gaps may help to improve ignitability through extension of discharge channel length and reduced heat loss from the early flame kernel to the electrodes, on highly boosted engines gap size may be limited by maximum sustainable breakdown voltages. A limit of around 36 kV for M10 sized spark plugs was identified by Corrigan *et al.* [324] of Ferrari in testing of a highly boosted single cylinder engine for Formula 1 research. A gap size of 0.8 mm allowed sparking at up to 50-60 bar cylinder pressure whilst a gap of 0.6 mm permitted sparking up to almost 80 bar. This came with a combustion stability penalty however. Alternative ignition systems have

been demonstrated to improve dilution tolerance. One of these is the Corona Ignition System which has been shown by a number of researchers to give benefits, including Idecheria *et al.* [325] of General Motors. This allowed halving of the CoV of IMEP at an air fuel ratio of 26:1 when tested against a conventional coil and plug ignition setup. Non-thermal transient plasma ignition systems have also been described, by Singleton *et al.* [326] of Transient Plasma Systems, together with collaborators at Sandia and Argonne National Laboratories. The EGR limit could be improved by 3-6% in comparison to a conventional ignition system. Neither of these systems have yet to come to market however, with primary focus remaining on development of ignition coil and spark plug based systems to improve dilution limits.

EGR may be an effective solution on vehicles of low to medium power output, but for a high performance vehicle, it is not considered appropriate. This is because the heat rejection requirements of an EGR cooler in this horsepower range are difficult to manage in terms of vehicle packaging. Water injection is seen as an interesting alternative. A pioneering rediscovery of the potential of water injection to mitigate knock was proposed by d'Adamo *et al.* [327] of the University of Modena in 2015. A number of papers were presented on the subject at the 5th International Conference on Knocking Combustion in Berlin in 2017. Hermann *et al.* [328] of Opel gave an overview of the possibilities, which include plenum water injection, Port Water Injection (PWI), mixed Gasoline/Water Direct Injection (GWDI) and Direct Water Injection (DWI). The primary motivation is to increase stoichiometric power on downsized engines. The direct injection systems gave best performance, but would be most costly to introduce in production. Plenum injection performed poorly whereas Port Water Injection (PWI) was seen as a good compromise. Heinrich *et al.* [329] of Trier University of Applied Sciences performed a number of comparisons of PWI and GWDI systems. The GWDI system was shown to give significant reductions in preignitions. Hunger *et al.* [330] of IAV, together with collaborators at Daimler, showed the benefits of the DWI system including the possibility of phasing the water injection timing to maximize the end of compression temperature reduction. Both Ferrari and Porsche presented activity on water injection at the 2019 SAENA ICE conference in Capri. Paltrinieri *et al.* [331] of Ferrari presented experimental activity with PWI on a boosted single-cylinder research engine, complemented by CFD and chemical kinetics calculations. Limits to knock mitigation synergies of EIVC and water injection were evidenced, with combustion stability eventually suffering as shown in Figure 2.44. Vacca and Bargende [332] of the University of Stuttgart, together with collaborators at Brandenburg University of Technology and Porsche, presented on a simulation approach to validate various water injection strategies. Chemical kinetics were included in CONVERGE 3D CFD software and the Bradley detonation diagram was used to interpret results. CFD was supported by experimental activity on a transparent research engine where both PWI and DWI strategies were trialled. It was found that although the DWI system give a better knock limited combustion phasing, exhaust temperatures were lower for the PWI system due in part to more homogenous water distribution. Other researchers have employed a purely simulation based approach. Franken *et al.* [333] in 2020 used detailed chemistry in a quasi-dimensional Stochastic Reactor Model (SRM) together with a Bradley diagram interpretation, to investigate the efficacy of water on knock suppression for a range of fuels. RON 90 fuel with 50-80% water to fuel ratio was calculated to be similar in terms of knock resistance to RON 100 gasoline.

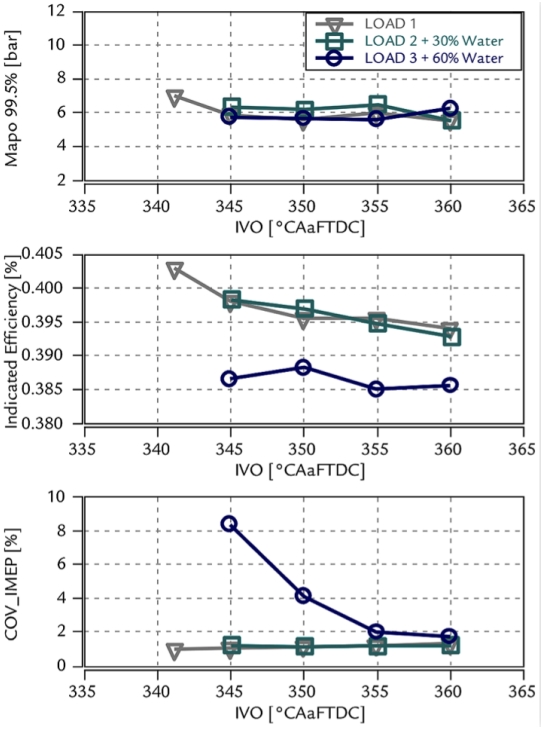

Figure 2.44: Combustion Stability Limitations of Combining Early Intake Valve Timing and High Water Injection Quantities, from Paltrinieri *et al.* [331]

Chemical kinetics is now routinely applied in CFD. Whereas in the past, dedicated chemistry solvers, notably CHEMKIN [334], needed to be coupled with 3D CFD code, modern CFD packages such as CONVERGE [335] and STAR-CCM+ [336] have integrated chemistry solvers. Whilst many surrogate reaction mechanisms have been widely applied over an extended period in ICE research, with perhaps the most obvious example being the historic Shell mech-

anism, updated mechanisms for even the most basic surrogate of gasoline - pure iso-octane - are still being published. Atef *et al.* [337] documented an improved iso-octane mechanism as recently as 2017. This was a large scale collaborative effort with authors from King Abdullah University of Science and Technology (KAUST), the University of Connecticut, National University of Ireland Galway and Lawrence Livermore National Laboratory. Primary validation data from rapid compression machines and shock tubes was in the range of 20-40 bar pressure and 632-1060 K temperature. Pressure conditions in the engine end-gas will routinely be significantly higher than this in full-load operation of modern downsized engines. One approach is to extrapolate trends to cover ranges beyond that of the rig experiments. Another is to apply a theoretically based *"ab-initio"* method. A review of the current status of "theory-informed chemical kinetics models" was given by Miller *et al.* [338] in 2020. Once again this was a large scale collaborative study with researchers from Argonne National Laboratory, Brown University, Columbia University, Sandia National Laboratories, the University of Colorado Boulder, the Technical University of Denmark and Southeast University, Nanjing. More theoretically based reaction modeling will undoubtedly have an impact on knocking analysis in internal combustion engines in the coming years.

The Miller cycle allows improvements in the knock limit without the necessity for additional cooling circuits or fluid systems. It is detrimental to volumetric efficiency however. It has been a key area of research and application in the last ten years. Whilst the original Miller concept is based on Early Intake Valve Closing [27], a similar effect can be achieved with Late Intake Valve Closing, as applied by Mazda in the 1990s [243]. A comparison of these two strategies was carried out by Luisi *et al.* [339] of Centro Ricerca Fiat (CRF) and Turin Polytechnic in 2015. EIVC has the disadvantage of reducing in-cylinder turbulence both for the early closing angle and the fact that a reduced lift is also frequently necessary to avoid excessive valve accelerations. In fact, on the 1.4 liter PFI test engine with a "MultiAir" Variable Valve Actuation (VVA) system, better knock limited combustion phasing at 2500 rpm for a given turbine inlet temperature was recorded for the LIVC strategy, as shown in Figure 2.45. This gain also translated into a relative reduction in component protection over-fueling. Such results depend somewhat on the base combustion system of the engine where testing is performed. A large scale project was undertaken by Ketterer *et al.* [340] of General Motors studying EIVC and LIVC strategies with dedicated combustion systems for each. Here it was found that at peak power the EIVC system had an advantage in terms of end of compression temperatures and hence knock limited combustion phasing, as it was more difficult to control the backflow of the LIVC concept at higher speeds.

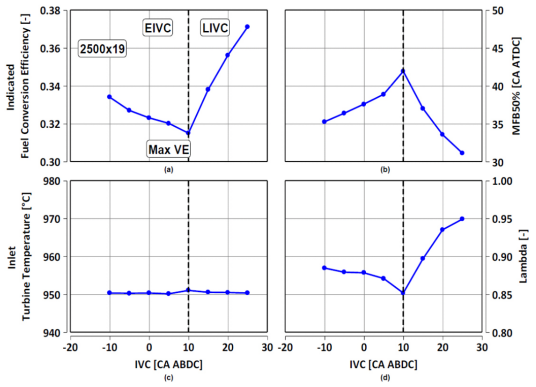

Figure 2.45: Comparison of EIVC and LIVC Miller Strategies on a 1.4 Liter VVA Engine at 2500rpm and 19 bar BMEP by Luisi et al. [339]

Gas dynamics tuning has long been known as a method of increasing the volumetric efficiency of high-performance NA engines and a detailed discussion was given by Blair of Queen's University Belfast in his book published in 1999 [341]. Finite amplitude wave reflections are harnessed in order to increase massflow in the intake system and pressure at the intake valve, in particular in the intake ramming period between Bottom Dead Center (BDC) and IVC[18]. The increased pressure before IVC also means increased temperature with respect to plenum conditions however. This hot charge is ingested by the cylinder and of course this increases the risk of knock. Such "positive" tuning is normally reserved for high-speed, high-performance NA engines where knock is unlikely to occur. In 2012, Taylor and collaborators at Mahle investigated tuning effects on a downsized turbocharged gasoline engine [342]. The standard turbocharged engine approach of "inert tuning" - use of very short intake runners to avoid wave action - was compared to conventional intake tuning for increasing volumetric efficiency and "anti-tuning", where the goal was to have low pressure at IVC. This last option means that the intake valve is open during an expansion in the intake system and hence local gas temperature will also be lower than plenum conditions.

[18] Whilst filling/emptying isentropic models are frequently applied at the intake valve, flow in the intake ducts depends on the pressure of oppositely moving waves in the intake system, each contributing to particle flow. The basic equation is shown in Equation 2.17 where c is the particle velocity, a_0 is the acoustic velocity for undisturbed conditions, p_0 is the pressure at undisturbed conditions, p is the pressure of the wave and γ is the ratio of specific heats. This needs to be applied separately for superimposed waves in opposite directions calculated in unsteady gas dynamics code whilst only the superposition pressure can be measured experimentally [341].

$$c = \pm \frac{2a_0}{\gamma - 1} \left[\left(\frac{p}{p_0} \right)^{\frac{\gamma-1}{\gamma}} - 1 \right] \tag{2.17}$$

It can therefore be considered a sort of gas-dynamics Miller cycle and in fact a 5% improvement in BSFC was obtained at high speed and load. The disadvantage is that volumetric efficiency decreases, as per an EIVC or LIVC strategy, and also that intake lengths of over one meter would be required for effective anti-tuning at 5000 rpm.

Prechamber research for automotive applications has increased in recent years. A large scale literature survey was performed by Toulson and Schock, of Michigan State University together with Attard, of Mahle Powertrain in 2010 [343]. Toulson and Attard had previously researched prechambers at Melbourne University. In the review, prechambers were classified based on presence of auxiliary fueling and volume as a percentage of clearance volume. The survey went back to 1918 and the Ricardo Dolphin engine mentioned in Ricardo's 1921 paper and already cited in the present work [33]. Attard published extensively on prechambers in the following years, with colleagues at Mahle Powertrain, both on lean combustion with an actively fueled prechamber [344–347] and highlighting the knock gains even for stoichiometric conditions and passive prechamber technology [348]. In this last work, testing was performed on a modern PFI engine with a pent-roof combustion chamber based on a GM Ecotec LE5 design. At Maximum Brake Torque (MBT) ignition timing, a PRF 96 blend with conventional spark ignition corresponded to PRF 86 with the prechamber igniter, as shown in Figure 2.46. Whilst there has been a lot of activity since then by a large number of universities, research organizations and car companies, it was not until 2020 that a manufacturer would once again prepare to go into production with a prechamber engine. The manufacturer was Maserati. Its engine also features an additional spark plug in the main chamber as described in the patent by Mazzoni *et al.* [349]. It produces 210 CV/L (154 kW/L) and has a compression ratio of 11:1 [350]. The secondary plug is shown mounted laterally in the combustion chamber in the patent application. An alternative layout with a secondary spark plug arranged in a manner to guarantee that "spark-coupled" injection strategies can still be used in catalyst heating was patented by Corrigan *et al.* [351] of Ferrari later the same year.

Research of CAI continued with increasing interest in Spark Assisted CAI techniques. Yun *et al.* [352] of GM used spark assistance to extend the maximum load limit of a stoichiometric EGR CAI engine. This relied on both external EGR and adjustable negative valve overlap for adequate dilution and charge temperature management. As had been observed by previous researchers, consuming part of the charge by flame-front propagation resulted in an extended overall burn duration and hence lower ringing noise. Manofsky *et al.* [353] also used a negative valve overlap strategy combined with external EGR and spark assistance to study stoichiometric load

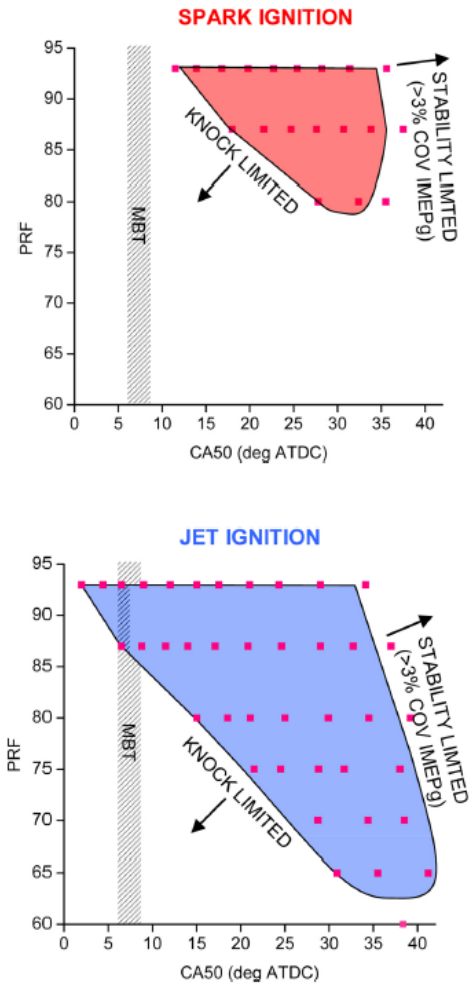

Figure 2.46: Knock Limit Benefits in Terms of Combustion Phasing (CA50) And Octane for a Passive Prechamber System, from Attard *et al.* [348]

extension on a HCCI engine. The engine had a compression ratio of 12.5:1 and direct injection. 7.5 bar IMEP was reached before knock began to occur. Up until that point, ringing intensity was well below the limit value. The operating map achieved is shown in Figure 2.47. Alternative techniques exist to extend HCCI load limits without knocking. A combination of boost and 60% EGR allowed Dec *et al.* [354] of Sandia to demonstrate 16 bar IMEP. Even if knock doesn't occur, ringing combustion is a problem with HCCI and hence much activity was carried out to connect pressure waves to heat release. Maria *et al.* [355] of MIT used cylinder pressure measurements and microphone analysis to correlate between acoustic and combustion data. A correlation between pressure oscillation amplitude Δp and maximum pressure rise rate $\frac{dp}{dt}$, originally demonstrated by Eng [264], was modified to account for expansion work from the initial autoignition event. This gave a consis-

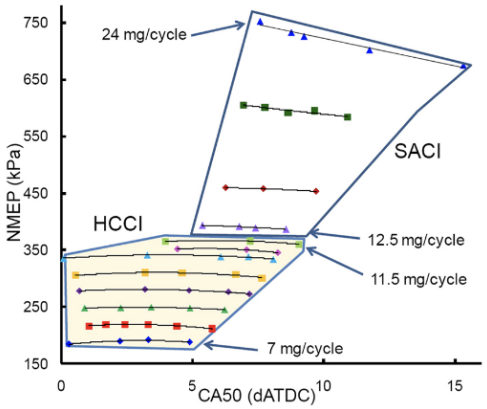

Figure 2.47: HCCI and SACI Operating Ranges from Manofsky *et al.* [353]

tent proportionality constant $\beta = \Delta p / \frac{dp}{dt}$ over a wider range of operating conditions than the original Eng correlation. The transition from controlled HCCI to knock was studied by Iijima *et al.* [356] of Nihon University. It was found that knocking intensity was correlated with time based maximum pressure rise rate in experiments on an optical access HCCI engine. For non-knocking combustion, multiple autoignition events took place over around 5° CA at 1200 rpm. For knocking combustion, a large end-gas region was seen to ignite with a reaction front velocity of around 540 m/s. In further measurements the following year [357], autoignition fronts at up to 1200 m/s were seen. Strong light emission from the CO-O reaction was observed at maximum pressure rise rate. Very strong knock resulted in higher excitation of the second transversal acoustic mode of the combustion chamber.

In 2019, a CAI engine finally made production. This was the Mazda Skyactiv-X engine which was described at the 28th Aachen Colloquium on Automobile and Engine Technology by Nakai *et al.* [358]. It has a compression ratio of 16.3:1 and is supercharged. The engine appears to function in a manner similar to that described by Urishihara *et al.* of Nissan in 2005, although it features only GDI fueling rather than a combined PFI/GDI setup. The engine transitions from HCCI to SACI to conventional SI as load is increased. A piezoelectric cylinder pressure transducer is used as the feedback device to manage the combustion process. The model based control system predicts both flame propagation and end-gas conditions. A 700 bar centrally mounted GDI system together with controllable swirl can be used to control mixture distribution and hence end-gas cooling. Depending on the operating regime, the engine can run stoichiometric, lean or lean with EGR. In some operating points it has a better BSFC than the company's diesel engine.

Ethanol, which had been shown to be effective against knock by Ricardo in the 1920s [33], has again been investigated by a number of researchers in recent years. Ethanol from biological sources is potentially carbon neutral and a further impetus for its use on the US market was with a view to greater US energy independence, as described by Kasseris and Heywood [359] of MIT. Ethanol also has a much higher latent heat of vaporization in comparison to typical non-oxygenated hydrocarbons used in gasoline blends. For stoichiometric mixture with air, it is four times higher than gasoline. This gives improved charge cooling, particularly on direct injection engines. Kasseris *et al.* showed that with a direct injection engine, this charge cooling benefit was almost linear as ethanol was added to premium gasoline, with a RON of 97, up to the maximum concentration tested of 85%. The chemical octane benefit may saturate at 30-40%. Ethanol as a fuel was also being tested by Steurs *et al.* [360] at the Swiss Federal Institute of Technology at the time and comparisons were made to a number of ignition delay models in the literature [361]. A large scale investigation was carried out by Leone [362] and colleagues at Ford, in collaboration with AVL, on a modern 3.5 L turbocharged GDI engine. Both "splash blends" (where ethanol was added to an existing gasoline in various concentrations) and "matched blends" (same RON and similar MON) were tested for E10, E20 and E30 fuels. Testing was performed both at the standard compression ratio of 10:1 and at increased compression ratios. Only marginal gains were observed for matched E20 and E30 blends and only for high load and retarded conditions. Adding 10% of ethanol to existing E10 fuel gives an improvement in RON of six units however, together with higher sensitivity, allowing a two point increase in compression ratio. The Lower Heating Value (LHV) of ethanol is significantly less than that of non-oxygenated gasolines and hence compression ratio needs to be increased together with RON in order to arrive at a similar or better fuel economy in terms of Miles Per Gallon (MPG). Chupka *et al.* [363] at the National Renewable Energy Laboratory performed Heat Of Vaporization (HOV) measurements on gasoline/ethanol blends using two different methodologies. HOV is a function of temperature and reduces to zero as this becomes critical. This is strongly the case for ethanol whose HOV halves from 50° C to 200° C. E20 at 50° C has an adiabatic temperature drop of 28° C in comparison to 21° C for E10. It is not clear how much of this HOV increase is included in the RON result on a CFR engine, where air temperature is controlled before fuel addition to the intake.

Using methane as a fuel could assist in reducing CO_2 from ICE vehicles, as described by Binder *et al* [364] of IAV. Methane can be produced from fossil fuels but also from biological sources or methanation of hydrogen. If the hydrogen is generated by electrolysis making use of carbon neutral electricity, a so-called Power-to-Gas (PtG) "e-Fuel" results. Energy is lost in each step going from electricity to an e-Fuel and hence such an approach

makes most sense as a method of storing energy when there is excess grid capacity. Exhaust gas after-treatment of methane engines is also difficult at low load and cold start. Hybridization and an electrically heated catalyst were suggested to combat this. Methane has better knock resistance than conventional gasoline however, and hence the compression ratio can be increased by around two units by switching fuels. An active prechamber, with an integrated air-assisted fuel injector, was also used in this study to further improve the knock-limit. This gave the possibility to raise the compression ratio a further two units. A final compression ratio of 17:1 was used with a specific power output of 58 kW/L. The potential of a methane based ICE was also demonstrated by Stoffels *et al* [365] of Ford in collaboration with Continental Powertrain, Luk and Schaeffler Technologies. Here, a strong downsizing approach was taken. A three cylinder engine of just 1 L capacity achieved 112 kW/L specific output with a compression ratio of 13:1. A 48 V electrically assisted compressor in series with a turbocharger with variable intake geometry was used to give adequate low end torque and transient response. Similar performance was demonstrated to a 1.5 L turbocharged GDI engine. 5% efficiency was gained from downsizing (largely enabled by methane's improved knock resistance) and a further 12% from the use of a 48V mild hybrid system. Considering the lower carbon density of methane in comparison to gasoline, CO_2 on a WLTC cycle could be reduced by 35% even if the fuel were fossil derived.

Hydrogen can also be used as an ICE fuel, as tested by Ricardo [33] one hundred years ago. Its high laminar flame speed allows significant dilution increases in comparison to gasoline, as already demonstrated in that period. Hydrogen also has good knock resistance in RON testing. The main obstacle to its use is the low density of the gas. This necessitates high pressure storage or cryogenic solutions, as described by Johnson *et al.* [366]. Despite tank pressures of 700 bar and the increased efficiency of fuel-cells in comparison to ICE, particularly in part-load conditions, hydrogen tank volumes are typically four times larger for a FCEV in comparison to gasoline fuel tanks of an ICE vehicle of similar range. If the hydrogen refueling network is developed in the coming years primarily for fuel-cell vehicles, it may make sense to further evaluate hydrogen also as an ICE fuel, in particular for applications where the engine operates consistently at high loads and/or peak efficiency. An estimated 45% brake thermal efficiency was exceeded at 2000 rpm and 13.5 bar BMEP by Matthias *et al.* [367] of Argonne National Laboratory in 2012. This result was based on measurements on a single-cylinder engine with turbocharger simulation and multi-cylinder friction estimation. The engine ran at around $\lambda = 3$ for most of the operating range with a compression ratio of 13:1. The engine efficiency map is shown in Figure 2.48.

Methanol is an alternative energy carrier which has the

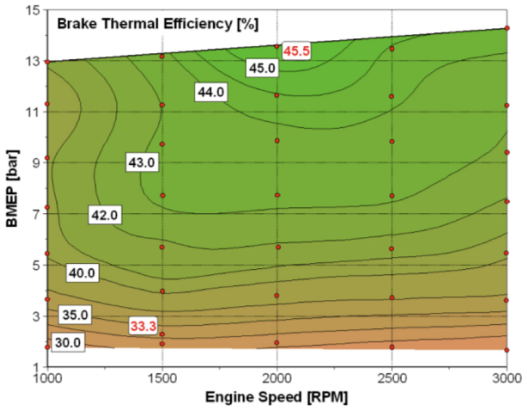

Figure 2.48: Hydrogen ICE Efficiency Map, from Matthias *et al.* [367]

advantage of being a liquid at ambient conditions. It can be created through a number of routes including notably the Fischer-Tropsch process [20]. Another method is the co-electrolysis of H_2 and CO_2. This is a Power-to-Liquid (PtL) e-fuel. Biological pathways are also available. Methanol is a very interesting fuel from a knock point of view with a blending RON value[19] in the range 115-130 [40] and has been used in racing series in the past, notably Indycar. It can be further processed to produce a synthetic gasoline. This gives a so-called "drop-in" solution to reduce CO_2 output from the existing SI vehicle fleet. This approach is being studied by the C3 (Closed Carbon Cycle) Mobility consortium. Over 30 companies are involved including vehicle and engine manufacturers, universities, research organizations and a major energy company [368].

Conventional gasoline is also likely to further evolve in the near future as well. Concawe, a research consortium of many major European energy companies, published two reports in 2020 on the benefits of moving to higher octane fuel. The first of these, by Williams *et al.* [369] studied the impact of increasing RON on a downsized three cylinder engine with a compression ratio of 12.2:1 and a maximum BMEP of 30 bar. RON was swept in steps from 95 up to 102. The combustion phasing was improved by around 5° CA of MFB50 (50% MFB) with the highest octane variant, widening the high efficiency region of the BSFC map. In Real Driving Emissions (RDE) type cycles, fuel efficiency was improved by as much as 4% at the tested compression ratio. Including the gain from compression ratio increases, the estimated benefit was a reduction in CO_2 of around 5% in both emissions cycles and real driving conditions. The addi-

[19] Octane values "blend non-linearly" by volume fraction and individual components often behave differently from a knock resistance point of view in combination with others. Blending of hydrocarbons to achieve a certain octane quality is therefore complex and generally supported by a combination of modeling and trial-and-error [40].

tional CO_2 emitted by refineries to produce higher octane fuel must also be taken into account for a Well-to-Wheel analysis. A follow-on report by Valdenaire *et al.* [370] suggested a significant saving in total CO_2 WtW emissions could be achieved if 50% of gasoline sales became RON 102 and engines were adapted to use of the fuel. This would likely require greater use of oxygenated fuel components and in particular MTBE.

Kalghatgi had introduced his "K-factor" concept in the previous decade. His collaborator, Amer [371] at Saudi Aramco, investigated the K-factor for a matrix of 15 fuels with decorrelated RON and Sensitivity at up to 3.4 bar absolute manifold pressure on a direct injection single cylinder engine with compression ratios of 8.5:1 and 10:1. As boost pressure increased, the K-factor was found to decrease as far as -0.93. Temperature at 15 bar compression pressure was suggested as an index to compare to RON and MON conditions. Kalghatgi in 2014 commented that PRF fuels were fundamentally not representative of modern gasolines and hence it would make sense to move to an n-heptane/toluene rating scale [372][20]. Kalghatgi showed that typical modern gasolines could be much better matched in terms of RON and Sensitivity and, as a consequence, in terms of knock limited performance on a modern boosted engine, with binary toluene/n-heptane blends. A perfect match of RON and Sensitivity is possible with a three component surrogate (iso-octane, n-heptane, toluene). Kalghatgi presented simple formulae to allow calculation of RON and S of such ternary mixtures based on toluene mole fraction [373]. Fitting of such blends was carried out to the Andrae kinetics mechanism and subsequent quasi-dimensional engine calculations showed good agreement with testing on a PFI single cylinder engine at 1.6 bar manifold pressure. In 2020, Gail of Shell together with colleagues and collaborators at RWTH Aachen University and Ferrari compared an alternative surrogate formulation to premium RON 98 gasoline in an RCM and a high performance GDI engine [374]. The surrogate was based on Toluene, n-Heptane and Iso-Pentane (THIP). It is easier to match fuel vapor pressure using these components than with a traditional TRF blend. Good agreement to the target gasoline was found both in RCM testing and in terms of the knock limit on the engine. A number of chemical kinetics mechanisms were compared to the experimental data including the 2012 LLNL model of Mehl *et al.* [375]. A simpler model was that of Tsurushima. This was applied by Kitada of Mitsubishi and compared to measurements of a 1.2 L three cylinder engine with compression ratio of 13:1 on PRF 95 fuel [376]. In order to match the experimental pressure curve, Low Temperature Heat Release (LTHR) had to be taken into account. This was shown to increase the end of compression temperature by almost 100 K. A modified version of the Douaud equation was proposed including a term for equivalence ratio ϕ as shown in Equation 2.18.

$$\tau = 0.01869 \left(\frac{OCN}{100}\right)^{3.4017} \left(\frac{P}{P_0}\right)^{-1.7} \phi^{-1.7} exp\left(\frac{3800}{T}\right) \tag{2.18}$$

The Douaud and Eyzat method is based on Arrhenius-like behavior, which can be prone to significant error for fuels with NTC regions. Yates had suggested a method to fit to ignition delay data of such a fuel using three ignition delay terms instead of one in 2005, as shown in Equation 2.16 [295]. Fandakov of the University of Stuttgart proposed an alternative approach based on two stage ignition with a triple Arrhenius fit for high temperature and double Arrhenius fit for low temperature conditions [377]. This was applied to ethanol containing surrogate blends based on chemical kinetics calculations with 500 species. A larger mechanism was used by Kim of Sandia in 2019 for ethanol containing blends. This LLNL mechanism featured 2871 species and 12,804 reactions [378]. Surrogates using nine base hydrocarbons were used to model alkylate, aromatic and ethanol blends with matched RON of 98. It was shown that at high temperatures, E30 had shorter ignition delay times than an aromatic blend, even allowing for charge cooling. LTHR was shown to be most significant for alkylates and least for ethanol. The alkylate fuel was the only one with a true NTC region, although regions of reduced temperature sensitivity were also visible for aromatic and to a lesser extent ethanol blends. The effect is that thermal stratification tends to decrease during compression and early combustion for alkylate blends, meaning more likelihood of autoignition in a cool zone and greater probability of fast sequential autoignition. This study also compared lean running with EGR in comparison to experimental results. It was shown that lean running did not improve the knock limit, and this was traced to an increase in LTHR and NO, both of which are significantly reduced by N_2 and CO_2 dilution.

Chemical kinetics are now routinely used either directly, or in look up table form, in 3D CFD. In a real engine with cyclic variability, the combustion phasing is generally managed such that knocking cycles are rare. They will typically be faster burning than the average cycle. RANS (Reynolds Averaged Navier Stokes) is still the most common 3D-CFD approach, but results in a prediction of an average combustion cycle. Large Eddy Simulations (LES) fundamentally calculate cyclic variability and hence are ideal for knocking investigations, but are more computationally intensive. In 2013 Fontanesi *et al.* [379] of the University of Modena applied LES calculations with detailed chemistry to a high performance Ferrari road car engine. Ignition delay was taken from pre-calculated look up tables as a function of pressure, temperature, mixture strength and residuals. Both the Andrae (138 species) and an LLNL

[20] Ricardo had suggested in 1922 to use another aromatic, benzene, as the knock resistant hydrocarbon in the rating scale [33] but in the end, iso-octane became the knock-resistant reference for RON and MON testing as already discussed. At the time typical octane values were in the range 40-60 and fuel sensitivity was also lower [54].

mechanism with 1389 species were applied. A knock margin was defined for each cell in the unburnt range of a number of spark advance angles. Three example cycles are shown in Figure 2.49. LES was also used to

Figure 2.49: Three LES Cycles Showing Flame-front Progress and Autoignition, from Fontanesi *et al.* [379]

study knock in an ICE by Robert *et al.* [380] of IFPEN in 2015 with a particular emphasis on the Deflagration to Detonation Transition. Three different spark timings with different corresponding knock amplitudes were simulated. Tabulated kinetics were once again employed. 15 LES cycles were compared to an experimental dataset of 500 cycles. A BPF MAPO calculation was performed from 5-9 kHz on both experimental and simulation data. A non-linearity of MAPO against mass burnt by autoignition was observed suggesting a mode transition. Realistic single cycle reactivity gradients also permitted calculating ξ in order to perform the Bradley correlation. Assumptions had to be made to estimate ε which depends on local length scales. The analysis in any case suggested that many cells were in the developing detonation region for the most advanced cycles simulated. A mathematical function was created to indicate if individual cycles were in the detonation peninsula. This agreed well with direct analysis of the LES data where coupling of autoignition and pressure fronts was observed. Often the DDT did not occur from the first autoignition location each cycle meaning that reacting flows must be simulated to evaluate detonation risk.

LES can also be applied to optimization of in-cylinder flow. As with any other computational technique, it is important to validate the methodology. Ritter *et al.* [381] of IFPEN compared LES simulations of charge motion and mixture formation in CONVERGE software to high speed PIV and Laser Induced Fluorescence (LIF) measurements of an optically accessible direct injection engine in 2020. 40 PIV cycles were compared to ten cycles in LES. It was remarked that ten LES cycles give a reliable average result, although it was spatially somewhat "noisier" than the average PIV results as can be seen in Figure 2.50. In-cylinder equivalence ratio distributions calculated with LES were also well aligned on average to LIF mixture measurements. Here 12 cycles were thought insufficient however to fully capture the real cyclic variability of the process. LES techniques are expected to become increasingly common in industrial environments, driven by improvements in processing power and software. This will enable optimization of cyclic variation in a much more direct manner in CFD than was possible in the past. As knocking cycles are generally the most advanced combustion cycles in a given population, understanding and reducing cyclic variability is key in improving the knock limited compression ratio that can be used.

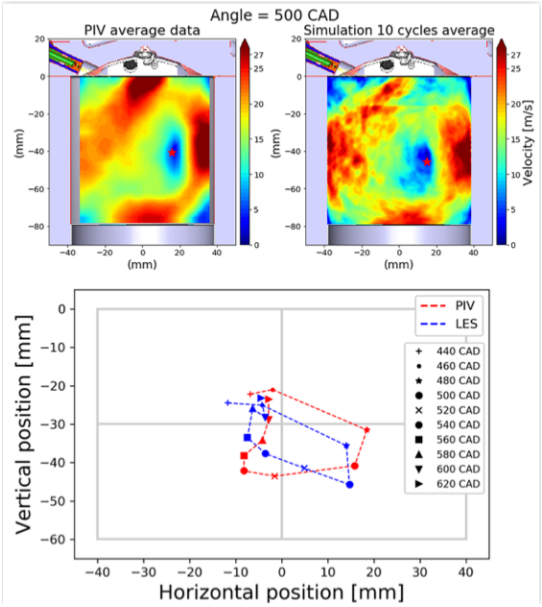

Figure 2.50: Comparison of Average PIV and LES Data of In-Cylinder Flow, from Ritter *et al.* [381]

A computationally less intensive alternative to LES is to approximate cyclic variability using RANS CFD. Corti *et al.* [382] of the University of Bologna, used calculated variability in equivalence ratio and turbulence in a sphere around the spark plugs of a 599 cm^3 two cylinder motorcycle engine, taken from RANS CFD, to perturb laminar flame speed and turbulence parameters in the model. D'Adamo *et al.* [383] of the University of Modena applied PDF (Probability Density Functions) of temperature and equivalence ratio in individual cells of a RANS simulation to estimate knocking probability in CFD. This was further developed in a subsequent publication [384]. Breda *et al.* [385], again of the University of Modena, would tune RANS calculations in STAR-CD software to match the statistically fast burning combustion profile of knocking cycles measured in an optically accessible GDI engine.

3D-CFD is now a standard combustion development tool, but researchers have continued to work on zero-dimensional models due to their computational simplicity and hence rapid speed. Turbulence and engine geometry effects can still be included, albeit indirectly. Bjerkborn *et al.* [386] of LOGE AB applied Monte Carlo techniques to a two zone Stochastic Reactor

Model (SRM). Here the mass of each zone is divided into a number of particles. The particles change from unburned to burned as the calculation progresses. Flame volume is assumed to be spherical but interacts with the combustion chamber walls. Detailed chemistry from a 200 species PRF mechanism was used both for ignition delay times and laminar flame speed. Kozarac *et al.* [387] of the University of Zagreb divided the unburnt region of a zero dimensional model into around 20 bins covering a range of thermal stratification of 200 K at each timestep. LTHR was included. A fractal model was used in 1D code for cyclic variation. Both LLNL and Andrae mechanisms were applied. Good agreement was demonstrated with KLSA of a CFR engine. Bozza *et al.* [298], of the University of Naples, also applied fractal combustion models in a 1-D engine simulation environment in the same year. A starting MFB curve was modified for cyclic variation based on experimental analysis. De Bellis *et al.* [388], also of the University of Naples, showed how cyclic variation could be correlated to combustion phasing and duration on a given engine. A three component surrogate reaction mechanism was employed and good agreement in terms of knock was seen, when comparing the fast-burning cycles from the simulation, with that those of high performance naturally aspirated V12 Lamborghini engine [389]. The fractal approach was also used by Fontanesi *et al.* [390] in knock tendency analysis of a small VVA engine with turbulence in the 1D model being calibrated from 3D CFD results. Kikusato *et al.* [391], at Waseda University, used a two-zone combustion model where chemical kinetics, in this case the original Shell model, were coupled to thermal calculations of the combustion chamber walls. Transient maneuvers showed that such temperatures may not stabilize for up to 20 seconds after a sudden load change. The model was then used to evaluate application of coatings to reduce heat losses, ideally without worsening the knock limit. The concept is to have a very dynamic wall temperature with variations of several hundred Kelvin in the cycle to avoid heating up the charge from the walls during compression and to avoid excess heat transfer during regular combustion. It was subsequently shown that this was possible through careful application of coatings with low thermal inertia and thicknesses of the order of 0.1 mm, although it became more difficult to achieve a knocking gain as load increased [392].

The concept of developing detonation, explained by Bradley in 2002 as depending both on the resonance factor ξ and ε, the rate at which heat release is loaded into the acoustic wave, was applied by a number of researchers to the SI engine "super knock" phenomenon. Superknock occurs when a Low Speed Pre-Ignition (LSPI) event turns into developing detonation. The LSPI itself is typically driven by particles or droplets of fuel/oil mixture. Peters *et al.* [393] of RWTH Aachen used dissipation elements in Direct Numerical Simulations (DNS) to estimate the dimension of the thermal gradient around exothermic centers in 2013. This depends on the integral time scale which is large when mean velocity gradients are low. Excitation times were calculated in chemical kinetics simulation. The outcome was then used in RANS 3D CFD simulations of a GDI engine over a range of conditions. Developing detonation was seen to be more likely at low speed and high load as expected. Lauer *et al.* [394], of the Technical University of Vienna, used Lagrangian tracking of droplets to infer tendency towards LSPI in a CFD model of a GDI engine in STAR-CD software in 2014. Liu [395] of Tsinghau University together with collaborators there, and at the University of Michigan and Cherry Automobile, studied super-knock both on a 1.6 L four cylinder turbocharged GDI engine and an optical RCM. On the engine, super-knock was found to take place only over a range of spark advance at low temperatures and high charge densities. In RCM testing, sequential autoignition was interpreted as normal knock and developing detonation as a super knock mode. Starting in the super knock mode in the RCM, whilst increasing the temperature, the combustion mode was seen to transition back to sequential autoignition. The difference in appearance of the various autoignition modes could be clearly seen in the optical access RCM as shown in Figure 2.51. In 2017, Liu together with Wang [36] of Tsinghau University, along with Reitz of the University of Wisconsin-Madison, published an extremely detailed review of the current status of the literature on knock and pre-ignition. Particular emphasis was placed on transitions from deflagration to detonation modes and the importance of shock wave reflections near the combustion chamber walls. Over 300 papers were reviewed with more emphasis on recent activity than in the current work.

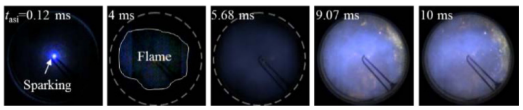

a. Normal flame propagation (p_{EOC} =11 bar, normal combustion condition)

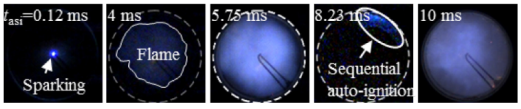

b. End gas sequential auto-ignition (p_{EOC} =14 bar, knock condition)

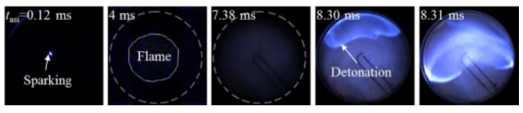

c. Detonation (p_{EOC} =25 bar, super-knock condition)

Figure 2.51: Flame-front Propagation, Sequential Autoignition and Detonation in a Rapid Compression Machine, from Liu *et al* [395]

Kalghatgi, who is acknowledged by Bradley as having

contributed to discussions in his 2002 paper [263], published on super knock in 2017. He showed that the resonance parameter ξ could be calculated from engine pressure data. Some assumptions were required to calculate the reactivity parameter ε. He used this theory to explain the conditions necessary to obtain super knock from preignition in modern downsized engines [396]. In 2018, Ohtomo *et al.* [397] of Toyota Central R&D Labs studied how to achieve autoignition without knock both in an RCM and in an engine through dilution. H_2 was mixed with gasoline in the engine intake to allow dilution levels up to 50%. A band was shown on a load / dilution diagram where autoignition was possible without knock. Cho *et al.* [398], of Seoul National University, separated the ξ term into equivalence ratio and temperature gradients. The RON test condition on iso-octane was simulated in a multi-zone zero-dimensional model using initial size and equivalence ratio gradients of rich and lean spots from Planar Laser Induced Fluorescence (PLIF) measurements at a higher engine speed. An RCM replicated pressure-temperature history that was expected in the engine. Local temperature was correlated with local equivalence ratio, due to specific heats and evaporative cooling. Lean spots are therefore more likely to be autoignition centers and lead to knock.

Optical measurements of conventional SI combustion have continued of course. Catapano *et al.* [399], of CNR (National Research Center), showed in testing on a GDI engine with a Bowditch piston, that autoignition generally occurred in regions of negative flame curvature. This could also be captured in CFD. The Shell model was also used in CFD and key reactive species concentrations from the model were correlated with experimental autoignition locations. The same researcher published a paper a few years later on split injection with a four cylinder 1.75 L engine with direct injection. Again a Bowditch piston was employed and optical measurements of the flame-front were taken at 50,000 frames per second. A new optically based knock index was described: MACLO (Maximum Amplitude of Centroid Luminosity Oscillation). When knock occurred, the flame centroid could be seen to oscillate at 6 kHz. Examination of centroid movement could also evidence multiple autoignitions, even if they were outside the field of view of the optical window [400]. An example is shown in Figure 2.52. Imaoka *et al.* [401], of Nissan, used laser induced phosphorescence thermography to measure piston crown temperatures in a 2 L normally aspirated GDI engine and a single cylinder equivalent. Despite using a piston bowl with a sharp edge, no hot spots were seen in this region. The study was notable also for using five separate cooling jackets - head inlet, center and exhaust sides, upper and lower liner. Lowering head intake side coolant temperature gave the greatest improvement in the knock limit. CFD suggested that 40% of the heat transfer to the charge was from the intake port. A plastic port liner improved the knock limit by 2° CA MFB50. Iijima *et al.* [402] of Nihon University performed optical measurements on a side spark and side valve engine at 500,000 frames per second. The engine had no cooling system and hence transitioned progressively into knock as it warmed up. Frequently, the first autoignition event led to subsequent events in the vicinity allowing optical identification of a reaction front. It was seen that such a front could propagate at a range of velocities from subsonic to supersonic, as shown in Figure 2.53. The knocking intensity as judged by cylinder pressure measurements was correlated with the reaction front velocity - strong pressure oscillations were correlated with detonation waves.

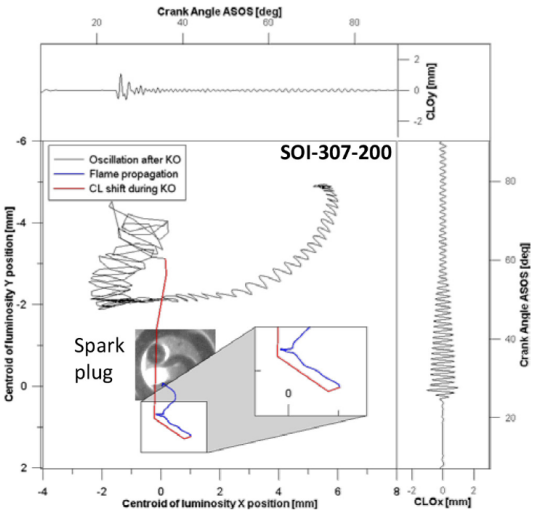

Figure 2.52: Flame Centroid Movement During Knocking Combustion as Measured by Catapano [400]

It is interesting that despite the fact that the CFR engine is almost 90 years old, and is the basis of fuel RON and MON measurements, it is still not fully understood today. Huber *et al.* [403] of Ingolstadt University of Applied Sciences performed investigations on modernizing the test procedure and engine using an ECU (Electronic Control Unit), PFI, lambda control and pressure indication in 2013. Pal *et al.* [404], at Argonne National Laboratory, created what they suspected to be the first 3D CFD model of a Waukesha CFR engine in 2018. Multicycle RANS with detailed chemistry was implemented in CONVERGE software. The G-equation was used for turbulence modeling, with laminar flame speeds from chemical kinetics. The engine was X-rayed to obtain the geometry of the head and water jacket to parameterize a 1D model. The engine was instrumented with intake, cylinder and exhaust dynamic pressure sensors, a lambda sensor and thermocouples. It was calculated that running iso-octane in the RON test condition, residuals were around 6%. Simulations suggested knock occurred towards the exhaust side, due to flame bias towards the intake, driven by asymmetric flow from the

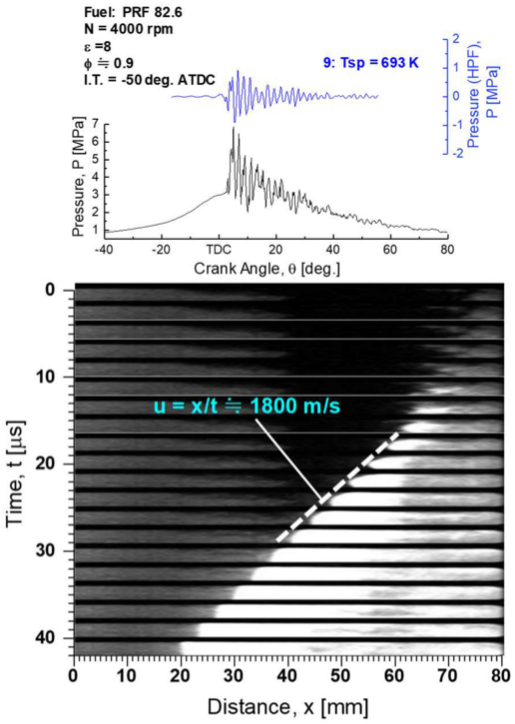

Figure 2.53: Supersonic Reaction Front Identifed by Iijima [402]

shrouded intake valve. Rockstroh *et al.* [405], also of Argonne National Laboratory, compared a wide range of cylinder-pressure based knock metrics to the standard CFR 501-C knockmeter. Correlation between the knockmeter and common modern indices such as MAPO was very poor. There was some correlation with peak pressure and rate of pressure rise. The knock meter features a low pass filter and hence is not sensitive to information in the 6 kHz range, which is the lowest acoustic mode commonly excited in this engine by knock. RON testing, according to ASTM D2699, is performed at maximum knocking lambda (and fixed ignition timing). The effects of these two variables had been investigated in 1931, just before the RON method was made official, by Campbell and collaborators [61]. The impact of this was revisited by the Argonne team in 2019 and described in a paper by Hoth [406]. It was found that peak knock lambda was generally slightly rich for all blends, but was around 0.88 for PRF fuels and as lean as 0.95 for aromatic and ethanol containing mixtures. This means that such fuels are not compared at the same lambda in standard RON tests. Paraffinic fuels were found to have a steeper gradient of knock with lambda, but also to give higher MAPO values for a given knock meter reading in the standard "peak knock lambda" test condition. These two effects somewhat compensate each other and mean that MAPO based RON values at stoichiometry are not dissimilar for fuels of different chemistry but similar RON. The MFB50 for a given spark timing was found to be within 1.5° CA for all fuels, with only a slight reduction for those containing high ethanol concentration.

Knock control understanding has also increased in the last ten years. With modern ECUs, it has become possible to introduce basic simulation models into real-time control systems. Xiao *et al.* [407] of Clemson University demonstrated the feasibility of a real-time capable model, which could suggest knock limited ignition timing, using a Douaud and Eyzat ignition delay model for knock and a Blizard and Keck turbulent entrainment model for flame-front propagation. It was suggested that such a model could be used for fuel adaptation, but would likely require cylinder pressure sensors. A similar system would appear to now be in production on the Mazda Skyactiv-X engine [358]. Corti *et al.* [408], of the University of Bologna, suggested a somewhat similar approach in 2017. A triple Arrhenius function was used for ignition delay times, based on the output of chemical kinetics calculations. A combustion progress variable was based on a linear fit through 10% and 50% MFB points and then extrapolation to zero and 100%. Both 10% and 50% MFB were assumed to be normally distributed. A further simplification was that when knock occurs, the entire mixture was assumed to autoignite. A normal distribution of unburnt gas temperature was considered and a calibrated temperature at intake valve closing initially imposed and then adjusted based on measured feedback. A 99th percentile MAPO was predicted by the model and it corresponded closely to experimental data when tested on a Ducati motorcycle engine.

A number of papers on knock statistics and control were published by Peyton Jones and collaborators at Villanova University. Spelina *et al.* [409] gave an overview of knock simulation and control in 2014 and she suggested that, although most production knock controllers aim for around 1% of strong knocking cycles, controller stability would be greatly improved by targeting around 20% of weak knocking events. Peyton Jones *et al.* [410] elaborated on this concept the following year and described a weighted error function to enable threshold optimization to correctly weight false-positive and false-negative errors. Further details on control oriented simulation techniques were published one year later with the importance of considering the stochastic element highlighted [411]. MAPO remains the most common knock index, but Siano [412] of the Istituto Motori CNR compared knock detection based on autoregressive models, a normalization of knock pressure oscillations and online calculated discrete wavelet transforms. The autoregressive model appeared to have an advantage in terms of sensitivity over the conventional MAPO approach.

Some of the highest efficiency knock-limited engines are currently found in Formula 1. Turbocharged engines returned to the sport in 2014 together with a fuel mass

flow limit of 100 kg/h. This effectively turned Formula 1 into a BSFC competition and hence development principally focuses on reducing knock to allow increasing of the compression ratio. As such, both EIVC and antituning are applied to minimize the end of compression temperature for a given geometric compression ratio, as documented by Rosetti *et al.* [413] of Ferrari and shown in Figure 2.54. The engines also run lean in full load

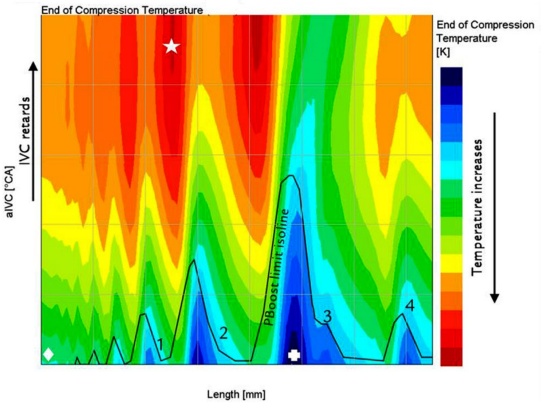

Figure 2.54: Influence of Intake Runner Length and Intake Valve Closing Angle on End of Compression Temperature for a Formula 1 Powertrain, from Rosetti *et al.* [413]

which gives a further knock limit improvement. A comparison of how volumetric efficiency and relative air fuel ratio have changed as the formula moved from normally aspirated to fuel-flow limited turbocharged engines was documented by Sassi *et al.* [28] of Ferrari and Shell and is repeated in Figure 2.55. Homogeneous lean SI combustion at high loads is rarely described in the literature. A recent paper by Clasen *et al.* [414] did explore this topic, although only at loads up to 17 bar IMEP and speeds in the range 1500-2500 rpm. In this operating area, the knock limit was actually found to worsen in combustion phasing terms moving from stoichiometric conditions to relative air fuel ratios of around 1.3. This is not a speed and load range of interest to racing applications and it would appear this trend does not hold at the much higher speeds and loads of Formula 1. The combination of antituning, EIVC and enleanment leads to long burn delays and hence significant activity was carried out to optimize the ignition system as documented by Corrigan *et al* [324] of Ferrari with collaborators at MOT (Motorentechnik, Optik und Thermodynamik). Whilst conventional spark ignition was used in early development, all manufacturers now use passive prechambers to further improve knocking performance, as confirmed by Symonds [415], Chief Technical Officer of Formula 1, in 2020 . Formula 1 also features a deep technical collaboration between engine and fuel suppliers. Fuels and engines are developed together, historically bringing evolutions of both engine hardware and fuel to the track on multiple occasions in a single season. Some of this activity has been published in the literature. These engines are quite far away from the CFR type in terms of design and operating conditions hence rapid compression machines and shock tubes are used to support development, as documented by Dauphin *et al.* [117] of Total together with collaborators at IFPEN and the University of Lille. Use of an RCM to characterize the anti-knock performance of high octane fuels was also presented by Burke [416] of RWTH Aachen together with collaborators at Shell and Ferrari. A Chemical Ignition Number (CIN) was proposed based on an iso-octane/ethanol scale where temperature, pressure and air fuel ratio were tailored to the target engine. These results can be used to calibrate chemical kinetics models to generate new fuel blends which are optimized for the pressure/temperature regime of these engines. The intention of the regulations [417] is to ensure that road-relevant components are used in the specific blends and hence fuel development is constrained.

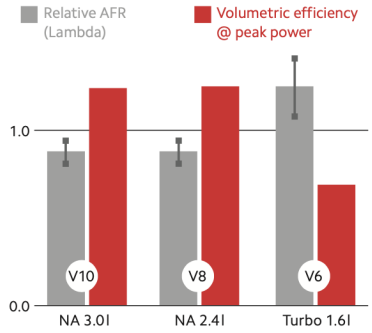

Figure 2.55: Changes in Relative Air Fuel Ratio and Volumetric Efficiency as Formula 1 Regulations Changed from Normally Aspirated V10 and V8 Engines to Knock-Limited Turbocharged Units, from Sassi *et al.* [28]

Mercedes published in 2018 that their Formula 1 engine had exceeded 50% thermal efficiency [418]. This is achieved at $>$ 40 bar IMEP at 11000rpm with peak cylinder pressures of the order of 250 bar. Current best road car technology is the Geely Hybrid engine which reaches 42.5% peak thermal efficiency and has a specific output of 75 kW/L as described by Zhang *et al.* [419]. A comparison between the engine types is given in Table 2.6 and will now be described, with comments on the applicability of racing knock mitigation techniques to road-car use. Where Formula 1 data in the literature is incomplete, estimated ranges are given.

The Formula 1 engine achieves very high Brake Thermal Efficiency due to its high compression ratio and waste heat recovery - effectively a form of turbo-compounding. Such a high compression ratio at extreme specific output can only be tolerated due to very effective knock mitigation. The combination of Miller and anti-tuning

Table 2.6: Comparison between Current Road-car and Formula 1 Engine Technology

	Production Roadcar	**Formula 1**
Swept Volume	1.5 L	1.6 L
Compression Ratio	13:1	16-18:1
Specific Output	75 kW/L@5500 rpm	≈390 kW/L@11000 rpm
Thermal Efficiency	42.5%	$>$ 50%
Dilution	$\lambda = 1$, ≈20% EGR	20-40% Enleanment
Intake Strategy	Miller and Detuning	Miller and Antituning
Ignition System	120 mJ Coil, Spark plugs	Prechamber
Fuel System	350 bar GDI	500 bar GDI
Fuel type	Commercial RON 95	100 $<$ RON $<$ 110
Waste heat recovery	None	From Turbine
Aftertreatment	TWC and GPF	None

gives very strong reductions in end of compression temperature. The anti-tuning system would require inlet runner lengths of the order of 1 m for road-car engine speeds and would be difficult to package. Variable runner length is also required to have effective anti-tuning over a reasonable speed range. The combination of strong Millerization and lean running requires a robust ignition system and prechambers are used to this effect. These also give good knock mitigation at high loads and generate turbulence in the main chamber increasing combustion speed. Extremely retarded conditions, such as catalyst heating, are difficult to achieve with prechambers but need not be run for a racing application. Prechamber engine layouts with secondary spark plugs have recently been proposed for road-car applications however. The possibility of designing a fuel to match the engine, albeit within regulatory limits, is of course a significant benefit. A number of new road-car fuels are currently under consideration however, including ethanol, methanol, methane, hydrogen and synthetic gasolines. Many of these have improved knock resistance in comparison to today's market gasolines. The Formula 1 engine is "over-square" with a bore to stroke ratio of 1.5 whereas thermal efficiency should be optimum at values of less than unity. Large bore areas permit large valves however, hence are appropriate for high specific power engines. This is particularly important if strong Millerization is applied, as available boost pressure may be limited. The cylinder swept volume of the Formula 1 engine is a rather small 267 cc and hence combustion chambers remain compact. This has long been known to benefit knock. Increased cylinder count to reduce cylinder swept volume would increase costs for road-car engines however, and also would increase friction and hence reduce part load efficiency. The high engine speed also reduces the time available for autoignition to occur and accelerates the flame-front. One of the key Formula 1 hybrid technologies - the electrified turbo - allows significant waste heat recovery along with turbocharger lag compensation. This system has also been recently announced for production by Garrett and Mercedes-AMG [420]. Waste heat recovery is most effective at high speeds and loads although some recuperation may already be possible on emissions cycles, depending on turbo-matching and road-load.

It can be seen therefore that the majority of knock-mitigating approaches in Formula 1 have an existing or potential road-car equivalent. The lack of exhaust after-treatment due to no emissions limits[21] is a an exception. A lean after-treatment system for full-load operation would not be desirable for road-car applications due to cost and packaging reasons, hence stoichiometric operation with EGR is preferred. The lack of an after-treatment system reduces exhaust back-pressure and hence trapped residual content. Knocking tendencies are therefore reduced.

Formula 1 has two other fundamental advantages over current road-car technology. One is the possibility to optimize the engine and turbocharger design for a narrow speed and load range. Compromises between competing objectives can therefore be avoided. Hybridization is a means of reducing the necessary operating range of road-car engines but an extreme hybridization approach would be required to fully limit the engine to single-point operation - for example a range extender. These engines are normally designed to be cheap rather than high performance as strong powertrain electrification is already expensive. Catalyst heating is another operating point that must currently be performed by the combustion engine in road-car applications. The introduction of electrically heated catalysts may mean less need to bias the combustion system design to cover this point in the near-future in comparison to the recent past and hence this compromise could maybe be avoided, or at least lessened. The second big advantage Formula 1 engines have is that continuous development with large budgets is invested into a single concept with a single target over a number of years. In some ways, this is similar to how WWII fighter aircraft piston engine development proceeded in the 1930s and 1940s, as described by Douglas [90]. Road-car engine development programs on the other hand, need to match strict budgetary and time limitations and have many more targets and constraints to satisfy. The fact that 42.5% efficiency has been achieved in production and $>$45% efficiency demonstrated in near-production research is therefore very impressive.

Splitter *et al.* [421] of Oak Ridge National Laboratory and the University of Tennessee Knoxville, published a paper in 2016 on historical analysis of octane number and spark-ignition engine specifications. Five key development periods were identified with the "Fuel Improvement Period" said to be up until 1955. This was based on US market data over an extended period. Data from this report (together with the assumption that the Ford Model T is representative of US vehicle sales in the 1920s) is shown in Figure 2.56. It can be seen that

[21] Emissions are currently unregulated but this is under consideration for future regulations [415]

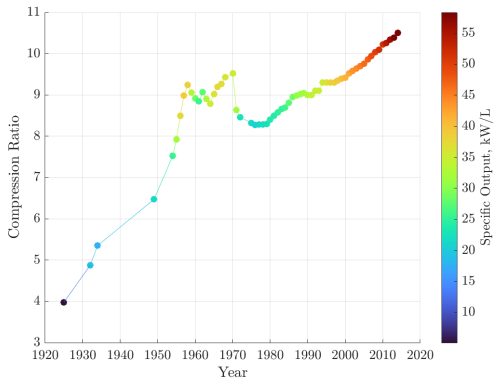

Figure 2.56: Changes in Average Compression Ratio and Specific Output of US Market Cars 1925-2014. Data from Splitter *et al.* [421]

both compression ratio and specific output increased dramatically from the 1920s until the mid 1950s. Improvements in fuel quality made a large contribution in this period, as noted by Splitter *et al.* and already discussed in the current paper. Compression ratio stabilized at around 9:1 and specific output at 34 kW/L until 1970. Compression ratio and specific output then fell, due primarily to the introduction of emissions legislation. This resulted in the consequent removal of leaded additives from gasoline and hence a reduction in fuel octane values, as shown in Figure 2.20. From the late 1970s onwards, both compression ratios and specific output began increasing again. Fuel antiknock quality has not markedly changed since then hence these gains are mostly due to more knock resistant engines. Increased specific output would normally require a compression ratio decrease for a given knock limit. This makes the improvements all the more impressive. These more recent gains have been primarily driven by better understanding of knock, developments in engine hardware and also improved powertrain calibration and control.

2.13 Conclusions

Engineers have sought to improve the efficiency of the ICE for over one hundred years and have been fighting against knock for all of that time. In the early period, a compression ratio of less than 5:1 was typical and Indicated Thermal Efficiency (ITE) was around 30%. This was at just 600 rpm. In 2020, Geely reached 42.5% Brake Thermal Efficiency (BTE) at around 2700 rpm with a compression ratio of 13:1 [419] whereas Formula 1 is now over 50% BTE at 11000 rpm [418], with compression ratios believed to be not far from the regulatory limit of 18:1. Specific power outputs have also increased dramatically in the same period. Although much progress has been made, knock remains a key limitation to further efficiency gains today, just as it was 100 years ago. Any gain in ICE efficiency will translate to reduced CO_2 emissions in the near term. Even with non-fossil fuel sources in the future, energy will always be at a premium and hence efficiency will remain of critical importance. Knock as a phenomenon was already defined in the introduction of this paper. In the following section, knock mitigation strategies which have been developed over the last 100 years are presented. Much of this knowledge has been hard won over an extended period, as has already been described.

2.13.1 Knock Mitigation Strategies

Knock can be avoided if the flame-front consumes all of the unburnt charge before autoignition has time to occur. Knock mitigation strategies therefore fall into two broad groups: those which seek to accelerate the rate of charge consumption by the flame-front (this will be referred to as FFA - Flame-Front Acceleration) and those which aim to reduce reaction rates in the end-gas (ERR - End-gas Reactivity Reduction). Guidelines for different component groups will now be given.

Charge Motion (primarily FFA):

Charge motion can assist in both mixture formation and flame-front acceleration. In terms of cylinder head design, both swirl and tumble motions can be created. A combination is also possible. Increasing tumble or swirl will generally result in a reduction in volumetric efficiency. Charge motion is favored by high piston speeds and hence high stroke to bore ratios.

Tumble is effectively transformed into turbulence at the end of compression and hence can accelerate especially the early phase of combustion. It is the predominant charge motion used with four-valve pent-roof type cylinder heads.

Swirl persists longer into the cycle and can improve later burn rates, especially when combined with squish. It was more commonly applied on cylinder heads with a single intake valve. It can also be achieved with a four-valve head through obstructing flow to one of the intake valves.

Squish is achieved by having a large parallel area on the piston and combustion chamber roof with a small distance between them. A flow is generated in the direction of the piston bowl close to TDC. This increases turbulence. As the piston descends, an anti-squish flow is created where the flame may be pulled by vacuum into the expanding squish volume. A strong squish effect is difficult to combine with valve overlap as the necessary piston pockets for high overlap reduce the available squish

area.

Whatever charge motion is adopted, care should be taken with undesirable secondary motions. These are flow tendencies which distort the flame front in an undesirable manner and hence can locally slow its progress. This increases the time available for autoignition to occur. Care should also be taken with cyclic variability of charge motion.

Both the quantity of turbulence and its spatial and temporal distribution should be optimized for best effects on combustion.

Perhaps the most direct way of accelerating the flame-front is to increase engine speed. This has a negative impact on friction and pumping work however. Increasing engine speed also means the end-gas is exposed to high temperatures and pressures for a shorter period of time, giving further knock benefits.

Charge Temperature Management (ERR):

As knock is largely a temperature driven phenomenon, all efforts should be taken to keep the charge as cool as possible until the flame-front arrives.

Intake systems should therefore be thermally isolated from hot parts of the cylinder head, particularly in regions of high flow and hence high heat transfer coefficient.

Charge cooling systems can reduce the temperature of the intake charge, in particular after it has been increased by a compression process.

Expansion of the charge can also take place in the intake system through appropriately timed wave action and/or in the cylinder by adopting an Early Intake Valve Closing strategy. Both of these techniques reduce volumetric efficiency and tumble however and so are limited by boost and combustion stability. A Late Intake Valve Closing strategy can also be used to reduce the effective compression ratio.

Combustion chamber components should also be adequately cooled. Typically the exhaust valves are the hottest region and this can be managed through sodium filled valves and direct cooling of guides and seats. The coolant circuit can and should be optimized in coupled calculations of the water jacket and the knock behavior in the cylinder. Cylinder flow motions and turbulence will also impact heat transfer behavior in the cylinder. Squish may have a positive impact on cooling of the end-gas if the piston temperature is lower than that of the charge during the squish and anti-squish period. Excessive cooling in the absence of knock will reduce overall efficiency. Careful use of coatings may enable a better compromise to be achieved between knocking tendency and excessive heat losses.

Mixture Formation (FFA & ERR):

Early SI engines used carburettor systems to achieve an approximately homogeneous mixture distribution. Mixing occurred primarily in the intake system and lighter and heavier fuel fractions were prone to separation. Mixture distribution to the cylinders was not necessarily even and closed loop control was difficult. Much of the fuel latent heat was lost to the walls of the intake system.

Port Fuel Injection creates a homogeneous distribution like a carburettor but has the advantage that the air fuel ratio can be tailored for each cylinder. Most latent heat is still lost to the walls however.

Gasoline Direct Injection systems create the possibility to tailor the mixture distribution to the operating point and hence a range of strategies can be applied. With correct timing of the injection event(s), maximum heat can be extracted from the charge which reduces the knocking tendency. Whilst late injection favors charge temperature reduction, there may be inadequate time for mixing. This can be alleviated somewhat with careful charge motion and spray pattern design. Extremely lean regions are unlikely to knock. Fuel concentration in the end-gas is correlated negatively with temperature however. Lean pockets may therefore be hotter and, combined with the fact that flame-fronts will consume them more slowly, can be at increased risk of autoignition if they are not lean enough. It is generally advantageous to achieve a slightly rich mixture near the spark plug at the time of ignition to maximize early flame kernel growth rates and stability.

In theory it should be possible to manage reactivity gradients to reduce the risk of autoignition events transitioning to damaging developing detonations.

Fuel (primarily ERR, secondary impact on FFA):

The knock resistance of fuels was correlated with the highest compression ratio an engine could achieve over 100 years ago and subsequently with testing in comparison to Primary Reference Fuels on a CFR research single-cylinder engine. These are known as the RON and MON tests.

The most common rating tests were conceived in the 1920s and 1930s when both fuel types and engine hardware were very different than they are today. Various methods have been proposed to correlate the rating values to modern engines with some success. The end-gas in a modern engine tends to be at lower temperatures for a given pressure than in the RON and particularly the MON test. Modern engines often perform best with fuels of high RON and low MON due to the combined effects of the rating method and the high sensitivity of modern fuels in comparison to the PRF test references.

The knock resistance of a fuel is correlated with its Ig-

nition Delay Time. This can be characterized in experimental facilities, typically against temperature and pressure. The delay time characteristic against temperature exhibits non-Arrhenius behavior for many fuel types, especially paraffins which make up the PRF scale. A Negative Temperature Coefficient region exists for many fuels. This has an impact on the severity of knock in the engine as this depends on reactivity gradients. NTC behavior is also correlated to pre-flame reactions. Experimental results can be compared to delay time maps coming from facilities such as RCMs and shock tubes to better understand knocking behavior. However, modern engines frequently run at higher pressure than these facilities can reliably achieve. Results from such facilities are therefore normally used to calibrate chemical kinetics software, which can be incorporated into 3D-CFD packages.

Liquid fuels evaporate before combustion. In doing so, they cool the charge. This effect is strongest for Direct Injection engines. Oxygenated hydrocarbons, particularly alcohols, have higher latent heat of vaporization than other typical gasoline components. High latent heat is beneficial for knock mitigation. The RON test is with fixed inlet air temperature and fuel is introduced to the intake system before the engine. There is therefore a partial charge cooling effect. The MON test on the other hand, controls the air/fuel mixture temperature upstream of the engine to a high temperature and hence is not sensitive to fuel latent heat. The volatility characteristics of the individual fuel components may cause separation in the intake system. This is of less importance on modern engines than it was with carburettor fuel systems.

The flame speed of a fuel may also have an impact on knock as faster flame-front propagation results in lower time for knock to occur. High flame speeds also mean more stable early flame kernel growth and hence better cyclic variability. Fuel flame speed effects are generally of second order importance to knock with respect to ignition delay times however, at least for typical hydrocarbons currently used in gasoline blending.

Dilution (ERR):

The benefits of charge dilution on knock were realized at an early point in the development of the ICE. Dilution renders the end-gas less reactive. This is partly because a given amount of heat release from the flame-front will result in a lower temperature rise in the chamber if the trapped mass is increased. Ignition delay time also depends on fuel/oxygen concentration and this is reduced by adding inert charge. Dilution can be with excess air, trapped or recirculated exhaust gas and/or introduction of additional fluids. All of these will reduce flame-speeds and hence there is a limit to how much can be applied.

Exhaust Gas Recirculation is commonly applied to increase the inert gas content in the cylinder. The exhaust gas should be cooled and ideally reactive species such as NO removed by catalysis before reintroduction to the engine. EGR cooling increases the total heat rejection requirement of the powertrain and may not be desirable for high performance applications. EGR should be well distributed in the intake system to avoid further increases in cyclic variability. There is some evidence that EGR may be less effective at very high load. Trapping of internal residuals has a detrimental effect on knock due to their high temperature and reactivity. This should be minimized by effective scavenging. Scavenging can be promoted by a combination of valve overlap and a favorable pressure gradient between the intake and exhaust systems. This is harder to achieve in a modern production engine which features a restrictive exhaust system due to the necessity to after-treat the gases to meet emissions limits.

Excess air is one of the simplest dilution strategies to apply. However, it is incompatible with emissions control by a three-way catalyst. It must therefore be used in conjunction with a lean after-treatment system to meet modern emissions limits which increases costs. In racing applications, notably Formula 1, excess air is applied to good effect to improve the knock limit at very high speeds and loads. It may be less effective at lower speeds and there is even evidence that it may be detrimental in some cases.

The most straightforward additional fluid to introduce is excess fuel. This was noted to benefit the knock limit in the early days of combustion research. Once again, three way catalysts only operate effectively in stoichiometric conditions and hence this approach is currently only used to protect engine components from over-heating in extreme operating conditions. Water injection may be used in addition or as an alternative. This was employed on WWII fighter aircraft and is enjoying renewed interest as a means of knock mitigation and temperature reduction compliant with stoichiometric operation. As for enrichment fueling, there is both a chemical benefit and a latent heat benefit. Direct injection of water gives maximum charge cooling for the same reasons that GDI systems mitigate knock more effectively. It is more complex and expensive to implement than low pressure port water injection.

Ignition system (FFA):

Ignition can be initiated in a spark-ignition engine by a conventional spark plug and coil. A high energy coil and large plug gap can result in a larger and more stable initial flame kernel. This is particularly important in dilute or stratified mixtures. A stable early flame kernel is key to guaranteeing low cyclic variability. Electrode design should aim to minimize kernel heat losses. Flow motion should aim to transport the kernel out of the gap, but not excessively, as blow-off or short-circuiting may oc-

cur. Large gap sizes mean high voltages are required to achieve a spark. This may limit the gap size for highly boosted engines.

A distributed ignition system results in multiple combustion initiation sites. This will result in faster combustion with lower cyclic variability. Distributed ignition may be achieved by a number of means including multiple spark plugs, a corona discharge system, and prechamber jets.

Prechamber jets also result in higher turbulence and radical seeding in the main chamber and so can give an additional performance improvement over other distributed ignition systems.

Combustion Chamber Design (FFA & ERR):

It has been known for at least 100 years that compact combustion chambers with short flame travel distances are beneficial for knock. The spark plug should therefore be arranged to minimize flame travel distance.

Smaller combustion chambers improve the knock limit. As knock generally occurs shortly after TDC, the bore size is the key dimension. Small bores are beneficial. For a given cylinder count and total swept volume, this implies a large stroke to bore ratio. This has a detrimental impact on volumetric efficiency however.

Using an increased number of cylinders can be an effective strategy. But this increases cost, heat transfer and potentially friction.

A bowl-in-piston design can be effective and was widely used in the past combined with squish. This is difficult to achieve together with valve overlap however.

Care should be taken to avoid protruding areas of the chamber which have poor heat-transfer to the coolant jacket.

Exhaust System Design (ERR):

Low exhaust system pressure drops should be aimed for to minimize trapped residuals.

Pressure wave tuning in the exhaust system can be used to achieve low pressure at the exhaust valve during valve overlap to further reduce residuals.

High flow exhaust ports, early exhaust valve opening and high exhaust valve lift may also contribute to more effective removal of burnt charge from the cylinder.

Closing Remarks:

If knocking is completely avoided, the engine is likely not running at its best possible efficiency. This may be due to excessively retarded combustion or an overly low compression ratio for the operating point. The target in the limiting condition should be to accept a given quantity of knock to permit the highest practicable compression ratio to be used. Control systems need to manage the combustion phasing and hence the knocking intensity to ensure an acceptable rate of damage accumulation in comparison to the engine's expected lifetime. Detailed combustion chamber design features and material choices may also lessen the damage which occurs for a given knocking intensity. Particular attention should be paid to the crevice zone and the piston rings.

2.14 Potential Future Research Directions

Powertrain engineering and the ICE is going through a seismic change. Whilst the ICE is commonly described as a mature technology, areas where further research activity is required to improve knocking limits and hence efficiency remain. There are many encouraging lines of research at the moment. An (incomplete) list of open points is as follows:

- The small spatial dimensions of exothermic centers which drive knock behavior, together with the extremely short timescales of autoignition chemistry in an ICE at elevated temperatures and pressures, mean that there is still much to understand here. Direct Numerical Simulation in CFD coupled with state-of-the art reaction mechanisms can allow exploring of the phenomenon but more effort is required to arrive at a fully predictive methodology and the development of tools to robustly validate it. Consideration should also be given to creation of a new generation of RCM and Shock Tube facilities to cover this experimental space. Downsizing has meant that many engines now operate outside of the current ranges of such devices.
- Standard methods of rating fuel knock resistance are long overdue an overhaul. The researchers who created the RON and MON methods did not expect that they would still be in use almost 100 years later. A number of suggestions on how such methods can be adapted have been proposed. A future rating scale should identify the possibility a fuel has to contribute to improved engine efficiency in a modern or near-future knock-limited powertrain. This will likely require testing at higher speeds than current RON and MON tests and over a range of dilution levels, compression ratios and loads. The opportunity should also be taken to move to a more modern combustion chamber and charge motion with direct injection fueling and a high energy ignition system. Modern cylinder pressure based feedback should also be introduced. Burn rate data could therefore

be produced together with knock limit results. Measurement of engine-out emissions should also be considered. The test procedure still needs to be possible in a relatively short time period. Modern automation systems and closed loop controllers should make this possible, potentially combined with slow transient rather than stationary operation.

- Much engine manufacturer activity still focuses on avoiding running into knock. As efficiency gains become harder to realize, the engine must be controlled to greater than borderline knock conditions where performance can be improved. Work on knock control systems and damage modeling, together with detailed activity to improve engine hardware design combined with materials to permit increased knock robustness, should be explored. Further understanding of shock wave behavior in engines and how to manage them to reduce damage is also needed.
- A number of potential future ICE fuels are currently being proposed including ethanol, methanol, methane, hydrogen, synthetic gasolines and more. All of these have valid reasons for being studied but it will be necessary to converge on a limited number of future fuels to permit engine manufacturers and energy companies to make the investments required to bring a new generation of products to market. There is a significant opportunity to improve the knock limit of the ICE and hence its efficiency if the right solution is backed. The most appropriate solution should be based on Well-to-Wheel and Total Life-cycle Analysis to have maximum beneficial environmental impact. An appropriate regulatory framework needs to exist in order to enable this to happen.
- The large range of potential fuels combined with the numerous possibilities to hybridize the ICE mean a predominantly experimental approach to identify the best solution would be prohibitively time-consuming and expensive. A fully integrated simulation methodology starting from a systems level and working down to CFD with integrated kinetics is required. Many of the proposed fuels are single-component and hence from a reaction modeling point of view, significantly simpler than existing gasolines. A number of promising alternatives will doubtlessly be identified and significant gains in knock-limited efficiency can be expected. These must then be validated experimentally. A large-scale international collaborative effort is likely needed, similar to what happened in the 1920s and 1930s driven by the CFR group. Such collaborations still exist today, but perhaps not at sufficient scale. This is particularly important as vehicle manufacturers' budgets must now be divided between electrification and ICE research and hence there should be a greater impetus for larger scale collaboration than considered in the recent past. A problem on a global scale demands global collaboration to find the best solution.

CHAPTER 3

CFD Modeling of Simple Combustion Chamber Acoustic Behavior

3.1 Abstract

Knock is one of the main limitations on Spark-Ignited (SI) Internal Combustion Engine (ICE) performance and efficiency and so has been the object of study for over one hundred years. Great strides have been made in terms of understanding in that time, but certain rather elementary practical problems remain. One of these is how to interpret if a running engine is knocking and how likely this is to result in damage.

Knocking in a development environment is typically quantified based on numerical descriptions of the high frequency content of a cylinder pressure signal. Certain key frequencies are observed, which Draper [78] explained with fundamental acoustic theory back in 1935. Since then, a number of approaches of varying complexity have been employed to correlate what is happening within the chamber with what is measured by a pressure transducer. Whilst such phenomena can be well described by 3D Computational Fluid Dynamics (CFD) with moving meshes, small time-steps and chemical kinetics, such an approach is computationally intensive. Analytical calculations or Finite Element Methods (FEM) on the other hand, can estimate modal frequencies but not their likelihood of occurrence.

In the present work, a simple stationary 3D CFD model, taking inspiration from an experiment by Draper [78] in 1934, is implemented in STAR CCM+ software. One or more autoignition events are simulated, and the corresponding frequency spectra and modal pressure distributions are described. It is shown that the model can reproduce the expected knocking frequencies from numerical analysis and experimental data. Sensitivity to autoignition and pressure transducer location is commented upon. Time Frequency Analysis (TFA) is applied to moving mesh data and demonstrates that little accuracy is lost in considering the stationary case. The current model is considered to be an appropriate means for analysis of knocking cycles with trace and moderate intensity, and can be used to bridge the gap between what is measured by a pressure transducer and what is occurring in the combustion chamber.

3.2 Introduction

In the early days of knock research, the primary means of diagnosing knock was using the human ear, as described by Ricardo [33] or the Dickinson Bouncing Pin indicator, used by Midgely [44] among others. In the 1930s, carbon granule microphones and piezoelectric transducers allowed for high frequency measurements of cylinder pressure in knocking engines. Draper [78] examined the frequency of these oscillations in both CFR (Cooperative Fuels Research) and NACA (National Advisory Committee for Aeronautics) research engines in 1934. He compared these frequencies to the volume acoustic modes of a flat-ended, right circular cylinder. The characteristic frequency observed for knock in the running CFR engine was around 6500 Hz at TDC (Top Dead Center), which corresponded to calculations of the first transverse mode of a cylinder, with a single nodal plane. In order to calculate the expected frequency in a running engine, certain assumptions are required, to estimate the gas properties in the chamber immediately after the knock event. Draper therefore also performed a simplified experiment, where a small explosive charge was detonated in the periphery of the combustion chamber whilst the engine was stationary, with the piston in a series of known positions. In this manner, gas properties and engine geometry were well defined. The primary oscillations observed were at 2600 Hz, which once again corresponded to the first transverse mode in the CFR engine, this time with air at approximately atmospheric pressure and temperature[1].

Acoustic mode calculations based on Bessel functions predict many more possible modes and indeed Draper [79] calculated 38 of these with expected frequencies up to 50 kHz in a follow up paper in 1938. This time, he had access to higher bandwidth electronic equipment. The only clearly identifiable mode was still at around 6500 Hz for the fired engine. It was commented that other frequencies were present, but that a higher film speed would be required to separate them[2]. Draper also suggested in this paper to use a knock index based on integrating and squaring the high frequency content. Practical knock indicators were developed, including by Draper, for use on military aircraft in WWII (World War II). A number of different devices were used, which generally gave knock feedback based on the presence of high frequency content in the signal, as described by Street [103], Costa [104] and Bogen and Faust [105] in the 1940s.

In the 1960s, Hoffman [140] investigated the knocking frequencies in a CFR engine over a range of fuels and operating conditions. A Kistler piezoelectric transducer was used. Once again, the main frequency content was found to be in the range 6000-7600 Hz.

In 1970, Barton *et al.* [167] used a variable cutoff frequency Band Pass Filter (BPF) to study frequency content of knocking cylinder pressure traces in a Removable Dome Head CFR engine (the original CFR engine has a flat head). The maximum cutoff frequency was 20 kHz.

[1] The explosive charge was small and was assumed to have little impact on the reference acoustic velocity of the chamber gases.

[2] Frequencies were identified by measuring the distance between peaks on the photographic time-based record and hence the greater the film speed, the more precise this estimate could be.

Root Mean Square (RMS) pressure was plotted against frequency, but the only clear peak due to knocking was again at around 6000 Hz. In 1978, Arrigoni *et al.* [172] showed frequency spectra from a knocking engine where two peaks could be clearly seen, one at around 9 kHz and another at around 14 kHz. The bore size of the engine was not stated but it was likely smaller than that of the CFR.

In the late 1970s and early 1980s, knock control was implemented in production vehicles. An accelerometer was generally used as the feedback sensor and correlation between the frequency spectra of accelerometers and pressure transducers was published in a number of papers. Conventional systems at the time focused on a bandwidth of 6-8 kHz, coherent with the studies in the 1930s and hence were focused on the first transverse mode. Nakamura *et al.* [183] compared frequency spectra of knocking and non-knocking cycles for both cylinder pressure and accelerometer signals. Five separate peaks were observed in the frequency range 8-22 kHz. These were compared to the modal frequencies predicted by Draper. The second transversal mode, at around 14 kHz in this study, was chosen as the most suitable for knock feedback, as background noise was shown to be present for non-knocking accelerometer data in the frequency range of the first mode.

Up until the 1980s, measured frequencies were generally compared with the expected modal frequencies from basic theory. However, in 1985 Schäpertöns and Lee [207] performed knocking calculations in two-dimensional CFD software. The "Shell" chemical kinetics model developed by Kirsch *et al.* [179] was integrated in the code. Pressure oscillations due to knock could be seen and the amplitude depended on the location of measurement within the chamber. A frequency analysis was not performed.

In 1994, Blunsdon *et al.* [227] implemented the Shell model in 3D (three-dimensional) CFD of a disk shaped combustion chamber using KIVA-II software. Multiple modes were excited with the first transversal being the predominant one. Supersonic wave propagation resulting from developing detonation was reproduced. Also in the 1990s, Time-Frequency Analysis (TFA) of knocking cylinder pressure and accelerometer data began to appear in the literature with Wigner-Ville (WV) and Wavelet Transform (WT) techniques being applied by Samimy *et al.* [232], Scholl *et al.* [233] and Burgdorf *et al.* [234] among others. These methods can cope with the fact that the resonant frequencies change with crank angle in a running engine, as they depend both on piston position and instantaneous gas properties.

In 2002, Carstens-Behrens *et al.* [272] applied the Finite Element Method (FEM) to calculate the acoustic modes of a complex pent-roof geometry. These were compared to TFA plots using the WV transform. The FEM approach has been applied frequently since, and can be seen as an extension of the original analytical technique applied by Draper. Like Draper's approach however, it does not predict the likelihood of each mode being excited. CFD models with integrated chemistry are also now standard practice, with ever more detailed models employed. Whereas in the past, a single representative cycle was simulated using Reynolds Averaged Navier Stokes (RANS) techniques, Large Eddy Simulations (LES) allow explicit simulation of cyclic variation, as demonstrated by Fontanesi *et al.* [379] in 2013 .

The CFR engine is likely the most studied engine of all time and indeed there have been a number of interesting papers in recent years. In 2018, Mittal [422] compared frequency spectra of the CFR engine with modern combustion chamber geometries and Draper's theoretical modes. The strongest mode was a little over 6 kHz, as had been identified by Draper. Five further peaks on the FFT (Fast Fourier Transform) could be seen between 10 and 20 kHz which corresponded closely in frequency terms to Draper's predictions. Frequency analysis of CFR knocking cylinder pressure data was also performed by Swarts and Kalaskar in 2020 [423]. Three distinct peaks could clearly be seen in the FFT analysis of RON testing of PRF (Primary Reference Fuel) 98, whilst a fourth group of peaks from 17-19 kHz were not easy to separate. 3D CFD modeling of the CFR engine appears to be a relatively recent phenomenon. Broatch *et al.* [404] presented a model of the CFR engine in CONVERGE in 2018. Although high frequency oscillations could be seen on the simulated pressure traces, the frequency spectra of the numerical data were not analyzed in the paper. Data analysis techniques have also evolved in the last years with greater emphasis on Time Frequency Analysis (TFA) such as Continuous Wavelet Transform (CWT) techniques, as described by Khosravi and Pitsch [424], or the Short-Time Fourier Transform, employed by Pla *et al.* [425].

Despite all the advances that have been made, it is still not immediately obvious to a development engineer, who must calibrate the knock limited ignition timing of an engine, what exactly is being measured by a cylinder pressure transducer. An engine's ignition timing must be calibrated over a range of speeds, loads, temperatures and a plurality of other variables. It is not currently feasible to perform dedicated CFD studies of all these possibilities, particularly if chemical kinetics, cyclic variability and higher frequency acoustic modes are of interest. Development engineers therefore frequently refer back to the original analytical work of Draper in interpreting knocking cylinder pressure data. A simple, fast-running model, which could be used to interpret cylinder pressure data for a given non-ideal geometry, would therefore be very useful.

In the present work it was decided, as a first approach, to reproduce the original Draper stationary engine experi-

ment of 1934 in STAR CCM+ CFD software. The goal is to gradually move towards the case of a modern high-performance knocking engine, only integrating greater model complexity if required to adequately explain experimental results.

3.3 Acoustic Theory

In 1935, Draper explained how to calculate acoustic mode frequencies of a plain ended, right circular cylinder starting from the basic wave equation in three dimensions. For cylindrical coordinates r, θ and z, this is shown in Equation 3.1 [78].

$$\frac{\partial^2\Phi}{\partial r^2} + \frac{1}{r}\frac{\partial\Phi}{\partial r} + \frac{1}{r^2}\frac{\partial^2\Phi}{\partial\theta^2} + \frac{\partial^2\Phi}{\partial z^2} = \frac{1}{c^2}\frac{\partial^2\Phi}{\partial t^2} \tag{3.1}$$

where Φ is the velocity potential and c is the reference acoustic velocity. Draper showed that the characteristic frequencies n of the cylindrical volume are given by Equation 3.2

$$n = c\sqrt{\frac{\beta^2}{4\pi^2} + \frac{g^2}{4h^2}} \tag{3.2}$$

where g describes the number of longitudinal modes, h is the combustion chamber height and the product of β and the cylinder radius a can only have certain values which depend on Bessel functions. Figure 3.1 shows the form of the first five Bessel functions of the first kind. If the piston is rather close to TDC (Top Dead Center), the main modes excited tend to be transverse modes and hence $g = 0$ in Equation 3.2. These modes have nodal planes in the cylinder axis and/or nodal cylinders coaxial with the engine cylinder. Table 3.1 shows how some transversal mode shapes are correlated with the values of βa and the Bessel function values.

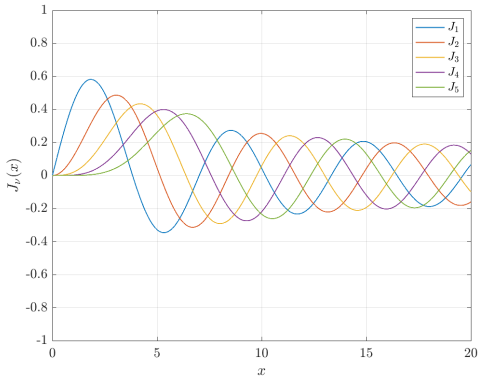

Figure 3.1: Bessel Functions of the First Kind (J_ν) of Independent Variable 'x' for $\nu = 1$ to 5

Figure 3.2 shows the frequencies of these modes for an engine with a $3\frac{1}{4}$" bore (82.55 mm, such as the CFR engine used by Draper) assuming the cylinder contents are air at standard atmospheric temperature and pressure. Each mode is given a short name "Fxy" where "x" is the number of nodal planes and "y" is the number of nodal cylinders (excluding the nodal cylinder at the bore wall). Longitudinal modes, where present, have a frequency which changes with piston height based on Equation 3.2 and hence in a running engine will vary with crank angle. Where both transversal and longitudinal modes are present, the transverse mode frequencies also become a function of piston height. Draper [78] showed in his original paper however, that primarily transverse modes are excited in a knocking engine, as the combustion chamber resembles a flat disk at the moment of knock occurrence.

Table 3.1: Mode Shapes and βa Product Dependence on Bessel Functions of the First Kind

Roots J_1	 F00	 F01	 F02
Peaks J_1	 F10	 F11	 F12
Peaks J_2	 F20	 F21	 F22
Peaks J_3	 F30	 F31	 F32
Peaks J_4	 F40	 F41	 F42

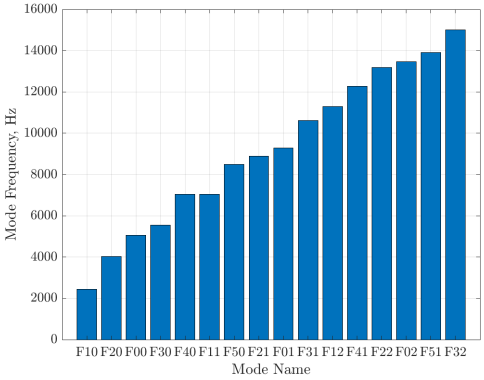

Figure 3.2: Transverse Modal Frequencies for a CFR Engine at Standard Atmospheric Conditions

3.4 Model Description

A CFD model of the Draper test case was built in SIMCENTER STAR-CCM+ version 2020.3. The cylinder bore was that of the CFR engine - 82.55 mm ($3\frac{1}{4}$") whilst the height was set to 24.5 mm (0.95"), a reference height for analysis in Draper's 1935 paper [78]). The sudden

heat release of an autoignition event is represented by superimposing a 1000 W heat source on a spherical surface obtained by subtracting a 2.5 mm diameter solid sphere from the fluid volume, as shown in Figure 3.3.

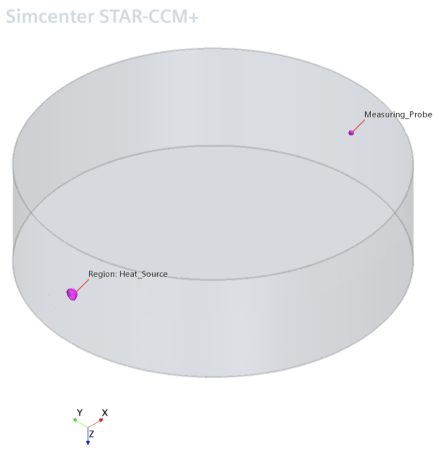

Figure 3.3: Simulated Fluid Domain

The heat source starts with a 0.03 ms delay from the beginning of the simulation and the duration of the source is fixed to 0.1 ms, as shown in Figure 4.2.

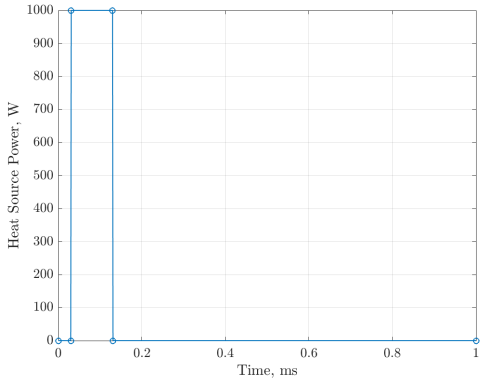

Figure 3.4: Superimposed Power Source Profile

No-slip boundary conditions are applied on the cylinder walls. Turbulence and heat transfer are neglected considering the flow as laminar and adiabatic. The fluid used for the simulation is air with temperature-dependent specific heat, whilst an ideal gas equation of state is applied. From a numerical standpoint, the Pressure-Implicit with Splitting of Operators (PISO) unsteady solver is used ensuring a quasi-second order time discretization. The chosen algorithm is suitable for transient cases where the convective Courant number is low. Due to this, a time step sensitivity was performed to reach as-reliable as possible results. Segregated third order numeric for flow and temperature is employed. Ambient pressure and temperature are fixed as initial conditions at 1 bar and 293 K respectively. For model validation and initial sensitivities, the time-varying pressure signal was monitored diametrically opposite the heat source as in the Draper experiments, see Figure 3.3.

Sensitivity to mesh size and numerical time-steps were performed to find the best compromise between accuracy of results and Central Processing Unit (CPU) efficiency. Four different mesh sizes were tested from 2 to 0.25 mm, whose characteristics are listed in Table 3.2 and shown in Figure 3.5. Mesh sensitivity was studied with a constant numerical time-step of 1 μs.

Table 3.2: Mesh Characteristics and CPU time (constant time step: 1 μs)

Name	Mesh Size mm	No. of Cells	Normalized CPU Time (20 CPUs)
Mesh-2	2.00	19922	100% (0.25 h)
Mesh-1	1.00	146335	183% (0.46h)
Mesh-05	0.50	1083111	1527% (3.8h)
Mesh-025	0.25	8433692	15527% (38.8h)

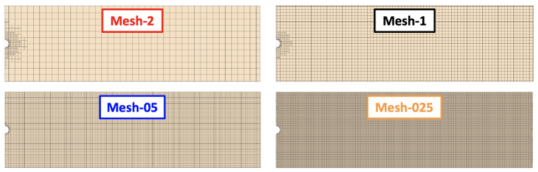

Figure 3.5: Section Plots of Tested Meshes, on the Left the Spherical Surface used as the Heat Source

As shown in Figure 3.6, the pressure signal is not overly sensitive to changing the mesh size when the numerical time-step is fixed. Frequency peaks do not change in the zone of key interest, as shown in Figure 3.7. However, a reduction of pressure oscillation amplitude is found when mesh density increases, due to an increase of numerical viscosity. Given the large impact on computation time, a mesh size of 1 mm was chosen.

Considering the characteristic velocity of the problem as being the velocity of sound, c =355 m/s, a mesh size Δx of 1 mm and a numerical time step Δt of 1 μs, the convective Courant number C can be calculated with Equation 3.3. For the Courant-Friedrichs-Lewy (CFL) condition to be satisfied, the Courant number must be less than unity.

$$C = c\frac{\Delta t}{\Delta x}, \text{ CFL Condition: } C < 1 \qquad (3.3)$$

As reported in Table 3.3, the numerical time step of 1 μs is more than suitable to track the evolution of pressure waves into the chamber when the mesh size is 1 mm. On the contrary, if a finer mesh is used, the numerical time step must be further reduced, leading to a significant increase of computational time, which is not justified by

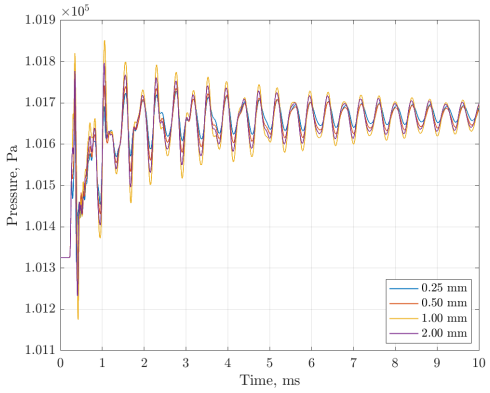

Figure 3.6: Pressure signal Variation with Mesh Resolution, constant timestep of 1 μs

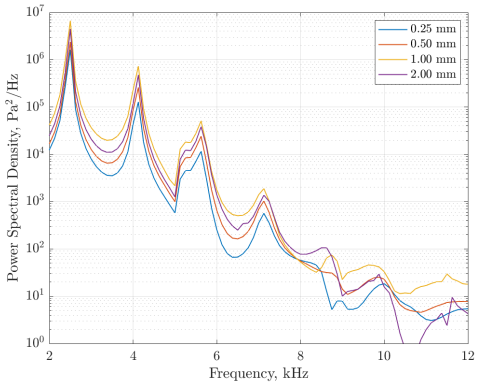

Figure 3.7: FFT Power Spectral Density Variation with Mesh Resolution, Constant Time Step of 1 μs. FFT Calculated from 2 ms until End of Run

higher quality of the results for the majority of cases. The sensitivity of the results to numerical time step was verified on the 1 mm mesh, as reported in Figure 3.8 and Figure 3.9. The pressure damping strongly increases when the numerical time step is not fine enough and the amplitude of pressure oscillations diminishes. Large differences in terms of pressure traces are found when the Courant number becomes higher than one, while the differences are reduced when the Courant number is low enough. Due to these effects, the 1 μs time-step was chosen as the best compromise between results accuracy and CPU efficiency, and it was adopted for the majority of the following activity.

Table 3.3: Courant Number for Different Tested Cases

Mesh Size mm	Time Step μs	Courant	CFL Condition
1.00	1.0	0.355	OK
1.00	2.0	0.710	OK
1.00	5.0	1.755	KO
1.00	10	3.550	KO
1.00	0.5	0.178	OK
0.50	1.0	0.710	OK
0.25	1.0	1.420	KO

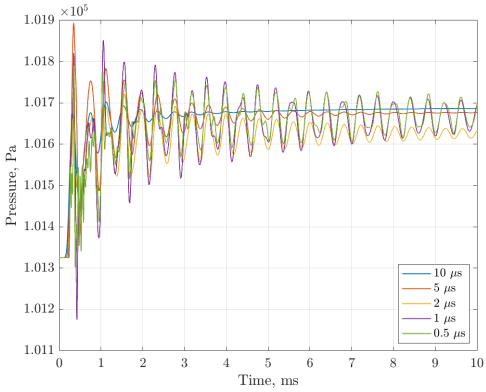

Figure 3.8: Pressure Signal Variation with Calculation Time Step, Constant Mesh Resolution of 1 mm

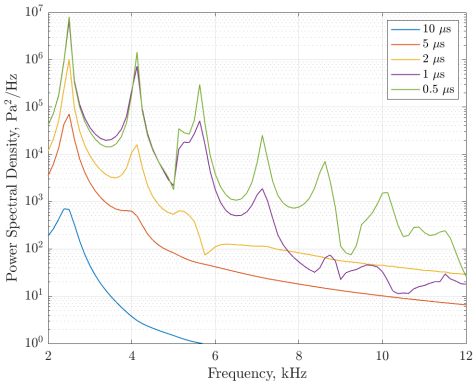

Figure 3.9: FFT Power Spectral Density Variation with Time Step, Constant Mesh Resolution of 1 mm. FFT Calculated from 2 ms until End of Run

3.5 Model Validation

Draper's original 1934 experiment featured a single pressure transducer mounted diametrically opposite the explosion source [78], as illustrated in Figure 3.3.

The sensor was a so-called "MIT indicator" and the acquired, amplified signal was rate of change of pressure with time. The amplifier had a frequency range of only around 10 kHz and the gain characteristic was not flat across this range. The gain dependence on frequency of the amplifier was described in the paper however, and has been replicated in the present study for the purposes of initial model validation.

Figure 3.10 shows the effect of the amplifier characteristic described by Draper on the pressure signal. A significant amount of high frequency information is clearly lost in the initial part of the acquisition. From around 5 ms onwards however, there is little difference between raw and filtered signals.

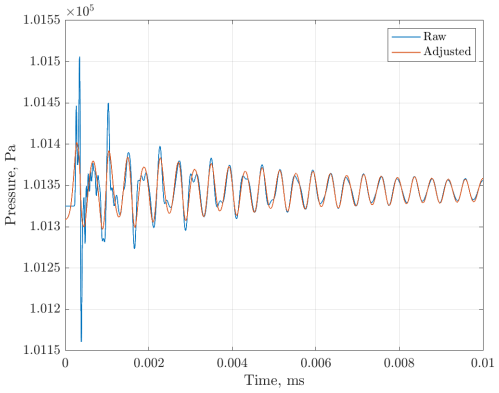

Figure 3.10: Effect of Amplifier Used by Draper on Pressure Data

The filtered rate of change of pressure from the model is compared to a figure from Draper's paper in Figure 3.11. No axes are present in the original photographic record and hence the image has been scaled to match the waveform from the model. It can only therefore be interpreted to confirm if the decay rate of the pressure oscillations with time and the form of the individual oscillations are similar, between model and historical experimental results. This would indeed appear to be the case as shown in Figure 3.11. Draper stated that the frequency of this signal was approximately 2600 Hz. He also noted that this was somewhat higher than the theoretical value of around 2400 Hz and attributed this to a potential temperature rise due to the explosive charge. The theoretical value determined in the current work is 2434 Hz and the model frequency, based on evaluating the distance between the peaks of the filtered signal as Draper likely did, is 2469 Hz. The model therefore appears to be adequately aligned both with the basic theory and the historical experiment.

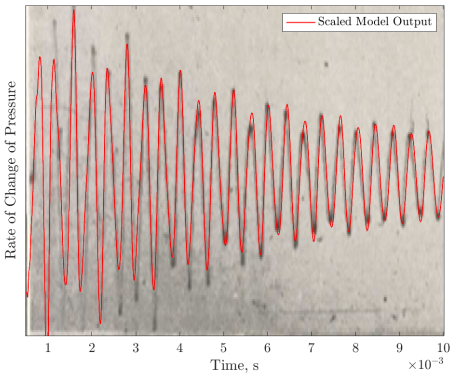

Figure 3.11: Comparison of Scaled Modeled Rate of Change of Cylinder Pressure with Figure 12 from Draper's Original Study [78]

3.6 Post Processing: Base Case

A total of 61 pressure measurement locations were implemented in the model with a view to post-processing, which was performed using MathWorks MATLAB R2020b. These "virtual sensors" were on a single plane offset into the chamber by 1 mm from the cylinder head face ($z = 1$ mm). The layout of sensors is shown in Figure 3.12. There are five groups of twelve, each group on a diameter concentric to the cylinder axis. A final 61st sensor was at the center of the chamber. These sensors can be analyzed in groups, in order to more easily understand the pressure wave behavior. An example is to track the initial pressure pulse originating near "Sensor 9" as it traverses the combustion chamber, as tracked by horizontally arranged sensors (those between Sensor 9 and Sensor 3). This is shown in Figure 3.13. It can be seen that the largest pressure amplitude is recorded by Sensor 9 as it is closest to the simulated heat source. By the time the wavefront has made its way to Sensor 3, the amplitude has diminished but the waveform has become more complex, as can be seen in Figure 3.13.

The initial reflections result in broadband frequency behavior, as evidenced by Time Frequency Analysis (TFA). A composite Continuous Wavelet Transform (CWT) scalogram from the results of all 61 sensors is shown in Figure 7.6, where it can be seen that a broad frequency spectrum is excited shortly after the explosion event. Later in the cycle, horizontal bands are evident, suggesting stable modal frequencies exist. The initial condition of the model was extended by 1 ms to reduce the impact of Cone Of Influence (COI) effects on the analysis of frequency behavior immediately after the ignition event.

FFT analysis was performed from 2 ms onwards. For

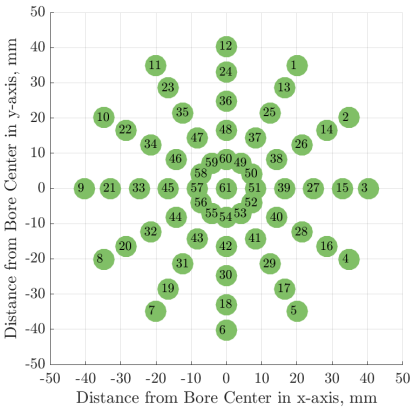

Figure 3.12: Virtual Pressure Sensor Location in Model

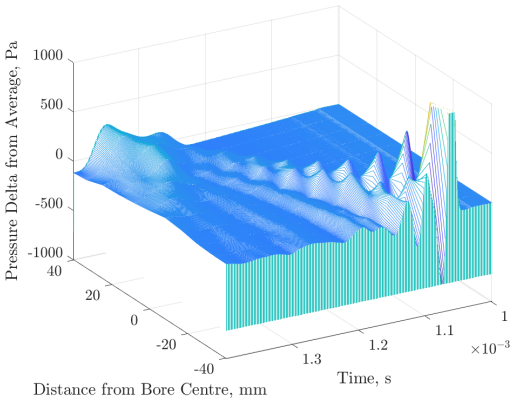

Figure 3.13: Propagation of Initial Acoustic Wave on Horizontal Sensor Group (Sensors 9-3)

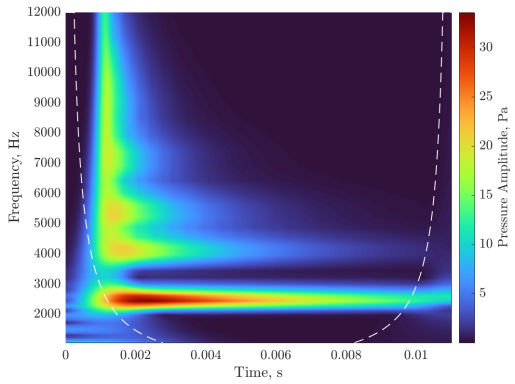

Figure 3.14: Composite CWT Scalogram of All Sensors, Cone Of Influence Boundary Overlaid on Scalogram

each sensor, peaks were identified on the Power Spectral Density (PSD) plot as shown in Figure 3.15 for Sensors 3 and 61. Theoretical modal frequencies are overlaid on the diagram. It is clear from Figure 3.15 that not all sensors see the same frequency information. The peaks from the FFT plot of all 61 sensors were therefore combined into a single diagram to visualize this dependency more clearly, as shown in Figure 3.16.

The strongest peak is at 2.4 kHz and is seen on the majority of sensors. However it is weak for every sixth sensor. These are the ones which lie on a theoretical nodal plane for F10, the closest theoretical mode in frequency terms, and hence this is expected. Interestingly, a weak peak is seen at 2.4 kHz even for Sensor 61, which is at the center of the chamber. This suggests a small geometrical asymmetry in the vibrations, likely due to the initial explosion event location.

The next strongest peak is at 4.1 kHz and is stronger on sensors of a lower number, which are those closer to the periphery. It agrees well with the theoretical frequency of the F20 mode. In contrast, a peak at 5.1 kHz is more evident on sensors closer to the center of the combustion chamber. This suggests it is indeed a circumferential mode, likely F00. Conversely, the peak at 5.7 kHz is more commonly observed for sensors of a lower number and is likely the F30 mode.

A series of narrow Band Pass Filters (BPF) were applied to the pressure/time data from all 61 sensors. The passband center frequencies were derived from the peaks of the average FFT diagram and that of Sensor 61. The FFT peak frequencies are listed in Table 3.4 together with the nearest theoretical frequencies and mode names. The passbands were from a factor of 0.95 to 1.05 of these frequencies. An Infinite Impulse Response (IIR) filter was used with steepness of 0.95.

Table 3.4: Frequency Peaks from Model Analysis and Comparison with Draper Frequencies

Peak	Freq. (Model)	Freq. (Theory)	Likely Mode
1	2444 Hz	2434 Hz	F10
2	4111 Hz	4035 Hz	F20
3	5111 Hz	5067 Hz	F00
4	5667 Hz	5557 Hz	F30
5	7111 Hz	7039 / 7052 Hz	F40 / F11
6	8556 Hz	8494 / 8878 Hz	F50 / F21
7	9222 Hz	9288 Hz	F01
8	10000 Hz	9923 Hz	F60
9	11111 Hz	11299 Hz	F12

The BPF pressure values of all sensors were fitted to surfaces using cubic interpolation, in order to more clearly visualize the mode shapes. These fitted BPF pressure distributions are shown in Figure 3.17 for the base case, corresponding to the original Draper stationary experiment with a piston height of 24.5 mm (0.95"). The standard deviation of pressure across the transducers was used to automatically select the most appropriate time-

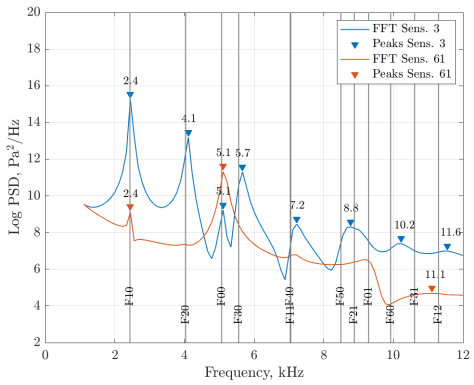

Figure 3.15: FFT from Sensor 3 and 61 with Peak Identification and Comparison with Theoretical Transversal Modal Frequencies

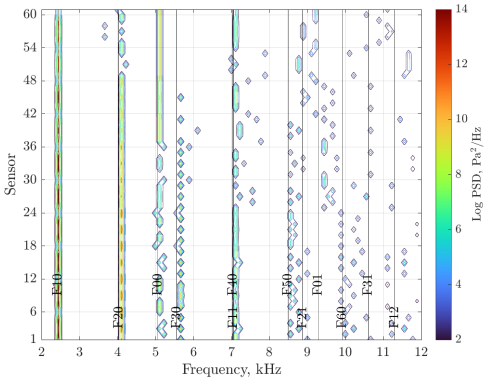

Figure 3.16: Contour Plot of FFT Peaks for all 61 Sensors. Theoretical Modal Frequencies Overlaid

step for each mode, shortly after 2 ms (and hence approximately 1 ms after the ignition event).

The first four modes are indeed F10, F20, F00 and F30 as expected. There is some overlap in the mode shape of F00 and F30 despite a very narrow and steep BPF being applied. The next mode shape, at 7111 Hz, shows elements of both F40 and F11 as expected, given that these two modes have almost identical theoretical frequencies. The mode at 8556 Hz is similar to the F50 pattern. The mode at 9222 Hz would appear to be the F21 mode, rather than the F01 which is closer in frequency terms in theory. It may in reality be a combination of both as it is not a pure F21 shape. The penultimate mode shown would indeed appear to be F60 based on both its frequency and pressure distribution. The final mode, on the other hand, looks more like F31 than its nearest neighbor in terms of theoretical frequency, F12. F31 is theoretically at 10611 Hz and hence is still rather close.

It can be seen that in general for the analyzed case, where an explosive event in the periphery of the combustion chamber was simulated, a wide range of modal frequencies are reproduced and their pressure distribution and frequencies agree well with the basic theory.

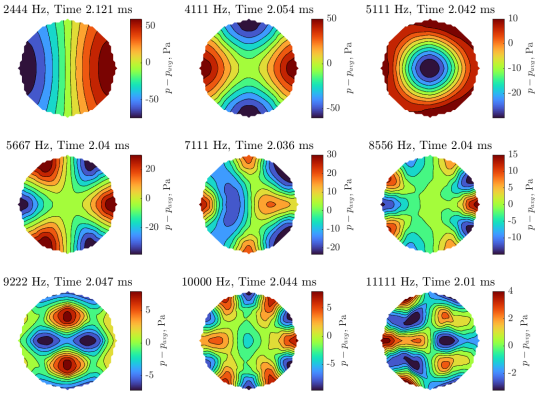

Figure 3.17: Band Pass Filtered Pressure Distributions at Approximately 2 ms for a Single Heat Source in Periphery of Combustion Chamber

3.7 Radial Ignition Site Sweep

A sensitivity to the location of the heat source was performed. It was swept from the center of the chamber to the periphery as shown in Figure 3.18. Twelve locations were considered, with the second location being only 1 mm offset from the center. For each case, the FFT peaks were analyzed for each sensor. The peak values were then averaged across the sensors and plotted against the radial offset of the ignition site from the combustion chamber center. The resulting contour plot is shown in Figure 3.19.

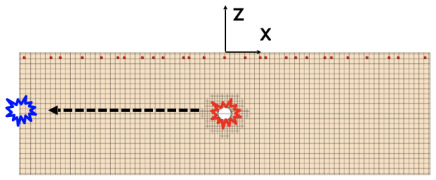

Figure 3.18: Radial Heat Source Location Sweep

The maximum radial offset is the same as for the Draper case and the strongest mode for this case is F10. This mode is almost absent from the central heat source case (zero radial offset), as are F20 and F30. Moving the heat source radially outwards, these modes become apparent. The F00 mode, on the other hand, is strongest for the central heat source case and weakens as it is moved to the periphery, although it remains present. The behavior close to 7 kHz is somewhat more complex to decipher as

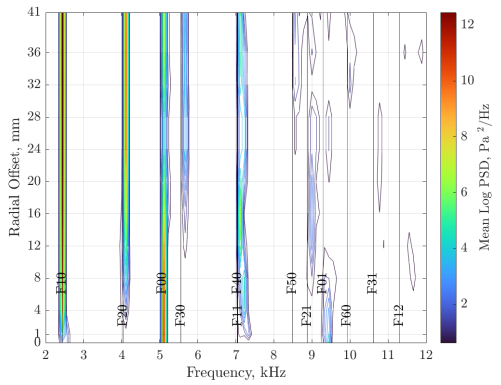

Figure 3.19: Contour Plot of Mean FFT Peak Response to Radial Heat Source Location Sweep

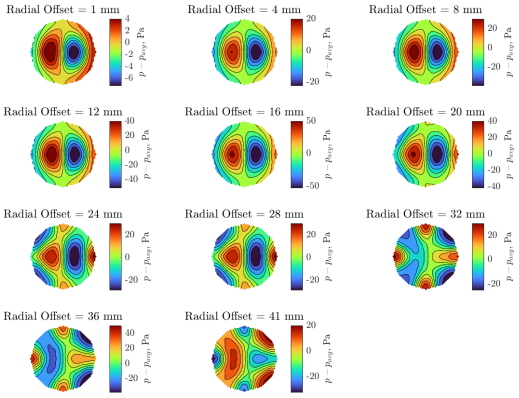

Figure 3.20: Pressure Distribution Variation with Heat Source Radial Offset for 7.1 kHz BPF Data

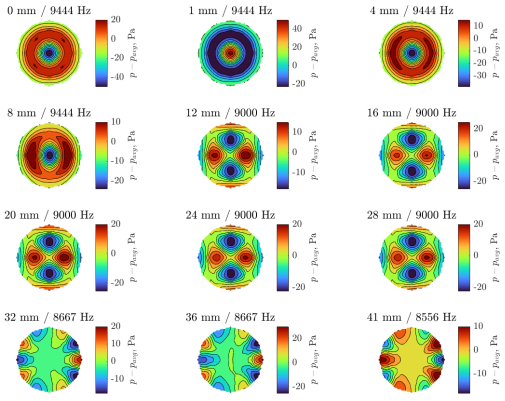

Figure 3.21: Pressure Distribution Variation with Heat Source Radial Offset for 8-10 kHz BPF Data

the theoretical frequency matches both the F40 and F11 modes. It would seem improbable that the F40 mode is excited for low values of radial offset, based on the response of F10, F20 and F30. The F11 mode is likely also present. In order to confirm this, the pressure distribution in this frequency range was analyzed for all ignition sites. The results are shown in Figure 3.20. Here it can be seen that for ignition sites close to the center of the chamber, only the F11 mode is present. For perfectly central ignition, it is not apparent. As the heat source is moved to the periphery, the F40 mode is also excited, although the pressure distribution suggests the F11 mode is still weakly present.

In the range 8.0-9.5 kHz, F50, F21 and F01 appear to be present. Based on frequencies, the F01 mode is predominant for central ignition, in the intermediate range F21 is prevalent and for heat sources close to the edge of the chamber F50 is strongest. This is confirmed by the BPF pressure distributions, as shown in Figure 3.21. The lowest frequency where a mode is present is shown at each radial offset. The F60 mode was already observed at 10 kHz, as shown in Figure 3.17.

3.8 Axial Ignition Site Sweep

The sensitivity to the axial location of the heat source was carried out as shown in Figure 3.22. This was with a view to moving the heat source location to the common position of the spark plug in a modern combustion chamber (the CFR engine features a side spark). With this heat source location, Sensor 61 cannot be used. Figure 3.23 shows the mean FFT response for Sensors 1-60. Despite the heat sources being coaxial with the cylinder in both cases, more complex frequency behavior is seen for the case where the axial position is not at the center of the chamber. Interestingly for this heat source location, some asymmetric modes are excited, including F10 and F11. For the central ignition case, a frequency is seen at 9.4 kHz whilst for the heat source in the "cylinder head" location, the closest peak is at 8.9 kHz. From examination of the pressure distribution, both of these peaks correspond to the F01 mode.

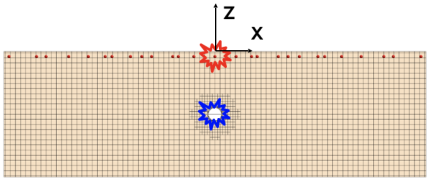

Figure 3.22: Axial Heat Source Location Sweep

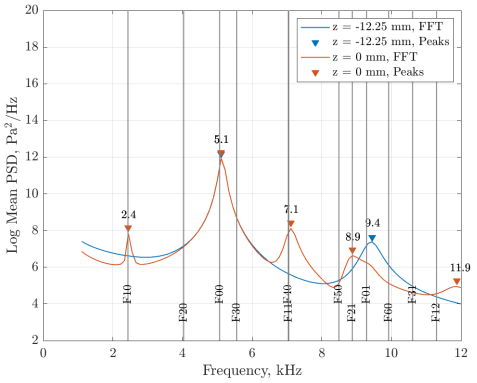

Figure 3.23: Mean FFT Response of Sensors 1-60 to Axial Heat Source Location Sweep

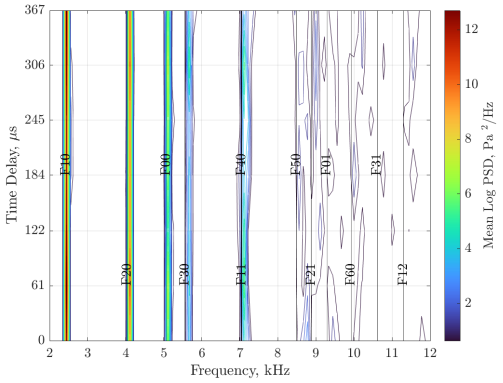

Figure 3.24: Mean FFT Peak Response to Time Delay in Periphery Heat Source Relative to Central Heat Source

3.9 Multiple Ignition Sites

The heat source at the top of the combustion chamber in the center can be thought of as a simplification of spark plug initiated heat release. When knock occurs, this heat source will already be present and hence there are potentially two stimuli which can excite the combustion chamber acoustic modes. Two heat sources were therefore implemented - one in the "spark plug location" and one in the periphery of the combustion chamber representing end-gas knock, in the same location as the original Draper experiment. As the stimulus in the periphery of the combustion chamber will occur some time after the spark plug ignition for knocking combustion, a time sweep was performed where the heat source in the periphery was activated with progressively larger delays. The delay time increment chosen, 61 μs, corresponds to the time for an acoustic wave to traverse half the bore radius. The results are shown in Figure 3.24. It can be seen that the frequencies excited are relatively independent of the time delay applied.

3.10 Prechamber Ignition

The majority of modern engines feature a single, approximately centrally mounted spark plug. However, in recent years, there is renewed interest in prechamber ignition systems [306, 307, 310, 343, 348]. Here, a small quantity of mixture is ignited by a conventional spark plug in a volume remote to the main chamber. Hot reactive jets then exit through a number of small diameter passageways into the main chamber. These become distributed ignition sources and so the number of ignition sites in the chamber depends on the number of passages. Although the prechamber is generally mounted centrally, the jets may travel some distance from the prechamber

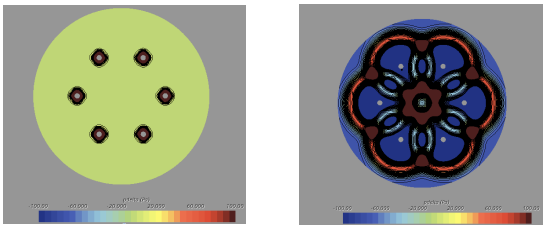

(a) Ignition + 0 μs **(b)** Ignition + 40 μs

Figure 3.25: Pressure Distribution in CFD for First Prechamber Ignition Case

before igniting the main chamber charge [305]. In order to study the effect of distributed ignition on pressure oscillations, six ignition sites were hypothesized for four different cases as described in Table 3.5. Images taken from CFD at the moment of heat source activation for the first case in Table 3.5 and shortly afterwards are shown in Figure 3.25.

Table 3.5: Prechamber Cases

No. Ign. Sites	Pitch Center Diameter	Offset
6	Bore Diam x 0.5	0 mm
6	Bore Diam x 0.5	1 mm
6	Bore Diam x 0.9	0 mm
6	Bore Diam x 0.9	1 mm

The mean FFT for each case is shown in Figure 3.26. It can be seen that where the ignition sites are arranged coaxially with the bore, the F10 mode at 2.4 kHz is very weak. As seen for the conventional spark ignition case, an offset of just 1 mm causes this mode to be strongly excited. The F00 mode at 5.1 kHz is similarly excited for all cases. For the 0.5x bore diameter ignition sites, peaks in the mean FFT diagrams are seen at 9.4 kHz. Figure 3.27 shows the pressure distributions at these three frequencies for the second case shortly after 3 ms. The

first two modes are confirmed as F10 and F00. The third mode appears to be a mix of F01 and F60. It can be seen that there are five peaks on the FFT of the 0.9x bore diameter cases. The F10 and F00 modes are in common with the 0.5x diameter cases. However, additional frequency content is seen at 4.1 kHz. The pressure distribution shortly after 3 ms in this frequency range is shown in Figure 3.28. The F20 mode is clear. A mixed F40/F11 pressure distribution is seen at 7.1 kHz, but is rather weak. The F60 mode is well defined. This is to be expected as six heat sources were introduced close to the periphery of the combustion chamber where this mode shows strongest pressure oscillations. In general, despite a very different initial pressure distribution for the prechamber cases in comparison to a single or twin ignition source, the frequencies excited are not markedly different from that of the previously analyzed cases, with the exception of the F60 mode, coherent with the number of heat sources.

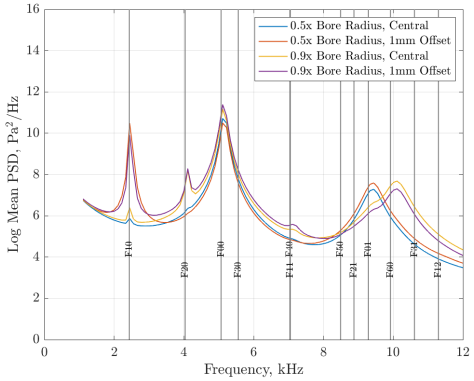

Figure 3.26: Prechamber Ignition Cases: Mean FFT Diagrams

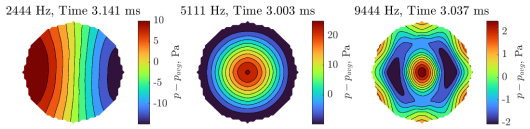

Figure 3.27: Prechamber Ignition: Pressure Distributions Shortly After 3 ms for 0.5x Bore Radius Case with 1mm Offset

3.11 Chamber Height

The height of the chamber was modified as a first approximation of piston movement, as was also performed by Draper in his stationary experiments [78]. Two heat sources were used once again - the central heat source high in the chamber and a second source once more near

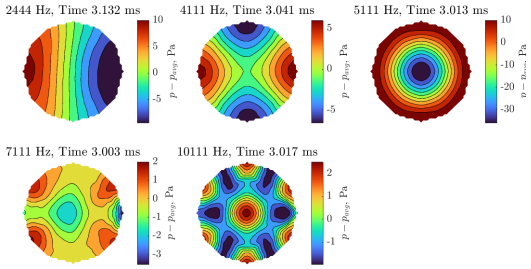

Figure 3.28: Prechamber Ignition: Pressure Distributions Shortly After 3 ms for 0.9x Bore Radius Case with 1mm Offset

the bore wall. This second source was at approximately 2 mm from the upper face of the chamber, so it could be maintained for all piston positions. This is shown in Figure 3.29. A time delay was applied to the second heat source, corresponding to the time it takes for an acoustic wave to traverse a distance equivalent to the cylinder radius for these gas conditions.

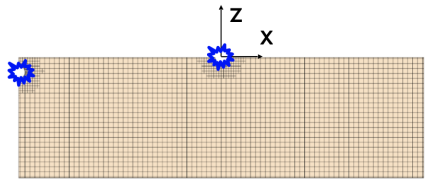

Figure 3.29: Heat Source Locations for Chamber Height Sweep

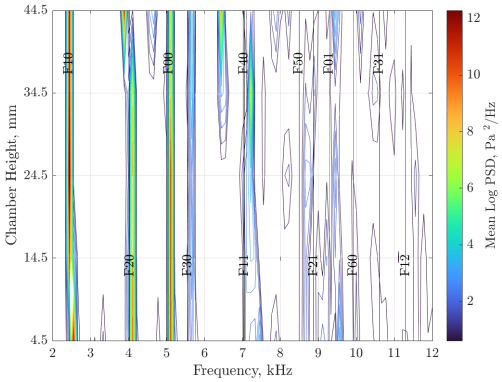

Figure 3.30: Mean FFT Peak Response to Piston Height

Figure 3.30 shows the response of the FFT peaks, once again averaged over 60 sensors, as the chamber height is modified. The F10, F20, F30 and F00 modes can all be clearly seen and are quite consistent over the sweep. The F20 mode perhaps moves to a lower frequency for the

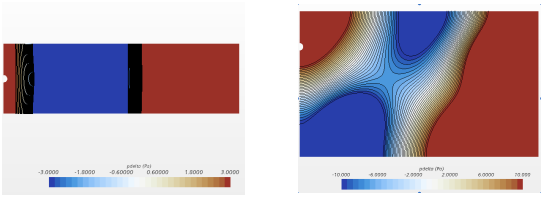

(a) Height = 24.5 mm **(b)** Height = 44.5 mm

Figure 3.31: Pressure Distribution in CFD in Vertical Plane at 1 ms for Two Different Piston Heights

44.5 mm case and also has a slightly modified pressure distribution. For the maximum chamber height investigated, new frequency content is apparent at 4.7 kHz. The pressure distribution in the measurement plane is similar to that at 5.1 kHz however - the F00 mode. For both 34.5 mm and 44.5 mm cases, a mode appears to be present at 6.4 kHz. Once again this has a similar appearance in the measurement plane to an F00 mode. Note that most likely the acoustic phenomena can no longer be considered in only two dimensions at this piston height, which is already greater than the bore radius of 41.3 mm. This is confirmed by examining pressure distributions in a vertical plane for the 24.5 mm case and 44.5 mm, as shown in Figure 3.31. The vertical pressure isolines in Figure 3.31a confirm essentially one-dimensional pressure behavior in the vertical plane and hence phenomena can be well described in the horizontal measurement plane of the virtual sensors. This is clearly not the case for the piston height presented in Figure 3.31b.

3.12 Moving Piston

When detonation occurs in a real ICE, the piston does not remain stationary. The two heat source experiment was therefore repeated with mesh cell height adjustment at each time-step to mimic piston motion. The piston height profile of a CFR engine with a compression ratio of 9:1 at 3000rpm was applied as shown in Figure 3.32. This speed was chosen as the entire piston stroke takes 10 ms - the standard calculated time thus far.

A starting mesh size of 0.5 mm was used together with a time-step of just 0.1 μs. Wavelet Synchro-Squeezed Transforms (WSST) were applied to the data from each pressure transducer. Time/frequency ridges were then extracted from each of these plots. Finally, for each time-step and frequency bin of the WSST, a ridge density was calculated by summing the number of sensors showing a ridge at this time/frequency location. The final plot is shown in Figure 3.33, where the theoretical modal frequencies (compensated for gas temperature) are overlaid.

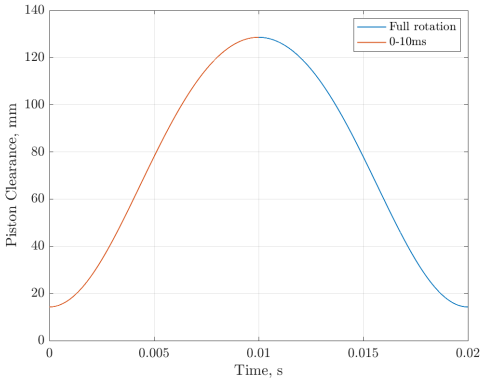

Figure 3.32: CFR Head to Piston Clearance at 3000rpm for Compression Ratio 9:1

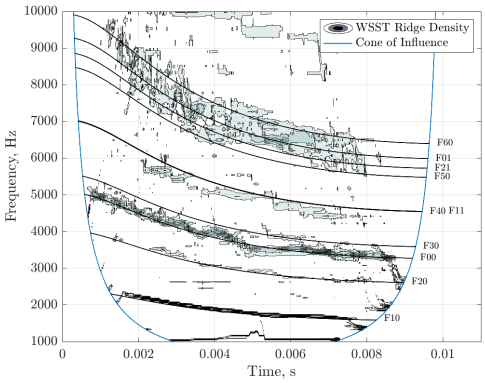

Figure 3.33: WSST Composite Ridge Density Plot for All Sensors, CFR Engine at 3000rpm, Central and Peripherical Ignition Sources with 11 μs Time Offset. Theoretical Transverse Modal Frequencies Overlaid

As has generally been seen thus far for the twin ignition case, the F10 and F00 modes are the strongest. The F20 mode is only weakly visible in the TFA whilst the F30 is even less evident. Some frequency content is seen in the region of the F40 and F11 modes. Given the weakness of F30, this is likely predominantly F11 rather than F40. The four highest frequency modes examined - F50, F21, F01 and F60 - form a wide band on the WSST ridge density plot. In general, the frequency resolution of a TFA is less than that of an FFT applied to a stationary case. However, it can be seen that there is good correspondence between the stationary and moving analysis, and the basic theory. This implies that it is not necessary to perform moving mesh calculations and consequently TFA in order to understand the underlying phenomena. A stationary case and FFT analysis is adequate to capture the key behavior, and these frequencies can be compensated based on expected acoustic velocities to extend them to a moving piston scenario.

3.13 Pressure Transducer Location Implications

Normally, the high frequency information from a single pressure transducer is summarized in a single index per cycle to give an indication of the knocking severity. Two common indices are MAPO (Maximum Amplitude of Pressure Oscillations) and IMPO (Integral of the Magnitude of Pressure Oscillations). The pressure oscillations Δp can be separated from an estimate of the average chamber pressure p_{avg} through high pass or band pass filtering. This is typically done over a range of crank angle $\theta_1 - \theta_2$ to avoid including spurious high frequency data. MAPO is defined in Equation 3.4 and IMPO in Equation 3.5.

$$\text{MAPO} = \mid \Delta p \mid_{max} \tag{3.4}$$

$$\text{IMPO} = \int_{\theta_1}^{\theta_2} \mid \Delta p \mid d\theta \tag{3.5}$$

These two indices have been applied to the data from the 60 pressure sensors for the moving piston case. As the CFD code outputs the mean chamber pressure p_{avg}, the difference between this and the individual sensor pressures was used to define Δp rather than using time-based filtering techniques. The resulting $\mid \Delta p \mid$ results from each sensor were then normalized with the mean $\mid \Delta p \mid$ value across all sensors. The MAPO and IMPO calculations were then performed and cubic interpolated surfaces have then been fitted to the results as shown in Figure 3.34. It can be seen that the normalized value of MAPO is much more sensitive to the sensor location than normalized IMPO. This is because the MAPO value is characterizing the initial peak of pressure generated by the heat source. The peak value is lower the further the sensor is from the heat source, at least for the case simulated of a non-reactive medium. IMPO on the other hand, has a value which increases with every pressure oscillation. It is therefore more strongly driven by standing waves in the chamber and less by the initial wave front. The MAPO surface indicates clearly the heat source locations whilst the IMPO surface resembles the superposition of mode shapes of F10, F20 and F00. In a real engine, the fact that the IMPO value increases for continuous small vibrations in the frequency range of interest also means that it is more susceptible to noise sources other than knocking combustion.

Developing detonation, which cannot be simulated without including reactive gas mixture, results in a shock wave which travels across the combustion chamber. The highest pressure may be when the shock wave reflects off the chamber wall at the opposite side from the initial autoignition location. Extending the model to include this knock mode will be the object of future activity.

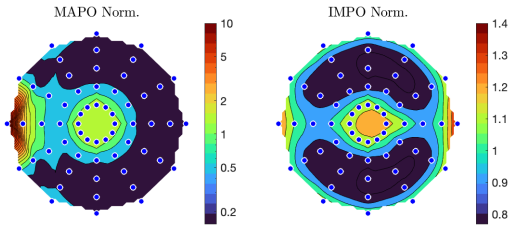

Figure 3.34: Effect of Sensor Location on Normalized MAPO and IMPO Values for the Moving Piston Case

3.14 Conclusions

An historic experiment from 1934 has been replicated in modern CFD software. The test case showed good alignment to the historic data and basic theory giving confidence in the model. In order to correctly predict modal frequencies, the CFL condition was shown to be of critical importance. A number of modifications were made to the stationary model in order to test sensitivities of modal frequencies to ignition sources and geometry. The following observations were made:

- The frequency content seen by an individual pressure transducer is highly dependent on its location with respect to modal pressure distributions. This is particularly the case for the F10 mode (transversal mode with a single nodal plane) for sensors in the periphery of the combustion chamber.
- Whilst the F10 mode is not excited by a heat source located axially and radially at the center of the combustion chamber, a 1 mm radial offset is enough for this asymmetric mode to become apparent.
- The F10 mode is also excited if a heat source on the bore centerline is not located axially at the midpoint of the chamber height.
- Multiple heat sources excite a greater number of frequencies. For the twin source case analyzed, the time delay between the activation of the heat sources does not seem to be of critical importance for the frequencies excited.
- Prechamber cases were considered through introduction of six heat sources arranged on a diameter in the combustion chamber. Despite more complex pressure distributions soon after the heat source activation, frequencies excited

were largely in common with the single and twin ignition site cases.

- A moving mesh case was calculated and analyzed with Wavelet Synchro-Squeezed Transforms. The time/frequency behavior was well aligned with basic theory and the stationary cases, which carry a much lower computational time penalty.
- Based on the model analysis, the MAPO knock index would seem much more sensitive to sensor location than IMPO

3.15 Future Activity

The main purpose of the reported investigation was to generate confidence in the methodology. It has been shown that the CFD model is well aligned to basic calculations of acoustic mode frequencies. Whilst the basic calculations are only strictly speaking appropriate for simple geometries, the CFD approach does not have this limitation. The next step is therefore to apply the CFD methodology to modern combustion chamber geometry and to compare the output with measured engine data. It is expected that the model will assist in the experimental data interpretation, through allowing the frequency information obtained to be translated into modes excited and therefore the possible stimuli.

The model at present fundamentally assumes acoustic wave behavior and hence sonic wave propagation velocities. This is not the case for extreme knock events such as mega-knock, where initial wavefront velocities may be supersonic [402]. In order to include these in the model, detailed chemistry would need to be introduced. This will also be examined in the near future, in particular with a view to understanding the time and complexity trade-offs in comparison to the simpler approach presented thus far.

CHAPTER 4

CFD Modeling of Modern Combustion Chamber Acoustic Behavior

4.1 Abstract

Knock has been studied by internal combustion engine researchers for well over a century. It remains perhaps the main limit on spark-ignition engine efficiency today. In an engine development environment, knock is typically described through quantification of the high frequency signal content of cylinder pressure measurements. A cylinder pressure transducer gives a point measurement in the combustion chamber volume. In non-knocking combustion cycles, there is little pressure variation across the chamber, hence this point measurement adequately represents the average gas pressure acting on the piston. This is not the case for knock, where autoignition leads to strong pressure gradients and standing wave behavior or even supersonic shock wave propagation. The resulting pressure signal is complex to interpret. Knocking phenomena can be simulated in Computational Fluid Dynamics (CFD), ideally using a combination of Large Eddy Simulations (LES), chemical kinetics, moving meshes and small time-steps. Such approaches are computationally intensive however, and may not be feasible to apply over the wide range of conditions for which an engine must be calibrated. A simpler model that could aid in cylinder pressure data interpretation would be invaluable as a support to calibration engineers.

To this end, a new methodology is proposed. This again uses CFD but concentrates on the pressure distributions in a combustion chamber following a localized exothermic event. The model is applied to modern engine geometry of high performance Normally Aspirated (NA) and turbocharged Direct Injection (DI) gasoline engines. Output from the CFD model is compared to experimental data at high load and beyond borderline knock conditions. It is shown that this approach can give new insight into experimental results interpretation, and allow firmer conclusions to be drawn on the relationship between knocking cylinder pressure measurements and the phenomena that are driving them.

4.2 Introduction

Engine researchers have been seeking to maximize the efficiency of Spark Ignition (SI) engines since as long as they have existed. It was realized at an early stage that increasing the compression ratio was an effective means of achieving this, but only if knock could be avoided or at least controlled [33], [32]. SI engine efficiency will continue to be fundamental even if carbon neutral fuels are adopted in the near future, as this will minimize the renewable energy expenditure necessary in their production [426].

A number of methods of measuring knock in a running engine have been applied over the years [187], [427] but high speed cylinder pressure measurements have been the most common approach in a development setting for a significant period [188], [428]. Such measurements typically exhibit oscillations of the pressure trace when knock occurs. These oscillations occur at characteristic frequencies, which Draper explained in the 1930s using acoustic theory [78]. The approach is based on the Wave equation, shown in cylindrical coordinates r, θ and z, in Equation 4.1. Here Φ is the velocity potential and c is the reference acoustic velocity.

$$\frac{\partial^2\Phi}{\partial r^2} + \frac{1}{r}\frac{\partial\Phi}{\partial r} + \frac{1}{r^2}\frac{\partial^2\Phi}{\partial\theta^2} + \frac{\partial^2\Phi}{\partial z^2} = \frac{1}{c^2}\frac{\partial^2\Phi}{\partial t^2} \quad (4.1)$$

Draper showed that the characteristic frequencies n of a cylindrical volume are given by Equation 4.2.

$$n = c\sqrt{\frac{\beta^2}{4\pi^2} + \frac{g^2}{4h^2}} \quad (4.2)$$

Here g describes the number of longitudinal modes, h is the combustion chamber height and the product of β and the cylinder radius a can only have certain values, which depend on Bessel functions.

Whilst acoustic theory can be directly applied to simple combustion chamber geometries, such as the Cooperative Fuels Research (CFR) engine used by Draper, modern combustion chambers are much more complex. Despite this fact, development engineers still apply Draper's method today [424]. Finite Element Methods (FEM) have been used to analyze complex combustion chamber geometries and predict potential resonant frequencies since at least 2002 [272]. Detailed CFD models encompassing moving meshes, combustion and auto-ignition chemistry and LES have also been applied more recently to study knock in detail [379]. The former approach is difficult to link to autoignition events however, and the latter complex to implement and requires significant computational resources.

Simple CFD models can be used to study how the combustion chamber of a modern engine responds in terms of pressure wave behavior for a given stimulus [429]. Such models are straightforward to implement, but it is not clear how closely such a model corresponds to experimental measurements in a modern high performance engine at extreme knocking conditions. If such a model could reliably aid in experimental data interpretation, it would be invaluable in development environments. This would be particularly true for cases where detailed knocking simulations are unavailable. Even in large organizations with mature CFD knock methodologies, it is unlikely to be feasible to simulate all knocking operating conditions encountered in engine calibration activity.

4.3 Engine Types

Two different high-performance engine geometries were considered in the present activity. The first of these was an NA V12 engine used in the Ferrari 812 Competizione. This features inlet-side DI and a compression ratio of 13.5:1. The second combustion chamber was that of the Ferrari SF90 Stradale. This has a centrally mounted direct injector and a compression ratio of 9.5:1. The compression ratio is lower due to the higher specific output enabled by boosting. Further details of the engines are shown in Table 4.1.

Table 4.1: Technical Specifications of Test Engines

Name	F140HB	F154FA
Type	V12 NA	V8 Turbo
Bore (mm)	94	88
Swept Volume (cc)	6496	3990
Injection System	Direct, Inlet Side	Direct, Central
Compression Ratio	13.5:1	9.5:1
Maximum Speed (rpm)	9500	8000
Specific Output (CV/L)[1]	128	195

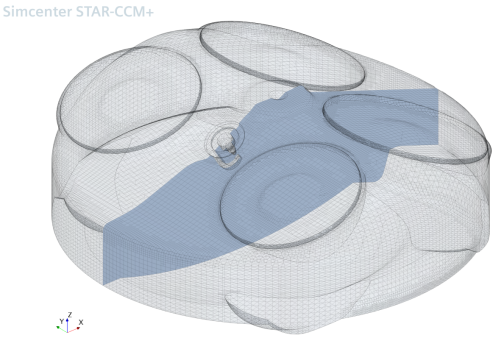

(a) V8 Combustion Chamber Geometry

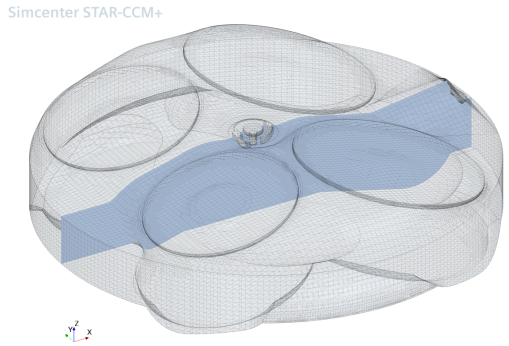

(b) V12 Combustion Chamber Geometry

Figure 4.1: Mesh Geometry of Combustion Chambers

4.4 CFD Activity

4.4.1 Model Description

CFD models were constructed in SIMCENTER STAR-CCM+ version 2020.3. A static mesh was created for each combustion chamber with a target mesh size of 1 mm as shown in Figure 4.1. Note that the combustion chamber of the V8 engine has a more pronounced piston bowl and pent-roof. The V12 combustion chamber is closer to that of an ideal cylinder. The V12 engine spark plug features two mass electrodes with a radial spark gap, whilst the turbo engine has a mass single electrode "J-type" design. In both cases, the mass electrodes are aligned with the engine symmetry plane. The height of the piston in both models was set at a value coherent with a crank angle of around 40° CA ATDC (After Top Dead Center), an angle shortly after knock is expected to occur.

The working fluid considered was air at atmospheric conditions. Turbulence and heat transfer were neglected. The Pressure-Implicit with Splitting of Operators (PISO) unsteady solver was used, ensuring a quasi-second order time discretization. Segregated third order numeric for flow and temperature was employed. A timestep of 0.5 μs was applied. This gives a Courant number of less than 0.2. This is significantly less than the minimum required for the Courant-Friedrichs-Lewy (CFL) condition. The sudden heat release of an autoignition event was represented by superimposing a 1000 W heat source on a spherical surface, obtained by subtracting a 2.5 mm diameter solid sphere from the fluid volume. This sphere was translated to simulate different cases. The heat source starts with a 0.03 ms delay from the beginning of the simulation and the duration of the source is fixed to 0.1 ms, as shown in Figure 4.2. This produces a pressure wave, which propagates across the chamber. This is an approximation of what happens in an engine following a localized autoignition event in the absence of Developing Detonation (DD).

4.4.2 Post-Processing

A total of 61 pressure measurement locations in a plane orthogonal to the cylinder axis were implemented in the model. This was with a view to post-processing, which was performed using MathWorks MATLAB R2020b. These "virtual sensors" were on a single plane offset into the chamber by 1 mm from the cylinder head face (z = -1 mm). The layout of sensors is shown in Figure 4.3. There are five groups of twelve, each group on a diameter concentric to the cylinder axis. A final 61st sensor was at the centre of the chamber. Additional

[1] 1 CV = 0.7355 kW

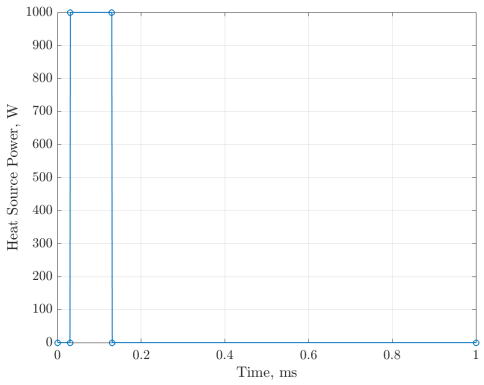

Figure 4.2: Superimposed Power Source Profile

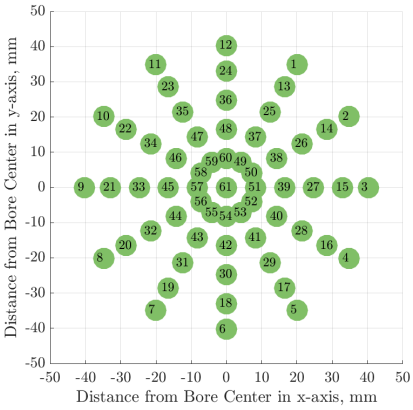

Figure 4.3: Virtual Pressure Sensor Layout in $z = -1$ mm plane

sensors were also added in x = 0 and y = 0 planes to examine three-dimensional modes where necessary. As knock typically occurs near Top Dead Center (TDC), the combustion chamber is somewhat similar to a flat disk. This is less the case than with some older engine designs however, such as the CFR. Oscillations in the z-planes are in any case thought to be most relevant. This will be commented upon later.

Frequency content of the pressure signals was analyzed both with Fast Fourier Transforms (FFT) and Continuous Wavelet Transforms (CWT). Surface fits of band pass filtered pressure distributions across the combustion chamber were used to view mode shapes directly.

4.4.3 CFD Base Case

Knock typically occurs when the majority of unburnt charge has already been consumed, in the so-called end-gas. The first case investigated in CFD was for an ignition source in the periphery of the chamber close to Sensor 9 (exhaust side). This will cause a pressure wave to propagate across the chamber in the direction of Sensor 3 (inlet side). The wave will reflect off the chamber walls and standing waves will result[2]. This case is similar to the Draper experiment of the 1930s [78].

A CWT filterbank was implemented with the Morse wavelet, a time-bandwidth product of 120 and 12 voices per octave. Wavelet transforms were performed on the data from each sensor and an average scalogram constructed, as shown in Figure 4.4. Data were extended by 1 ms before the ignition event to reduce Cone Of Influence (COI) effects. The highest amplitudes are associated with the initial pressure front and are visible as a wide-frequency-band, short-term event. Horizontal bands can be seen on both plots. Those at lower frequencies persist to the end of the calculated time[3]. The lowest band is very clear and somewhat above 2 kHz for both combustion chambers. At higher frequencies, the bands are of lower amplitude and separation is less distinct. Note that already differences can be seen between the combustion chambers, with stronger bands visible for the V12 chamber at around 5 and 6 kHz.

For these stationary cases, FFT analysis can be conveniently applied. This was performed from 2 ms onwards to more clearly identify resonance behavior after the initial ignition event. Power Spectral Density (PSD) plots were performed for each sensor. The results depend highly on sensor location, as is evidenced in Figure 4.5. Theoretical modal frequencies based on bore diameters and Draper's approach are overlaid. Peaks in the PSD are also identified. The nomenclature of Draper is used to name each mode: FXY where X = number of nodal planes and Y = number of nodal cylinders. It can be seen that, for these cases, Sensor 3 shows much more signal energy than Sensor 61. The strongest peak for Sensor 3 corresponds to mode F10, as expected. This peak is much weaker, although still present, for Sensor 61. Sensor 61 on the other hand shows strongest signal content at frequencies corresponding to the F00 mode, again in line with expectations. The F10 peak is closer to the theoretical frequency for the V12 combustion chamber in comparison to the V8. This may suggest that the equivalent acoustic diameter of the V8 chamber is smaller than the bore size in the plane orthogonal to initial wavefront direction of travel. This may be due to the V8 combustion chamber featuring a piston bowl, whereas the piston of the V12 is flatter to achieve its much higher compression ratio.

The PSD peaks were combined into a single contour plot for all sensors for clearer visualization of the results.

[2]Note that the initial wave will reflect off the upper and lower chamber boundaries as it moves across the combustion chamber. By the time it arrives at the bore wall, it will have lost some energy and also the waveform will have been modified.

[3]Wave attenuation is proportional to frequency [430]

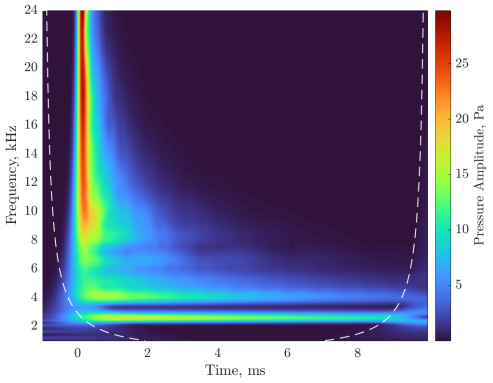

(a) V8 Combustion Chamber

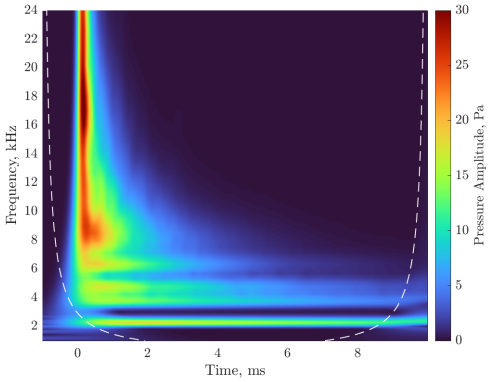

(b) V12 Combustion Chamber

Figure 4.4: Mean CWT Scalograms for Base Case, Cone Of Influence (COI) Overlaid.

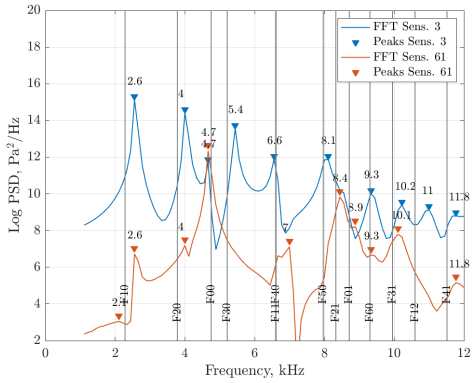

(a) V8 Combustion Chamber

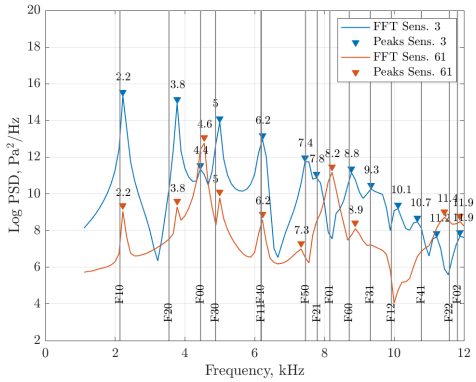

(b) V12 Combustion Chamber

Figure 4.5: Combustion Chambers for the Base Case. Peaks are Identified and Theoretical Frequencies Overlaid.

This is shown in Figure 4.6. Certain patterns can be seen. For example, the F10 peak is weaker on every sixth sensor. This is as expected, given that every sixth sensor is on a node for this mode. The modes with radial nodal planes should be most evident on sensors near the periphery of the combustion chamber *i.e.* those of lower number, for the chosen sensor numbering scheme. This would generally appear to be the case. Conversely, the F00 mode should be most obvious for sensors near the center, *i.e.* with a high sensor number. This is the case for the V12 chamber whereas for the V8, peaks are also seen at this frequency by sensors near the periphery. At higher frequencies, the picture becomes less clear as there is lower signal energy and modes are less well spaced.

In order to visualize mode shapes, Band Pass Filtering (BPF) was used. Multiple narrow pass bands were defined based on the peaks identified in the PSD plots. For each frequency of interest, BPF pressure values of all sensors were fitted to surfaces using cubic interpolation. These fitted BPF pressure distributions are shown in Figure 4.7. Timesteps were chosen which showed maximum pressure variation across the chamber for each frequency range of interest shortly after 2 ms. These diagrams allow pressure modes to be confirmed visually. In ascending frequency order, the F10, F20, F00 and F30 modes can all be clearly seen for both chambers. For the V8 combustion chamber, the peaks at 6556 Hz and 7000 Hz both correspond to an overlay of the F40 and F11 modes. For the V12 chamber in contrast, the F11 mode appears to dominate at 6222 Hz and little evidence of F40 can be seen. F50 and F60 are evident for the V12 chamber at 7333 Hz and 8778 Hz respectively. F60 can also be seen for the V8 chamber, in this case at 8889 Hz. For this chamber, there may be an overlapping mode with pressure variation on the cylinder axis. A complex mode shape at 8111 Hz for the V8 is also seen and is not obviously F50, the nearest theoretical mode expected. F21 and F01 theoretical frequencies are also nearby and hence multiple modes may be overlapping. At still higher frequencies, the mode shapes become more complex and their amplitudes weaker making interpretation more difficult.

Standing waves in other planes may also become signifi-

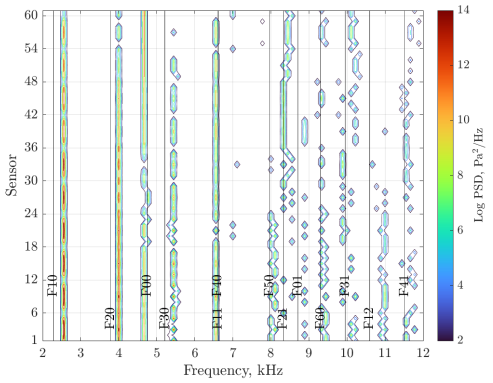

(a) V8 Combustion Chamber

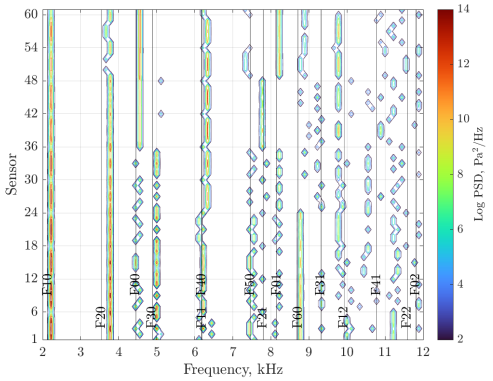

(b) V12 Combustion Chamber

Figure 4.6: Contour Plots of PSD Peaks for both Combustion Chambers and the Base Case. Theoretical Frequencies Overlaid.

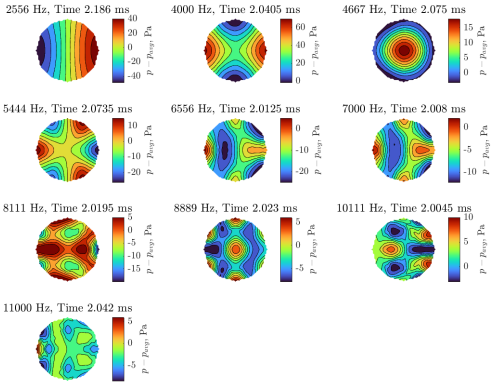

(a) V8 Combustion Chamber

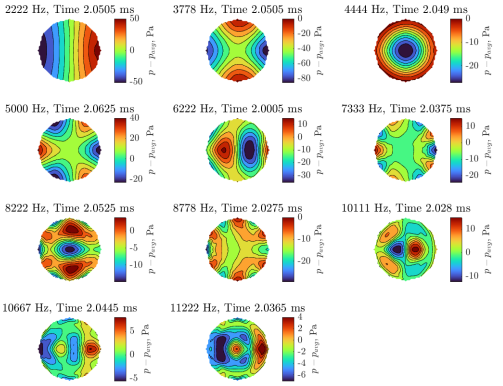

(b) V12 Combustion Chamber

Figure 4.7: Mode Visualization for both Combustion Chambers and the Base Case

cant at high frequencies. To examine this, further sensors were added to the model in the $x = 0$ and $y = 0$ planes. These showed that pressure isolines were generally close to parallel to the cylinder axis. The exceptions were that an axial mode was found for the V8 chamber at 8889 Hz, coherent with the distance between head and piston at the center of the chamber of 19 mm, and for the V12 at 11222 Hz, corresponding to its average chamber height of 16 mm.

In general it can therefore be said that up to around 8 kHz for the V8 case and 10 kHz for the V12[4], pressure modes excited by an ignition event in the periphery of the combustion chamber are primarily in planes orthogonal to the bore axis. This may not be the case if the piston is at a lower position, as this will lower the frequency of the axial modes of the cylinder. The piston will generally be close to TDC at the moment of autoignition for knocking cycles in a typical combustion engine however. This will be commented upon in the experimental section.

[4]This corresponds to around 24 kHz and 30 kHz for the V8 and V12 chambers respectively for realistic acoustic velocities in a running engine

4.5 Ignition Location Sensitivity Sweeps

The modes that are excited by knock, and their relevant strength, depend not only on the combustion chamber geometry, but also the location of the autoignition event. Sweeps of the heat source location were therefore performed for both geometries.

4.5.1 Radial Sweeps

The ignition site was moved from around the position of Sensor 9 (x = -44 mm), to around the position of Sensor 3 (x = +44 mm, in steps of 11 mm, for both combustion chambers. The results can be seen in Figure 4.8. Here, the frequency peaks identified from all 61 sensors

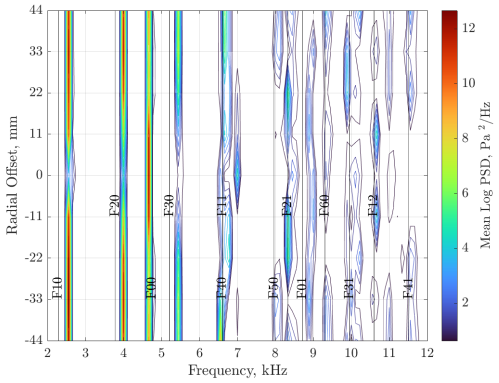

(a) V8 Combustion Chamber

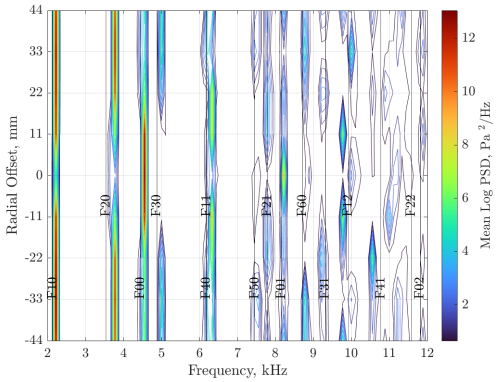

(b) V12 Combustion Chamber

Figure 4.8: Average FFT Peak Sensitivity to Ignition Site Radial Offset in x Direction

are combined in a single vector per test case. In general, it would be expected to see a weakening of the modes with maximum pressure variation near the edge of the combustion chamber, and strengthening of those with pressure variation near the center, as the ignition site is moved from the periphery to the middle of the chamber. Indeed, this pattern is clear for F10, F20, F30, F50 and F00 for both chambers. F40 is expected to overlay with F11 and in fact peaks on the FFTs were detected in the relevant frequency range of these modes over the entire sweep. The F21 and F12 modes appear at intermediate ignition site distances, again coherent with their modal pressure distribution. There is therefore a clear connection between autoignition radial offset from the center of the chamber and the relative strength of each mode.

The sweep was then performed in the y-direction, again in steps of 11 mm from the center. The results for all sensors are shown in Figure 4.9. The patterns of frequencies excited are generally similar to the x-sweep when considering the composite values from all sensors.

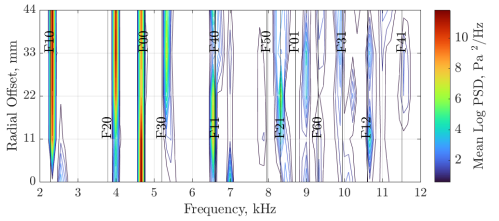

(a) V8 Combustion Chamber

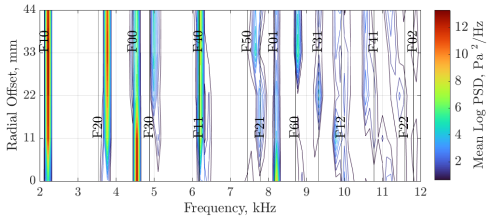

(b) V12 Combustion Chamber

Figure 4.9: Average FFT Peak Sensitivity to Ignition Site Radial Offset in y Direction

4.5.2 Angular Sweep

Knock generally occurs when the flame-front has already consumed the majority of the unburnt charge. It is therefore more likely to occur near the periphery of the combustion chamber, especially for typical modern engines with spark plugs near the center[5]. The most practically interesting sweep is therefore an angular sweep of ignition sites near the bore wall. For a purely cylindrical combustion chamber, the average of frequencies excited across the chamber would not of course change and the mode shapes would simply rotate. Modern combustion chambers have more complex forms however, hence more interesting results could be expected.

The heat source was moved angularly around the cylinder axis in steps of 15° from 0° (combustion chamber symmetry plane, exhaust side) to 180° (combustion chamber symmetry plane, intake side). The radial distance was maintained constant at 44 mm. The results are shown in Figure 4.10a. Note that, for the V8 geometry, F10 does not have a constant frequency as the angular offset is changed. When the ignition source is close to Sensor 9 or 3 (0° or 180°), the frequency of F10 is higher than if the ignition source is close to Sensor 12 (90°). This effectively means that, acoustically speaking, the combustion chamber is smaller in the x direction than in the y direction. For the V12 combustion chamber in contrast, F10 is very stable with angular heat source location. Some frequency shifts can be seen for F20 on the other hand, perhaps due to the valve pockets.

The mode behavior in the predicted frequency range

[5]Note that many earlier engines, including the CFR, featured a side mounted spark plug.

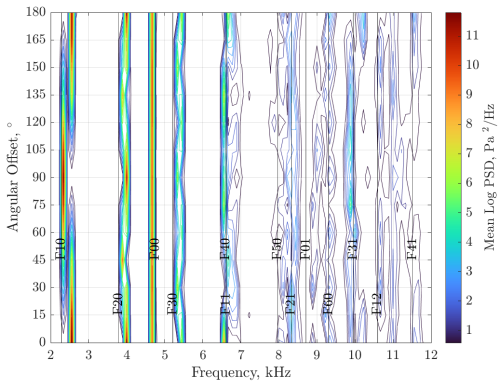

(a) V8 Combustion Chamber

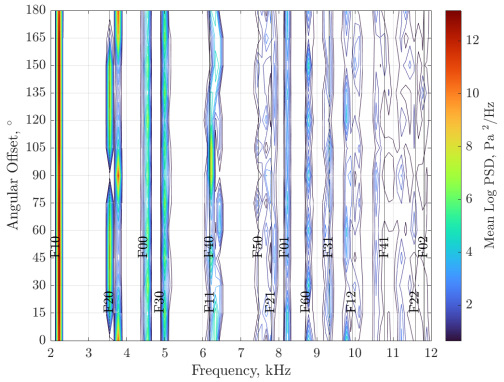

(b) V12 Combustion Chamber

Figure 4.10: FFT Peak Values for Angular Sweep

of F11 and F40 was examined over the angular sweep for the V8 geometry. The strongest frequency peak was considered in each case. The results are shown in Figure 4.11. The results show that mode transitions occur as the ignition source moves around the chamber border. The pressure distributions suggest that 6556 Hz corresponds to F40 and 6778 Hz to F11. Note that the 180° source excites the F11 mode more strongly than the 0° case, where F40 appears predominant. Recall that the piston bowl of the V8 is offset from the center of the chamber, as shown in Figure 4.1.

4.6 Experimental Tests

4.6.1 Raw Data Analysis and Thresholding

Testing was carried out on the V8 engine at 3000 rpm and full load. This corresponds to 26 bar of Indicated Mean Effective Pressure (IMEP). An ignition timing

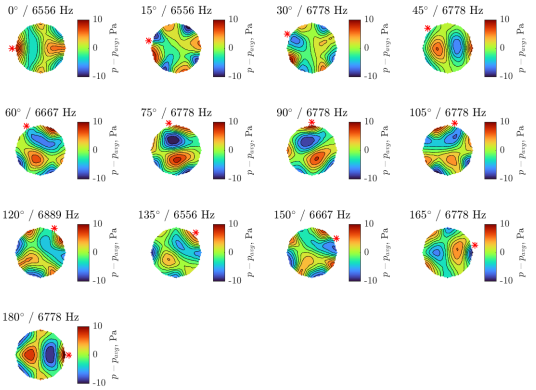

Figure 4.11: Angular Sweep Predominant Mode Shift for Frequencies in Range 6.4-7.0 kHz, V8 Combustion Chamber. Heat source location is shown with '*'

sweep was performed beyond the range of standard calibration activity, in order to generate a large number of strongly knocking cycles. The engine was instrumented with one Kistler 6044 M8 size flush-mounted piezoelectric sensor per cylinder, connected through a Kistler 5064C charge amplifier to an AVL Indimaster 672 acquisition system. The crank angle resolution was 0.1° CA, which corresponds to a sampling frequency of 180 kS/s at 3000 rpm. Cylinder 5 was chosen for detailed analysis as it showed the strongest knocking behavior. The sensor location corresponds to that of Sensor 18 in the CFD analysis, although offset of course in the z plane. Raw data from a 500 cycle acquisition are shown in Figure 4.12.

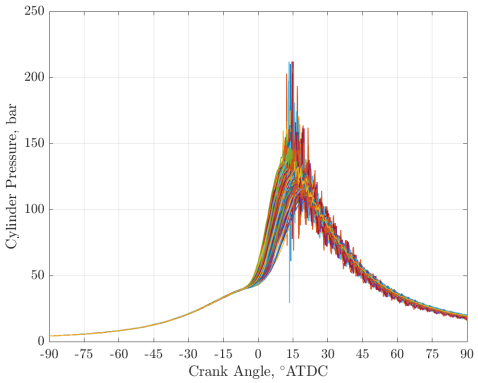

Figure 4.12: Experimental Data from Cylinder 5 at 3000 rpm Full Load and Advanced Ignition Timing, V8 Combustion Chamber

Maximum Amplitude of Pressure Oscillation (MAPO) and Integral of the Modulus of Pressure Oscillations (IMPO) algorithms were implemented in MATLAB. The pressure oscillations, Δp, were separated from an

estimate of the average chamber pressure, p_{avg}, using a High Pass Filter (HPF). An Infinite Impulse Response (IIR) HPF with a cutoff frequency of 4.0 kHz and an attenuation of 60 dB at the stopband frequency of 3.4 kHz was specified. An angular window, $\theta_1 - \theta_2$, of -90 to +90° ATDC was chosen. MAPO for the present activity is defined in Equation 4.3 and IMPO in Equation 4.4. MAPO was used as the main reference.

$$\text{MAPO} = \mid \Delta p \mid_{max} \tag{4.3}$$

$$\text{IMPO} = \int_{\theta_1}^{\theta_2} \mid \Delta p \mid d\theta \tag{4.4}$$

A Low Pass Filtered (LPF) cylinder pressure curve was constructed based on the difference between the original and the HPF version. A single-zone First-Law heat release analysis, with temperature-dependent gas parameters, was implemented. The average gas temperature was estimated using the State Equation. Apparent Heat Release (AHR) was normalized to give an estimate of Mass Fraction Burned (MFB). The normalization was based on the average value of cumulative AHR from 70-90° CA ATDC. Knocking cycles are associated with higher heat transfer - as much as three times that of normal cycles according to the literature [195, 256]. This will be commented upon later.

It is common with experimental knocking datasets to separate the cycles into "knocking" and "non-knocking" populations. There are a number of ways in which this can be performed. Frequently, a knock index such as MAPO or IMPO is first calculated for all cycles. A threshold is then set to separate between the two classes. This threshold generally compensates for the fact that high frequency content will be present also for non-knocking cycles. One approach, is to define a threshold of MAPO as a function of engine speed. This assumes that non-knock driven high frequency noise depends only on this operating parameter. In reality, it will depend also on engine load, combustion phasing, sensor type, sensor location and other variables. A pragmatic approach was suggested by Gail *et al.* [374], where the noise was characterized using the median of the dataset and the knocking threshold was set as a factor of this value. It may be the case that a unique factor is not appropriate for all conditions however. It is often stated that knocking cycles follow a lognormal distribution [280], [409]. The first mention of this in the literature may have been in the 1980s by Iwata *et al.* [194]. In that paper, it was actually stated that knock indices of both non-knocking and knocking cycles follow a lognormal distribution but that these two distributions are distinct. It was furthermore suggested that this observation could be used to separate between knocking and non-knocking cycles. This approach has been applied to the current dataset as shown in Figure 4.13. It can be seen that the experimental data deviates from the single lognormal probability fit at around a MAPO value of 20 bar. This corresponds to 2.5 times the median value of the dataset. This factor is coherent with past activity in terms of threshold setting [374].

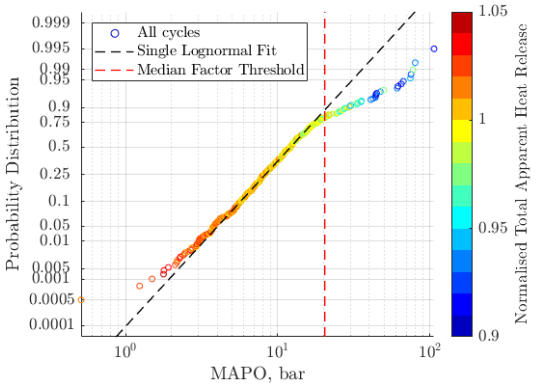

Figure 4.13: Lognormal MAPO Statistics and Comparison with Median Factor Threshold Method and Normalised Total Apparent Heat Release, V8 Data

Note that the cycles above this threshold are also those with a total AHR of less than 95% of the mean value of this dataset. Recall that this is "Apparent" heat release *i.e.* that which results in a measurable increase in pressure on the piston. It is therefore affected by heat transfer. The low values for the knocking cycles are hence most likely driven by increased heat losses rather than reduced combustion completeness. A similar effect attributed to knock has already been reported in the literature [302].

4.6.2 Time Frequency Analysis

The threshold value appears appropriate for separating knocking and non-knocking data. This enables these two classes of cycle to be compared. Figure 4.14 shows mean Continuous Wavelet Transforms for knocking and non-knocking cycles. The greater high frequency signal content of the knocking cycles is immediately apparent. Note that even for the non-knocking dataset, a horizontal band at around 7 kHz can be seen. This corresponds to the F10 mode, which is very easily excited, even by stimuli close to the center of the chamber [429]. Some higher frequency content is also visible, although clear bands cannot be discerned. For the knocking cycles, a strong vertical band at around 12° ATDC can be seen on the scalogram. This corresponds to an impulsive event, which is likely the incident wave from autoignition.

In order to understand the evolution of high frequency data with crank angle across individual cycles, the maximum value of pressure amplitude at each crank angle from the CWT was extracted for each cycle, for frequen-

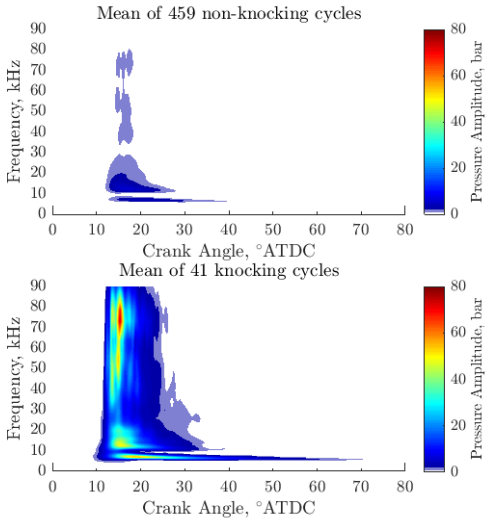

Figure 4.14: Mean Continous Wavelet Transform Scalograms for Knocking and Non-knocking Cycles

cies above 4000 Hz. The cycles were then sorted in ascending order of MAPO for visualization, as shown in Figure 4.15. It is interesting to note that the high frequency signal content arrives relatively late in the cycle in comparison to flamefront propagation. This is clear if the pressure amplitude data is plotted against MFB values, as shown in Figure 4.16. It can be seen that for low MAPO cycles, high frequencies are present after MFB90 (90% MFB). For most cycles, significant high frequency content appears after around MFB80. For the strongest cycles in the dataset, high frequencies are visible from as early as MFB50, but there is a strong increase at around MFB80-90.

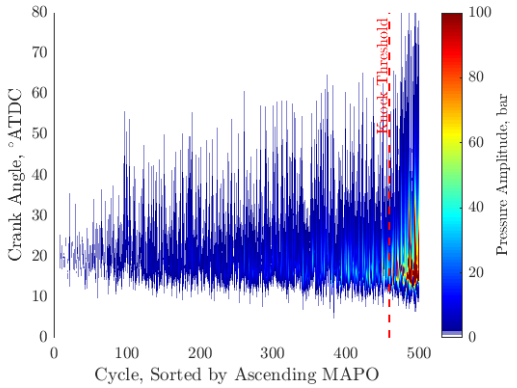

Figure 4.15: Maximum Pressure Amplitude versus Crank Angle for All Cycles, Sorted in Order of Ascending MAPO

This increase is most likely driven by strong autoignition

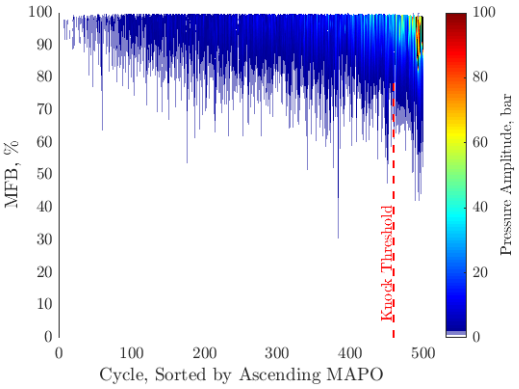

Figure 4.16: Maximum Pressure Amplitude versus Mass Fraction Burned for All Cycles, Sorted in Order of Ascending MAPO

events. The rise at MFB50 could be due to fast combustion or initial autoignition events of lower severity. It may be the case, based on Figure 4.16, that weak autoignition is occurring late during flame-front propagation even for low MAPO cycles. As described by Zeldovich [208] in 1980, the consequences of an initial autoignition event depend on the reactivity gradient around the exothermic center. The strongest pressure wave behavior is expected when conditions are such that the incident pressure wave emanating from the exothermic center becomes coupled with local autoignition chemistry. This can lead to DD and supersonic shock-waves. This theory was expanded upon by Bradley *et al.* [263] in 2002 who indicated that a second parameter, related to exothermic center dimensions, was also important. Figure 4.13 clearly suggests two classes of cycles in the dataset. Figure 4.16 suggests that autoignition may be present for the majority of cycles. The threshold between the two classes of cycles may therefore represent a change in autoignition behavior rather than a level below which no autoignition occurs.

4.6.3 CFD Supported Pressure Signal Analysis

The most relevant CFD case was considered to be the angular sweep of an ignition source near the bore wall. The FFT peak data for this sweep and Sensor 18 only are shown in Figure 4.17.

In order to directly compare experimental data to the CFD model, the experimental time intervals of the pressure signal were scaled based on the estimated acoustic velocity, c. This acoustic velocity was calculated based on mean gas properties from the single zone heat release analysis already described. These adjusted data were resampled to a uniform timestep of 1 μs and then FFT

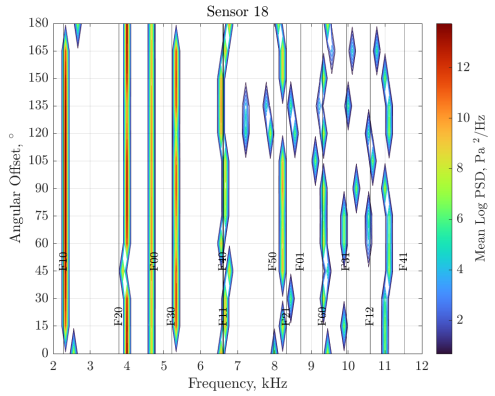

Figure 4.17: FFT Peak Data for Angular Heat Source Sweep with V8 Chamber, Sensor 18

analysis was performed. The mean PSD plots for non-knocking and knocking data, adjusted in this manner, are shown in Figure 4.18. The peaks identified in FFT analysis of the CFD angular sweep for Sensor 18 can be directly compared and are overlaid for comparison. Note that a range of frequencies for several modes were identified in the CFD analysis. This is due to the combustion chamber not having a unique acoustic diameter.

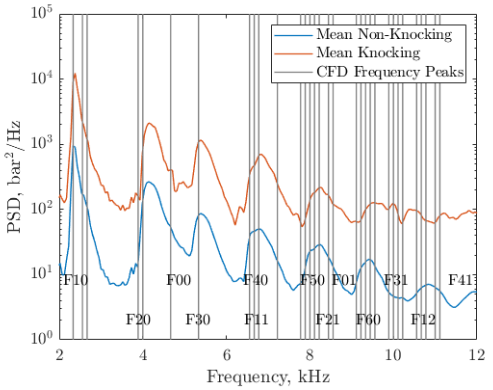

Figure 4.18: Mean Acoustic Velocity Compensated Power Spectral Density Plots of Experimental V8 Dataset. Peaks Identified in CFD Angular Sweep are Overlaid

It can be seen that there is generally good agreement between the peaks evident on the PSD plot of experimental data and those identified in CFD. The predominant F10 mode appears to be associated with the largest acoustic diameter of the chamber. This is expected for all ignition sites that are not at 0° or 180°, as shown in Figure 4.17. The experimental peak for the F20 mode is at a slightly higher frequency than for the model value. A small peak due to F00 can only be discerned for the knocking cycles and is well aligned in frequency terms to the model. F30 is clear for both sets of cycles and here too the PSD peak frequency is well aligned with the model. There is evidence of multiple peaks present in the F40/F11 region for the knocking dataset. The lower frequencies should correspond to F40 and the higher F11, according to Figure 4.11. Figure 4.17 suggests that higher frequencies may be associated with a knock origin at an angular offset of ±45° (exhaust valve region) or 180° (symmetry plane, inlet side) and those at lower frequencies in the range ±120-150° (inlet valve region). Note that the experimental peak in the F40/F11 band is more pronounced at a higher frequency for strong knocking cycles than those classified as non-knocking.

Some further statements on potential autoignition site locations can be made by considering relative mode strengths. Figure 4.19 shows how the PSD values for F10, F20, F30 and F00 change over the angular sweep at the position of Sensor 18 in CFD. The data have been fitted by a 3-sine function.

Three regions can be identified on this diagram based on relative mode strengths. Local pressure oscillations associated with the F10 mode at the sensor location will only be weaker than those of F20 if the sensor is close to the F10 nodal plane. The F10 nodal plane orientation depends on the heat source location. In particular, Figure 4.19 shows the exact range where F20 driven oscillations are stronger than F10 (for the given sensor) to be associated with an autoignition location at ±0-27° or ±152-180° . If, on the other hand, F20 is weaker than F30, the sensor must lie close to one of the two nodal planes of F20. This implies an autoignition event in the range ±13-53° or ±125-146°. The F00 mode is seen rather weakly by this sensor, which is mounted near the periphery. It can be compared to the value of F30 however, to identify when the sensor lies close to a nodal plane of this mode, where that nodal plane is not shared with F10. This occurs at around ±62° and ±118°. This angular region was reduced where overlapping with the others to avoid successive double counting of cycles.

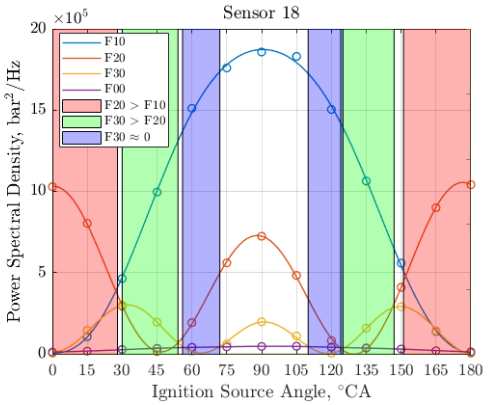

Figure 4.19: Strength of Some Key Modes for Sensor 18 in CFD Model over Angular Sweep

Considering each cycle individually, estimates on autoignition location can be made by comparing the relative mode strengths read by the sensor. Results are shown in Figure 4.20. The number of cycles identified in each region was normalized by the number of cycles expected in that region if autoignition sites were uniformly distributed in the chamber. Slightly more than 70% of cycles could be characterized based on this method with just one sensor. The results suggest that strong knocking cycles are biased towards the sectors of the chamber close to ±45° and ±135°. This is the area of the valve pockets. The exhaust valve pockets are considered more likely, given the high frequency peak in the F40/F11 region shown on the PSD for the strong knocking cycles. The non-knocking (or mostly likely weakly knocking) cycles on the other hand, are consistent with an autoignition site in the region ±60° or ±120°. Figure 4.17 does not show a frequency shift for the F40/F11 band between these two angular possibilities, hence estimating which is most likely cannot be ascertained by this method for the low-knocking cycles.

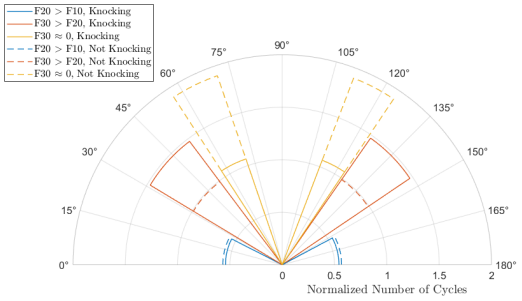

Figure 4.20: Possible Knock Locations in Combustion Chamber based on Relative Strength of F10, F20 and F30 Modes

4.6.4 Validation of Knock Location

The relative acoustic mode analysis suggested that strong knocking cycles were most likely driven by autoignition events in the exhaust valve pocket or inlet valve pocket regions. For a simple combustion chamber geometry, it would not be possible to further distinguish between these possibilities. The asymmetry of the combustion chamber under investigation however, led to a F40/F11 mode transition in CFD, which depended on the autoignition location, as shown in Figure 4.11. CFD-supported experimental analysis therefore suggested the exhaust side pocket as the likely source. In an effort to independently validate this assertion, a detailed CFD study using a different methodology was employed. This detailed model does not make use of experimental data, as it is intended for design and validation of combustion systems before they arrive in experimental test facilities. In the following paragraphs, a brief description of the model is reported. Further details of the modeling approach (applied to a different combustion system) can be found in [331].

3D-CFD simulations were carried out in STAR-CD v4.30. Calculations were performed using a RANS (Reynolds Averaged Navier-Stokes) approach and the $k - \varepsilon$ RNG (Re-Normalization Group) turbulence model [431]. The ideal gas equation of state was adopted to close the set of RANS equations. Viscosity was modeled as a function of temperature by Sutherland's equation. Specific heat and thermal conductivity were considered as temperature dependent using polynomial functions. The non-slip condition was imposed at solid walls and temperature was fixed. The near-wall flow was modeled via a high-Reynolds approach to save computational cost, thus wall functions were adopted for both velocity and thermal boundary layers. The numerical solver uses a PISO solution algorithm and a second order Monotone Advection and Reconstruction Scheme (MARS) for momentum, temperature, turbulence and species transport equations. Time steps were variable in the range 1-8 μs, to keep the CFL number to approximately unity.

The computational domain included the combustion chamber and the intake and exhaust ports. Boundary conditions of pressure and temperature were taken from a one-dimensional unsteady gas dynamics model of the test setup. Geometrical symmetry was exploited, thus only half of the domain was simulated in order to reduce the computational effort. The computational mesh was created using trimmed cell technology. Global average mesh size was 0.75 mm in the cylinder and ports; once the initial mesh had been created, a local subdivision of cells was performed around the spark plug. Globally, the number of fluid cells for the full-cylinder was approximately 1 million at Bottom Dead Center (BDC). The software uses a dynamic cells addition/removal feature, to remove or add cell layers as the piston moves, thereby preventing the layers from becoming excessively compressed.

A Lagrangian approach was applied for spray modeling of the multi-hole gasoline injector. The injected spray parcels were represented using a Monte-Carlo method. Single-component Lagrangian phase was constituted of gasoline, whose properties were tailored to match the real fuel properties used at the test bench facility. The same applies to the vapor phase of the evaporated droplets. In order to replicate the particle size distribution of the liquid phase exiting from the injector, a Rosin-Rammler distribution was adopted, while the secondary break-up was modeled following the recommendation of Reitz [432]. For each nozzle hole, a unique injection rate profile was used.

The flame front was modeled with the commonly used ECFM-3Z (Extended Coherent Flame Model - 3 Zone)

approach. In the CFM combustion model family, the flamelet hypothesis assumes a time-scale separation between the turbulent eddy turn-over time and the chemistry time-scale, the latter being at least one order of magnitude smaller. Therefore, the reaction rate is controlled by the turbulent kinetic energy, which acts as a surface amplifier for reactant interface, while the flame front preserves its laminar inner structure. The burn rate, $\dot{\omega}$, in every computational cell is given by the expression $\dot{\omega} = -Y_F \rho_u \Sigma S_L$, where Y_F and ρ_u are the fuel mass fraction and the unburnt mixture density respectively and Σ is the flame surface density. S_L is the laminar flame speed at the cell thermodynamic condition. Its values were pre-computed using an offline method, using a detailed chemistry approach, as previously described in [331].

Pre-ignition kinetics were not directly resolved in ECFM-3Z. Rather, an auto-ignition delay time, τ_d, was computed, and used to establish the time when knock occurred. To accomplish this task, an ignition progress variable function, Y_{igi}, was defined to track the development of the reactions prior to auto-ignition: $\frac{dY_{igi}}{dt} = Y_{TF} F(\tau_d)$, where Y_{TF} is the fuel mass fraction. Once the critical delay is reached, *i.e.* $Y_{igi} > Y_{TF}$, an extra flame surface is added in the unburnt gases. The auto-ignition delay is calculated based on semi-empirical correlations of RON, pressure, residual gas fraction and unburnt temperature.

Ignition timing was adjusted in the detailed 3D-CFD model to phase the combustion coherently with the mean experimental pressure trace with the autoignition model deactivated. Figure 4.21 shows the alignment between the experimental pressure trace and that of the detailed model. The detailed model is clearly well aligned in terms of average cylinder pressure.

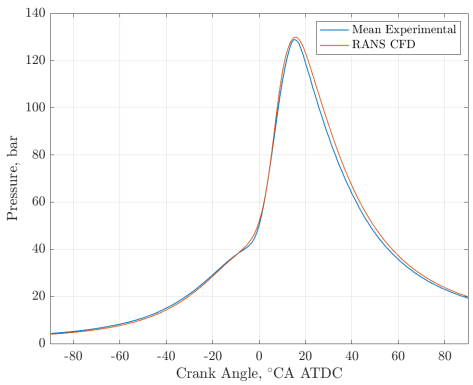

Figure 4.21: Comparison between Mean Experimental Cylinder Pressure and Detailed 3D-CFD Cylinder Pressure

The autoignition model was then activated. The knock onset location can be seen in Figure 4.22a at 10° CA.

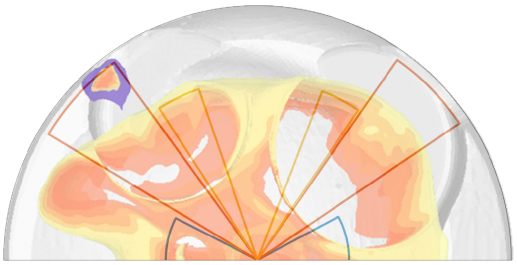

(a) Autoignition Onset at 10° CA ATDC

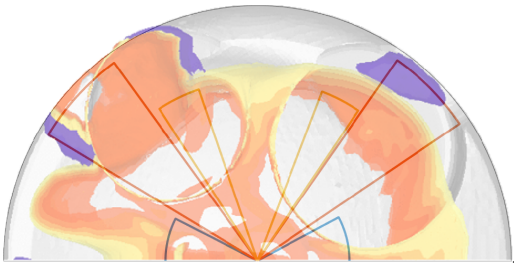

(b) Autoignition Onset at 11° CA ATDC

Figure 4.22: Comparison of autoignition onset location from detailed CFD calculations with probable knock location of strong knocking cycles evaluated through frequency analysis of experimental pressure data supported by the simple "acoustic" CFD model. Note that the exhaust pocket (left hand side of images) was considered most likely from the latter method.

Figure 4.22b shows that just 1° CA later, the autoignition reaction front has grown significantly. This rapid reaction front velocity would most likely cause the generation of a pressure wave, in a manner analogous to the heat source of the simple CFD model. The timing of the autoignition event is coherent with the CWT analysis in Figure 4.14. In both Figure 4.22a and Figure 4.22b, the probable knock locations for the strongly knocking cycles from Figure 4.20 are overlaid. The autoignition onset location is confirmed to be in the sector considered most probable from the previous analysis *i.e.* that associated with the exhaust valve pocket.

Knowledge of the most knock prone regions of the combustion chamber is valuable, as it permits actions to be taken to address these problem areas. This may include acting on the chamber cooling to inhibit pre-flame reactions. Alternatively, modifying port and piston geometry, or the injector spray pattern, can encourage the flame front to consume these regions before autoignition can occur. If this can be done without creating issues in other parts of the chamber, the overall knock limit should be improved. This would enable an increase of compression ratio or a reduction in spark retard, hence improving efficiency. Whilst a range of methods already exist to locate knock in an engine, such as optical sensors [251],

[252] or three or more pressure transducers [239], [284]. Such approaches tend to be more expensive, or more invasive, than the methodology described in the current manuscript.

4.6.5 Future Activity

It has been described above how estimates can be made of the location of knock from just a single pressure transducer combined with CFD-supported acoustic analysis of the chamber. An independent fully CFD based methodology suggested a similar knocking location. An additional sensor would enable further possibilities for both frequency based methods and conventional triangulation techniques. This would likely increase accuracy and robustness. It may be the case that only two sensors are required to fully locate the autoignition region using such a combined approach. In contrast, the pure triangulation method based only on relative wavefront arrival times requires at least three sensors [239]. The possibility of being able to obtain similar information with one less sensor has obvious appeal - particularly in a development environment with a near-production engine. This will be the object of future investigation.

4.7 Conclusions

- A CFD analysis of combustion chamber acoustic modes has been applied to modern combustion chamber geometry
- Acoustic modes and their frequencies were found to be quite close to predictions based on analytical methods applied to simple, cylindrical geometry, in particular for the lower modes
- The V8 turbocharged engine combustion chamber was found to exhibit two characteristic acoustic diameters due to its geometry. This led to frequency shifts and mode shifts considering an ignition event near the bore wall over a range of geometric angles.
- The V12 NA combustion chamber, whose geometry is closer to a perfect cylinder, exhibited resonant frequencies and mode shapes better aligned to basic acoustic theory applied to the bore diameter.
- Experimental testing in strong knocking conditions for the V8 combustion chamber showed good alignment in terms of frequency peaks in FFT analysis with the CFD model (corrected for acoustic velocity)
- A method of thresholding MAPO values based on a dual-lognormal distribution correlated well with Apparent Heat Release approaches and thresholding based on a factor of the Median MAPO value
- The change in the relative mode strengths seen by a pressure transducer over the angular location sweep gives information on the likely knock origin. Possible autoignition locations were identified for the V8 chamber, associated with the valve pocket regions. The exhaust valve pocket was thought more likely for the strongly knocking cycles based on FFT analysis indicative of a mode shift. This preferred knock location was confirmed using an independent fully CFD based methodology.
- Whilst the information for identifying the autoignition location is somewhat limited when only a single transducer is available, it is thought that a second transducer would open up significant possibilities to extend frequency based localization combined with wavefront arrival based triangulation methods. This will be the object of further study

CHAPTER 5

Fuel Development and Understanding

5.1 Abstract

Fuel and engine development have been inextricably linked since the birth of the automobile. The most famous, but least flattering example, was the introduction of Tetra-Ethyl Lead to enable increased compression ratios in the 1920s and 1930s. There has been a lot more to fuel development over the last century than just anti-knock additives however.

Whilst in the early years, automotive manufacturers carried out significant research on fuels, this has waned in recent years, with some notable exceptions. In Formula 1 however, engines and fuels are co-developed. Methodology in support of such development includes chemical kinetics mechanism development, supported by rig testing for ignition delay time measurements. These can then be incorporated in full engine CFD calculations and results validated in experimental engine testing.

The main issue for passenger car engines is not to decide what fuel is most desirable and to create it - it is to properly understand the behavior of market fuel and exploit it. The Formula 1 methodology developed by Ferrari and Shell was thus harnessed to design and validate a surrogate fuel to represent a high performance, high octane, full boiling range gasoline. A surrogate based on toluene, n-heptane and iso-pentane was blended and tested in a CFR engine, a rapid compression machine and finally in a high performance production engine. Good correlation was found to the target market gasoline giving confidence in use of such a surrogate for future engine simulation activity.

5.2 Introduction

As described in Chapter 2, fuel development for much of the 20th Century focused on reducing knock. The main feedback on the fuel knock resistance was the Octane Number. The original octane test was the Research Octane Number method (RON), created by the Co-operative Fuels Research (CFR) group in the 1920s. In the 1930s, a revised test - the Motor Octane Number method (MON) was developed to better correspond to the knock behavior of vehicles of the period. The MON test results in higher in-cylinder temperatures for a given in-cylinder pressure. As engines evolved over the 20th Century, improvements in design led to reduced temperatures for a given pressure. This meant that the RON test once again became the most relevant and for turbocharged and intercooled engines, the temperature for a given pressure may be even cooler than for the RON test. This led Kalghatghi to introduce the "K-value" concept. This effectively extrapolates to "beyond RON" conditions starting from the MON and RON values of the fuel [286].

Strictly speaking, the RON and MON tests only tell of the knock behavior of a fuel in the CFR engine at its reference conditions. Despite the fact that engine design has changed markedly since the 1930s, the RON and MON test are still used for fuel rating today. Whilst in the early part of the 20th Century, octane values improved over time, for a number of years premium unleaded has been sold with a standard RON value of 95. Super-premium blends exist with higher octane values, but most manufacturers will design their engines to tolerate the most common market fuels. Fuel for road cars has therefore largely become a boundary condition to respect rather than a development pathway.

This is not the case in Formula 1. Here, engines and fuels are co-developed to achieve the best overall performance. All engine manufacturers have close partnerships with their fuel and oil suppliers. The technical partner for Ferrari is Shell. The author of this thesis worked for a number of years with Shell to develop fuels for Formula 1 applications. For a period, as many as five new fuel blends would be brought to the race track per season. Whilst the fuel regulations for Formula 1 [417] approximately correspond to EN-228 (which governs standard commercial unleaded fuel), in practice Formula 1 suppliers produce laboratory blends selecting the most appropriate molecules to optimize performance rather than refining based on a given crude oil. The final blends must feature at least six components but in practice, 70% of the fuel may be made up of just two.

This is very different to commercial gasoline blends. These are produced through successive refinery operations for a given base stock and successive integration of additives. The process results in hundreds of different molecules for a given blend. The quality control on the fuel is through testing of its physical properties and octane values together with some limits on the percentage of certain constituent families which may be present. It is therefore rather difficult to say what a commercial gasoline actually is from a chemical perspective - different blends of different molecules may comply with the same regulatory values.

This is an issue when combustion must be simulated. A common way to simplify the problem is through surrogate blends. The simplest analogue of gasoline is pure iso-octane. This by definition has both a RON and MON value of 100. Standard unleaded EN-228 petrol has a minimum RON of 95 and a minimum MON of 85. This means that it corresponds to a mixture of 95% iso-octane in n-heptane in the RON test and 85% iso-octane in n-heptane in the MON test. Therefore its sensitivity (S = RON-MON) will be approximately 10. A two-component blend of iso-octane and n-heptane (known as a Primary Reference Fuel or PRF) clearly cannot have a non-zero sensitivity. Both iso-octane

and n-heptane are paraffins. These represent just a part of the constituents of typical modern gasoline. A common approach is to introduce a further component to represent the aromatic part of a fuel - typically toluene. This results in a Toluene Reference Fuel (TRF). A TRF can match both the RON and MON values of a commercial gasoline, but may be quite different in terms of physical properties, such as the distillation curve.

5.3 Collaboration with Shell and RWTH Aachen University

The author of the present work approached Shell to see if the same tool-chain used to develop Formula 1 blends could be applied to produce a simple surrogate, that well represented Ferrari's development fuel. This could then be used in Computational Fluid Dynamics (CFD) software. This tool-chain is based on empirical blending studies, chemical kinetics mechanisms, CFR engine evaluations and Rapid Compression Machine (RCM) testing.

Shell suggested a new surrogate formulation based on toluene, n-heptane and iso-pentane. This can also match RON and MON values of commercial fuels but has the advantage of enabling tuning of volatility, characterized in this case by Dry Vapor Pressure Equivalent (DVPE). This is shown in Figure 5.1. The gasoline blend targeted had a RON value of 98, as used by Ferrari in production engine development. This was referred to as Reference Premium Gasoline (RPG) in the study. Testing in RON and MON conditions was performed on a CFR engine. Volatility characteristics were also evaluated. It is shown in Table 5.1 that the process was successful in matching the target parameters. The codename of the successful surrogate was KM9096.

Table 5.1: Some Properties of Reference Premium Gasoline and THIP Surrogate

Fuel Type	DVPE, kPa	RON	MON	LHV, MJ/kg
Reference Fuel	87.9	98.0	87.9	42.16
Surrogate	85.1	97.9	88.0	42.77

The autoignition delay time characteristics of the reference gasoline, and that of the THIP surrogate blended based on Shell's empirical functions, were tested in the RCM at the Physico-Chemical Fundamentals of Combustion (PCFC) institute at RWTH Aachen University. The results are shown in Figure 5.2. Note that a Negative Temperature Coefficient (NTC) region can be seen on the ignition delay results of both the reference gasoline and the surrogate. There is some deviation in the ignition delay results at very high temperatures between the two fuels, despite the very similar RON and MON values. Note also that the error bars are generally overlapping however.

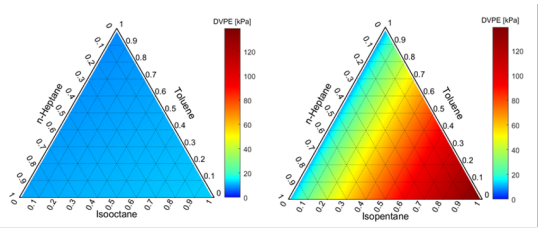

Figure 5.1: Ternary plots showing DVPE (Chevron method, [433]) of TPRF and THIP surrogates, from [374]

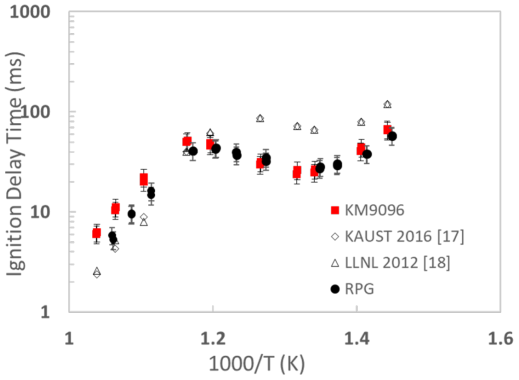

Figure 5.2: IDT (closed symbol) and 1st stage IDT (open symbol) plotted against 1000/T for the isopentane-containing surrogate fuel (KM9096) and the RPG tested. 20% error bars on the individual measurements are included for IDT, from [374]

5.4 Engine Testing

The agreement was deemed satisfactory and hence the surrogate blend was tested in a back-to-back fashion against the RPG in a F154FA engine at Ferrari's facilities in Maranello. The author was responsible for this activity. Details of the test engine are given in Table 5.2. The test condition was at 3000 rpm with an absolute manifold pressure of 2 bar.

Knock in an internal combustion engine occurs if a region of unburnt charge, commonly known as the end-gas, auto-ignites before the flame front initiated by the spark plug has time to consume it. The end-gas heating is largely driven by the combustion chamber pressure history as in a rapid compression machine. Part of the end-gas compression is due to the movement of the engine piston but a large part is driven by the flame-front consuming fresh charge and hence releasing heat which

Table 5.2: Details of F154FA V8 Turbocharged Engine

Engine Type	F154FA
Swept Volume	3990 cm^3
Number of Cylinders	8
Bore	88 mm
Stroke	82 mm
Number of Valves	4
Injector Location	Central
Fuel Pressure	350 bar
Specific Output	195 CV/L

results in a pressure increase across the entire combustion chamber. Whilst the piston-driven pressure rise is a highly repeatable phenomenon, the rate at which the flame front propagates shows significant cyclic variability. Evidence for this can be seen comparing the variability of cylinder pressure measurements with respect to engine crank angle during the compression and combustion phases, as shown in Figure 5.3.

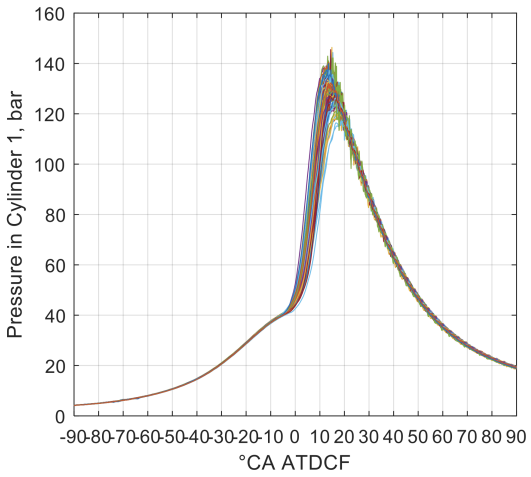

Figure 5.3: 100 Consecutive cycles of cylinder pressure data with constant ignition timing. The pressure rise due to combustion can be seen at around -5° CA After Top Dead Center Firing (ATDCF)

Figure 5.4 shows two consecutive cycles from the same dataset. Cycle 239 exhibits a faster pressure rise followed by an autoignition event leading to a high frequency oscillation on the pressure trace. The cylinder pressure trace is high pass filtered and the amplitude of the pressure oscillation is taken as an indication of the severity of the knock of that cycle. This is known as the Maximum Amplitude Pressure Oscilation (MAPO) value [279]. Cycle 238 has a value of 1.2 bar whilst that of Cycle 239 is 14.6 bar. The cyclic variability of knocking in an engine means that statistical values are normally constructed using a population of some hundreds of cycles in order to adequately characterize the knock propensity for a given ignition timing and fuel. Two indices were considered. The first was the 99.5th percentile MAPO value. A common method of calibration is to aim for a 99.5th percentile MAPO of the engine speed divided by 1000. This is the method that has historically been used by Ferrari for road car development testing.

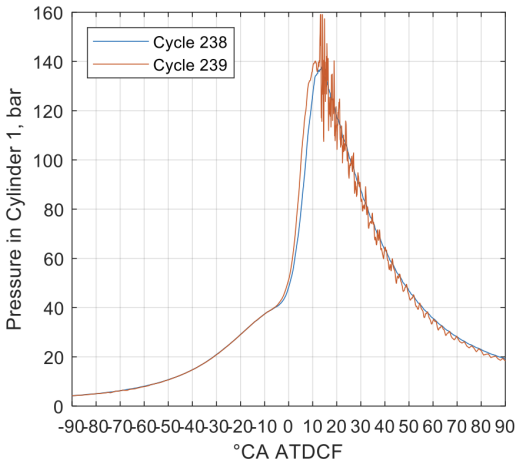

Figure 5.4: Example of consecutive cycles, the second of which is knocking

A second index was also used. Here, the number of cycles with a MAPO value over a certain threshold was divided by the total number of cycles in the dataset. The threshold is based on a factor of the median MAPO value. The median is a useful method of characterizing the base "noise" level of non-knocking cycles in the dataset. As knock is statistically rare, the median value is highly unlikely to be knocking. Cycles above the threshold are considered to be knocking. The factor of the median that is used to set the threshold is a tuning factor in the calculation, to give adequate noise robustness and hence to avoid false positives. A desired percentage of knocking cycles can be targeted through adjusting the ignition timing. This method was developed by the author when working in Formula 1 and will be referred to as 'Knock Frequency'. It tends to be more severe in terms of likely engine damage than that of the 99.5th percentile MAPO target, as is appropriate for a racing vehicle. Using two methods gives two estimates of knock-limited combustion phasing differences for the different fuels, hence increasing robustness in interpretation of the results.

The tests of the RPG and surrogate KM9096 were bracketed by a development fuel, C103, which was available in larger quantities. This fuel had a higher RON and lower MON than that of the reference premium grade or the surrogate. The testing order was: C103, RPG, C103, KM9096, C103. The results over the entire com-

bustion phasing sweeps are shown in Figure 5.5 using the 99.5thpercentile MAPO index and in Figure 5.6 using the index developed in Formula 1. Considering firstly the C103 results, it can be seen that the repeatability in terms of the knocking response for a given combustion phasing is of the order of 0.5° CA. C103 clearly permits a more advanced combustion phasing for a given level of knock in comparison to the other fuels as would be expected by its higher RON and higher sensitivity (high sensitivity is generally found to be advantageous in modern TGDI engines [434]).

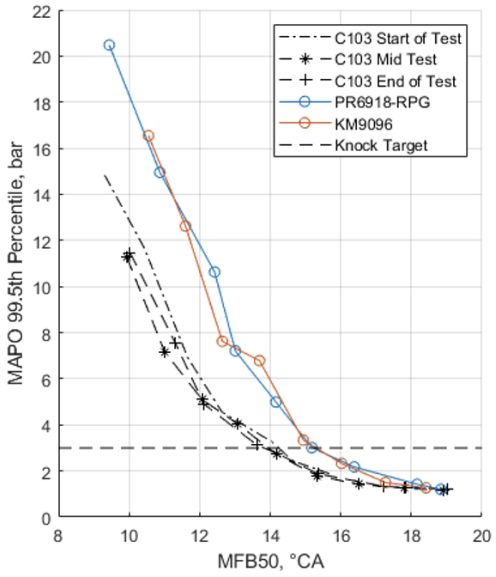

Figure 5.5: MAPO 99.5th Percentile over Combustion Phasing Sweep for RPG and Surrogate Blends (KM9096) together with Bracketing Fuel (C103)

A precise value of combustion phasing must be chosen during engine calibration defined by the target knock limit. Figure 5.7 shows average knock limited combustion phasing values for the C103 tests based on the two indices and thresholds discussed. Error bars are defined using the repeatability of the C103 knock limit over the three tests at the threshold values. These error bars are then also applied to the RPG and KM9096 results. It can be seen that the error bars for the knock limit values between RPG and KM9096 are overlapping, indicating that the difference in their knock limit is within the repeatability of the test procedure.

It is also apparent in Figure 5.7 that the Formula 1 derived knock calibration is approximately 1° CA advanced from the production calibration in this activity. This will result in higher performance, but of course must be shown to not introduce reliability issues in durability testing.

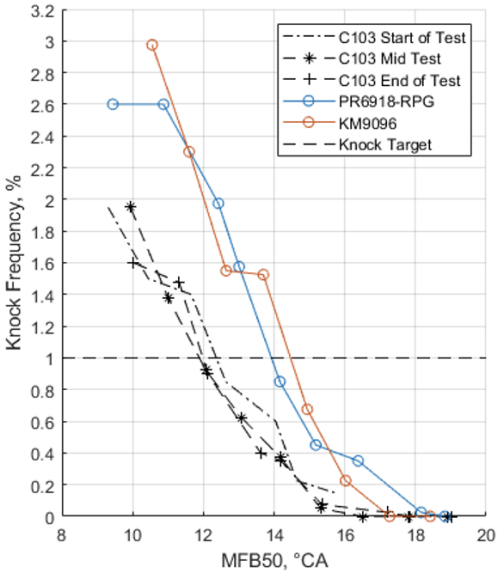

Figure 5.6: Knock Frequency over Combustion Phasing Sweep for RPG and Surrogate Blends (KM9096) together with Bracketing Fuel (C103)

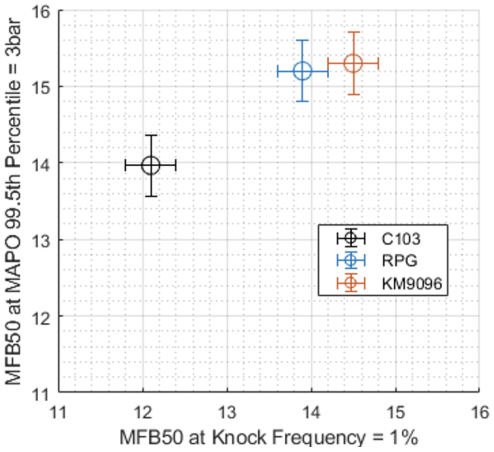

Figure 5.7: Comparison of Reference Gasoline (RPG) and Surrogate (KM9096) Knock Limits. Bracketing Fuel (C103) was used to Define Error Bars

5.5 Conclusion

The main goal of this activity was to see if methodologies developed together by Shell and Ferrari in Formula 1 activities could be used to aid in production development. A second goal was to compare production and Formula 1 knock calibration approaches. The For-

mula 1 derived knock calibration was shown to be more advanced by 1° CA in comparison to the production calibration. The surrogate fuel gave the same knock limit as the reference commercial gasoline to within experimental repeatability for both indices. This means that in simulation studies, if the simple THIP surrogate can be modeled reliably in reaction mechanisms, the predictivity of the engine knock limit should be greatly improved. Further details of the activity can be found in the Journal Paper [374].

CHAPTER 6

Prechambers

6.1 Abstract

The vast majority of gasoline engines in production now and in the past have featured a spark plug as the ignition system. In Formula 1, regulations state that combustion can only be initiated by a spark plug connected to a conventional ignition coil. Whilst in most modern engines the spark plug is mounted in a "open" combustion chamber, this need not necessarily be the case.

Already 100 years ago, Ricardo experimented with prechamber ignition. There was also a period of great interest in the 1970s. At the time it was linked to running lean, which made increasingly stringent emissions legislation more difficult to comply with. Formula 1 engine manufacturers adopted the technology for the 2014 engine regulations to maximize performance and efficiency at high speeds and loads. Some research activity on fundamental understanding of Formula 1 prechamber systems is presented.

Prechambers give large improvements in engine combustion stability and knock limitations in full load conditions. They are more problematic at part load and in particular at highly retarded combustion phasing, as is shown. Such an operating strategy is key for catalyst heating for modern passenger vehicles. A new engine concept making use of both a prechamber and a conventional igniter, arranged to permit high combustion stability in catalyst heating, is presented. Experimental results show the potential of this system, which has also been granted a patent.

6.2 Introduction

There is considerable interest in prechambers at present. As mentioned above, they are not a new technology. Ricardo [33] described a prechamber engine in 1922. A drawing from the original paper is shown in Figure 6.1. The prechamber was fed through a check valve by air fuel mixture. Air was fed into the main chamber by a conventional intake valve with late opening timing. Turbulence was generated in the prechamber as the piston rose during the compression stroke. It was observed that the combustion in the prechamber was very fast. The mixture in the main chamber was lean but could be ignited by the flame emanating from the prechamber, where the mixture was much richer. The engine was described as a "stratified charge" concept and could run much leaner than a conventional premixed configuration.

Running lean reduces maximum cycle temperatures. This means that heat loss is reduced and the ratio of specific heats, γ, is also higher. Efficiency is therefore improved. If adequate combustion stability and flame speeds can be guaranteed when running lean, the knock limit should also improve. This is because ignition delay times increase lean of stoichiometry, hence end-gas reactions are suppressed.

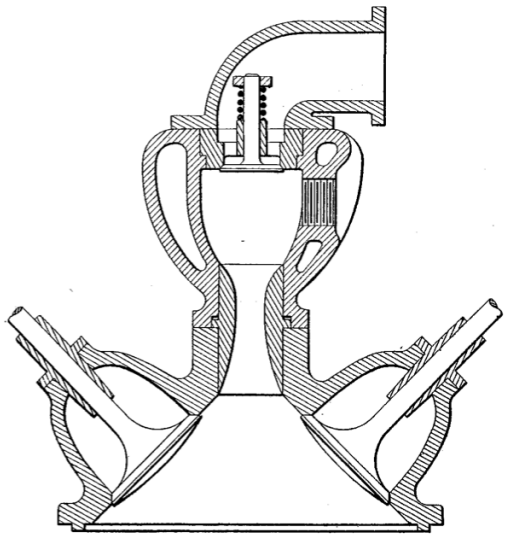

Figure 6.1: Ricardo Stratified Charge Prechamber Engine, from [33]

Despite the promising results obtained by Ricardo, prechamber engines did not become common. There was a resurgence of interest however, in the 1970s. This was a period of fuel shortages and new emissions legislation, which initially required only oxidation catalysis. A number of automotive manufacturers experimented with prechamber engines at the time, as documented by the Environmental Protection Agency [160]. Honda brought a vehicle to market with its Compound Vortex Controlled Combustion system [161]. As found by Ricardo, one of the main advantages was to facilitate lean running. This was incompatible however, with use of a Three Way Catalyst (TWC). This became a standard item in the late 1970s driven by more stringent regulatory limits on NO_x.

Whilst further production vehicles did not come to the market, research efforts continued. A large review was written by Toulson *et al.* in 2010 [343]. The author of the current thesis read this paper in 2011 [435] and proposed to apply the technology in Formula 1 for the new boosted regulations foreseen for 2014. Activity at Ferrari did not proceed at this time on the prechamber, and in fact Mercedes were the first team to run the technology in 2014. In this same season, a research program on prechambers was begun at Ferrari led by the author, initially in collaboration with Mahle Powertrain.

Prechamber engines are frequently divided into two

classes: active and passive prechamber systems. An active prechamber has independent fueling of the main chamber. Ricardo's engine is one such example. This is particularly useful for lean burn engines, as it allows a locally close to stoichiometric mixture to be guaranteed near the spark plug, even if conditions are globally very lean. Current Formula 1 regulations [417] only permit one injector per cylinder and a maximum of four valves. This effectively implies a passive prechamber system is the only one that can be used. Here, the mixture in the prechamber must be fed from the main chamber. With suitable main chamber stratification, it may still be possible to guarantee a locally stoichiometric or slightly rich mixture at the spark plug within the prechamber and still have a lean overall λ value. As Formula 1 engines run lean to maximize thermal efficiency [28], this is a key target of development. Some lessons learned in Formula 1 prechamber development will be described, as will subsequent activity carried out in road car development by the author and colleagues.

6.3 Formula 1 Prechamber Research

Experimental activity at Ferrari Gestione Sportiva began in 2015 on a single cylinder research engine. The first prechamber used featured a volume of approximately 2% of the main chamber clearance volume and six 1 mm diameter holes. This was consistent with literature recommendations. The installation can be seen in Figure 6.2. Initial results in Feburary of 2015 were

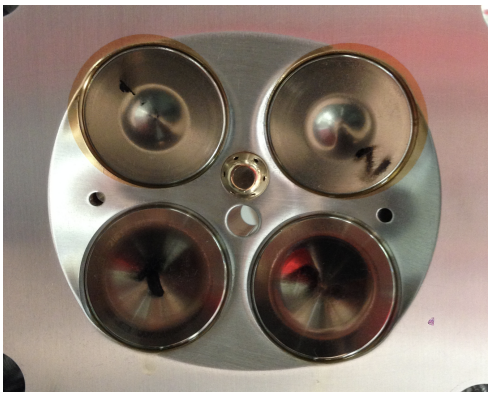

Figure 6.2: First Ferrari Formula 1 Prechamber Installation from 2015

promising - CoV (Coefficient of Variation) of IMEP (Indicated Mean Effective Pressure) dropped from 3.5% to 1.2% in comparison to the conventional spark plug igniter [436]. 10-50% Mass Fraction Burned was also significantly improved and emissions of HC and CO were less than half of the conventional values. An accelerated program was led by the author to introduce the technology on the race engine. The system was used from the Canada GP on the 6th of June onwards - less than four months after the fireup on the single cylinder engine. The first race win came shortly afterwards.

Development of course continued. As the engine ran globally lean, much effort was made on getting adequate fuel to the prechamber. A number of interesting experimental studies were performed to understand the system better. Optical measurements using a UV intensified camera system were performed by MOT GmbH. This allowed visualization of the prechamber jets, as shown in Figure 6.3. Three of the jets were visible the camera system and were seen to exit from the prechamber at around Top Dead Center. Note that the jets are much more intense for the lower λ values.

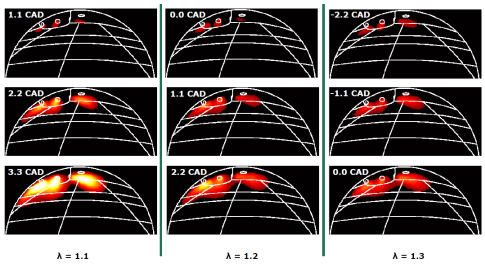

Figure 6.3: Prechamber Jet Optical Investigations on Ferrari Formula 1 Research Engine, 2015 [437]

As prechamber air fuel ratio appeared critical, a dedicated engine layout was proposed by the author to study this. This single cylinder engine featured port fueling for the main chamber and a single-hole direct injector to adjust the prechamber air-fuel ratio. Unlike in a conventional active system, this injector was mounted in the main chamber. This concept only functioned if the injector tip was close to a prechamber nozzle hole and angled such that an injector jet could target a prechamber opening. This is shown in Figure 6.4 This layout allowed the prechamber λ to be targeted independently of the main chamber with a cylinder head layout coherent with Formula 1 regulations. The goal was to size the injector opening for prechamber enrichment on the single-hole injector, then return to a multihole injector which would fuel both main and prechambers in the desired ratio. The research activity confirmed that the best approach was to use the quantity of prechamber fueling which maximized early burn rates, irrespective of global lambda. This mean that the difference in main and prechamber air fuel ratios, $\Delta\lambda$, needed to be coherent with the global lambda target. For example, for a global λ of 1.3, a prechamber λ value of 0.9 was found to be optimum which means a $\Delta\lambda$ of 0.4. In fact, running at constant global lambda of 1.3, it was possible to sweep $\Delta\lambda$ and confirm the impact on knock limited combustion phasing. This is shown in Figure 6.5. It can be seen that if

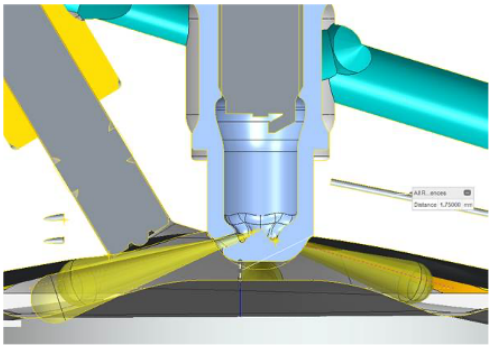

Figure 6.4: Ferrari Formula 1 Research Engine for Prechamber Enrichment Studies, 2015 [438]

it is not possible to enrich the prechamber when running globally lean, the knock limit can suffer significantly.

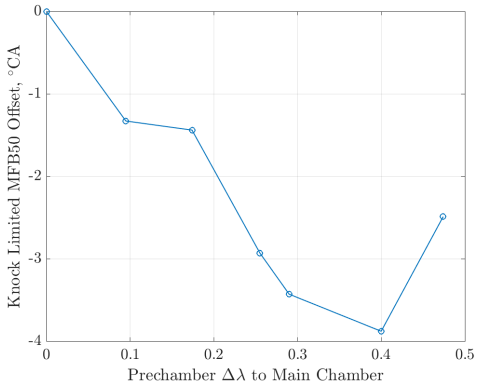

Figure 6.5: Effect of Enriching the Prechamber on the Knock Limited Combustion Phasing of Research Formula 1 Single Cylinder Engine Running at $\lambda = 1.3$ [438]

Whilst it was relatively straightforward to enrich the prechamber with the engine layout shown in Figure 6.4, in 2016 another arrangement was used. Here the injector was much further from the prechamber hence achieving prechamber enrichment was more difficult. A study was carried together with LaVision using a local infrared based HC sensor (ICOS) in motored, fueled engine testing. The probe was installed in the prechamber in the position of the spark plug. Like this, the dynamics of prechamber fueling could be studied. Some results are shown in Figure 6.6. The injection timing used here was at TDC during valve overlap. Despite this early injection timing however, the fuel only was seen to arrive in the prechamber in significant quantities late in the compression stroke. Modifications to the cylinder head and injector spray pattern were made to improve prechamber fueling and performance increases were found.

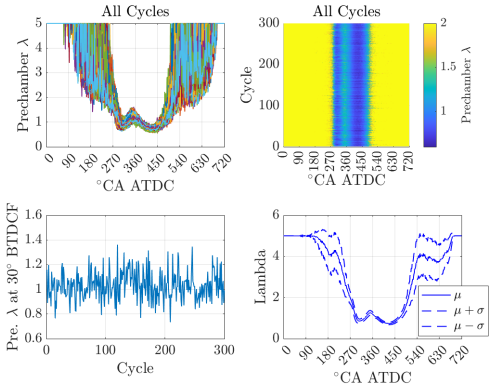

Figure 6.6: Dynamics of Air Fuel Mixture Transport to Prechamber for Motored Fueled Research Formula 1 Single Cylinder Engine Running at $\lambda = 1.3$ [439]

Formula 1 engines run lean at high load. Active prechambers are not allowed hence much of the challenge is to guarantee an optimum mixture in the prechamber at the time of ignition, as described above. If this can be achieved, combustion is much more stable. This gives a direct knock limit improvement, and also makes the engine more tolerant to further dilution or Millerisation in comparison to a standard SI system. This in turn further boosts efficiency and performance, hence why prechambers are now ubiquitous in Formula 1.

6.4 Road Car Prechamber Research

The promising results seen in Formula 1 research were communicated to colleagues in production car development. Initial testing on a multicylinder engine took place shortly afterwards. Whilst performance improvements were seen in full load conditions [440], issues were observed with combustion stability at low loads. Activity moved to single cylinder engine testing to better understand potential applicability for a road car application.

Single cylinder testing showed that low loads were challenging but certain prechamber design features could improve the minimum stable load value. Bigger problems were found in terms of retardability [441]. Figure 6.7 shows an ignition timing sweep from Maximum Brake Torque (MBT) in the retarded direction for both conventional and prechamber igniters in the same test engine. Note that for the conventional spark plug, when the ignition is retarded such that the mean Indicated Mean Effective Pressure (IMEP) is less than 40% of the starting value, no misfires are observed

as evidenced by the non-zero minimum high pressure IMEP values (IMEPH). For the prechamber on the other hand, misfires are already occurring at IMEP values of just less than 80% of the starting value. In combustion phasing terms, the prechamber begins to show misfires at a Mass Fraction Burned 50% (MFB50) value of 35° ATDC whereas the conventional igniter shows no misfires still at 75° ATDC. Such extremely retarded combustion phasing is used to generate high exhaust enthalpy in order to rapidly heat the after-treatment system shortly after engine start. Formula 1 does not have emissions regulations hence no after-treatment system is present and the combustion phasing retard requirement is much more modest[1].

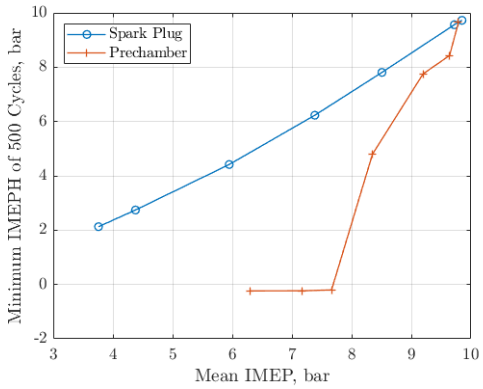

Figure 6.7: Retardability Issues of Prechamber at 2000 rpm Over Retard Sweep

Considerable development effort was spent to alleviate the issue but only modest improvements were found. Discussions also took place with a number of automotive consultancies at the time and the catalyst heating condition seemed to be a major obstacle for introducing a prechamber system in a modern production vehicle. It was decided to pursue an alternative approach.

6.5 New Ferrari Prechamber Engine Concept

Ferrari engines are relatively large compared to typical road car applications and have much higher power output. They therefore have large after-treatment systems. To preserve the characteristic Ferrari engine sound, long exhaust primaries are normally used. This means that there is a significant temperature drop along the exhaust line from the cylinder head to the catalyst inlet. This results in Ferrari having very high engine out enthalpy requirements in catalyst heating operating points. High retardability is thus a necessity.

To meet this requirement, the SF90 Stradale featured a new combustion chamber layout in comparison to past applications. The injector is mounted centrally and the spark plug is positioned in between the exhaust valves. During catalyst heating, a "spark-coupled" injection strategy is used. This is a short injection event phased to around spark timing which generates local turbulence and enrichment near the spark plug. This greatly assists in improving ignitability for late combustion events - where turbulence generated by the ports has significantly decayed. It was desired to keep this feature for the prechamber engine.

A novel engine concept was therefore devised by the author and his colleagues. The prechamber was positioned in the center of the combustion chamber. This should maximize burning rates in high load knock limited conditions and hence power output. A conventional spark plug was retained between the exhaust valves for the catalyst heating condition. Finally, the fuel injector was moved to the exhaust side of the chamber. A patent application was written for this concept by the author and the patent was granted by the European patent office in 2019 [351]. The layout as shown in the patent application can be seen in Figure 6.8

6.6 New Prechamber Concept Testing

The first point to clarify when it came to the experimental program was whether the spark-coupled injection strategy would still be as effective as hoped. In order to do this, a comparison was made with the production combustion chamber on a single cylinder engine. Combined port and direct injection was employed, somewhat similarly to the strategy described in Section 6.3. The direct injector used was a multi-hole rather than single hole design however. With small injection quantities injected in parallel with the spark event, this still allows investigation of the spark coupled mechanism efficacy. The engine was run in a catalyst heating operating condition, and the proportion of fueling fed to the direct injector gradually increased. This was performed both for the standard, central injection concept and the new exhaust side configuration [442]. As shown in Figure 6.9, without the direct injector fueling, both combustion systems give a standard deviation (σ) of IMEP of around 0.5 bar in the catalyst heating operating point. As fuel is gradually apportioned to the direct injector, the σ value drops to around 0.3 bar for the standard system and then remains flat. For the new concept, the σ value drops slightly lower before gradually increasing with very high quantities of fuel injected in this event. The new system

[1] This is true for Formula 1 regulations from 2014 onwards. Some years earlier, exhaust blown diffuser techniques led to extreme enthalpy requirements at low torque also in Formula 1 [28]

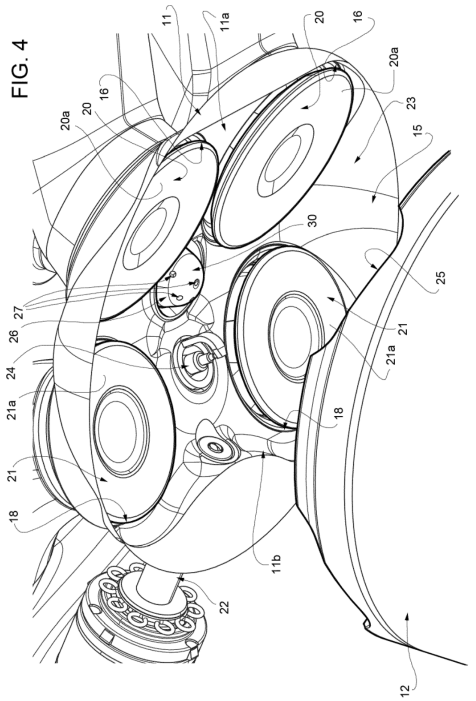

Figure 6.8: Layout of New Patented Ferrari Prechamber Combustion System featuring an Exhaust Side Direct Injector, a Centrally Mounted Prechamber and a Secondary Spark Plug in between [351]

also seems less favorable in terms of particulate emissions at high quantities of fuel injected directly in such a manner. There is therefore a trade-off between the combustion stability gain and particulate emissions for such a spark-coupled injection strategy. Figure 6.10 shows this relationship directly. It can be seen that the new concept actually gives a better compromise between particulate emissions and combustion stability in the area of maximum interest (in the lower left of the figure).

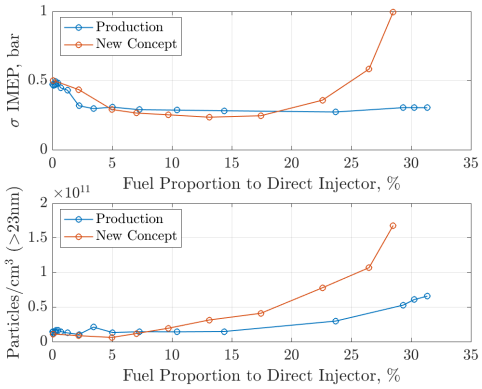

Figure 6.9: Comparison of Spark Coupled Injection Strategy for Previous Ferrari Engine and New Combustion Concept

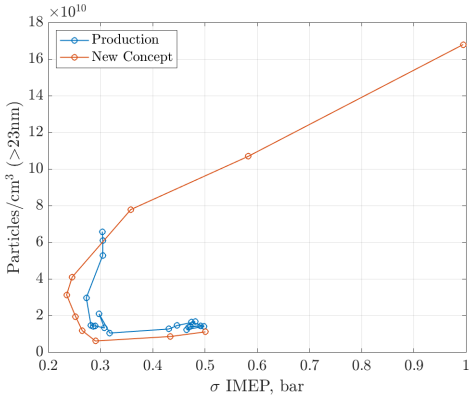

Figure 6.10: Combustion Stability / Particulate Emisison Trade-off for Production Combustion System and New Concept

The emissions feasibility of the concept having been demonstrated, testing therefore proceeded to the maximum power condition. Formula 1 experience suggested that prechamber engines did not require high tumble values. In order to confirm this, a number of intake port inserts were produced to allow convenient comparison testing on the single cylinder research engine [443]. The port designs are shown in Figure 6.11.

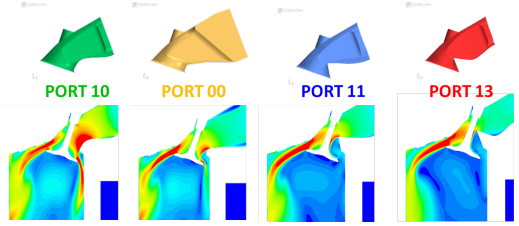

Figure 6.11: Intake Port Designs for Various Tumble Levels [443]

Combustion phasing sweeps for each port at 7000 rpm are shown in Figure 6.12. It can be seen that the prechamber combined with most of the tumble levels improves the knock limit with respect to current production technology. It would also appear that high tumble actually has an antagonistic effect on the prechamber combustion system. In fact, best performance is for the lowest tumble values. The direct correlation between tumble and knock limited combustion phasing for the prechamber engine is shown in Figure 6.13. A linear best fit line is also shown.

The experimental activity to date has demonstrated the feasibility of this new combustion concept. The necessity for additional spark plugs and ignition coils, together

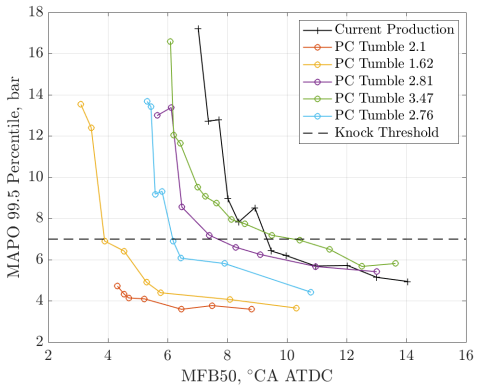

Figure 6.12: Effect of Tumble on Prechamber (PC) Knock Limit and comparison to Current Production Technology

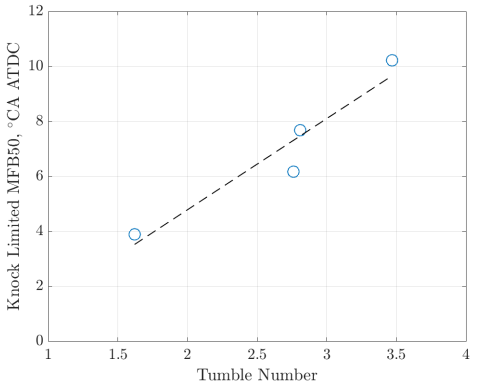

Figure 6.13: Correlation between Tumble and Knock Limited Combustion Phasing for Prechamber Engine

with a more complex Engine Control Unit (ECU) software structure, means that it is more expensive to implement in production than current technology.

6.7 Conclusion

Prechambers were originally explored by Ferrari in racing activity but have since been researched also for production applications. Similar benefits were found for high load conditions in both cases, namely improved knock limited performance and greater combustion stability. The additional operating regimes required of a production vehicle, primarily due to emissions requirements, mean that it is difficult to cover all operating conditions without a secondary igniter. A novel combustion chamber layout was therefore proposed and patented. Detailed analysis of prechamber data in knocking conditions will be presented in the next chapter.

CHAPTER 7

Knocking Data for Standard and Prechamber Igniters

7.1 Abstract

Knock has historically been one of the main limitations on spark ignition engine compression ratio and hence efficiency. The trend to downsizing or rightsizing in recent years, driven by ever reducing CO_2 targets, has increased the relevance of the knock limit for typical engine operating conditions. Even for scenarios where an engine is run on carbon neutral fuel, thermal efficiency will always be fundamental in terms of best use of scarce resources. Knock therefore remains a relevant topic for current and future research.

Knock is typically quantified through analysis of high pass filtered cylinder pressure signals. For spark ignition engines, this is relatively unproblematic. A promising technology for further combustion engine efficiency gains however, is prechamber ignition. It has been noted that prechamber combustion systems result in significant high frequency content on the cylinder pressure trace in the bandwidth of interest for knock. It is therefore more difficult to accurately determine the knock limit for such engines, which is necessary in order to make a fair comparison to traditional spark ignition systems.

There is relatively little detail on this key topic in the existing literature. Accordingly, this study compares knocking experimental data from the same high performance single-cylinder research engine with both spark ignition and prechamber combustion systems. Established and new approaches of interpreting the knocking data are examined, applying both high frequency and low frequency techniques to cylinder pressure signals, complemented by statistical methods. The analysis conducted demonstrates that for knocking prechamber combustion, three distinct combustion stages are detected. The high-frequency content of the prechamber pressure signal is also more complex and is analyzed in detail. A significant gain in knock-limited combustion phasing is thus confirmed for the prechamber igniter, at appropriate levels of knock, in comparison to the standard spark plug system.

7.2 Introduction

The automobile industry is going through a period of huge transition. CO_2 produced by vehicles must be reduced drastically in the coming years to meet the objectives of the Paris agreement [29]. In July of 2021, the European Commission presented its *"Fit for 55"* package. This proposes that the CO_2 from new passenger cars be reduced to zero by 2035 [444]. In 2020 however, around 95% of passenger cars sold in the European Union (EU) featured an Internal Combustion Engine (ICE) [445]. The ICE therefore has a role to play in reducing CO_2 emissions in the coming years. Zero CO_2 pathways also exist for the ICE, such as "e-Fuels"[1] [446], where renewable electricity is used to create carbon neutral gasoline. These synthetic gasolines offer interesting possibilities to permit cleaner and more efficient combustion [447]. Other areas of current research include hydrogen combustion engines [448]. Whichever fuel is utilized, maximum efficiency should always be sought. This will reduce CO_2 emissions if the fuel is fossil derived and minimize upstream energy expenditure, if the fuel is from renewable sources.

Engine researchers have striven to maximize the efficiency of the Spark Ignition (SI) engine since its inception. It was realized at an early stage that increasing the compression ratio was an effective means of achieving this, but only if knock could be avoided or at least controlled [32, 33]. Knock in an SI engine occurs when a region of the unburnt charge ignites ahead of an advancing flame-front in the so called end-gas. Autoignition is more likely to occur if the unburnt charge is at high temperature and pressure. The autoignition almost always begins at one or a number of localized regions known as hot-spots or exothermic centers [219]. Once a localized autoignition event takes place, what happens next depends on the size of this exothermic center [263] and the reactivity gradient around it [208]. A pressure wave is frequently, but not always, generated. For moderate knocking, this propagates at sonic velocity across the chamber and is then reflected by the chamber boundary. Standing waves result which produce vibrations at key frequencies dictated by the acoustic modes of the combustion chamber volume. These cause vibrations in the engine structure that give rise to the characteristic sound. It is also possible that the initial pressure wave becomes coupled with local autoignition chemistry and thus generates a reaction front traveling at well above sonic velocities. This results in very strong pressure wave behavior and hence is likely to cause engine damage. This phenomenon is sometimes referred to as "super-knock" [393] and is an example of Developing Detonation (DD). Further information on the phenomenon of knock and the history of its research can be found in [427].

The feedback on knock was originally the human ear. In the 1920s, dedicated instrumentation was developed, most notably the "Bouncing Pin Indicator". A number of methods of measuring knock in a running engine have been applied over the years [187], but high speed cylinder pressure measurements have been the most common approach in a development setting for a significant period [188, 428]. Such measurements typically exhibit oscillations of the pressure trace when knock occurs. These oscillations occur at characteristic frequencies, which Draper [78] explained in the 1930s using acous-

[1] Carbon neutral hydrocarbon fuels made through a combination of electrolysis of H_2O using renewable electricity and CO_2 from carbon capture

tic theory applied to a cylindrical volume. How the characteristics of these oscillations are modified by changing the location of the pressure wave stimulus for modern combustion chamber geometries has recently been demonstrated [429].

It should be noted however, that combustion chamber resonances are not uniquely excited by knock. This was a key area of study for HCCI (Homogeneous Charge Compression Ignition) engines in the past and a formula for "Ringing Intensity" was given by Eng [264] in 2002. This is shown in Equation 7.1. β is a constant to be tuned with experimental data, P is the cylinder pressure, γ is the ratio of specific heats of the trapped charge and T is the gas temperature. The equation implies that ringing intensity correlates with high pressure rise rates and high peak cylinder pressures. Such conditions can be generated by any type of fast combustion - not only autoignition.

$$\text{Ringing Intensity} \approx \frac{1}{2\gamma} \frac{\left(\beta \frac{dP}{dt}_{max}\right)^2}{P_{max}} \sqrt{\gamma R T_{max}} \tag{7.1}$$

A modified version of the equation to account for expansion work from the initial autoignition event was proposed by Maria *et al.* [355]. Bradley and Kalghatgi [265] directly linked the pressure oscillation ΔP to the resonance parameter $\xi = a/u_a$ where a is the acoustic velocity and u_a is the autoignition propagation velocity relative to the unburnt gas. This is shown in Equation 7.2 and assumes a small exothermic center dimension and isentropic compression and expansion. It is therefore of greatest relevance to small knock events and especially in the absence of developing detonation.

$$\frac{\Delta P_{max}}{P} \approx \xi^{-2} \tag{7.2}$$

Acoustic theory states that waves will be generated where volumetric expansion from a point location is rapid relative to local acoustic velocity [430]. This condition may be verified also for combustion modes other than autoignition. In a prechamber combustion system, air/fuel mixture is ignited in a small "prechamber" volume by a conventional spark plug. This volume is linked to the main chamber by one or a number of orifices. Combustion in the prechamber results in a pressure rise relative to the main chamber, which drives hot reactive jets into the main combustion volume [449]. The resulting combustion in the main chamber originates from these jets, which can be considered approximately as point sources [305]. Combustion is typically very rapid in this period and hence pressure waves may be generated locally. Prechamber jets reaching sonic conditions at nozzle outlet may also result in shock-waves, further complicating cylinder pressure data interpretation [450]. Prechamber engines are not new - a prechamber engine was described by Ricardo [33] as far back as 1922 and there was much research on the technology for passenger cars in the 1970's [160]. A production car was brought to the market by Honda in this period - the CVCC (Compound Vortex Controlled Combustion) engine [161]. Gussak *et al.* [451] described research in the Soviet Union and results on a Volga automobile in the same decade. The technology at the time was principally used to aid in running lean. This fell out of favor due to ever stricter emissions limits in the period and a lack of suitable, cost-effective exhaust gas after-treatment solutions. An extensive review of prechamber engines was given by Toulson *et al.* [343] in 2010 and in recent years, there has been renewed interest in the field. This is both for lean running [344] and also for knock limit extension in stoichiometric conditions [348]. In 2020, Maserati S.p.A. announced that it would bring a prechamber engine to the market in 2021 [350]. Other manufacturers, component suppliers and research organizations are also studying the technology. In order to evaluate if moving from spark ignition to prechamber ignition is warranted, it is important to have a robust methodology for comparing both systems at their respective knock limits to accurately quantify the benefits. This is not covered in detail in the existing literature, hence is the focus of the present work.

7.3 Test Engine and Procedure

Testing was performed on a specifically designed prototype Single Cylinder Engine (SCE). The combustion architecture of the SCE is based on the geometry of the F140HB V12 normally aspirated engine found in the Ferrari 812 Competizione high performance production automobile. Some key details of the multicylinder engine are shown in Table 7.1.

Table 7.1: Technical Specifications of Multicylinder Engine

Name	F140HB
Type	V12 NA
Bore (mm)	94
Swept Volume	6500 cc
Injection System	Direct, 350 bar
Compression Ratio	13.6:1
Maximum Speed (rpm)	9500
Specific Output (CV/L)	128

This engine normally features a centrally mounted conventional Spark Plug (SP). The cylinder head of the SCE was modified to allow swapping between the conventional plug and a PreChamber Igniter (PCI) mounted in the same, central location in an M12 threaded hole. The prechamber used in this investigation is a passive de-

sign *i.e.* with no auxiliary fueling or active scavenging. The prechamber volume is less than 3% of the main chamber clearance volume, hence would be described as a *"small prechamber"* using the classification system of Toulson *et al.* [343]. A Gasoline Direct Injector (GDI) is mounted laterally on the intake side. Air-fuel mixture, formed in the main chamber by a single injection event, moves into the prechamber volume principally during the compression process, due to the pressure differential between the two volumes. Combustion is initiated in the prechamber using a conventional spark plug and a single spark event. Residuals are primarily scavenged from the prechamber during the expansion stroke when prechamber pressure is higher than that of the main chamber. Cooling, lubrication, intake and exhaust systems were properly designed to reproduce boundaries of the reference multicylinder engine. In particular, intake and exhaust system lengths, diameters and volumes were designed using one-dimensional unsteady gas dynamics software (GT-Power) to replicate insofar as is possible the dynamic pressures at the intake and exhaust valves during the valve open periods for the chosen operating condition. The experimental installation is shown in Figure 7.1. It is acknowledged that single cylinder testing can never fully replicate the complexities of a multicylinder engine. Friction will not be aligned and the effect of multiple cylinders on tuning cannot be fully reproduced. Differences are also inevitable in the cooling circuit, although here that of the multicylinder was replicated as faithfully as was possible. Single cylinder testing does however, have the advantage of being much more flexible, rapid and cost effective in the initial evaluation of novel concepts.

The experimental setup was fully instrumented to determine the crank angle and time based thermodynamic and mechanical states of the engine. A Kistler 6045B piezoelectric cylinder pressure transducer with a natural frequency in the region of 76 kHz was installed. This was flush mounted in the periphery of the chamber between the intake and exhaust valves. This is preferable to a centrally mounted location, as many acoustic modes excited by knocking have a node at the geometric center of the combustion chamber [429]. The signal was amplified by a Kistler 5011 charge amplifier with 200 kHz bandwidth and acquired by an AVL Indimicro 602 indication system. This features anti-aliasing filters at 100 kHz. An AVL 365X crank encoder was used as the reference timing signal. The acquisition resolution was 0.1° Crank Angle (CA), which corresponds to 300 kS/s at 5000 rpm. The indicating measurement chain and a schematic of the SCE installation is shown in Figure 7.2

Combustion phasing sweeps were performed for both conventional spark plug and prechamber igniters. Testing in the present activity was carried out at 5000 rpm and Wide Open Throttle (WOT) conditions with stoichiometric equivalence ratio. This is a high speed and load in comparison to typical driving conditions on the road. The compression ratio for this application however, is chosen considering full load performance. If knock can be improved in such conditions, a higher compression ratio can be specified, bringing efficiency gains at lower loads and speeds. Gasoline fuel with a Research Octane Number (RON) of 91 was used to render the engine more knock prone, as it was initially found that the prechamber allowed operation significantly beyond Maximum Brake Torque (MBT) ignition timing on conventional premium gasoline.

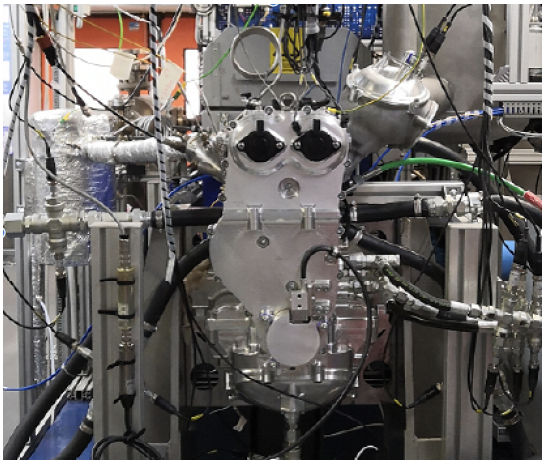

Figure 7.1: Single-Cylinder Engine Installation on Test Bench

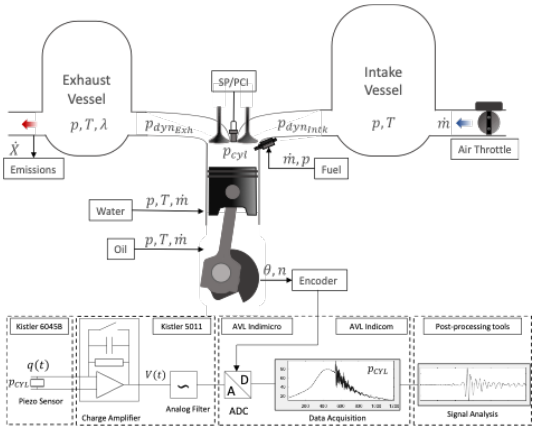

Figure 7.2: Single-Cylinder Engine Layout and In-Cylinder Pressure Measurement Chain

7.4 Experimental Results

Post-processing of indicating data was performed in MATLAB R2020b. An initial assessment and thresholding of the experimental results was made using the common MAPO (Maximum Amplitude Pressure Oscil-

lation) index, before proceeding to examine knocking and non-knocking cycles in more detail using a range of techniques.

7.4.1 MAPO Analysis and Thresholding

The results with the conventional spark plug will first be described and then contrasted with those from the prechamber ignition system. As a starting point for data interpretation, the MAPO algorithm was used. This is defined in Equation 7.3, where P_{bpf} is the Band Pass Filtered (BPF) cylinder pressure.

$$\text{MAPO} = \mid P_{bpf} \mid_{max} \tag{7.3}$$

The passband for the BPF was chosen as 3-30 kHz. 512 cycles were acquired at each ignition timing. Knocking cycles feature high MAPO values. Various percentiles of the MAPO index are shown for each combustion phasing investigated. Combustion phasing here is defined using the cyclic average 50% Mass Fraction Burned (MFB50) value based on a single-zone First Law analysis of the pressure trace.

The 99.5$^{\text{th}}$ percentile MAPO value (MAPO$_{99.5\%}$) was compared to a threshold based on the engine speed for the conventional spark plug. This is a well known calibration methodology for SP engines. The speed-dependent threshold allows for the fact that cylinder pressure data generally feature more high frequency noise content as engine speed increases, even in the absence of knock. This allowed a baseline "knock-limited" (KL) combustion phasing value to be chosen for the conventional igniter. This combustion phasing will be referred to as Spark Plug Knock Limit (SP KL). Figure 7.3 shows the results. Combustion phasing values are expressed in comparison to this chosen knock limit for the standard plug. MAPO percentile values are normalized to the 99.5$^{\text{th}}$ percentile value for the spark plug measurement at this knock limit. It can be seen that there is a steep gradient of the normalized MAPO percentile values in the region of SP KL for the standard igniter. Retarding from the knock limit, the data for the SP drop significantly and then flatten out. Advancing, they increase significantly; doubling in a step of two degrees of CA.

The PCI data on the other hand look quite different. At SP KL combustion phasing, the 99.5$^{\text{th}}$ percentile MAPO value is already slightly higher than for the conventional plug. Advancing the combustion phasing however, there is little increase until around 8° CA advanced from the spark plug limit. Thereafter, the percentiles increase much more steeply than seen for the standard plug. It is likely that the knock limit of the prechamber is in this region. Three measurement points will be compared in detail to confirm this: the baseline knock limited SP

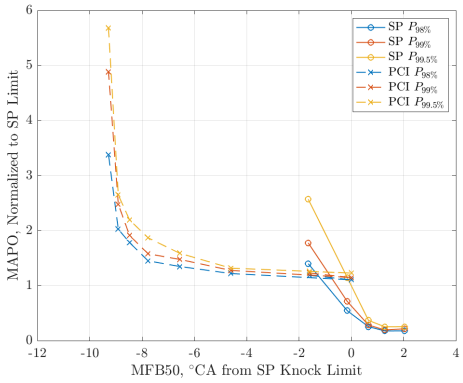

Figure 7.3: Normalized MAPO Percentiles over Combustion Phasing Sweep

measurement, the PCI at the same combustion phasing, and the second most advanced PCI measurement of the sweep.

The distribution of MAPO values for each file was analyzed using log-normal probability plots, as suggested by Iwata *et al.* [194]. Iwata stated that both non-knocking datasets and knocking datasets follow a log-normal distribution. They are two distinct populations however, with different fitting terms. This fact can be used to set a threshold value to discern between knocking and non-knocking cycles. Figure 7.4 shows the results. If the cycles were distributed in a single log-normal manner, we would expect them all to group around the log-normal best fit line. This condition is verified only for the retarded PCI measurement. For the knocking spark ignition measurement on the other hand, it can be seen that the higher MAPO cycles clearly diverge from the fit line. A similar phenomenon is observed for the advanced PCI measurement at a similar cumulative probability, but this corresponds to higher MAPO values than for the SP. An identical threshold to separate between non-knocking and knocking cycles was fixed at 0.5 standard deviations from the log-normal best fit line. This results in 27 cycles being classified as knocking for the SP at its KL. 12 cycles were classified as knocking for the PCI for the file advanced by 9° CA from SP KL combustion phasing.

7.4.2 Mean Angle Based Band Pass Filtered Data

With the cycles classified into knocking and non-knocking groups, further detailed analysis could be performed. The profiles of absolute BPF cylinder pressure data, $\mid P_{bpf} \mid$, were compared against crank angle for the reference datasets, separated into knocking and non-knocking. Mean values are shown in Figure 7.5. The raw measurements were fitted with a spline algo-

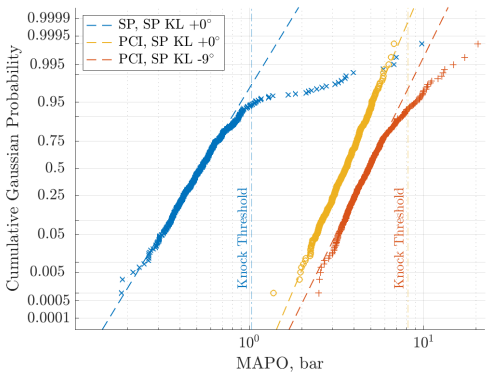

Figure 7.4: Log-normal Analysis and Threshold Setting for Spark Plug and Prechamber Measurement Files

rithm. The crank angle phasing of each measurement is shown relative to its MFB50 value. For the SP

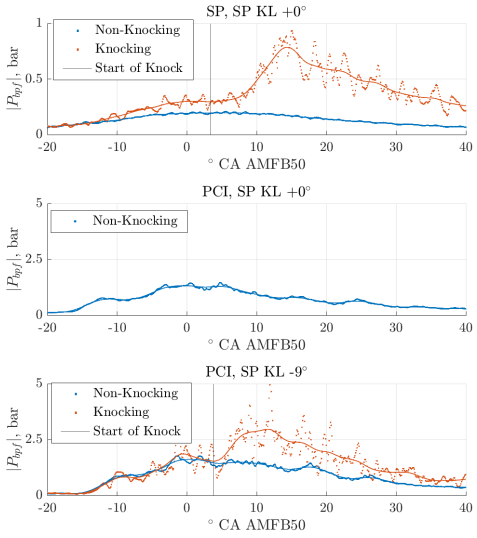

Figure 7.5: Mean Absolute High Pass Filtered Cylinder Pressure for Various Measurements

non-knocking cycles, the signal increases gradually to a peak around MFB50 and then smoothly decreases again. For the knocking SP cycles, there is greater BPF signal content already from 10° CA before MFB50. Note that knocking cycles are frequently correlated with faster burning even before knock occurs. This is because fast combustion leads to higher temperatures and pressures in the end-gas. Instead of decreasing after MFB50, there is an increase in the BPF cylinder pressure up until a peak at around 14° CA after MFB50 (AMFB50). The last point at which the gradient of the fitted BPF signal is zero, prior to this peak, was used as an indicator for the Start Of Knock (SOK).

The non-knocking PCI cycle averages are very similar between the measurement at SP KL combustion phasing and the advanced condition. The signal is less smooth with an initial rise up until around -13° CA AMFB50 and a second rise up until around -4° CA AMFB50. These peaks likely correspond to the arrival of the jets in the prechamber and the maximum burn rate respectively. For the knocking PCI cycles only, once again a further rise can be seen after MFB50. This is around three times higher than the equivalent peak for the SP knocking data when both are compared to their respective non-knocking mean curves. The zero gradient is at a similar relative angle to MFB50 as for the SP case. This suggests that autoignition begins with a similar amount of unburnt charge in the chamber. This does not necessarily mean that all of the remaining charge subsequently autoignites - localized autoignition events can occur in parallel with flame front propagation. Both the quantity of charge involved in autoignition and the rate at which it is consumed contribute to average pressure rises. Other factors, such as reactivity gradients around the initial autoignition site and its initial size, may determine if an autoignition proceeds in a relatively benign manner or proceeds into much more damaging developing detonation [263].

7.4.3 Continuous Wavelet Transforms

For greater insight into the nature of the high frequency content for all measurements, but in particular for the non-knocking prechamber cycles, Time Frequency Analysis (TFA) was performed. Continuous Wavelet Transforms (CWT) were used to this end, as they simultaneously permit fine time resolution at high frequencies and good frequency resolution at lower frequencies. Use of CWTs has been reported in the literature for knocking cycle analysis since at least 2000 [271]. A filter bank was constructed in MATLAB using the Morse wavelet, a time-bandwidth product of 60, 12 voices per octave and the same frequency range as used for the BPF (3-30 kHz). The results are shown in Figure 7.6.

For the SP KL cycles selected as non-knocking, the only frequency content identified in the range of interest is at around 6 kHz. This is the expected frequency of the first transversal mode, F10, for this chamber. For the knocking SP cycles, this mode can also be seen and is stronger. A broader range of frequencies are excited shortly after MFB50 for cycles over the knock threshold. This is clear evidence of an impulsive event - most likely rapid autoignition. It is well aligned with the SOK defined in Figure 7.5. Thereafter, some key frequency bands can be seen at around 10 kHz and 14 kHz. The specific frequencies excited will be examined in more detail in a later section.

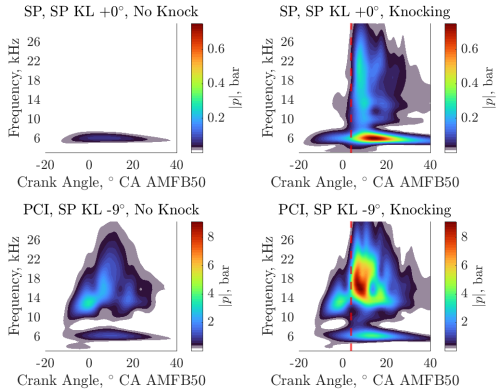

Figure 7.6: Continous Wavelet Transforms of Knocking and Non-Knocking Cycles for SP and PCI Measurements. Estimated Start of Knock Overlaid

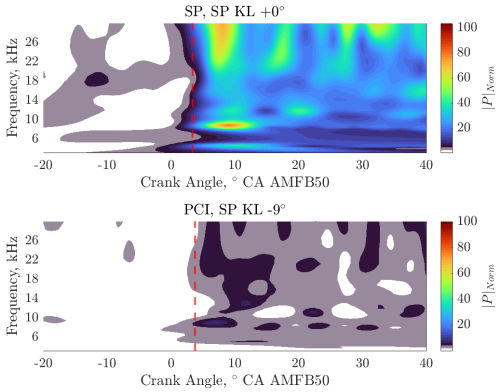

Figure 7.7: Ratio of Knocking to Non-Knocking Pressure Magnitude from CWT Analysis. Estimated Start of Knock Overlaid.

For the PCI case, already for non-knocking cycles there is much greater high frequency content. Once again the F10 mode is observed, but there is a new feature on the scalogram which emerges at around 10° CA before MFB50. This is much too soon to be end-gas knock and in fact coincides in angular terms with start of main chamber heat release. As this is driven by the jet arrival in the chamber, the jets are the likely cause - potentially shock waves, as described in [450]. Alternatively, pressure waves could be generated by initial rapid combustion from the jet locations in the main chamber. The data feature is present both for knocking and non-knocking PCI cycles. For the knocking PCI cycles, a broadband region shortly after MFB50 is excited, somewhat similarly to the spark ignition knocking case. This could once again be attributed to autoignition. This is overlaid however, on an additional time/frequency region also present for the non-knocking PCI cycles. An explanation for this region is not immediately apparent, although it does emerge at around peak heat release rates. The peak heat release rates are only around 1.5 times higher for the PCI case in comparison to the SP measurement and hence the global Heat Release Rate (HRR) by itself may not justify the noise. The fact that the main-chamber heat release for the prechamber initially occurs very rapidly in multiple locations may mean that burn rates in these regions are much higher than the overall factor of 1.5 suggests.

In an attempt to exclude non-knocking high frequency content, the mean scalograms for the knocking data were normalized using those for the non-knocking cycles. The results are shown in Figure 7.7. The files are qualitatively similar in that there is very little normalized content before the SOK line. The normalized content thereafter is much stronger for the SP in comparison to the PCI measurement however.

7.4.4 Discrete Wavelet Transforms

The CWT method gives detailed information in time-frequency space but is computationally intensive. A related method which can be implemented in a real-time system is the Discrete Wavelet Transform (DWT) [412]. The DWT approach is based on the Mallat multi-resolution algorithm [452]. As with the CWT, signal evaluation is carried out at different scales where the frequency resolution is better at low-frequency but at the cost of poor temporal resolution and frequency resolution is coarser at higher frequencies but with a finer temporal resolution. Unlike the CWT, the signal is only decomposed into octave bands. This methodology is applicable for the detection of abnormal combustion phenomena in which low-frequencies tend to develop and exist for longer periods, while high-frequency events tend to exist for shorter times. In practice, in the DWT approach, the signal is high-pass filtered at successively reducing octaves, to provide details at the next (coarser) level (with D_j coefficients), and low-pass filtered and sub-sampled to obtain approximations (with coefficients A_j), where j represents the level of decomposition. The process is illustrated in Figure 7.8.

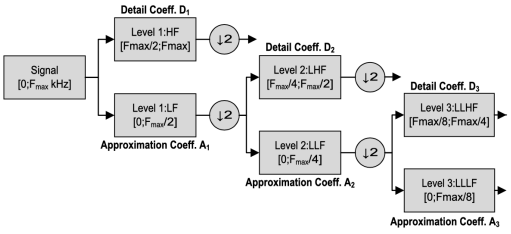

Figure 7.8: DWT Signal Decomposition

The composition of the filter bank depends on the choice of the wavelet function. In this work, a Daubechies

wavelet was chosen. The multilevel DWT decomposition is obtained by the recursive application of the analysis filter bank on the low-frequency bands (the approximation coefficients, A_j). Then, the process is repeated until the desired resolution is reached. Figure 7.9 shows the DWT decomposition for all levels for the pressure signal for the two different combustion systems, SP and PCI, for single cycles with the same (knocking) MAPO value. The maximum frequency was 72 kHz.

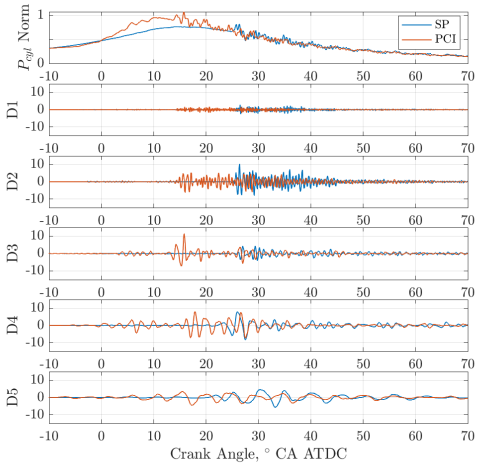

Figure 7.9: DWT Five Level Multiresolution Analysis for Knocking SP and PCI Cycle of Similar MAPO

Both the SP and PCI cycles show similar behaviour at the D5 frequency level (4-9 kHz), related to the F10 mode. For D4 (9-18 kHz) in the case of the PCI, the oscillations are clearly stronger. This band corresponds to the "background noise" identified even on non-knocking PCI cycles in Figure 7.6. There also appears to be greater signal content for the PCI in the next band, D2 (18-36 kHz), whilst for the highest band, D1 (36-72 kHz), the signals are subjectively similar again, but with signal content beginning sooner for the prechamber case. It may be advantageous to construct a single knock index per cycle which is robust to prechamber noise based on such decompositions. This will be the object of future study.

7.4.5 Acoustic Velocity Compensated Frequency Analysis

In order to study in more detail the frequencies present in the measurements, Fast Fourier Transform (FFT) analysis was performed. FFT analysis is appropriate for signals that are not changing in frequency during the analyzed time interval. This is clearly not the case in an engine, where gas properties and temperatures are highly variable. The mean gas temperatures and thermodynamic properties can be estimated using a First Law analysis. This was performed on the measured datasets. The gas temperature at Bottom Dead Center (BDC) before compression was taken from correlated GT Power simulations of the test case, as was the trapped mass. Acoustic velocity was calculated as a function of crank angle for each cycle in the dataset. This velocity was normalized to acoustic velocity at standard atmospheric conditions (estimated as 343 m/s). The time-base of the pressure signals was then adjusted by scaling with the ratio of instantaneous to reference velocities. FFT analysis was subsequently performed to give an equivalent power spectrum at reference acoustic conditions.

For a flat cylindrical volume with constant gas properties, acoustic mode frequencies can be calculated using the methodology of Draper [78]. Modern combustion chambers are somewhat more complex in comparison to the CFR engine analyzed by Draper in his experiments. Their modal frequencies can be estimated with Finite Element Analysis (FEA) [272] or with Computational Fluid Dynamics (CFD) [429]. The CFD approach was applied to the combustion chamber of interest in the present work. An average power spectrum was taken from the CFD for a peripheral heat source over an angular location sweep. As the CFD analysis was performed at standard atmospheric conditions, the datasets could be directly compared. The results are shown in Figure 7.10. Modes follow Draper's naming convention and some example mode shapes are shown schematically in Table 7.2.

Table 7.2: Mode Shape Naming Convention: FXY where X = No. of nodal planes and Y = No. of nodal Cylinders. Nodal planes and cylinders shown.

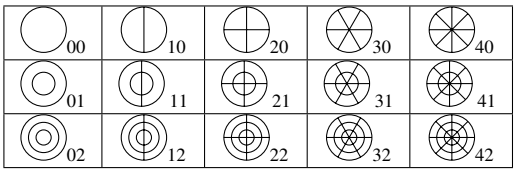

Considering firstly the spark plug dataset, the only clear peak on the Power Spectral Density (PSD) plot for the non-knocking cycles corresponds closely to the F10 frequency predicted by the CFD. For the knocking spark ignition cycles on the other hand, seven peaks can be observed. Six of these correspond to modes that only feature nodal planes: F10, F20, F30, F40, F50 and F60[2]. These are all well matched to the CFD in frequency terms. F00 can be seen but is rather weak. For this mode, the experimental result is shifted in comparison

[2]F40 and F01 have overlapping frequencies but past activity has shown that F40 is dominant for stimuli close to the bore wall [429]

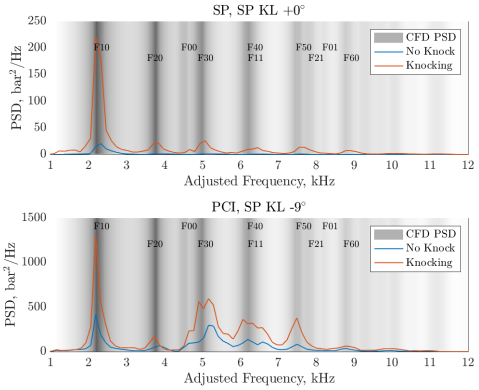

Figure 7.10: Comparison of Experimental Knocking and Non-Knocking Power Spectral Density for SP and PCI to CFD based Acoustic Analysis

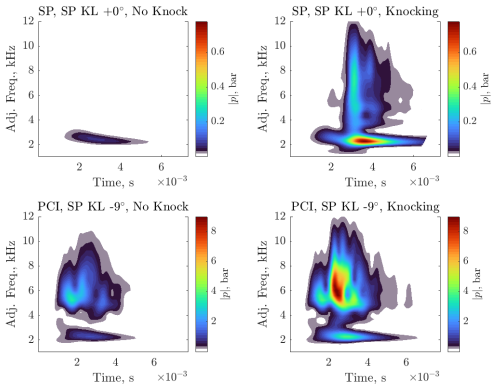

Figure 7.11: Continous Wavelet Transforms of Knocking and Non-Knocking Cycles for SP and PCI Measurements following Acoustic Velocity Compensation

to the CFD by around 200 Hz. In general it can be stated that for the SP KL measurement, all the significant frequency content in the range of interest for knocking analysis is explained by combustion chamber resonant modes.

If we now consider the prechamber measurements, once again the picture is more complex. For the non-knocking cycles, a greater range of frequencies are excited and in fact the F10-F60 modes would all appear to be present. F30 is particularly strong. The peaks are less distinct in the range of 4.5-8 kHz in comparison to the SP cases however. The prechamber jets may also be exciting the F11 mode at around 6 kHz (acoustically compensated). For knocking cycles, similar frequency peaks are seen but of higher magnitude. CWT analysis was once again performed, but this time with the acoustic velocity compensated pressure signals. The results are shown in Figure 7.11. Here it can be seen that the content from 4.5-8 kHz is present for the prechamber dataset from before the knock event and it persists also afterwards. Although it is rather a wide band, the fact that, following acoustic velocity compensation, it appears relatively stable in frequency terms over an extended duration, suggests that acoustic modes are of relevance to this data feature.

7.4.6 Heat Release Estimation

Heat release analysis from pressure measurements was first demonstrated by Rassweiler and Withrow[3] in 1938 [75]. The basic method has not changed much since. It assumes that the average pressure acting on the piston corresponds to that measured by the pressure transducer. The transducer gives a local pressure measurement, which may differ significantly from the average pressure at any given instant when waves exist. This can at least partly be handled through filtering. The data can also be fitted to one or a number of Wiebe functions [453]. This was demonstrated by Corti *et al.* for knocking datasets for conventional spark ignition [277].

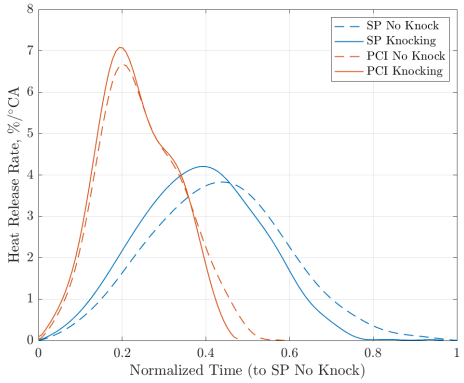

Figure 7.12: Average Heat Release Rates for SP and PCI, Knocking and Non-Knocking

Figure 7.12 shows the Heat Release Rate (HRR) analysis for the datasets of interest. The raw pressure data were filtered with a Low Pass Filter (LPF) with a corner frequency of 3 kHz and a steepness of 0.95. This should exclude the influence of pressure oscillations driven by the combustion chamber acoustic modes, the lowest of which is around 6 kHz as shown in Figure 7.6. For the non-knocking SP case, the burn rate follows the classical expected profile and in fact can be fitted successfully with a single Wiebe function. The Wiebe fit function for

[3]The same researchers also published some of the earliest photographic records of knock [74]

MFB is shown in Equation 7.4.

$$MFB_{Wiebe} = 100 * \left(1 - e^{-a\left(\frac{\theta-\theta_{SOB}}{\Delta\theta}\right)}\right) \quad (7.4)$$

Crank angle, θ, is normalized based on Start of Burn (SOB) and burn duration ($\Delta\theta$) whereas a and m are the form parameters. The error of this fitting (calculated as the average absolute difference between measured and fitted MFB) was just 0.24% for the non-knocking SP case. Attempting to fit the knocking SP data in the same way gives an error of 1.8%. The curve shape is more complex after around MFB50 - this is evidence of the additional heat release process of autoignition. The prechamber heat release profile is quite different. It shows a very rapid early heat release rate which then decays and is followed by an inflection point. The single Wiebe fit cannot cope well with this and in fact the error is much higher - around 0.8% for the non-knocking case and 2.3% for the average of knocking cycles. The best and worst cases for use of the single Wiebe fit are shown in Figure 7.13.

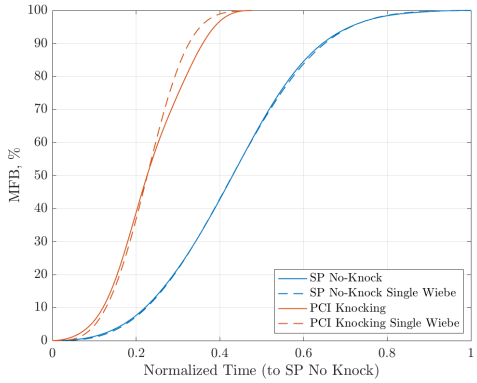

Figure 7.13: Average Heat Release Rates for SP and PCI, Knocking and Non-Knocking

A second Wiebe function was added. The fit parameters were explored using a Genetic Algorithm (GA) optimizer. The start point was randomized and ten runs were completed with only the best result retained. The results are shown in Figure 7.14 and the average error is less than 0.1%. The second Wiebe in this case physically represents an acceleration of burn rates shortly after peak HRR - likely driven by autoignition. Note the start of the “bulge" in the HRR curve which is well aligned with the Start Of Knock determined using high frequency data (Figure 7.5).

The double Wiebe function was also used to account for the early rapid burn with prechamber combustion. Once again the GA optimizer was run multiple times with randomized starting points. The results are shown in Figure 7.15. The average absolute fit error is 0.2%.

For the knocking PCI cycles, a further Wiebe function was required. This is because there are three distinct

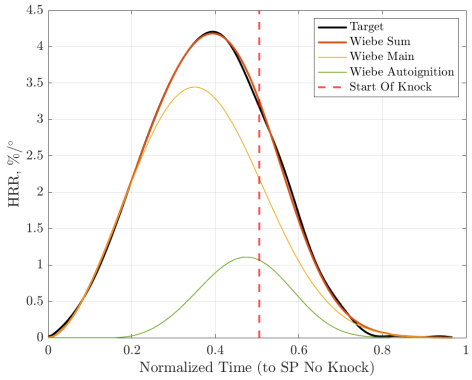

Figure 7.14: Double Wiebe fit for Knocking Spark Plug Cycles. Start Of Knock based on BPF Data Overlaid

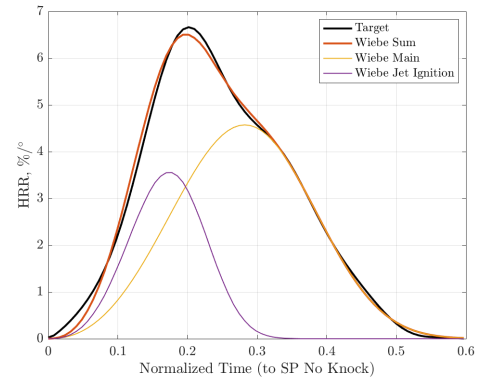

Figure 7.15: Double Wiebe fit for non-Knocking Prechamber Cycles.

combustion processes: initial fast combustion driven by prechamber jets, conventional flame-front propagation once the jets are no longer present, and autoignition. The results are shown in Figure 7.16. Note the excellent alignment between the HRR inflection point and the start of knock as identified in Figure 7.5. High frequency data and low frequency data are therefore in agreement on when autoignition occurs for both SP and PCI combustion systems. For the spark plug, the corresponding MFB value is 64% and for the prechamber 71%. It is clear from the above figures that this autoignition does not result in isochoric consumption of all the remaining charge. For the SP, from SOK to MFB99 takes 16° CA and for the PCI 8° CA. For the SP, this represents around a 25% reduction in duration in comparison to the non-knocking case. For the PCI, the corresponding reduction is 20%. Post-autoignition HRR acceleration does not therefore suggest that the PCI knock is more severe than that of the SP. Once again it must be recalled that this is the average chamber value and locally rates may differ significantly.

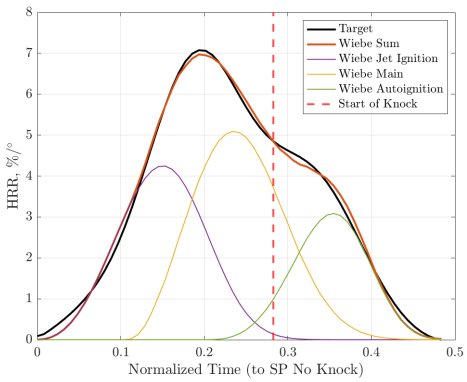

Figure 7.16: Triple Wiebe fit for Knocking Prechamber Cycles

The heat release analysis performed here was for "apparent heat release" only *i.e.* that which results in a pressure increase on the piston, net of heat transfer. Negative apparent heat release was calculated after end of combustion and it was realized that this was in effect an indicator of heat transfer. As knock has long been associated with higher heat losses [73, 195], this apparent negative heat release was compared between knocking and non-knocking cycles for both igniter types. It was found that mean post-knock apparent negative heat release was 8% higher for knocking SP cycles in comparison to non-knocking cycles. The equivalent figure for the PCI was 12% higher for knocking cycles in comparison to non-knocking. Note that this particular index should not be sensitive to transducer location, unlike high frequency techniques such as MAPO. It may indicate that the prechamber knocking cycles at SP KL-9° are more severe. There are fewer cycles classified as knocking for the PCI in comparison to the SP at its knock limit however. Hence in terms of severity of this index multiplied by the number of knocking cycles, the two datasets are comparable.

7.4.7 Combined Heat Release and Continuous Wavelet Transform Analysis

A method of identifying the beginning of autoignition which results in knock has already been demonstrated and is in agreement with HRR analysis. The angle of maximum BPF signal content may also be of interest. It is possible to visually inspect a dataset in its entirety using a combination of CWT and MFB analysis. At each increment of MFB, the average pressure amplitude across all frequencies in the CWT is taken for the corresponding crank angle. This is performed for each cycle, then these vectors are combined in a matrix. For visualization, the individual cycle values are then sorted by MAPO value from minimum to maximum. The end result is shown in Figure 7.17.

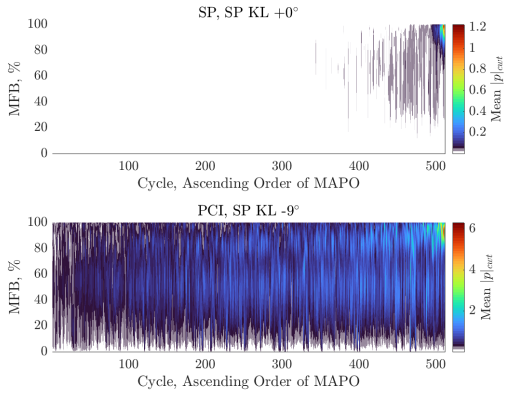

Figure 7.17: Comparison of Experimental Knocking and Non-Knocking Power Spectral Density for SP and PCI to CFD based Acoustic Analysis

For the spark plug case, very little high frequency content is seen for the vast majority of cycles. Recall that only 27 were classified as knocking. In the upper right part of the diagram, a triangular shaped region is evident. This implies that maximum BPF signal content is late in the cycle but progressively earlier for the strongest knocking cycles. For the highest MAPO cycles, the high frequency content is evident from around MFB70. This is somewhat later than the SOK identified in Figure 7.5 but recall that this was based on the beginning of the rise up to the maximum value. For the PCI measurement, high frequency content is clearly evident from the beginning of combustion. Once again however, a triangular region can be identified in the upper right. This is somewhat smaller (recall that just 12 cycles were classified here as knocking). The background noise level is also much higher. For mean data, this can be compensated as shown in Figure 7.5.

7.4.8 Knock Probability Analysis

Knock is a cyclically variable phenomenon. Part of this is driven by cyclic variation of flame-front propagation. Normally when an engine is said to be in a "borderline knock" condition, only a certain percentage of cycles will be knocking. These will generally be the most advanced cycles in the population, as already described. Cyclic variability depends on the combustion system and in particular on variations in early burn rates [260]. A prechamber ignition system results in very fast early burn rates with low cyclic variability. The knock limit improvement of the prechamber is partly due to this phenomenon. It is possible to quantify this from the data.

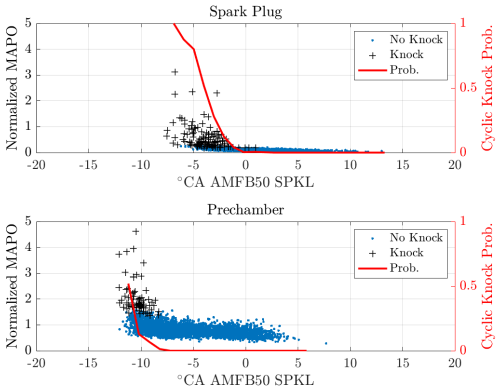

Figure 7.18: Calculation of Single Cycle Knock Probability for Given Combustion Phasing

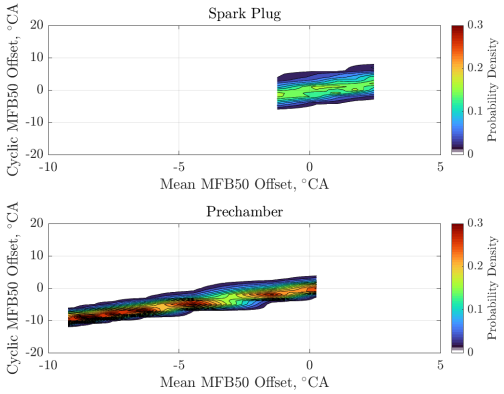

Figure 7.19: Variability of Cyclic MFB50 over Combustion Phasing Sweeps

The knock thresholds for all measurements in the sweep were defined using the method demonstrated in Figure 7.4. All cycles in each combustion phasing sweep were then classified as knocking or not-knocking. The cycles were grouped into bins at discrete combustion phasing intervals. At each interval, the ratio of knocking to non-knocking cycles was calculated. This gives a single-cycle knock probability - the likelihood that a single cycle will result in knock if it has a given combustion phasing. The results are shown in Figure 7.18.

The final population knock probability depends on the single-cycle knock probability and the cyclic variation of combustion phasing. Histograms of cyclic MFB50 were therefore created for each distinct dataset in the sweep. A surface was then interpolated between each histogram. This is shown in Figure 7.19. It can be seen that there is greater variation in cyclic MFB50 for the spark plug in comparison to the prechamber. MFB50 follows an approximately normal distribution for both igniters. The standard deviation is a function of average combustion phasing, as can be seen for the prechamber dataset - more advanced phasings show lower cyclic variability. This is not obvious for the spark plug but this is likely due to the narrower range of spark timings investigated.

The single-cycle knock probability and the cyclic MFB50 distributions can be combined to give a global knock probability for a given mean combustion phasing. This is shown in Figure 7.20. This figure allows us to quantify how much of the prechamber's advantage in terms of knock-limited combustion phasing is due to its reduced cyclic variation. If there were no contribution, the offset between the single-cycle knock probability curves would be equal to the offset between the population knock probability curves. This is not the case. The single cycle offset is 8° CA whilst for the population the offset is 9° CA. Reduced cyclic variability is therefore contributing just 1° CA of the overall gain. It also results in a steeper population knock probability increase as

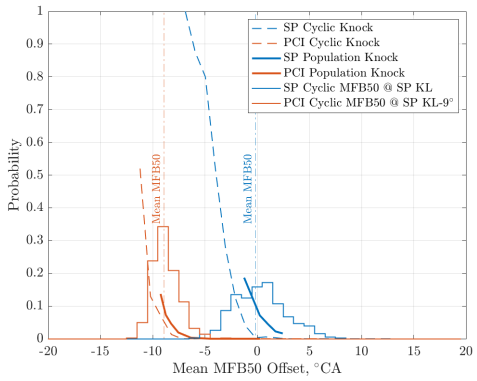

Figure 7.20: Comparison of Cyclic and Population Knock Probabilities. Cyclic MFB50 variation for the SP KL and PCI SP KL-9° measurements are overlaid.

combustion phasing is advanced. The knock limited benefit of reduced cyclic variability from prechamber combustion would be of greater importance in more challenging conditions, such as with dilute mixtures or water injection combined with Miller intake valve lift profiles [331].

7.5 Summary of Results

A wide range of techniques have been applied in this work to study a SP dataset at a known knock limit with a PCI dataset advanced by 9° CA of MFB50. Table 7.3 summarizes some key indices generated in this investigation. It can generally be stated that high frequency pressure based indices rank the knocking PCI cycles as more severe by around a factor of three. Whilst such measurements are susceptible to relative

transducer and knock locations in the chamber, the same cannot be said for the negative heat release index. This suggests that the PCI knocking cycles are 1.5 times more severe. Note however, that there are 2.3 times more SP knocking cycles than PCI knocking cycles for the datasets analyzed in this study, based on an identical thresholding routine. The burn rate analysis on the other hand, suggests slightly more unburnt charge at the beginning of autoignition for the SP measurements and a more significant relative reduction in burn rates post-autoignition. Here the differences to the PCI are rather small.

Table 7.3: Summary of Knock Indices for SP KL and PCI with 9° CA Advance. All pressure based indices are normalized to threshold MAPO 99.5th MAPO values for standard SP calibration activity

Index	SP	PCI
MAPO $P_{99.5}$	0.7	2.0
Lognormal Threshold	0.2	1.5
Cycles Over Lognormal Threshold, n_{knock}	27	12
Mean peak ΔP_{bpf} to non-knocking	0.12	0.31
n_{knock} . Mean Peak ΔP_{bpf}	3.2	3.7
MFB at Autoignition	64%	71%
Post Knock Burn Duration Reduction, PKBDR	23%	19%
n_{knock} . PKBRF	621%	228%
Negative Late HRR Ratio, NLHRRR	108%	112%
n_{knock} . NLHRRR	2916%	1344%

In balance, considering the overall picture, the PCI with 9° CA of MFB50 advance can be considered similar, or even slightly less severe, in its knocking tendency to the SP at its knock limit. The SP knock limit was defined by established calibration methodology. The knock limit benefit of the prechamber is therefore thought to be appropriately quantified and not overestimated as a result of a more permissive calibration approach to knock.

7.6 Conclusions

A detailed analysis of knocking datasets for both conventional spark plug ignition and prechamber ignition has been performed for a high performance engine over full-load combustion phasing sweeps. The following observations were made:

- MAPO values in retarded conditions are significantly higher for prechamber combustion in comparison to conventional spark ignition
- Despite this, a method to separate data into knocking and non-knocking populations, originally suggested by Iwata *et al.* [194], could be used to good effect with no requirement for individual threshold tuning for the two combustion systems.
- For conventional spark ignition and non-knocking cycles, the only high frequency noise on the pressure trace is due to the F10 chamber resonance mode at around 6 kHz. The noise profile against crank angle has a gradual rise and fall.
- For the prechamber, in retarded conditions the high frequency content is much more complex. The F10 mode is still excited but so are all transversal modes with nodal planes up until at least F60. F00 and F11 are also likely present. In crank angle terms, two rises in high frequency content are likely associated with jet arrival in the main chamber and peak heat release rate, which is much higher for prechamber ignition.
- For spark ignition knocking cycles, all frequency content could be well explained by transverse acoustic modes from F10 to at least F60, as expected. F10 is present even before autoignition is identified whereas the other modes appear to be excited by an impulsive event - likely the onset of knock. A similar data feature is identified for the prechamber knocking cycles.
- For both spark ignition and prechamber combustion, key frequencies in spectral analysis were well aligned to CFD based acoustic studies of the combustion chamber geometry.
- Wiebe fit analysis of HRR profiles showed three distinct combustion processes for the knocking prechamber cycles: initial burn rate acceleration by prechamber jets, conventional flame-front propagation, and autoignition driven acceleration of burn rates. Burn rate acceleration for prechamber and spark ignition knocking cycles was similar in proportional terms, whilst relative knocking heat losses were somewhat higher with the PCI igniter.
- Analysis of knocking probability on cyclic and population bases suggested that almost all the gain in knock-limited combustion phasing for the prechamber was due to “average cycle” effects with only a minor contribution from improved combustion stability.
- The range of methods employed confirm that the knock limited combustion phasing benefit of the prechamber considered in this investigation, is of the order of 9 °CA of MFB50. This can clearly make a significant contribution to improving engine efficiency, in particular if combined with increased compression ratio.

7.7 Future Activity

This work has described knocking characteristics of standard and prechamber igniters to generate confidence that appropriate and comparable borderline knock conditions can be identified for both systems. Future activity will look more closely at combustion in the prechamber, through use of prechamber pressure indication, and knocking locations in the main chamber. Operating conditions will also be extended and higher compression ratios will be investigated, together with revised prechamber geometries. An improved real-time capable cyclic knock index will also be studied, based on the DWT approach.

CHAPTER 8

Knock in Transients

8.1 Abstract

Knock in a research setting has long been studied on engine test beds [33]. Here, the engine is generally held at constant speed and load for an extended period before performing a measurement. This ensures thermal stability. Engines for road vehicles however, frequently operate in transient conditions. This is the case by definition during an acceleration. It is therefore important to understand the differences in knocking behavior between stationary and transient cases.

Transient events may differ from steady state operation for a number of reasons. A key aspect is component temperature. An engine running indefinitely at full load will have higher combustion chamber component temperatures than an engine that has been running at low load where full load is then requested. As knock is largely linked to high temperatures, this implies there may be an additional knock margin for such events in comparison to how engines are typically calibrated.

A simple model was developed by the author to harness this knock margin in Formula 1. This has now been applied to passenger car development at Ferrari. It is shown that despite more limited instrumentation availability on a production passenger vehicle, this model can still be used to good effect to offer improved engine performance in transient conditions.

8.2 Introduction

In the 1930s, the Cooperative Fuels Research (CFR) group performed extensive testing on the road in order to devise representative knock testing procedures for the engine test bench. One of the first road test methods was the "Uniontown" procedure [65], named for the location where testing was performed in 1933. Investigations were performed of knock behavior during acceleration uphill starting from different vehicle speeds in the range of 10-60 miles per hour. In this way, for each car and fuel, a profile of knock intensity (judged aurally) against vehicle speed could be constructed. It was decided that the reference for each car and fuel would be the highest knock intensity recorded at any speed. This fuel could then be compared in the same car to bracketing references at their maximum knock speed[1]. This procedure was known as the CFR "Road-Test Method for Conducting Antiknock Tests". Correlation to the Research Octane Number (RON) engine test method was seen to be poor. The RON procedure was modified to have higher speed (900 rpm) and both coolant and mixture temperatures were increased[2]. This would become the CFR Motor Octane Number (MON) test, devised in the same research program as the Uniontown road tests [65]. Correlation with road testing was greatly improved. Fuels at the time had octane numbers in the range of 60-70. No specific mention of possible reasons for transient phenomena in the vehicle tests was made.

Fuel refining evolved significantly, in part driven by research as part of the war effort in the late 1930s and early 1940s. Octane ratings for aircraft engine fuels exceeded 100 [90]. The CFR road test procedure was revised in 1940 to give the "Borderline method". Here acceleration events were performed beginning at high gears from low vehicle speeds. Knock tended to die out as the vehicle accelerated. The engine speed at which knock could no longer be discerned was noted and gave one point on the curve. The procedure was then repeated with adjusted ignition timing characteristics until a final "borderline knock curve" could be produced, as shown in Figure 8.1. Once again the profile of knocking behavior was observed to vary with fuel type. Engine speed was thought to be the most representative variable to measure knock against. Knock was found to typically be most problematic at low speeds.

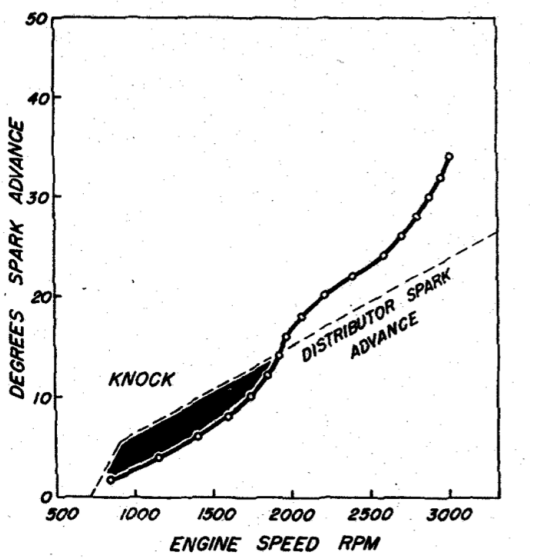

Figure 8.1: "Borderline" Ignition Timing showing Knock Region in Comparison to Distributor Advance Curve, from Risk [91]

The issue of fuel knock behavior dependence on operating conditions was studied in great detail in the American Petroleum Research Project 45, described by Lovell [112] in 1948. 29 different operating conditions were considered, but once again this was in stationary testing. Rapid Compression Machines began to be

[1] it was noted that different fuels produced maximum knock at different speeds in the same vehicle

[2] the intake system was deliberately heated on engines of the period to improve mixture formation

used to better understand reaction kinetics in the same period [122].

In the 1960s, the stationary test methods were once again called into question [134]. It was noted that both fuels and engines had changed significantly since the procedures were devised. Knocking was observed in road testing at higher speeds due to a combination of automatic transmissions and engine design. The MON test was said to be decreasing in relevance due to efforts to lower engine temperatures in comparison to 1930s vehicles. Fuel sensitivity (RON-MON) had also greatly increased. It was stated by Bartholomew that single cylinder fuel testing should still be relevant to road use if *"the program of pressure, temperature and time in the knocking cylinders is duplicated in the cylinder of the test engine"*, among other conditions. Dynamics of liquid fuel vaporizing in the intake system were also mentioned and in fact a "Distribution Octane Number" was used to account for such effects at the time [136]. Once again, no effort was made to introduce a transient engine test procedure.

In the late 1970s, electronic control of knock in production vehicles was introduced [176] and such devices would become ubiquitous in the 1980s [180, 181]. These generally reacted on the ignition timing. An alternative approach was proposed by Gillbrand [182] at Saab which acted on boost pressure. This system allowed for higher boost pressure in transient maneuvers, where less knock was observed. The thermal inertia of the combustion chamber was credited as the reason why this could be achieved.

Despite the possibilities of modern control systems, knock is still typically measured in a research setting and calibrated for production engines in stationary conditions. Concerns about fuel mixture dynamics in the inlet system are eliminated by direct injection hence the thermal dynamics of the combustion chamber should dominate in transient events, providing intake air temperature remains constant.

8.3 Formula 1 Experience

In 2014, the author of the present work devised and carried out a research study to investigate the effect of transients on knock. It was suspected that the combustion chamber surface temperature would be the most relevant parameter influencing the knock behavior in a fast acceleration, but this is not straightforward to measure directly. The temperature reading of a miniature modified indication sensor with a thermocouple on the diaphragm was therefore used as a surrogate. This is shown in Figure 8.2. Research was initially carried out on a Formula 1 single-cylinder engine, as this gave best control of boundary conditions [454]. Full load ramps to 14200 rpm were executed at various engine speed gradients, starting from stabilized conditions at 5000 rpm and 35 bar Indicated Mean Effective Pressure (IMEP). Ramp rates were decided based on representative full load engine speed gradients for each gear ratio used at the track. It was found that temperature decreased approximately linearly with speed gradient. This is because the engine is moving from a lower power to a higher power condition and hence the chamber is heating up over the ramp.

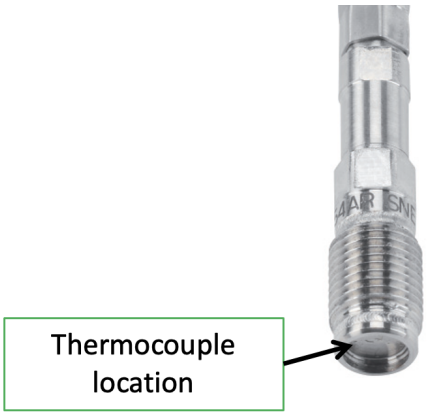

Figure 8.2: Miniature Indication Sensor with Temperature Instrumented Diaphragm

Two other effects were noted. Firstly, even if careful attention was paid to ensure constant air fuel ratio over the ramp, to maintain combustion phasing for a given speed and load, a fast ramp required more ignition advance. This was attributed to the effect of lower combustion chamber temperatures on laminar flame speeds. This means that if an engine is calibrated in stationary conditions for a given combustion phasing, it will likely run more retarded in a fast ramp even if all conditions other than combustion chamber component temperature are matched. The ignition timing was therefore adjusted to maintain the same combustion phasing, characterized by 50% Mass Fraction Burned (MFB50) as achieved in stationary calibration. Note that in stationary conditions, this combustion phasing was knock-limited. The second observation was that this combustion phasing no longer produced knock in the fast ramp. In fact, the combustion phasing could be progressively advanced as ramp rate was increased to take advantage of this phenomenon. The potential for advance was well correlated with the measurement of the temperature sensor, as shown in Figure 8.3. This implied that the sensor was measuring a temperature pertinent to the knocking behavior of the engine. Note that it was possible to advance by almost 10° CA of MFB50 in the fastest and hence coolest ramps - a very significant amount. This had obvious implications both for engine design (the optimum compression ratio to minimize lap-time was likely higher than previously assumed) and calibration methodology.

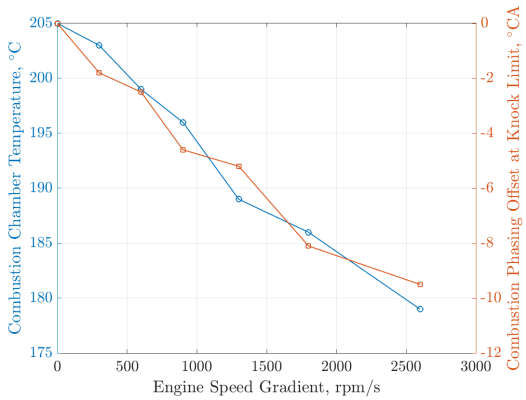

Figure 8.3: Effect of Engine Speed Gradient on Combustion Chamber Temperature and Knock Limited Combustion Phasing at 10500 rpm following Ramp from Thermal Stabilization at 5000 rpm

Figure 8.3 shows the effect which had been hoped for. It implied that there was the potential to increase power in an engine speed gradient, such as occurs at the exit of a corner, in comparison to the standard calibration conditions, which were approximately thermally stabilized. Such conditions were more representative of the engine temperature at the end of the straight just before corner entry. Note that the lap-time benefit of additional engine power depends on where it is applied. The benefit is maximum at corner exit, as speed increases achieved here will correspond to a higher speed for the entire straight. Extra power just before braking on the other hand, has almost no effect on lap-time. The conditions at which the engine was being calibrated were therefore not the most lap-time relevant!

It was not desired to add additional sensors to the race car, hence a modeling approach was adopted to replicate the temperature sensor's output. As this model was to be implemented into the Engine Control Unit (ECU) on an individual cylinder basis, as simple an approach as possible was desired. The sensor was mounted in the multi-cylinder race engine and a playback measurement performed on a transient powertrain test bed [455]. This featured an engine start in the pit, followed by a lap to grid, a race start and three laps, as shown in Figure 8.4. A simple model was constructed in MATLAB Simulink, as shown in Figure 8.5. The model featured only three inputs - engine speed, coolant temperature and peak cylinder pressure. The thermal inertia of the combustion chamber was represented by a numerical integrator block. Cylinder gas temperature was assumed to be proportional to peak cylinder pressure by a proportionality constant (Constant 1). A second constant (Constant 2) represented the convective heat transfer coefficient between the gas and the combustion chamber metal. The convective heat transfer coefficient for the coolant was assumed proportional to engine speed (which is linked directly to water pump speed) by Constant 3. The final tuning term, was the combustion chamber thermal inertia represented by the integrator function. Despite the very simple model structure, the model error was acceptably small, as shown in Figure 8.6.

The model output was also registered in stationary conditions during standard calibration activity. The final step was to introduce a new map structure in the ECU to actuate an ignition offset as a function of the difference between the actual estimated combustion chamber temperature whilst the car was running at the track, and that of the chamber at the same speed and load point in the calibration activity. This model was extremely effective and allowed up to 12° CA of additional ignition advanced to be applied in critical moments of the race (such as the start) when combustion chamber temperatures were suitably low [456].

8.4 Model Application for Road Cars

The goal of race engine calibration is to extract the maximum performance at all times, within an acceptable engine damage budget. This damage budget may also depend on the phase of the race weekend - for example it makes more sense to push the engine hard during qualifying in comparison to practice sessions. A road car development program on the other hand, generally has fixed targets of performance to achieve. The thermal model was not therefore considered until a production development vehicle was not meeting its desired in-gear acceleration performance.

The maneuver was a full load acceleration in from low speed. The engine was knock limited in stationary conditions in this speed range, hence it was thought there would be good potential to increase performance taking advantage of thermal effects. This was verified by performing ignition timing sweeps at various ramp rates corresponding to different gear ratios [457], similarly to the Formula 1 single cylinder activity. The results are shown in Figure 8.7. As was seen in the racing activity, a significant improvement in the knock limited ignition timing was possible, harnessing the thermal advantage of fast ramp rates. A similar temperature sensor as employed in the racing activity was once again used. This confirmed that knock limit improvements were once again correlated with chamber temperature, as shown in Figure 8.8

The Formula 1 engine featured cylinder pressure transducers hence peak cylinder pressure was already available as an input to the thermal model. This was not the case for the production intent vehicle. Peak pressure

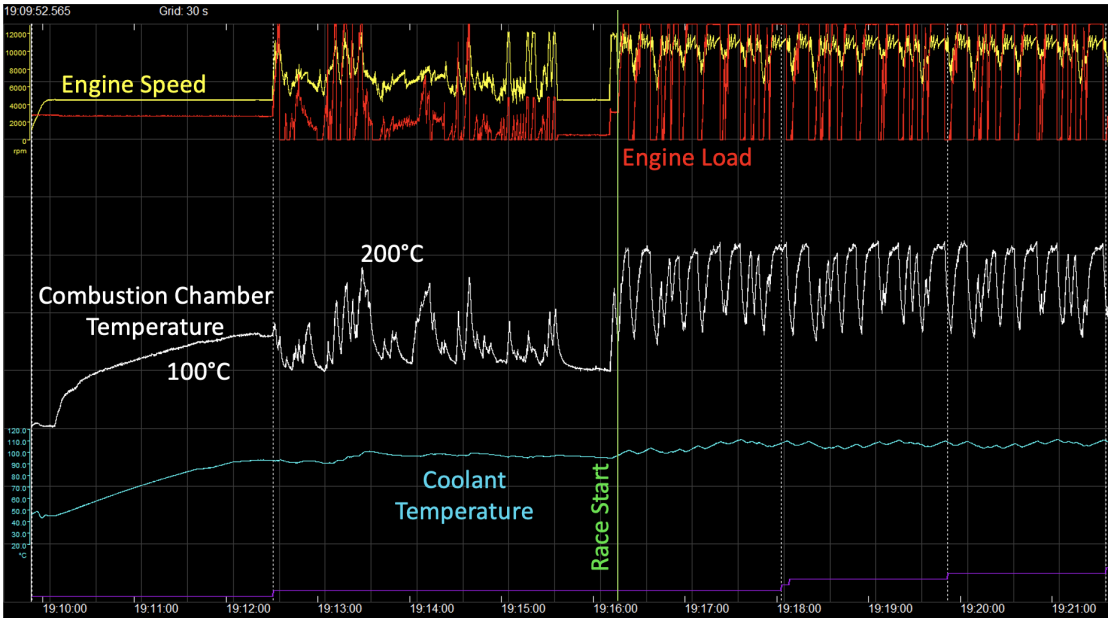

Figure 8.4: Transient Test Cycle with Temperature Measurement for Model Development and Tuning [455]

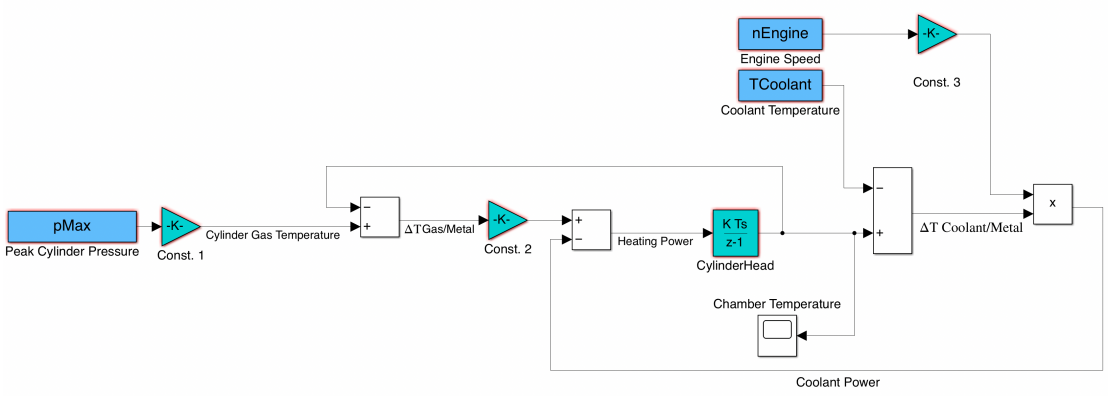

Figure 8.5: Simulink Model of Combustion Chamber Temperature

maps were reconstructed based on experimental data as a function of speed, load and ignition timing. Whilst typical temperature errors for the Formula 1 application were within $\pm 5°$ C, the error was approximately two times larger for the production application. At least part of this may be due to the uncertainty in peak cylinder pressure estimation.

Once again, a map structure was created where the modeled temperature of the chamber estimated by the ECU during transient maneuvers could be compared to the reference chamber temperature during calibration. The ignition offset based on this temperature difference is shown in Figure 8.9

This transient calibration approach, taken directly from Formula 1 activities, allowed the vehicle to meet the target acceleration values, which were not possible without this feature.

8.5 Conclusions

Knock in transient maneuvers has been rather neglected in terms of research and calibration effort over the years. In the early days of the motor car, adequate instrumentation did not exist to characterize and fully understand the phenomenon. In the middle of the 20th Century, transient effects were dominated by fuel dynamics in the intake system. In the 1980s, some researchers begin to find possibilities to take advantage of transient maneu-

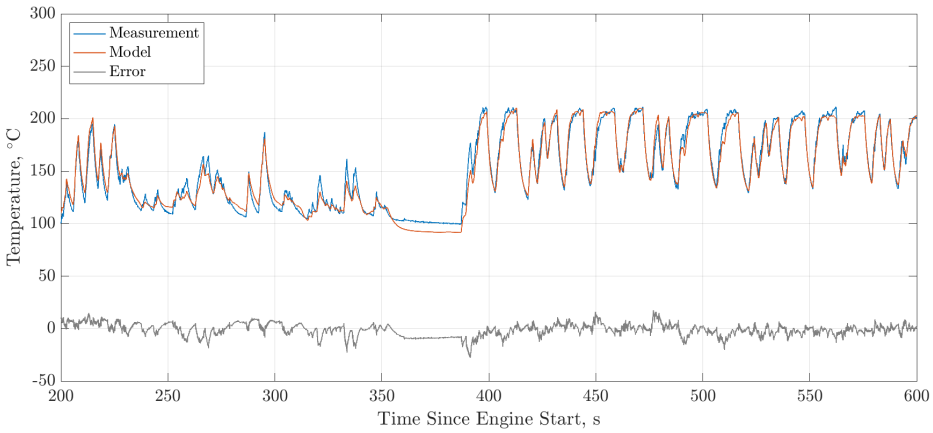

Figure 8.6: Thermal Model Validation on Transient Test Cycle

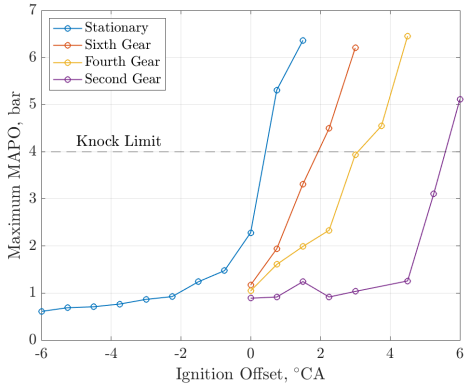

Figure 8.7: Effect of Engine Speed Gradient on Knock Response at Full Load 4000 rpm following Ramp from Thermal Stabilization at 2000 rpm Partial Load

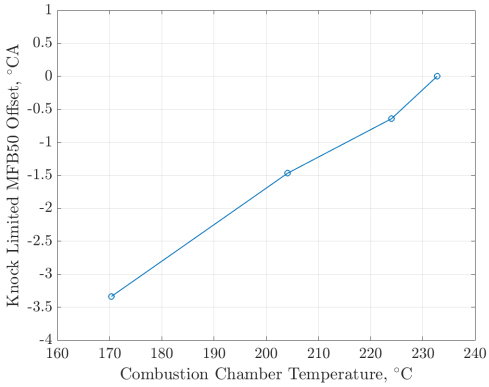

Figure 8.8: Effect of Engine Speed Gradient on Knock Response at Full Load 4000 rpm following Ramp from Thermal Stabilization at 2000 rpm Partial Load

vers to improve knock limited performance, but there has been relatively little in the literature since. Formula 1 gave both the motivation and the tools to study the phenomenon and to control it in highly dynamic situations. It has been shown that even for production engines without cylinder pressure indication, techniques developed in Formula 1 can be applied to good effect.

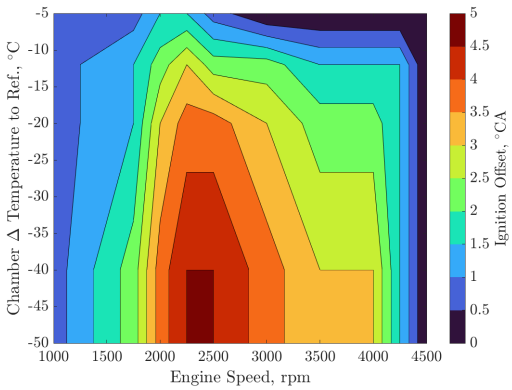

Figure 8.9: Ignition Offset Map based on Combustion Chamber Temperature Difference to Calibration Conditions

CHAPTER 9

Closing Remarks

THROUGHOUT the three years of this PhD, the author has sought to use his experience from a Formula 1 background to reinterpret road car development and technology. Maximizing engine performance has been a key theme. Whilst the physics of what limits this are, of course, identical for road and race applications, the boundary conditions are rather different.

Knock has been the primary focus throughout. This is partly as it has been perhaps the main development driver in Formula 1 since turbocharged engines returned to the sport in 2014. It is also because high performance road car engines are increasingly downsized to minimize fuel consumption in part load, but with turbocharging to also guarantee high performance when required. Improving the knock limit is also a large efficiency benefit, as it is the main limitation on the compression ratio and hence theoretical cycle efficiency. A significant portion of time was invested in a large scale literature survey covering one hundred years of activity on the subject. This led to a number of realizations:

- The experience with Tetra-Ethyl Lead is a lesson from history. This was said to be a *"gift from God"* in the 1920s as it allowed for great improvements in fuel efficiency. Even if there were some warning signs already then, it was not for another fifty years that its negative health effects would come to be realized after much damage had already been done. We are currently in a period where there is great focus on reducing carbon dioxide emissions but also, perhaps, an appetite for apparent silver bullet solutions. Abandoning combustion engines and replacing all road transport with battery driven vehicles is seen by some as an obvious solution. Great attention must be paid here to potential negative externalities associated with the necessary raw materials extraction and high energy expenditure in production of such energy storage systems. As has been seen countless times in the past, it is very easy to create a new problem in a rushed effort to solve an existing one. Whilst electrification no doubt has a key role to play, perhaps a more balanced technical solution portfolio would be advantageous.
- The activities of the CFR group in the 1920s and 1930s are admirable for the scale and intensity of the international collaboration. Researchers from companies around the world worked closely and quickly to develop new fuel rating procedures which we are still using today. The current effort to find technical solutions to combat climate change could take some inspiration from this. Instead it appears to be an overly politically driven debate, which risks to not identify the best pathway to success.
- Some very interesting experiments were performed in the past to aid in fundamental understanding. An excellent example of this is Draper's research on combustion chamber acoustics comparing fired and stationary engine data. It is now technically possible to perform very complex experiments and simulations. Perhaps when the goal is understanding, rather than replication, there is still room for simplification of complex problems to gain greater insight.
- It is sometimes said *"there is nothing new in engineering"*. Whilst this may be an exaggeration, it is certainly the case that faced with similar problems, engineers have developed similar solutions over the years. The prechamber is one example

that has come and gone several times over the last century and is currently enjoying somewhat of a renaissance. It is therefore useful for engineers to try to gain an historical overview of their subject area rather than concentrating only on the most recent research. Often it is implicitly assumed that recent papers will refer back to the most relevant historical activity. Some very useful historic publications appear to have been overlooked however - an excellent example being Iwata's dual log-normal knock thresholding approach from the 1980s.

Fuel development was and remains a key area of knock research since the early years of the automobile. The most intense fuel development in recent years is arguably in Formula 1. Whilst vehicle manufacturers generally don't seek to develop their own fuels, methodologies used by teams and fuel suppliers can be recycled to better understand commercial blends. This enables more accurate simulation of new combustion concepts to maximize performance and efficiency. Similar methodologies will undoubtedly be key in investigating future carbon-neutral fuels.

Prechambers are an interesting technology for improving an engine's knock limit and have become ubiquitous in Formula 1. They are much more difficult to apply to a production vehicle due to issues with retard-ability and hence catalyst heating. A new combustion concept has therefore been proposed, patented and demonstrated in physical testing. Similar experimental techniques as developed in Formula 1 were used in its validation and to aid understanding. This new concept enables significant knock limited performance improvements with emissions capabilities at least on a par with existing combustion systems. The necessity of a secondary igniter does increase engine cost however.

In order to improve an engine's knock limit, measurements of knock must be well understood. Part of this is understanding the chamber acoustic behavior. A new method of interpreting cylinder pressure measurements supported by simple CFD models taking inspiration from historic activity has therefore been developed.

Experimental data from both spark ignition and prechamber combustion has been interpreted making use of historic and new techniques. In particular, it appears to be possible to make some estimate on knock location from a single pressure transducer. A detailed comparison between prechamber and standard ignition systems at the knock limit has also been performed using a wide range of methodologies. Such an approach allows for robust quantification of new combustion system performance gains - in particular where high frequency signal content on cylinder pressure traces is not uniquely driven by autoignition.

Finally, whilst almost all of the literature and activity on knock concentrates on stationary measurements, a new method of understanding and harnessing knock behavior in transients has been brought from Formula 1 into a production environment. This has allowed a road-car vehicle to meet acceleration targets which otherwise would not have been possible.

The Internal Combustion Engine is sometimes described as a mature technology. This implies that it is well understood and there is little left to be learned. At no time in the

three years of this research did the author have the impression there was nothing left to explore! We are entering a period of great uncertainty for automotive powertrains. The stakes have never been higher. It is only by maintaining an open mind, learning the lessons of the past, and collaborating in an open and honest way with our fellow engineers and scientists that we can ensure we find the best solution for our world, and that of our children.

Bibliography

[1] Benz & Co., "European patent DE37435C: Fahrzeug mit gasmotorenbetrieb," 1886.

[2] Wikipedia. Peugeot type 5. [Online]. Available: https://en.wikipedia.org/wiki/Peugeot_Type_5

[3] Daimler. Mercedes-benz W 125 (1937). [Online]. Available: https://media.daimler.com/marsMediaSite/ko/en/9904219

[4] Wikipedia. Alfa romeo 158. [Online]. Available: https://it.wikipedia.org/wiki/Alfa_Romeo_158

[5] Ferrari. Ferrari website. [Online]. Available: www.ferrari.com

[6] Brand Finance. Brand finance automotive industry 2021. [Online]. Available: https://brandirectory.com/rankings/auto

[7] FIA. Formula 1 regulations. [Online]. Available: https://www.fia.com/regulation/category/110

[8] M. Tutuianu, P. Bonnel, B. Ciuffo, T. Haniu, N. Ichikawa, A. Marotta, J. Pavlovic, and H. Steven, "Development of the world-wide harmonized light duty test cycle (WLTC) and a possible pathway for its introduction in the european legislation," *Transportation Research Part D: Transport and Environment*, vol. 40, pp. 61–75, 2015. [Online]. Available: https://www.sciencedirect.com/science/article/pii/S1361920915001030

[9] A. Hamilton, P. Reznikoff, and G. M. Burnham, "Tetra-Ethyl Lead," *Journal of the American Medical Association*, vol. 84, no. 20, pp. 1481–1486, May 1925. [Online]. Available: https://doi.org/10.1001/jama.1925.02660460017008

[10] R. Sayers, A. Fieldner, W. Yant, and B. Thomas, "Experimental Studies on the Effect of Ethyl Gasoline and its Combustion Products," U.S. Bureau of Mines, Tech. Rep. 597996515, 1927.

[11] J. P. Leake, L. Kolb, L. Schwartz, G. C. Lake, W. Harrison, C. W. Mitchell, W. M. Clark, E. Elvove, C. Remsburg, C. Kinyoun, J. Bloomfield, W. Hall, and W. A. Simkins, "Investigation of Health Hazard from Tetraethyl Lead Gasoline," United States Public Health Service, Tech. Rep. Public Health Bulletin No. 163, Jun 1926.

[12] US Government, "An Act to provide research and technical assistance relating to air pollution control ," *Public Law*, vol. 159, no. 360, pp. 322–323, July 1955.

[13] US Goverment, "Motor Vehicle Air Pollution Control Act - An Act to amend the Clean Air Act to require standards for controlling the emission of pollutants from certain motor vehicles, to authorize a research and development program with respect to solid-waste disposal, and for other purposes ," *Public Law*, vol. 89, no. 271, pp. 992–1001, October 1965.

[14] C. C. Patterson, "Contaminated and Natural Lead Environments of Man," *Archives of Environmental Health*, vol. 11, no. 3, pp. 344–360, 1965, PMID: 14334042. [Online]. Available: https://doi.org/10.1080/00039896.1965.10664229

[15] Health Effects Branch of the EPA, "EPA's Position on the Health Effects of Airborne Lead," Environmental Protection Agency, Tech. Rep. 736F72001, November 1972.

[16] R. Engel, D. Hammer, R. Horton, N. Lane, and L. Plumlee, "Environmental lead and public health," Environmental Protection Agency, Tech. Rep. AP-90, March 1971.

[17] United Nations Environment Program. Era of leaded petrol over, eliminating a major threat to human and planetary health. [Online]. Available: https://www.unep.org/news-and-stories/press-release/era-leaded-petrol-over-eliminating-major-threat-human-and-planetary

[18] J. Ewing, *Faster, Higher, Farther: The Volkswagen Scandal*. New York: W. W. Norton & Company, 2017, ISBN: 978-0393254501.

[19] Z. Samaras, A. Balazs, A. Kontses, A. Dimaratos, P. Aakko, N. Ligterink, J. Andersson, T. Scarbrough, and L. Ntziachristos, "Online AGVES Meeting: LDV Exhaust," 2021. [Online]. Available: https://circabc.europa.eu/faces/jsp/extension/wai/navigation/container.jsp?FormPrincipal:_idcl=FormPrincipal:_id1&FormPrincipal_SUBMIT=1&id=26f3d67f-7c5d-480a-aa67-a98f84bea785&javax.faces.ViewState=Tx1v0f1FNzoEOsXuYotF5l+zvirDAhWbC+9F9B5OKokobtKDuwqRGpKWA/udXIw7hZtDDkMnxLw09zjgxaddQzY0LvZYsOAawMp0Wp6eO+D1I6rxAk0Li2aaG1PcqiEXk+u5gSqQ0iXCtUPjHH+n3hvODyI=

[20] G. Kalghatgi, *Fuel/Engine Interactions*. SAE International (Warrendale), 2013.

[21] J. B. Heywood, *Internal Combustion Engine Fundamentals*. McGraw-Hill, Singapore, 1988.

[22] N. A. Otto, "US Patent US194047A: improvement in gas-motor engines," 1877.

[23] J. A. Gatowski, E. N. Balles, K. M. Chun, F. E. Nelson, J. A. Ekchian, and J. B. Heywood, "Heat release analysis of engine pressure data," in *1984 SAE International Fall Fuels and Lubricants Meeting and Exhibition*. SAE International, 1984. [Online]. Available: https://doi.org/10.4271/841359

[24] S. H. Mansouri and J. B. Heywood, "Correlations for the viscosity and Prandtl Number of hydrocarbon-air combustion products," *Combustion Science and Technology*, vol. 23, no. 5-6, pp. 251–256, 1980. [Online]. Available: https://doi.org/10.1080/00102208008952416

[25] T. Leroy, J. Chauvin, G. Le Solliec, and G. Corde, "Air path estimation for a turbocharged SI engine with variable valve timing," in *Proceedings of the American Control Conference*, 2007, pp. 5088 – 5093.

[26] F. Leach, G. Kalghatgi, R. Stone, and P. Miles, "The scope for improving the efficiency and environmental impact of internal combustion engines," *Transportation Engineering*, vol. 1, p. 100005, 2020. [Online]. Available: https://www.sciencedirect.com/science/article/pii/S2666691X20300063

[27] R. Miller, "Supercharging and internal cooling cycle for high output," in *Transactions of the American Society of Mechanical Engineers*. ASME, Jul 1947.

[28] L. Sassi, I. Kitsopanidis, and G. Lovett, "Evolutions in F1 engine technology: Pursuing performance from today's power unit through efficiency," Presented at the 37th Engine Symposium, Vienna, 2016.

[29] United Nations Framework Convention on Climate Change, "Report of the Conference of the Parties on its twenty-first session, held in Paris from 30 November to 13 December 2015," 2016, Accessed: 01/11/2021. [Online]. Available: https://unfccc.int/resource/docs/2015/cop21/eng/10a01.pdf

[30] European Environment Agency, "Monitoring of CO2 emissions from passenger cars – Regulation (EU) 2019/631," December 2020. [Online]. Available: https://www.eea.europa.eu/data-and-maps/data/co2-cars-emission-18

[31] European Automobile Manufacturers Association, "ACEA Press Release: Fuel Types of New Cars," November 2020. [Online]. Available: https://www.acea.be/uploads/press_releases_files/20201105_PRPC_fuel_Q3_2020_FINAL.pdf

[32] D. Clerk, "Cylinder Actions In Gas and Gasoline Engines," in *Pre-1964 SAE Technical Papers*. SAE International, Jan 1921, SAE Technical Paper No. 210043. [Online]. Available: https://doi.org/10.4271/210043

[33] H. R. Ricardo, "Recent research work on the internal-combustion engine," in *Pre-1964 SAE Technical Papers*. SAE International, 1922, SAE Technical Paper 220001. [Online]. Available: https://doi.org/10.4271/220001

[34] J. M. Towers and R. L. Hoekstra, "Engine Knock, A Renewed Concern In Motorsports - A Literature Review," Nov 1998, SAE Technical Paper 983026. [Online]. Available: https://doi.org/10.4271/983026

[35] X. Zhen, Y. Wang, S. Xu, Y. Zhu, C. Tao, T. Xu, and M. Song, "The Engine Knock Analysis – An Overview," *Applied Energy*, vol. 92, pp. 628–636, 2012. [Online]. Available: https://www.sciencedirect.com/science/article/pii/S0306261911007859

[36] Z. Wang, H. Liu, and R. D. Reitz, "Knocking Combustion in Spark-Ignition engines," *Progress in Energy and Combustion Science*, vol. 61, pp. 78 – 112, 2017. [Online]. Available: http://www.sciencedirect.com/science/article/pii/S0360128516300764

[37] G. Kalghatgi, "Knock Onset, Knock Intensity, Superknock and Preignition in Spark Ignition Engines," in *International Journal of Engine Research*. SAGE Journals, Oct 2017. [Online]. Available: https://doi.org/10.1177/1468087417736430

[38] E. M. Chapman and V. S. Costanzo, "A Literature Review of Abnormal Ignition by Fuel and Lubricant Derivatives," *SAE International Journal of Engines*, vol. 9, no. 1, pp. 107–142, sep 2015. [Online]. Available: https://doi.org/10.4271/2015-01-1869

[39] C. F. Kettering, "Fuel Research Developments," in *Pre-1964 SAE Technical Papers*. SAE International, Jan 1921, SAE Technical Paper 210012. [Online]. Available: https://doi.org/10.4271/210012

[40] P. Richards, *Automotive Fuels Reference Book, 3rd ed.* Warrendale: SAE International, Mar 2014, ISBN: 978-0-7680-0638-4.

[41] H. L. Horning, "Effect of Compression on Detonation and its Control," in *Pre-1964 SAE Technical Papers*. SAE International, Jan 1923, SAE Technical Paper 230033. [Online]. Available: https://doi.org/10.4271/230033

[42] L. Brooke, *Ford Model T: The Car That Put the World on Wheels*. Minneapolis: Motorbooks, 2008, ISBN: 978-0-7603-2728-9.

[43] H. C. Dickinson, "Resume of Bureau of Standards Fuel Study," in *Pre-1964 SAE Technical Papers*. SAE International, Jan 1921, SAE Technical Paper 210004. [Online]. Available: https://doi.org/10.4271/210004

[44] T. Midgely and T. A. Boyd, "Methods of Measuring Detonation in Engines," in *Pre-1964 SAE Technical Papers*. SAE International, Jan 1922, SAE Technical Paper 220004. [Online]. Available: https://doi.org/10.4271/220004

[45] E. J. Martin and D. F. Caris, "A New Electrical Engine-Indicator," in *Pre-1964 SAE Technical Papers*. SAE International, Jan 1928, SAE Technical Paper 280050. [Online]. Available: https://doi.org/10.4271/280050

[46] A. Trowbridge, "Photographic Recording of Engine Data," in *Pre-1964 SAE Technical Papers*. SAE International, Jan 1922, SAE Technical Paper 220007. [Online]. Available: https://doi.org/10.4271/220007

[47] D. MacKenzie and R. K. Honaman, "The Velocity of Flame Propagation in Engine Cylinders," in *Pre-1964 SAE Technical Papers*. SAE International, Jan 1920, SAE Technical Paper 200010. [Online]. Available: https://doi.org/10.4271/200010

[48] G. L. Clark and A. L. Henne, "Ultraviolet Spectroscopy of Engine-Fuel Flames," in *Pre-1964 SAE Technical Papers*. SAE International, Jan 1927, SAE Technical Paper 270002. [Online]. Available: https://doi.org/10.4271/270002

[49] H. K. Cummings, "Methods of Measuring the Antiknock Value of Fuels," in *Pre-1964 SAE Technical Papers*. SAE International, Jan 1927, SAE Technical Paper 270003. [Online]. Available: https://doi.org/10.4271/270003

[50] T. Midgely and R. Janeway, "Laws Governing Gaseous Detonation," in *Pre-1964 SAE Technical Papers*. SAE International, Jan 1923. [Online]. Available: https://doi.org/10.4271/230004

[51] B. Bryson, *A Short History of Nearly Everything*. London: Transworld, 2003, ISBN: 0-552-99704-8.

[52] D. Rosner and G. Markowitz, "A 'gift of God'?: The public health controversy over leaded gasoline during the 1920s," *American Journal of Public Health*, vol. 75, no. 4, pp. 344–352, May 1985. [Online]. Available: https://doi.org/10.2105/ajph.75.4.344

[53] R. Sayers and A. Fieldner, "Exhaust Gases from Engines Using Ethyl Gasoline," U.S. Bureau of Mines, Tech. Rep., Feb 1925.

[54] E. Graham, "Detonation Specifications for Automotive Fuels," in *Pre-1964 SAE Technical Papers*. SAE International, Jan 1927, SAE Technical Paper 270006. [Online]. Available: https://doi.org/10.4271/270006

[55] R. N. Janeway, "Combustion Control by Cylinder-Head Design," in *Pre-1964 SAE Technical Papers*. SAE International, Jan 1929, SAE Technical Paper 290016. [Online]. Available: https://doi.org/10.4271/290016

[56] C. H. Barton, C. H. Sprake, and R. Stansfield D, "Comparison of Antiknock Ratings Determined in Different Laboratories," in *Pre-1964 SAE Technical Papers*. SAE International, Jan 1930, SAE Technical Paper 300019. [Online]. Available: https://doi.org/10.4271/300019

[57] J. M. Campbell, W. G. Lovell, and T. A. Boyd, "Detonation Characteristics of Some of the Fuels Suggested as Standards of Antiknock Quality," in *Pre-1964 SAE Technical Papers*. SAE International, Jan 1930, SAE Technical Paper 300018. [Online]. Available: https://doi.org/10.4271/300018

[58] C. H. Barton, C. H. Sprake, R. Stansfield, and O. Thornycroft, "Knock Rating of Motor Fuels," in *Pre-1964 SAE Technical Papers*. SAE International, Jan 1931, SAE Technical Paper 310021. [Online]. Available: https://doi.org/10.4271/310021

[59] C. S. Kegerreis, "Carbureter Design for the C. F. R. Detonation Engine," in *Pre-1964 SAE Technical Papers*. SAE International, Jan 1931, SAE Technical Paper 310020. [Online]. Available: https://doi.org/10.4271/310020

[60] E. Graham, "Jacket and Cylinder-Head Temperature Effects upon Relative Knock-Ratings," in *Pre-1964 SAE Technical Papers*. SAE International, Jan 1931, SAE Technical Paper 310023. [Online]. Available: https://doi.org/10.4271/310023

[61] J. M. Campbell, W. G. Lovell, and T. A. Boyd, "Influence of Carbureter Setting and Spark Timing on Knock Ratings - Annual Meeting Paper," in *Pre-1964 SAE Technical Papers*. SAE International, Jan 1931, SAE Technical Paper 310025. [Online]. Available: https://doi.org/10.4271/310025

[62] H. F. Huf, J. R. Sabina, and J. B. Hill, "Effect of Sound Intensity on Knock Ratings," in *Pre-1964 SAE Technical Papers*. SAE International, Jan 1931, SAE Technical Paper 310026. [Online]. Available: https://doi.org/10.4271/310026

[63] Cooperative Fuel Research Committee, "CFR Research Method of Tests for Knock Characteristics of Motor Fuels," *SAE Transactions*, vol. 34, pp. 277–280, 1939. [Online]. Available: http://www.jstor.org/stable/44467952

[64] ASTM International, "Standard Test Method for Research Octane Number of Spark-Ignition Engine Fuel," *ASTM Standard 2699-19e1*, Revised July 2019. [Online]. Available: www.astm.org

[65] C. B. Veal, H. W. Best, J. M. Campbell, and W. M. Holaday, "Antiknock Research Coordinates Laboratory and Road Tests," in *Pre-1964 SAE Technical Papers*. SAE International, Jan 1933, SAE Technical Paper 330015. [Online]. Available: https://doi.org/10.4271/330015

[66] ASTM International, "Standard Test Method for Motor Octane Number of Spark-Ignition Engine Fuel," *ASTM Standard D2700-19e1*, Revised July 2019. [Online]. Available: www.astm.org

[67] C. B. Veal, "C. F. R. Committee Report on 1934 Detonation Road Tests," in *Pre-1964 SAE Technical Papers*. SAE International, Jan 1935, SAE Technical Paper 350094. [Online]. Available: https://doi.org/10.4271/350094

[68] T. A. Boyd, "1937 Road Knock Tests," in *Pre-1964 SAE Technical Papers*. SAE International, Jan 1938, SAE Technical Paper 380145. [Online]. Available: https://doi.org/10.4271/380145

[69] J. M. Campbell and W. G. Lovell, "Application of Statistical Concepts to the Knock-Rating Problem," in *Pre-1964 SAE Technical Papers*. SAE International, Jan 1938, SAE Technical Paper 380169. [Online]. Available: https://doi.org/10.4271/380169

[70] E. Beale and R. Stansfield, "The Sunbury Knock Indicator," in *Pre-1964 SAE Technical Papers*. SAE International, Jan 1937, SAE Technical Paper 370118. [Online]. Available: https://doi.org/10.4271/370118

[71] D. B. Brooks and R. B. Cleaton, "The Precision of Knock Rating - 1936-1938 - Report from Cooperative Fuel Research Committee," in *Pre-1964 SAE Technical Papers*. SAE International, Jan 1939, SAE Technical Paper 390176. [Online]. Available: https://doi.org/10.4271/390176

[72] C. F. Marvin, "Observations of Flame in an Engine," in *Pre-1964 SAE Technical Papers*. SAE International, Jan 1934, SAE Technical Paper 340112. [Online]. Available: https://doi.org/10.4271/340112

[73] G. M. Rassweiler and L. Withrow, "Flame Temperatures Vary with Knock and Combustion-Chamber Position," in *Pre-1964 SAE Technical Papers*. SAE International, Jan 1935, SAE Technical Paper 350091. [Online]. Available: https://doi.org/10.4271/350091

[74] L. Withrow and G. M. Rassweiler, "Slow Motion Shows Knocking and Non-Knocking Explosions," in *Pre-1964 SAE Technical Papers*. SAE International, Jan 1936, SAE Technical Paper 360126. [Online]. Available: https://doi.org/10.4271/360126

[75] G. M. Rassweiler and L. Withrow, "Motion Pictures of Engine Flames Correlated with Pressure Cards," in *Pre-1964 SAE Technical Papers*. SAE International, Jan 1938, SAE Technical Paper 380139. [Online]. Available: https://doi.org/10.4271/380139

[76] T. A. Boyd, "Engine Flame Researches," in *Pre-1964 SAE Technical Papers*. SAE International, Jan 1939, SAE Technical Paper 390173. [Online]. Available: https://doi.org/10.4271/390173

[77] N. MacCoull and G. T. Stanton, "The Measurement of Engine Knock by Electro-Acoustic Instruments," in *Pre-1964 SAE Technical Papers*. SAE International, Jan 1936, SAE Technical Paper 360104. [Online]. Available: https://doi.org/10.4271/360104

[78] C. S. Draper, "The Physical Effects of Detonation in a Closed Cylindrical Chamber," National Advisory Committee for Aeronautics, Tech. Rep. NACA-TR-493, Jan 1935. [Online]. Available: https://ntrs.nasa.gov/citations/19930091567

[79] C. Draper, "Pressure Waves Accompanying Detonation in the Internal Combustion Engine," in *Power Plants and Propellers Session, Sixth Annual Meeting, I. Ae. S.* Institute of Aeronautical Sciences, Jan 1938.

[80] A. M. Rothrock and R. C. Spencer, "A Photographic Study of Combustion and Knock in a Spark-Ignition Engine," National Advisory Committee for Aeronautics, Tech. Rep. NACA-TR-622, Jan 1938. [Online]. Available: https://ntrs.nasa.gov/citations/19930091697

[81] S. D. Heron, "Fuel Requirements of the Gasoline Aircraft-Engine," in *Pre-1964 SAE Technical Papers*. SAE International, Jan 1930, SAE Technical Paper 300024. [Online]. Available: https://doi.org/10.4271/300024

[82] R. Du Bois and V. Cronstedt, "High Output in Aircraft Engines," in *Pre-1964 SAE Technical Papers*. SAE International, Jan 1937, SAE Technical Paper 370150. [Online]. Available: https://doi.org/10.4271/370150

[83] A. Nutt, "Detonation Rating of Aviation Fuels," in *Pre-1964 SAE Technical Papers*. SAE International, Jan 1933, SAE Technical Paper 330054. [Online]. Available: https://doi.org/10.4271/330054

[84] C. B. Veal, "Rating Aviation Fuels-in Full-Scale Aircraft Engines - A report of the Cooperative Fuel Research Committee," in *Pre-1964 SAE Technical Papers*. SAE International, Jan 1936, SAE Technical Paper 360112. [Online]. Available: https://doi.org/10.4271/360112

[85] H. K. Cummings, "Rating Aviation Fuels in Full-Scale Aircraft Engines - Completion of First Program and Progress on Second Program-Report of the Cooperative Fuel Research Committee," in *Pre-1964 SAE Technical Papers*. SAE International, Jan 1938, SAE Technical Paper 380177. [Online]. Available: https://doi.org/10.4271/380177

[86] R. Stansfield and H. B. Taylor, "A New Laboratory Method for Rating Aviation Fuels of High Octane Number," in *Pre-1964 SAE Technical Papers*. SAE International, Jan 1939, SAE Technical Paper 390018. [Online]. Available: https://doi.org/10.4271/390018

[87] ASTM International, "Standard Test Method for Supercharge Rating of Spark-Ignition Aviation Gasoline," *ASTM Standard D909-18e1*, Revised July 2018. [Online]. Available: www.astm.org

[88] T. Dillstrom, "A High-Power Spark-Ignition Fuel-Injection Engine," in *Pre-1964 SAE Technical Papers*. SAE International, Jan 1934, SAE Technical Paper 340117. [Online]. Available: https://doi.org/10.4271/340117

[89] H. C. Tsien, "Basic problems in the design of high-output aircraft engines," in *Pre-1964 SAE Technical Papers*. SAE International, Jan 1938, SAE Technical Paper 380111. [Online]. Available: https://doi.org/10.4271/380111

[90] C. E. Douglas, *The Secret Horsepower Race - Western Front Fighter Engine Development*. Horncastle: Tempest Books, 2020, ISBN: 978-1911658504.

[91] T. H. Risk, "Factors Affecting the Antiknock Performance of Post-War Fuels," in *Pre-1964 SAE Technical Papers*. SAE International, Jan 1944, SAE Technical Paper 440169. [Online]. Available: https://doi.org/10.4271/440169

[92] D. P. Barnard and R. B. Cragin, "Volatility Decreases and Availability of High Knock Rating Aviation Fuels," in *Pre-1964 SAE Technical Papers*. SAE International, Jan 1940, SAE Technical Paper 400120. [Online]. Available: https://doi.org/10.4271/400120

[93] E. W. Hives and F. L. Smith, "High-Output Aircraft Engines," in *Pre-1964 SAE Technical Papers*. SAE International, Jan 1940, SAE Technical Paper 400133. [Online]. Available: https://doi.org/10.4271/400133

[94] W. H. Hubner, "Better Fuels for Better Engines . . . ," in *Pre-1964 SAE Technical Papers*. SAE International, Jan 1940, SAE Technical Paper 400165. [Online]. Available: https://doi.org/10.4271/400165

[95] J. M. Campbell, R. J. Greenshields, and W. M. Holaday, "1940 Road Detonation Tests - (Compiled from Report 1 of The Cooperative Fuel Research Committee)," in *Pre-1964 SAE Technical Papers*. SAE International, Jan 1941, SAE Technical Paper 410107. [Online]. Available: https://doi.org/10.4271/410107

[96] A. M. Rothrock, "Fuel rating - its relation to engine performance," in *Pre-1964 SAE Technical Papers*. SAE International, Jan 1941, SAE Technical Paper 410088. [Online]. Available: https://doi.org/10.4271/410088

[97] D. B. Brooks, "Development of reference fuel scales for knock rating - report of coordinating fuel research committee of coordinating research council, inc." in *Pre-1964 SAE Technical Papers*. SAE International, Jan 1946, SAE Technical Paper 460230. [Online]. Available: https://doi.org/10.4271/460230

[98] S. D. Heron, "Mutual adaptation of aircraft fuels and engines," in *Pre-1964 SAE Technical Papers*. SAE International, Jan 1947, SAE Technical Paper 470214. [Online]. Available: https://doi.org/10.4271/470214

[99] E. J. Gay and H. T. Mueller, "Fuel antiknock quality - a basis for selection of compression ratio," in *Pre-1964 SAE Technical Papers*. SAE International, Jan 1947, SAE Technical Paper 470238. [Online]. Available: https://doi.org/10.4271/470238

[100] E. A. Droegemueller, D. S. Hersey, and W. A. Kuhrt, "The relation cooling of intake-charge to engine performance," in *Pre-1964 SAE Technical Papers*. SAE International, jan 1944. [Online]. Available: https://doi.org/10.4271/440214

[101] M. R. Rowe and G. T. Ladd, "Water injection for aircraft engines," in *Pre-1964 SAE Technical Papers*. SAE International, Jan 1946, SAE Technical Paper 460192. [Online]. Available: https://doi.org/10.4271/460192

[102] E. F. Obert, "Detonation and Internal Coolants," in *Pre-1964 SAE Technical Papers*. SAE International, Jan 1948, SAE Technical Paper 480173. [Online]. Available: https://doi.org/10.4271/480173

[103] J. W. Streett, "The Detection of Detonation and Other Operating Abnormalities in Aircraft Engines by Means of Special Instrumentation," in *Pre-1964 SAE Technical Papers*. SAE International, Jan 1945, SAE Technical Paper 450012. [Online]. Available: https://doi.org/10.4271/450012

[104] P. J. Costa, "Detonation in Flight - Its Effect on Fuel Consumption and Engine Life," in *Pre-1964 SAE Technical Papers*. SAE International, Jan 1945, SAE Technical Paper 450191. [Online]. Available: https://doi.org/10.4271/450191

[105] J. S. Bogen and W. J. Faust, "Aircraft Detonation Indicators," in *Pre-1964 SAE Technical Papers*. SAE International, Jan 1947, SAE Technical Paper 470233. [Online]. Available: https://doi.org/10.4271/470233

[106] J. H. Goffe and J. W. Wheeler, "Development of Detonation Instrumentation for Automotive Vehicles," in *Pre-1964 SAE Technical Papers*. SAE International, Jan 1947, SAE Technical Paper 470245. [Online]. Available: https://doi.org/10.4271/470245

[107] E. F. Fiock, "The Present Status of Combustion Research," in *Pre-1964 SAE Technical Papers*. SAE International, Jan 1941, SAE Technical Paper 410122. [Online]. Available: https://doi.org/10.4271/410122

[108] A. M. Rothrock and R. C. Spencer, "A High-Speed Motion-Picture Study of Normal Combustion, Knock and Preignition in a Spark-Ignition Engine," National Advisory Committee for Aeronautics, Tech. Rep. NACA-TR-704, Jan 1941. [Online]. Available: https://ntrs.nasa.gov/citations/19930091782

[109] C. D. Miller and H. L. Olsen, "Identification of knock in NACA high-speed photographs of combustion in a spark-ignition engine," National Advisory Committee for Aeronautics, Tech. Rep. NACA-TR-761, Jan 1943. [Online]. Available: https://ntrs.nasa.gov/citations/19930091840

[110] C. D. Miller, H. L. Olsen, J. Logan, Walter O, and G. E. Osterstrom, "Analysis of Spark-Ignition Engine Knock as Seen in Photographs Taken at 200,000 Frames Per Second," National Advisory Committee for Aeronautics, Tech. Rep. NACA-TR-857, Jan 1946. [Online]. Available: https://ntrs.nasa.gov/citations/19930091929

[111] H. L. Olsen and C. D. Miller, "The Interdependence of Various Types of Autoignition and Knock," National Advisory Committee for Aeronautics, Tech. Rep. NACA-TR-912, Jan 1948. [Online]. Available: https://ntrs.nasa.gov/citations/19930091978

[112] W. G. Lovell, "Engine Knock and Molecular Structure of Hydrocarbons," in *Pre-1964 SAE Technical Papers*. SAE International, Jan 1948, SAE Technical Paper 480219. [Online]. Available: https://doi.org/10.4271/480219

[113] C. F. Kettering, "Fuels and Engines for Higher Power and Greater Efficiency," in *Pre-1964 SAE Technical Papers*. SAE International, Jan 1945, SAE Technical Paper 450195. [Online]. Available: https://doi.org/10.4271/450195

[114] E. R. Retailliau, H. A. Ricards, and M. C. Jones, "Precombustion Reaction in the Spark-Ignition Engine," in *Pre-1964 SAE Technical Papers*. SAE International, Jan 1950, SAE Technical Paper 500191. [Online]. Available: https://doi.org/10.4271/500191

[115] D. Pastell, "Precombustion Reactions in a Motored Engine," in *Pre-1964 SAE Technical Papers*. SAE International, Jan 1950, SAE Technical Paper 500198. [Online]. Available: https://doi.org/10.4271/500198

[116] W. Cornelius and J. D. Caplan, "Some Effects of Fuel Structure, Tetraethyl Lead, and Engine Deposits On Precombustion Reactions in a Firing Engine," in *Pre-1964 SAE Technical Papers*. SAE International, Jan 1952, SAE Technical Paper 520250. [Online]. Available: https://doi.org/10.4271/520250

[117] R. Dauphin, J. Obiols, D. Serrano, Y. Fenard, A. Comandini, L. Starck, G. Vanhove, and N. Chaumeix, "Using RON Synergistic Effects to Formulate Fuels for Better Fuel Economy and Lower CO2 Emissions," in *2019 JSAE/SAE Powertrains, Fuels and Lubricants*. SAE International, Dec 2019, SAE Technical Paper 2019-01-2155. [Online]. Available: https://doi.org/10.4271/2019-01-2155

[118] W. J. Levedahl and H. P. Broida, "Emission Spectra on Autoignited Heptane-Air Mixtures," *Analytical Chemistry*, vol. 24, no. 11, pp. 1776–1780, 1952. [Online]. Available: https://doi.org/10.1021/ac60071a019

[119] J. Mason and H. Hesselberg, "Engine Knock as Influenced by Precombustion Reactions," in *Pre-1964 SAE Technical Papers*. SAE International, Jan 1954, SAE Technical Paper 540229. [Online]. Available: https://doi.org/10.4271/540229

[120] B. M. Sturgis, "Some Concepts of Knock and Antiknock Action," in *Pre-1964 SAE Technical Papers*. SAE International, Jan 1955, SAE Technical Paper 550249. [Online]. Available: https://doi.org/10.4271/550249

[121] N. Semenov, "Advances of Chemical Kinetics in the Soviet Union," *Nature*, vol. 151, no. 3824, pp. 185–187, 1943. [Online]. Available: https://doi.org/10.1038/151185a0

[122] C. F. Taylor, E. S. Taylor, J. C. Livengood, W. A. Russell, and W. A. Leary, "Ignition of Fuels by Rapid Compression," in *Pre-1964 SAE Technical Papers*. SAE International, Jan 1950, SAE Technical Paper 500178. [Online]. Available: https://doi.org/10.4271/500178

[123] J. Livengood and P. Wu, "Correlation of Autoignition Phenomena in Internal Combustion Engines and Rapid Compression Machines," *Symposium (International) on Combustion*, vol. 5, no. 1, pp. 347 – 356, 1955. [Online]. Available: http://www.sciencedirect.com/science/article/pii/S0082078455800471

[124] E. B. Rifkin and C. Walcutt, "A Basis for Understanding Antiknock Action," in *Pre-1964 SAE Technical Papers*. SAE International, Jan 1957, SAE Technical Paper 570046. [Online]. Available: https://doi.org/10.4271/570046

[125] D. Diggs, "Effect of Combustion Time on Knock in a Spark-Ignition Engine," in *Pre-1964 SAE Technical Papers*. SAE International, Jan 1953, SAE Technical Paper 530242. [Online]. Available: https://doi.org/10.4271/530242

[126] R. Meagher, R. L. Johnson, and K. G. Parthemore, "Correlation of Engine Noises With Combustion Phenomena," in *Pre-1964 SAE Technical Papers*. SAE International, Jan 1955, SAE Technical Paper 550269. [Online]. Available: https://doi.org/10.4271/550269

[127] R. H. Perry and H. V. Lowther, "knock-knock: Spark Knock, Wild Ping, or Rumble?" in *Pre-1964 SAE Technical Papers*. SAE International, Jan 1959, SAE Technical Paper 590019. [Online]. Available: https://doi.org/10.4271/590019

[128] H. F. Hosteller and W. R. Tuuri, "Knock, Rumble, and Ping," in *Pre-1964 SAE Technical Papers*. SAE International, Jan 1959, SAE Technical Paper 590020. [Online]. Available: https://doi.org/10.4271/590020

[129] W. M. Wiese, "If you Squeeze them, must they Scream?" in *Pre-1964 SAE Technical Papers*. SAE International, Jan 1959, SAE Technical Paper 590023. [Online]. Available: https://doi.org/10.4271/590023

[130] J. A. Warren and J. B. Hinkamp, "New Instrumentation for Engine Combustion Studies," in *Pre-1964 SAE Technical Papers*. SAE International, Jan 1956, SAE Technical Paper 560059. [Online]. Available: https://doi.org/10.4271/560059

[131] H. Ricardo, "Some Early Reminiscences," in *Pre-1964 SAE Technical Papers*. SAE International, Jan 1955, SAE Technical Paper 550282. [Online]. Available: https://doi.org/10.4271/550282

[132] A. W. Pope, "Single-Cylinder Engine Fuel Research," in *Pre-1964 SAE Technical Papers*. SAE International, Jan 1959, SAE Technical Paper 590034. [Online]. Available: https://doi.org/10.4271/590034

[133] F. D. Buerstetta, I. A. Caputo, E. S. Corner, T. M. Korn, and E. C. Younghouse, "Are Octane Numbers and Hydrocarbon Type Enough?" in *Pre-1964 SAE Technical Papers*. SAE International, Jan 1960, SAE Technical Paper 600140. [Online]. Available: https://doi.org/10.4271/600140

[134] E. Bartholomew, "New Knock-Testing Methods needed to Match Engine and Fuel Progress," in *Pre-1964 SAE Technical Papers*. SAE International, Jan 1961, SAE Technical Paper 610200. [Online]. Available: https://doi.org/10.4271/610200

[135] B. Brewster and R. V. Kerley, "Automotive Fuels and Combustion Problems," in *Pre-1964 SAE Technical Papers*. SAE International, Jan 1963, SAE Technical Paper 630416. [Online]. Available: https://doi.org/10.4271/630416

[136] P. L. Gerard and C. J. DiPerna, "Multifaceted Octane Numbers for Diverse Engine Requirements," in *1965 International Automotive Engineering Congress and Exposition*. SAE International, Feb 1965, SAE Technical Paper 650094. [Online]. Available: https://doi.org/10.4271/650094

[137] F. B. Fitch and R. H. Thena, "Fuel Requirements of Passenger Cars Throughout the World," in *1969 International Automotive Engineering Congress and Exposition*. SAE International, Feb 1969, SAE Technical Paper 690210. [Online]. Available: https://doi.org/10.4271/690210

[138] M. Gluckstein and C. Walcutt, "End-Gas Temperature-Pressure Histories and Their Relation To Knock," in *Pre-1964 SAE Technical Papers*. SAE International, Jan 1961, SAE Technical Paper 610044. [Online]. Available: https://doi.org/10.4271/610044

[139] J. H. Johnson, P. S. Myers, and O. A. Uyehara, "End-Gas Temperatures, Pressures, Reaction Rates, and Knock," in *Mid-Year Meeting*. SAE International, Feb 1965, SAE Technical Paper 650505. [Online]. Available: https://doi.org/10.4271/650505

[140] R. A. Hoffman, "A New Technique for Determining the Knocking Resistance of Fuels," in *Pre-1964 SAE Technical Papers*. SAE International, Jan 1961, SAE Technical Paper 610202. [Online]. Available: https://doi.org/10.4271/610202

[141] C. F. Taylor, "The Effects of Cylinder Size On Detonation and Octane Requirement," in *Pre-1964 SAE Technical Papers*. SAE International, Jan 1962, SAE Technical Paper 620522. [Online]. Available: https://doi.org/10.4271/620522

[142] S. Curry, "The Relationship Between Flame Propagation and Pressure Development During Knocking Combustion," in *Pre-1964 SAE Technical Papers*. SAE International, Jan 1963, SAE Technical Paper 630095. [Online]. Available: https://doi.org/10.4271/630095

[143] W. W. Haskell and J. L. Bame, "Engine Knock -An End-Gas Explosion," in *Mid-Year Meeting*. SAE International, Feb 1965, SAE Technical Paper 650506. [Online]. Available: https://doi.org/10.4271/650506

[144] L. B. Graiff, "The Mode of Action of Tetraethyllead and Supplemental Antiknock Agents," in *National Fuels and Lubricants and Transportation Meetings*. SAE International, Feb 1966, SAE Technical Paper 660780. [Online]. Available: https://doi.org/10.4271/660780

[145] US Government, "The Clean Air Act - An Act to improve, strengthen, and accelerate programs for the prevention and abatement of air pollution ," *Public Law*, vol. 88, no. 206, pp. 392–401, December 1963.

[146] W. G. Burwell and D. R. Olson, "The Spontaneous Ignition of Isooctane Air Mixtures under Steady Flow Conditions," in *Mid-Year Meeting*. SAE International, Feb 1965, SAE Technical Paper 650510. [Online]. Available: https://doi.org/10.4271/650510

[147] W. Jost and A. Martinengo, "Recent Investigations of Reaction Processes by Means of Adiabatic Compression," in *Mid-Year Meeting*. SAE International, Feb 1966, SAE Technical Paper 660347. [Online]. Available: https://doi.org/10.4271/660347

[148] A. A. Quader, P. S. Myers, and O. A. Uyehara, "UV Absorbance Histories and Knock in a Spark Ignited Engine," in *Mid-Year Meeting*. SAE International, Feb 1969, SAE Technical Paper 690519. [Online]. Available: https://doi.org/10.4271/690519

[149] US Government, "Clean Air Ammendments of 1970 - An Act to amend the Clean Air Act to provide a more effective program to improve the quality of the Nation's air ," *Public Law*, vol. 91, no. 604, pp. 1676–1713, December 1970.

[150] Office of Air Programs of the EPA and National Environmental Research Center, "Health hazards of lead," Environmental Protection Agency, Tech. Rep. 400R72001, April 1972.

[151] EPA Office of Air Quality Planning and Standards, "National Ambient Air Quality Standard for Lead," Environmental Protection Agency, Tech. Rep. EPA 600177502, December 1977.

[152] C. R. Angle and M. S. McIntire, "Lead: Environmental Sources and Red Cell Toxicity in Urban Children," Environmental Protection Agency, Tech. Rep. EPA-650/1-75-003, Jun 1975.

[153] E. L. Dage, "The Health and Environmental Impacts of Lead and an Assessment of a Need for Limitations," Environmental Protection Agency, Tech. Rep. EPA-560/2-79-001, Apr 1979.

[154] E. M. Shelton, M. L. Whisman, and P. W. Woodward, "Trends in Motor Gasolines: 1942-1981," United States of America Department of Energy, Tech. Rep. DOE/BETC/RI-82/4, Jun 1982.

[155] EPA Technology Assessment and Evaluation Branch, "Octane Requirements of 1975 Model Year Automobiles Fueled with Unleaded Gasoline," Environmental Protection Agency, Tech. Rep. EPA-AA-TAEB 75-28, Aug 1975.

[156] L. C. Duke, S. S. Lestz, and W. E. Meyer, "The Relation Between Knock and Exhaust Emissions of a Spark Ignition Engine," in *1970 Automotive Engineering Congress and Exposition*. SAE International, Feb 1970, SAE Technical Paper 700062. [Online]. Available: https://doi.org/10.4271/700062

[157] J. L. Hodges, "The Effect of Exhaust Recycle on Knock-Limited SI Engine Performance," in *1975 Automotive Engineering Congress and Exposition*. SAE International, Feb 1975, SAE Technical Paper 750025. [Online]. Available: https://doi.org/10.4271/750025

[158] C. R. Morgan and S. S. Hetrick, "The Effects of Engine Variables and Exhaust Gas Recirculation on Emissions, Fuel Economy, and Knock-Part II," in *1976 Automotive Engineering Congress and Exposition*. SAE International, Feb 1976, SAE Technical Paper 760198. [Online]. Available: https://doi.org/10.4271/760198

[159] J. A. Gething and S. S. Lestz, "Knocking and Performance Characteristics of Low Octane Primary Reference Fuels Blended with Methanol," in *1978 Automotive Engineering Congress and Exposition*. SAE International, Feb 1978, SAE Technical Paper 780079. [Online]. Available: https://doi.org/10.4271/780079

[160] W. Roessler and A. Muraszew, "Evaluation of Prechamber Spark Ignition Engine Concepts," Environmental Protection Agency, Tech. Rep. EPA-650/2-75-023, Feb 1975.

[161] T. Date, S. Yagi, A. Ishizuya, and I. Fujii, "Research and development of the Honda CVCC engine," in *National West Coast Meeting*. SAE International, 1974. [Online]. Available: https://doi.org/10.4271/740605

[162] N. C. Blizard and J. C. Keck, "Experimental and Theoretical Investigation of Turbulent Burning Model for Internal Combustion Engines," in *1974 Automotive Engineering Congress and Exposition*. SAE International, Feb 1974, SAE Technical Paper 740191. [Online]. Available: https://doi.org/10.4271/740191

[163] D. R. Lancaster, "Effects of Engine Variables on Turbulence in a Spark-Ignition Engine," in *1976 Automotive Engineering Congress and Exposition*. SAE International, Feb 1976, SAE Technical Paper 760159. [Online]. Available: https://doi.org/10.4271/760159

[164] D. R. Lancaster, R. B. Krieger, S. C. Sorenson, and W. L. Hull, "Effects of Turbulence on Spark-Ignition Engine Combustion," in *1976 Automotive Engineering Congress and Exposition*. SAE International, Feb 1976, SAE Technical Paper 760160. [Online]. Available: https://doi.org/10.4271/760160

[165] I. Nagayama, Y. Araki, and Y. Iioka, "Effects of Swirl and Squish on S.I. Engine Combustion and Emission," in *SAE Technical Paper*. SAE International, 02 1977, SAE Technical Paper 770217. [Online]. Available: https://doi.org/10.4271/770217

[166] H. I. S. Allwood, G. A. Harrow, and L. J. Rose, "A Multichannel Electronic Gating and Counting System for the Study of Cyclic Dispersion, Knock and Weak Mixture Combustion in Spark Ignition Engines," in *1970 Automotive Engineering Congress and Exposition*. SAE International, Feb 1970, SAE Technical Paper 700063. [Online]. Available: https://doi.org/10.4271/700063

[167] R. K. Barton, S. S. Lestz, and L. C. Duke, "Knock Intensity as a Function of Engine Rate of Pressure Change," in *1970 Automotive Engineering Congress and Exposition*. SAE International, Feb 1970, SAE Technical Paper 700061. [Online]. Available: https://doi.org/10.4271/700061

[168] P. Chiampo, F. de Cristofaro, and R. Gozzelino, "Relationship of Flame Front Pattern to Pressure and High-Speed Knock on Commercial Engines," in *1973 International Automotive Engineering Congress and Exposition*. SAE International, Feb 1973, SAE Technical Paper 730087. [Online]. Available: https://doi.org/10.4271/730087

[169] C. V. Ferraro, "A knock intensity meter based on kinetic criterion," in *1978 Automotive Engineering Congress and Exposition*. SAE International, Feb 1978, SAE Technical Paper 780154. [Online]. Available: https://doi.org/10.4271/780154

[170] V. Arrigoni, G. M. Cornetti, G. Spallanzani, F. Calvi, and A. Tontodonati, "High Speed Knock in S.I. Engines," in *International Automobile Engineering and Manufacturing Meeting*. SAE International, Feb 1974, SAE Technical Paper 741056. [Online]. Available: https://doi.org/10.4271/741056

[171] G. M. Cornetti, F. De Cristofaro, and R. Gozzelino, "Engine Failure and High Speed Knock," in *1977 International Automotive Engineering Congress and Exposition*. SAE International, Feb 1977, SAE Technical Paper 770147. [Online]. Available: https://doi.org/10.4271/770147

[172] V. Arrigoni, G. F. Calvi, B. Gaetani, F. Giavazzi, and G. F. Zanoni, "Recent Advances in the Detection of Knock in S.I. Engines," in *1978 Automotive Engineering Congress and Exposition*. SAE International, Feb 1978, SAE Technical Paper 780153. [Online]. Available: https://doi.org/10.4271/780153

[173] K. W. Randall and J. D. Powell, "A Cylinder Pressure Sensor for Spark Advance Control and Knock Detection," in *1979 Automotive Engineering Congress and Exposition*. SAE International, Feb 1979, SAE Technical Paper 790139. [Online]. Available: https://doi.org/10.4271/790139

[174] M. Kondo, A. Niimi, and T. Nakamura, "Indiscope-A New Combustion Pressure Indicator with Washer Transducers," in *SAE Automobile Engineering and Manufacturing Meeting*. SAE International, Feb 1975, SAE Technical Paper 750883. [Online]. Available: https://doi.org/10.4271/750883

[175] B. Kraus, P. E. Godici, and W. King, "Reduction of Octane Requirement by Knock Sensor Spark Retard System," in *1978 Automotive Engineering Congress and Exposition*. SAE International, Feb 1978, SAE Technical Paper 780155. [Online]. Available: https://doi.org/10.4271/780155

[176] T. F. Wallace, "Buick's Turbocharged V-6 Powertrain For 1978," in *1978 Automotive Engineering Congress and Exposition*. SAE International, Feb 1978, SAE Technical Paper 780413. [Online]. Available: https://doi.org/10.4271/780413

[177] A. M. Douaud and P. Eyzat, "Four-Octane-Number Method for Predicting the Anti-Knock Behavior of Fuels and Engines," in *1978 Automotive Engineering Congress and Exposition*. SAE International, Feb 1978, SAE Technical Paper 780080. [Online]. Available: https://doi.org/10.4271/780080

[178] M. P. Halstead, L. J. Kirsch, A. Prothero, and C. P. Quinn, "A mathematical model for hydrocarbon autoignition at high pressures," *Proceedings of the Royal Society A*, 1975. [Online]. Available: https://doi.org/10.1098/rspa.1975.0189

[179] L. Kirsch and C. Quinn, "A Fundamentally based Model of Knock in the Gasoline Engine," *Symposium (International) on Combustion*, vol. 16, no. 1, pp. 233 – 244, 1977. [Online]. Available: http://www.sciencedirect.com/science/article/pii/S0082078477803287

[180] Y. Boccadoro and T. Kizer, "Adaptive Spark Control with Knock Detection," in *SAE International Congress and Exposition*. SAE International, Feb 1984, SAE Technical Paper 840447. [Online]. Available: https://doi.org/10.4271/840447

[181] H. Decker and H.-U. Gruber, "Knock Control of Gasoline Engines - A Comparison of Solutions and Tendencies, with Special Reference to Future European Emission Legislation," in *SAE International Congress and Exposition*. SAE International, Feb 1985, SAE Technical Paper 850298. [Online]. Available: https://doi.org/10.4271/850298

[182] P. Gillbrand, "Knock Detector System Controlling Turbocharger Boost Pressure," in *Passenger Car Meeting and Exposition*. SAE International, Jun 1980, SAE Technical Paper 800833. [Online]. Available: https://doi.org/10.4271/800833

[183] N. Nakamura, E. Ohno, M. Kanamaru, and T. Funayama, "Detection of Higher Frequency Vibration to improve Knock Controllability," in *Passenger Car Meeting and Exposition*. SAE International, Oct 1987, SAE Technical Paper 871912. [Online]. Available: https://doi.org/10.4271/871912

[184] T. Priede and R. K. Dutkiewicz, "The Effect of Normal Combustion and Knock on Gasoline Engine Noise," in *SAE Noise and Vibration Conference and Exposition*. SAE International, May 1989, SAE Technical Paper 891126. [Online]. Available: https://doi.org/10.4271/891126

[185] N. Collings, S. Dinsdale, and D. Eade, "Knock Detection by Means of the Spark Plug," in *SAE International Congress and Exposition*. SAE International, Mar 1986, SAE Technical Paper 860635. [Online]. Available: https://doi.org/10.4271/860635

[186] K. Sawamoto, Y. Kawamura, T. Kita, and K. Matsushita, "Individual Cylinder Knock Control by Detecting Cylinder Pressure," in *Passenger Car Meeting and Exposition*. SAE International, Oct 1987, SAE Technical Paper 871911. [Online]. Available: https://doi.org/10.4271/871911

[187] C. A. Amann, "Classical Combustion Diagnostics for Engine Research," in *SAE International Congress and Exposition*. SAE International, Feb 1985, SAE Technical Paper 850395. [Online]. Available: https://doi.org/10.4271/850395

[188] C. Amann, "Cylinder-Pressure measurement and Its Use in Engine Research," in *1985 SAE International Fall Fuels and Lubricants Meeting and Exhibition*. SAE International, Oct 1985, SAE Technical Paper 852067. [Online]. Available: https://doi.org/10.4271/852067

[189] M. J. McNally, J. D. Benson, J. C. Callison, J. P. Graham, T. Wusz, and B. Evans, "Coordinating Research Council Quantifying Performance of Knock-Sensor Equipped Vehicles with Varying Octane Level Fuels," in *1989 SAE International Fall Fuels and Lubricants Meeting and Exhibition*. SAE International, Sep 1989, SAE Technical Paper 892037. [Online]. Available: https://doi.org/10.4271/892037

[190] D. L. Sutton and D. Williams, "Knock protection—future fuels and engines," in *International Conference on Fuel Efficient Power Trains and Vehicles*. SAE International, Sep 1984, SAE Technical Paper 841289. [Online]. Available: https://doi.org/10.4271/841289

[191] A. By, B. Kempinski, and J. M. Rife, "Knock in Spark Ignition Engines," in *SAE International Congress and Exposition*. SAE International, Feb 1981, SAE Technical Paper 810147. [Online]. Available: https://doi.org/10.4271/810147

[192] W. R. Leppard, "Individual-Cylinder Knock Occurence and Intensity in Multicylinder Engines," in *SAE International Congress and Exposition*. SAE International, Feb 1982, SAE Technical Paper 820074. [Online]. Available: https://doi.org/10.4271/820074

[193] K. M. Chun and J. B. Heywood, "Characterization of Knock in a Spark-Ignition Engine," in *SAE International Congress and Exposition*. SAE International, Feb 1989, SAE Technical Paper 890156. [Online]. Available: https://doi.org/10.4271/890156

[194] T. Iwata, K. Sakakibara, and H. Haragucti, "A New Method to Automatically Optimize the Knock Detection Level in the Knock Control System," in *Passenger Car Meeting and Exposition*. SAE International, Sep 1989, SAE Technical Paper 891964. [Online]. Available: https://doi.org/10.4271/891964

[195] W. Lee and H. J. Schaefer, "Analysis of Local Pressures, Surface Temperatures and Engine Damages under Knock Conditions," in *SAE International Congress and Exposition*. SAE International, Feb 1983, SAE Technical Paper 600140. [Online]. Available: https://doi.org/10.4271/830508

[196] Y. Nakagawa, Y. Takagi, T. Itoh, and T. lijima, "Laser Shadowgraphic Analysis Of Knocking In S.I. Engine," in *20th FISITA Congress (1984), Vienna, Austria*. SAE International, Jan 1984, SAE Technical Paper 845001. [Online]. Available: https://doi.org/10.4271/845001

[197] P. M. Najt, "Evaluating Threshold Knock with a Semi-Empirical Model—Initial Results," in *1987 SAE International Fall Fuels and Lubricants Meeting and Exhibition*. SAE International, Nov 1987, SAE Technical Paper 872149. [Online]. Available: https://doi.org/10.4271/872149

[198] U. Spicher and H.-P. Kollmeier, "Detection of Flame Propagation During Knocking Combustion by Optical Fiber Diagnostics," in *1986 SAE International Fall Fuels and Lubricants Meeting and Exhibition*. SAE International, Oct 1986, SAE Technical Paper 861532. [Online]. Available: https://doi.org/10.4271/861532

[199] M. D. Checkel and J. D. Dale, "Computerized Knock Detection from Engine Pressure Records," in *SAE International Congress and Exposition*. SAE International, Mar 1986, SAE Technical Paper 860028. [Online]. Available: https://doi.org/10.4271/860028

[200] H. Ando, J. Takemura, and E. Koujina, "A Knock Anticipating Strategy Basing on the Real-Time Combustion Mode Analysis," in *SAE International Congress and Exposition*. SAE International, Feb 1989, SAE Technical Paper 890882. [Online]. Available: https://doi.org/10.4271/890882

[201] J. A. Harrington, "Water Addition to Gasoline-Effect on Combustion, Emissions, Performance, and Knock," in *SAE International Congress and Exposition*. SAE International, Feb 1982, SAE Technical Paper 820314. [Online]. Available: https://doi.org/10.4271/820314

[202] J. Klimstra, "The Knock Severity Index – A Proposal for a Knock Classification Method," in *1984 SAE International Fall Fuels and Lubricants Meeting and Exhibition*. SAE International, Oct 1984, SAE Technical Paper 841335. [Online]. Available: https://doi.org/10.4271/841335

[203] Y. Iwashita and A. Saito, "Observation of Knock Using a High Speed Shutter TV Camera System," in *1983 SAE International Fall Fuels and Lubricants Meeting and Exhibition*. SAE International, Oct 1983, SAE Technical Paper 831696. [Online]. Available: https://doi.org/10.4271/831696

[204] T. Hayashi, M. Taki, S. Kojima, and T. Kondo, "Photographic Observation of Knock with a Rapid Compression and Expansion Machine," in *1984 SAE International Fall Fuels and Lubricants Meeting and Exhibition*. SAE International, Oct 1984, SAE Technical Paper 841336. [Online]. Available: https://doi.org/10.4271/841336

[205] Y. Takagi, T. Itoh, and T. Iijima, "An Analytical Study on Knocking Heat Release and its Control in a Spark Ignition Engine," in *SAE International Congress and Exposition*. SAE International, Feb 1988, SAE Technical Paper 880196. [Online]. Available: https://doi.org/10.4271/880196

[206] H. Sakai, H. Noguchi, M. Kawauchi, and H. Kanesaka, "A New Type of Miller Supercharging System for High-Speed Engines - Part 1 Fundamental Considerations and Application to Gasoline Engines," in *1985 SAE International Off-Highway and Powerplant Congress and Exposition*. SAE International, Sep 1985, SAE Technical Paper 851522. [Online]. Available: https://doi.org/10.4271/851522

[207] H. Schäpertöns and W. Lee, "Multidimensional Modelling of Knocking Combustion in SI Engines," in *SAE International Congress and Exposition*. SAE International, Feb 1985, SAE Technical Paper 850502. [Online]. Available: https://doi.org/10.4271/850502

[208] Y. Zeldovich, "Regime classification of an exothermic reaction with nonuniform initial conditions," *Combustion and Flame*, vol. 39, no. 2, pp. 211 – 214, 1980. [Online]. Available: http://www.sciencedirect.com/science/article/pii/0010218080900176

[209] A. K. Oppenheim, "The Knock Syndrome — Its Cures and Its Victims," in *1984 SAE International Fall Fuels and Lubricants Meeting and Exhibition*. SAE International, Oct 1984, SAE Technical Paper 841339. [Online]. Available: https://doi.org/10.4271/841339

[210] A. Oppenheim, "Dynamic features of combustion," *Philosophical Transactions of the Royal Society of London. Series A*, vol. 315, pp. 471–508, 1985.

[211] R. Maly and G. Ziegler, "Thermal Combustion Modeling — Theoretical and Experimental Investigation of the Knocking Process," in *Passenger Car Meeting & Exposition*. SAE International, Feb 1982, SAE Technical Paper 820759. [Online]. Available: https://doi.org/10.4271/820759

[212] D. Cuttler and N. Girgis, "Photography of Combustion During Knocking Cycles in Disc and Compact Chambers," in *SAE International Congress and Exposition*. SAE International, Feb 1988, SAE Technical Paper 880195. [Online]. Available: https://doi.org/10.4271/880195

[213] P. O. Witze, J. K. Martin, and C. Borgnakke, "Measurements and Predictions of the Precombustion Fluid Motion and Combustion Rates in a Spark Ignition Engine," in *SAE Technical Paper*. SAE International, Oct 1983, SAE Technical Paper 831697. [Online]. Available: https://doi.org/10.4271/831697

[214] A. D. Gosman, Y. Y. Tsui, and C. Vafidis, "Flow in a model engine with a shrouded valve-a combined experimental and computational study," in *SAE Technical Paper*. SAE International, Feb 1985, SAE Technical Paper 850498. [Online]. Available: https://doi.org/10.4271/850498

[215] J. C. Kent, A. Mikulec, L. Rimal, A. Adamczyk, S. R. Mueller, R. Stein, and C. C. Warren, "Observations on the Effects of Intake-Generated Swirl and Tumble on Combustion Duration," in *SAE Technical Paper*. SAE International, Sep 1989, SAE Technical Paper 892096. [Online]. Available: https://doi.org/10.4271/892096

[216] Y. Otobe, O. Goto, H. Miyano, M. Kawamoto, A. Aoki, and T. Ogawa, "Honda Formula One Turbo-charged V-6 1.5L Engine," in *SAE International Congress and Exposition*. SAE International, Feb 1989, SAE Technical Paper 890877. [Online]. Available: https://doi.org/10.4271/890877

[217] R. R. Maly, R. Klein, N. Peters, and G. Konig, "Theoretical and Experimental Investigation of Knock Induced Surface Destruction," in *International Congress & Exposition*. SAE International, Feb 1990, SAE Technical Paper 900025. [Online]. Available: https://doi.org/10.4271/900025

[218] G. Konig and C. G. W. Sheppard, "End Gas Autoignition and Knock in a Spark Ignition Engine," in *International Fuels & Lubricants Meeting & Exposition*. SAE International, Oct 1990, SAE Technical Paper 902135. [Online]. Available: https://doi.org/10.4271/902135

[219] G. König, R. R. Maly, D. Bradley, A. K. C. Lau, and C. G. W. Sheppard, "Role of Exothermic Centres on Knock Initiation and Knock Damage," in *International Fuels & Lubricants Meeting & Exposition*. SAE International, Oct 1990, SAE Technical Paper 902136. [Online]. Available: https://doi.org/10.4271/902136

[220] R. Herweg and R. R. Maly, "A Fundamental Model for Flame Kernel Formation in S. I. Engines," in *SAE Technical Paper*. SAE International, Oct 1992, SAE Technical Paper 922243. [Online]. Available: https://doi.org/10.4271/922243

[221] J. Pan, C. G. W. Sheppard, A. Tindall, M. Berzins, S. V. Pennington, and J. M. Ware, "End Gas Inhomogeneity, Autoignition and Knock," in *International Fall Fuels and Lubricants Meeting and Exposition*. SAE International, Oct 1998, SAE Technical Paper 982616. [Online]. Available: https://doi.org/10.4271/982616

[222] U. Spicher, H. Kröger, and J. Ganser, "Detection of Knocking Combustion Using Simultaneously High-Speed Schlieren Cinematography and Multi Optical Fiber Technique," in *International Fuels & Lubricants Meeting & Exposition*. SAE International, Oct 1991, SAE Technical Paper 912312. [Online]. Available: https://doi.org/10.4271/912312

[223] C. K. Westbrook, W. J. Pitz, and W. R. Leppard, "The Autoignition Chemistry of Paraffinic Fuels and Pro-Knock and Anti-Knock Additives: A Detailed Chemical Kinetic Study," in *International Fuels & Lubricants Meeting & Exposition*. SAE International, Oct 1991, SAE Technical Paper 912314. [Online]. Available: https://doi.org/10.4271/912314

[224] P. Ronney, M. Shoda, S. Waida, C. Westbrook, and W. Pitz, "Knock Characteristics of Liquid and Gaseous Fuels in Lean Mixtures," in *International Fuels & Lubricants Meeting & Exposition*. SAE International, Oct 1991, SAE Technical Paper 912311. [Online]. Available: https://doi.org/10.4271/912311

[225] S. Brussovansky, J. B. Heywood, and J. C. Keck, "Predicting the Effects of Air and Coolant Temperature, Deposits, Spark Timing and Speed on Knock in Spark Ignition Engines," in *International Fuels & Lubricants Meeting & Exposition*. SAE International, Oct 1992, SAE Technical Paper 922324. [Online]. Available: https://doi.org/10.4271/922324

[226] M. Nakano, S. Nakahara, K. Akihama, S. Kubo, and S. Yamazahi, "Predictions of the Knock Onset and the Effects of Heat Release Pattern and Unburned Gas Temperature on Torque at Knock Limit in S.I. Engines," in *1995 SAE International Fall Fuels and Lubricants Meeting and Exhibition*. SAE International, Oct 1995, SAE Technical Paper 952408. [Online]. Available: https://doi.org/10.4271/952408

[227] C. A. Blunsdon and J. Dent, "The Simulation of Autoignition and Knock in a Spark Ignition Engine with Disk Geometry," in *International Congress & Exposition*. SAE International, Mar 1994, SAE Technical Paper 940524. [Online]. Available: https://doi.org/10.4271/940524

[228] G. T. Kalghatgi, P. Snowdon, and C. R. McDonald, "Studies of Knock in a Spark Ignition Engine with "CARS" Temperature Measurements and Using Different Fuels," in *International Congress & Exposition*. SAE International, Feb 1995, SAE Technical Paper 950690. [Online]. Available: https://doi.org/10.4271/950690

[229] H. Shoji, A. Saima, and K. Shiino, "Simultaneous Measurement of Light Emission and Absorption Behavior of Unburned Gas During Knocking Operation," in *International Fuels & Lubricants Meeting & Exposition*. SAE International, Oct 1993, SAE Technical Paper 932754. [Online]. Available: https://doi.org/10.4271/932754

[230] M. Golombok, G. T. Kalghatgi, and A. Tindall, "Heat Release and Knock in Paraffinic and Aromatic Fuels and the Effect of an Ashless Anti-knock Additive," in *1995 SAE International Fall Fuels and Lubricants Meeting and Exhibition*. SAE International, Oct 1995, SAE Technical Paper 952405. [Online]. Available: https://doi.org/10.4271/952405

[231] M. Kaneyasu, N. Kurihara, K. Katogi, and H. Tokuda, "Engine Knock Detection Using Multi-Spectrum Method," in *International Congress & Exposition*. SAE International, Feb 1992, SAE Technical Paper 920702. [Online]. Available: https://doi.org/10.4271/920702

[232] B. Samimy, G. Rizzoni, and K. C. Leisenring, "Improved Knock Detection by Advanced Signal Processing," in *International Congress & Exposition*. SAE International, Feb 1995, SAE Technical Paper 950845. [Online]. Available: https://doi.org/10.4271/950845

[233] D. Scholl, S. Russ, and W. Stockhausen, "Detection of Spark Knock Oscillations: Dependence on Combustion Temperature," in *International Congress & Exposition*. SAE International, Feb 1997, SAE Technical Paper 970038. [Online]. Available: https://doi.org/10.4271/970038

[234] K. Burgdorf and A. Karlström, "Using Multi-Rate Filter Banks to Detect Internal Combustion Engine Knock," in *International Fuels & Lubricants Meeting & Exposition*. SAE International, May 1997, SAE Technical Paper 971670. [Online]. Available: https://doi.org/10.4271/971670

[235] K. Burgdorf and I. Denbratt, "Comparison of Cylinder Pressure Based Knock Detection Methods," in *International Fuels & Lubricants Meeting & Exposition*. SAE International, Oct 1997, SAE Technical Paper 972932. [Online]. Available: https://doi.org/10.4271/972932

[236] K. Burgdorf, "A Contribution to Knock Statistics," in *SAE Technical Paper*. SAE International, Oct 1998, SAE Technical Paper 982475. [Online]. Available: https://doi.org/10.4271/982475

[237] K. Burgdorf and J. Chomiak, "A New Knock Form - an Experimental Study," in *International Fall Fuels and Lubricants Meeting and Exposition*. SAE International, Oct 1998, SAE Technical Paper 982589. [Online]. Available: https://doi.org/10.4271/982589

[238] B. Stiebels, M. Schreiber, and A. S. Sakak, "Development of a New Measurement Technique for the Investigation of End-Gas Autoignition and Engine Knock," in *International Congress & Exposition*. SAE International, Feb 1996, SAE Technical Paper 960827. [Online]. Available: https://doi.org/10.4271/960827

[239] P. M. Liiva, J. N. Valentine, J. M. Cobb, and W. P. Acker, "Use of Multiple Pressure Transducers to Find In-Cylinder Knock Location," in *International Fuels & Lubricants Meeting & Exposition*. SAE International, Oct 1992, SAE Technical Paper 922368. [Online]. Available: https://doi.org/10.4271/922368

[240] K. Gschweitl, E. Gotthard, and A. Kampitsch, "Real Time Knock Analysis for Automatic Engine Mapping and Calibration," in *SAE Brasil '94*. SAE International, Nov 1994, SAE Technical Paper 942399. [Online]. Available: https://doi.org/10.4271/942399

[241] B. Grandin, H.-E. Ångström, P. Stålhammar, and E. Olofsson, "Knock Suppression in a Turbocharged SI Engine by Using Cooled EGR," in *International Fall Fuels and Lubricants Meeting and Exposition*. SAE International, Oct 1998, SAE Technical Paper 982476. [Online]. Available: https://doi.org/10.4271/982476

[242] T. Ueda, T. Okumura, S. Sugiura, and S. Kojima, "Effects of Squish Area Shape on Knocking in a Four-Valve Spark Ignition Engine," in *International Fuels & Lubricants Meeting & Exposition*. SAE International, May 1999, SAE Technical Paper 1999-01-1494. [Online]. Available: https://doi.org/10.4271/1999-01-1494

[243] T. Goto, K. Hatamura, S. Takizawa, N. Hayama, H. Abe, and H. Kanesaka, "Development of V6 Miller Cycle Gasoline Engine," in *International Congress& Exposition*. SAE International, Mar 1994, SAE Technical Paper 940198. [Online]. Available: https://doi.org/10.4271/940198

[244] M. Hitomi, J. Sasaki, K. Hatamura, and Y. Yano, "Mechanism of Improving Fuel Efficiency by Miller Cycle and Its Future Prospect," in *International Congress& Exposition*. SAE International, Feb 1995, SAE Technical Paper 950974. [Online]. Available: https://doi.org/10.4271/950974

[245] N. Ueda, H. Sakai, N. lso, and J. Sasaki, "A Naturally Aspirated Miller Cycle Gasoline Engine - Its Capability of Emission, Power and Fuel Economy," in *International Congress& Exposition*. SAE International, Feb 1996, SAE Technical Paper 960589. [Online]. Available: https://doi.org/10.4271/960589

[246] Y. Iwamoto, K. Noma, O. Nakayama, T. Yamauchi, and H. Ando, "Development of Gasoline Direct Injection Engine," in *SAE Technical Paper*. SAE International, Feb 1997, SAE Technical Paper 970541. [Online]. Available: https://doi.org/10.4271/970541

[247] J. Harada, T. Tomita, H. Mizuno, Z. Mashiki, and Y. Ito, "Development of Direct Injection Gasoline Engine," in *SAE Technical Paper*. SAE International, Feb 1997, SAE Technical Paper 970540. [Online]. Available: https://doi.org/10.4271/970540

[248] J. Yang and R. W. Anderson, "Fuel Injection Strategies to Increase Full-Load Torque Output of a Direct-Injection SI Engine," in *SAE Technical Paper*. SAE International, Feb 1998, SAE Technical Paper 980495. [Online]. Available: https://doi.org/10.4271/980495

[249] W. Anderson, J. Yang, D. D. Brehob, J. K. Vallance, and R. M. Whiteaker, "Understanding the thermodynamics of direct injection spark ignition (DISI) combustion systems: An analytical and experimental investigation," in *SAE Technical Paper*. SAE International, Oct 1996, SAE Technical Paper 962018. [Online]. Available: https://doi.org/10.4271/962018

[250] J. Willand, R.-G. Nieberding, G. Vent, and C. Enderle, "The Knocking Syndrome - Its Cure and Its Potential," in *International Fall Fuels and Lubricants Meeting and Exposition*. SAE International, Oct 1998, SAE Technical Paper 982483. [Online]. Available: https://doi.org/10.4271/982483

[251] G. Töpfer, J. Reissing, H.-J. Weimar, and U. Spicher, "Optical Investigation of Knocking Location on S.I.-Engines with Direct-Injection," in *SAE 2000 World Congress*. SAE International, Mar 2000, SAE Technical Paper 2000-01-0252. [Online]. Available: https://doi.org/10.4271/2000-01-0252

[252] H. Philipp, A. Hirsch, M. Baumgartner, G. Fernitz, C. Beidl, W. Piock, and E. Winklhofer, "Localization of Knock Events in Direct Injection Gasoline Engines," in *SAE 2001 World Congress*. SAE International, Mar 2001, SAE Technical Paper 2001-01-1199. [Online]. Available: https://doi.org/10.4271/2001-01-1199

[253] F. Westin, B. Grandin, and H.-E. Ångström, "The Influence of Residual Gases on Knock in Turbocharged SI-Engines," in *International Fuels & Lubricants Meeting & Exposition*. SAE International, Oct 2000, SAE Technical Paper 2000-01-2840. [Online]. Available: https://doi.org/10.4271/2000-01-2840

[254] O. Stenlåås, P. Einewall, R. Egnell, and B. Johansson, "Measurement of Knock and Ion Current in a Spark Ignition Engine with and without NO Addition to the Intake Air," in *SAE 2003 World Congress & Exhibition*. SAE International, Mar 2003, SAE Technical Paper 2003-01-0639. [Online]. Available: https://doi.org/10.4271/2003-01-0639

[255] A. A. Burluka, K. Liu, C. Sheppard, A. J. Smallbone, and R. Woolley, "The Influence of Simulated Residual and NO Concentrations on Knock Onset for PRFs and Gasolines," in *2004 Powertrain & Fluid Systems Conference & Exhibition*. SAE International, Oct 2004, SAE Technical Paper 2004-01-2998. [Online]. Available: https://doi.org/10.4271/2004-01-2998

[256] B. Grandin and I. Denbratt, "The Effect of Knock on Heat Transfer in SI Engines," in *SAE 2002 World Congress & Exhibition*. SAE International, Mar 2002, SAE Technical Paper 2002-01-0238. [Online]. Available: https://doi.org/10.4271/2002-01-0238

[257] B. Grandin, I. Denbratt, J. Bood, C. Brackmann, P.-E. Bengtsson, A. Gogan, F. Mauss, and B. Sundén, "Heat Release in the End-Gas Prior to Knock in Lean, Rich and Stoichiometric Mixtures With and Without EGR," in *SAE 2002 World Congress & Exhibition*. SAE International, Mar 2002, SAE Technical Paper 2002-01-0239. [Online]. Available: https://doi.org/10.4271/2002-01-0239

[258] A. Gogan, B. Sundén, H. Lehtiniemi, and F. Mauss, "Stochastic Model for the Investigation of the Influence of Turbulent Mixing on Engine Knock," in *2004 Powertrain & Fluid Systems Conference & Exhibition*. SAE International, Oct 2004, SAE Technical Paper 2004-01-2999. [Online]. Available: https://doi.org/10.4271/2004-01-2999

[259] M. Sjöberg and J. E. Dec, "Effects of Engine Speed, Fueling Rate, and Combustion Phasing on the Thermal Stratification Required to Limit HCCI Knocking Intensity," in *2005 SAE Brasil Fuels & Lubricants Meeting*. SAE International, May 2005, SAE Technical Paper 2005-01-2125. [Online]. Available: https://doi.org/10.4271/2005-01-2125

[260] P. G. Aleiferis, A. M. K. P. Taylor, J. H. Whitelaw, K. Ishii, and Y. Urata, "Cyclic Variations of Initial Flame Kernel Growth in a Honda VTEC-E Lean-Burn Spark-Ignition Engine," in *SAE Technical Paper*. SAE International, Mar 2000, SAE Technical Paper 2000-01-1207. [Online]. Available: https://doi.org/10.4271/2000-01-1207

[261] F. Zhao, D. L. Harrington, and M.-C. D. Lai, *Automotive Gasoline Direct-Injection Engines*. SAE International, Warrendale, 2002.

[262] J. Yi, S. Wooldridge, G. Coulson, J. Hilditch, C. O. Iyer, P. Moilanen, G. Papaioannou, D. Reiche, M. Shelby, B. VanDerWege, C. Weaver, Z. Xu, G. Davis, B. Hinds, and A. Schamel, "Development and Optimization of the Ford 3.5L V6 EcoBoost Combustion System," *SAE Int. J. Engines*, vol. 2, pp. 1388–1407, Apr 2009. [Online]. Available: https://doi.org/10.4271/2009-01-1494

[263] D. Bradley, C. Morley, X. J. Gu, and D. R. Emerson, "Amplified Pressure Waves During Autoignition: Relevance to CAI Engines," in *SAE Powertrain & Fluid Systems Conference & Exhibition*. SAE International, Oct 2002, SAE Technical Paper 2002-01-2868. [Online]. Available: https://doi.org/10.4271/2002-01-2868

[264] J. A. Eng, "Characterization of pressure waves in HCCI combustion," in *SAE Powertrain & Fluid Systems Conference & Exhibition*. SAE International, 2002. [Online]. Available: https://doi.org/10.4271/2002-01-2859

[265] D. Bradley and G. Kalghatgi, "Influence of autoignition delay time characteristics of different fuels on pressure waves and knock in reciprocating engines," *Combustion and Flame*, vol. 156, no. 12, pp. 2307 – 2318, 2009. [Online]. Available: http://www.sciencedirect.com/science/article/pii/S0010218009002272

[266] J. Hyvönen, G. Haraldsson, and B. Johansson, "Operating Conditions Using Spark Assisted HCCI Combustion During Combustion Mode Transfer to SI in a Multi-Cylinder VCR-HCCI Engine," in *SAE Technical Paper*. SAE International, Apr 2005. [Online]. Available: https://doi.org/10.4271/2005-01-0109

[267] T. Urushihara, K. Yamaguchi, K. Yoshizawa, and T. Itoh, "A Study of a Gasoline-fueled Compression Ignition Engine - Expansion of HCCI Operation Range Using SI Combustion as a Trigger of Compression Ignition," in *SAE Technical Paper*. SAE International, Apr 2005, SAE Technical Paper 2005-01-0180. [Online]. Available: https://doi.org/10.4271/2005-01-0180

[268] T. Suzuki, H. Ohara, A. Kakishima, K. Yoshida, and H. Shoji, "A Study of Knocking Using Ion Current and Light Emission," in *Small Engine Technology Conference & Exposition*. SAE International, Sep 2003, SAE Technical Paper 2003-32-0038. [Online]. Available: https://doi.org/10.4271/2003-32-0038

[269] H. Hirooka, S. Mori, and R. Shimizu, "Effects of High Turbulence Flow on Knock Characteristics," in *SAE 2004 World Congress & Exhibition*. SAE International, Mar 2004, SAE Technical Paper 2004-01-0977. [Online]. Available: https://doi.org/10.4271/2004-01-0977

[270] T. Shinagawa, T. Okumura, S. Furuno, and K.-O. Kim, "Effects of Hydrogen Addition to SI Engine on Knock Behavior," in *2004 SAE Fuels & Lubricants Meeting & Exhibition*. SAE International, Jun 2004, SAE Technical Paper 2004-01-1851. [Online]. Available: https://doi.org/10.4271/2004-01-1851

[271] Z. Zhang and E. Tomota, "A New Diagnostic Method of Knocking in a Spark-Ignition Engine Using the Wavelet Transform," in *CEC/SAE Spring Fuels & Lubricants Meeting & Exposition*. SAE International, Jun 2000, SAE Technical Paper 2000-01-1801. [Online]. Available: https://doi.org/10.4271/2000-01-1801

[272] S. Carstens-Behrens, M. Urlaub, J. F. Böhme, J. Förster, and F. Raichle, "FEM Approximation of Internal Combustion Chambers for Knock Investigations," in *SAE 2002 World Congress & Exhibition*. SAE International, Mar 2002, SAE Technical Paper 2002-01-0237. [Online]. Available: https://doi.org/10.4271/2002-01-0237

[273] H. A. Noubari and G. A. Dumont, "Towards an Improved Knock Detection and Quantification using Wavelets and Entropy-based Noise Compensation," in *SAE 2005 Noise and Vibration Conference and Exhibition*. SAE International, May 2005, SAE Technical Paper 2005-01-2269. [Online]. Available: https://doi.org/10.4271/2005-01-2269

[274] J. M. Borg, G. Saikalis, S. Oho, and K. C. Cheok, "Knock Signal Analysis Using the Discrete Wavelet Transform," in *SAE 2006 World Congress & Exhibition*. SAE International, Apr 2006, SAE Technical Paper 2006-01-0226. [Online]. Available: https://doi.org/10.4271/2006-01-0226

[275] J. M. Borg and A. C. Alkidas, "Characterization of Autoignition in a Knocking SI Engine Using Heat Release Analysis," in *Powertrain & Fluid Systems Conference and Exhibition*. SAE International, Oct 2006, SAE Technical Paper 2006-01-3341. [Online]. Available: https://doi.org/10.4271/2006-01-3341

[276] R. Worret, S. Bernhardt, F. Schwarz, and U. Spicher, "Application of Different Cylinder Pressure Based Knock Detection Methods in Spark Ignition Engines," in *Spring Fuels & Lubricants Meeting & Exhibition*. SAE International, May 2002, SAE Technical Paper 2002-01-1668. [Online]. Available: https://doi.org/10.4271/2002-01-1668

[277] E. Corti and D. Moro, "Knock Indexes Thresholds Setting Methodology," in *SAE World Congress & Exhibition*. SAE International, Apr 2007, SAE Technical Paper 2007-01-1508. [Online]. Available: https://doi.org/10.4271/2007-01-1508

[278] A. Hettinger and A. Kulzer, "A new method to detect knocking zones," *SAE International Journal of Engines*, vol. 2, no. 1, pp. 645–665, 2009. [Online]. Available: https://doi.org/10.4271/2009-01-0698

[279] N. Cavina, E. Corti, G. Minelli, D. Moro, and L. Solieri, "Knock Indexes Normalization Methodologies," in *The Sustainable Mobility Challenge at the National Congress of the Italian Thermotechnical Association (ATI)*. SAE International, Sep 2006, SAE Technical Paper 2006-01-2998. [Online]. Available: https://doi.org/10.4271/2006-01-2998

[280] J. Naber, J. R. Blough, D. Frankowski, M. Goble, and J. E. Szpytman, "Analysis of Combustion Knock Metrics in Spark-Ignition Engines," in *SAE 2006 World Congress & Exhibition*. SAE International, Apr 2006, SAE Technical Paper 2006-01-0400. [Online]. Available: https://doi.org/10.4271/2006-01-0400

[281] V. Mittal, B. M. Revier, and J. B. Heywood, "Phenomena that Determine Knock Onset in Spark-Ignition Engines," in *2007 Fuels and Emissions Conference*. SAE International, Jan 2007, SAE Technical Paper 2007-01-0007. [Online]. Available: https://doi.org/10.4271/2007-01-0007

[282] A. Abhijit and J. Naber, "Ionization signal response during combustion knock and comparison to cylinder pressure for si engines," *SAE International Journal of Passenger Cars - Electronic and Electrical Systems*, vol. 1, no. 1, pp. 349–364, 2008. [Online]. Available: https://doi.org/10.4271/2008-01-0981

[283] G. G. Zhu, I. Haskara, and J. Winkelman, "Stochastic Limit Control and Its Application to Knock Limit Control Using Ionization Feedback," in *SAE 2005 World Congress & Exhibition*. SAE International, 2005, SAE Technical Paper 2005-01-0018. [Online]. Available: https://doi.org/10.4271/2005-01-0018

[284] M. Castagné, J. P. Dumas, S. Henriot, F. A. Lafossas, and T. Mazoyer, "New Knock Localization Methodology for SI Engines," in *SAE 2003 World Congress & Exhibition*. SAE International, Mar 2003, SAE Technical Paper 2003-01-1118. [Online]. Available: https://doi.org/10.4271/2003-01-1118

[285] M. Rothe, T. Heidenreich, U. Spicher, and A. Schubert, "Knock Behavior of SI-Engines: Thermodynamic Analysis of Knock Onset Locations and Knock Intensities," in *SAE 2006 World Congress & Exhibition*. SAE International, Apr 2006, SAE Technical Paper 2006-01-0225. [Online]. Available: https://doi.org/10.4271/2006-01-0225

[286] G. Kalghatgi, "Fuel Anti-Knock Quality - Part I. Engine Studies," in *SAE 2002 World Congress & Exhibition*. SAE International, Sep 2001, SAE Technical Paper 2001-01-3584. [Online]. Available: https://doi.org/10.4271/2001-01-3584

[287] G. T. Kalghatgi, "Fuel Anti-Knock Quality- Part II. Vehicle Studies - How Relevant is Motor Octane Number (MON) in Modern Engines?" in *SAE 2002 World Congress & Exhibition*. SAE International, Sep 2001, SAE Technical Paper 2001-01-3585. [Online]. Available: https://doi.org/10.4271/2001-01-3585

[288] V. Mittal and J. B. Heywood, "The shift in relevance of fuel RON and MON to knock onset in modern SI engines over the last 70 years," *SAE International Journal of Engines*, vol. 2, no. 2, pp. 1–10, 2009. [Online]. Available: https://doi.org/10.4271/2009-01-2622

[289] G. Plassat, S. Guichaous, N. Dioc, J. Milpied, N. Jeuland, A. Marchal, and P. Schmelzle, "Impact of fuel properties on the performances and knock behaviour of a downsized turbocharged DI SI engine - focus on octane numbers and latent heat of vaporization," *SAE International Journal of Fuels and Lubricants*, vol. 2, no. 1, pp. 118–126, 2009. [Online]. Available: https://doi.org/10.4271/2009-01-0324

[290] J. Kusaka, Y. Daisho, and K. Nakama, "Effect of ethanol on knock in spark ignition gasoline engines," *SAE International Journal of Engines*, vol. 1, no. 1, pp. 1366–1380, 2008. [Online]. Available: https://doi.org/10.4271/2008-32-0020

[291] J. A. Topinka, M. D. Gerty, J. B. Heywood, and J. C. Keck, "Knock Behavior of a Lean-Burn, H2 and CO Enhanced, SI Gasoline Engine Concept," in *SAE 2004 World Congress & Exhibition*. SAE International, Mar 2004, SAE Technical Paper 2004-01-0975. [Online]. Available: https://doi.org/10.4271/2004-01-0975

[292] A. Swarts, A. Yates, C. Viljoen, and R. Coetzer, "Standard Knock Intensity Revisited: Atypical Burn Rate Characteristics identified in the CFR Octane Rating Engine," in *2004 SAE Fuels & Lubricants Meeting & Exhibition*. SAE International, Jun 2004, SAE Technical Paper 2004-01-1850. [Online]. Available: https://doi.org/10.4271/2004-01-1850

[293] C. Elmqvist, F. Lindström, H.-E. Ångström, B. Grandin, and G. Kalghatgi, "Optimizing Engine Concepts by Using a Simple Model for Knock Prediction," in *SAE Powertrain & Fluid Systems Conference & Exhibition*. SAE International, Oct 2003, SAE Technical Paper 2003-01-3123. [Online]. Available: https://doi.org/10.4271/2003-01-3123

[294] T. Noda, K. Hasegawa, M. Kubo, and T. Itoh, "Development of Transient Knock Prediction Technique by Using a Zero-Dimensional Knocking Simulation with Chemical Kinetics," in *SAE 2004 World Congress & Exhibition*. SAE International, Mar 2004, SAE Technical Paper 2004-01-0618. [Online]. Available: https://doi.org/10.4271/2004-01-0618

[295] A. D. B. Yates, A. Swarts, and C. L. Viljoen, "Correlating Auto-Ignition Delays And Knock-Limited Spark-Advance Data For Different Types Of Fuel," in *2005 SAE Brasil Fuels & Lubricants Meeting*. SAE International, May 2005, SAE Technical Paper 2005-01-2083. [Online]. Available: https://doi.org/10.4271/2005-01-2083

[296] M. Mehl, T. Faravelli, E. Ranzi, T. Lucchini, A. Onorati, F. Giavazzi, P. Scorletti, and D. Terna, "Kinetic modeling of knock properties in internal combustion engines," in *Powertrain & Fluid Systems Conference and Exhibition*. SAE International, Oct 2006, SAE Technical Paper 2006-01-3239. [Online]. Available: https://doi.org/10.4271/2006-01-3239

[297] G. D'Errico, T. Lucchini, A. Onorati, M. Mehl, T. Faravelli, E. Ranzi, S. Merola, and B. M. Vaglieco, "Development and Experimental Validation of a Combustion Model with Detailed Chemistry for Knock Predictions," in *SAE World Congress & Exhibition*. SAE International, Apr 2007, SAE Technical Paper 2007-01-0938. [Online]. Available: https://doi.org/10.4271/2007-01-0938

[298] E. Torella, F. Bozza, and D. Siano, "Cycle-by-cycle analysis, knock modeling and spark-advance setting of a "downsized" spark-ignition turbocharged engine," *SAE International Journal of Engines*, vol. 2, no. 2, pp. 381–389, 2009. [Online]. Available: https://doi.org/10.4271/2009-24-0020

[299] T. Hattrell, C. G. W. Sheppard, A. A. Burluka, J. Neumeister, and A. Cairns, "Burn Rate Implications of Alternative Knock Reduction Strategies for Turbocharged SI Engines," in *SAE 2006 World Congress & Exhibition*. SAE International, Apr 2006, SAE Technical Paper 2006-01-1110. [Online]. Available: https://doi.org/10.4271/2006-01-1110

[300] L. Liang, R. D. Reitz, C. O. Iyer, and J. Yi, "Modeling Knock in Spark-Ignition Engines Using a G-equation Combustion Model Incorporating Detailed Chemical Kinetics," in *SAE World Congress & Exhibition*. SAE International, Apr 2007, SAE Technical Paper 2007-01-0165. [Online]. Available: https://doi.org/10.4271/2007-01-0165

[301] P. Eckert, S.-C. Kong, and R. D. Reitz, "Modeling Autoignition and Engine Knock Under Spark Ignition Conditions," in *SAE 2003 World Congress & Exhibition*. SAE International, Mar 2003, SAE Technical Paper 2003-01-0011. [Online]. Available: https://doi.org/10.4271/2003-01-0011

[302] E. Corti and C. Forte, "Combination of in-cylinder pressure signal analysis and CFD simulation for knock detection purposes," *SAE International Journal of Engines*, vol. 2, no. 2, pp. 268–380, 2009. [Online]. Available: https://doi.org/10.4271/2009-24-0019

[303] A. P. Kleemann, P. Menegazzi, S. Henriot, and A. Marchal, "Numerical Study on Knock for an SI Engine by Thermally Coupling Combustion Chamber and Cooling Circuit Simulations," in *SAE 2003 World Congress & Exhibition*. SAE International, Mar 2003. [Online]. Available: https://doi.org/10.4271/2003-01-0563

[304] S. Shih, E. Itano, J. Xin, M. Kawamoto, and Y. Maeda, "Engine Knock Toughness Improvement Through Water Jacket Optimization," in *SAE Powertrain & Fluid Systems Conference & Exhibition*. SAE International, Oct 2003, SAE Technical Paper 2003-01-3259. [Online]. Available: https://doi.org/10.4271/2003-01-3259

[305] S. Couet, P. Higelin, and B. Moreau, "APIR: A new firing concept for the internal combustion engines - sensitivity to knock and in-cylinder aerodynamics," in *International Spring Fuels & Lubricants Meeting*. SAE International, 2001. [Online]. Available: https://doi.org/10.4271/2001-01-1954

[306] M. Kettner, M. Rothe, A. Velji, U. Spicher, D. Kuhnert, and R. Latsch, "A New Flame Jet Concept to Improve the Inflammation of Lean Burn Mixtures in SI Engines," in *SAE Technical Paper*. SAE International, Oct 2005, SAE Technical Paper 2005-01-3688. [Online]. Available: https://doi.org/10.4271/2005-01-3688

[307] J. Getzlaff, J. Pape, C. Gruenig, D. Kuhnert, and R. Latsch, "Investigations on Pre-Chamber Spark Plug with Pilot Injection," in *SAE Technical Paper*. SAE International, Apr 2007, SAE Technical Paper 2007-01-0479. [Online]. Available: https://doi.org/10.4271/2007-01-0479

[308] Y. Kawabata and D. Mori, "Combustion Diagnostics & Improvement of a Prechamber Lean-Burn Natural Gas Engine," in *SAE Technical Paper*. SAE International, Mar 2004, SAE Technical Paper 2004-01-0979. [Online]. Available: https://doi.org/10.4271/2004-01-0979

[309] H. Winter, G. Kogler, E. Schnessl, A. Wimmer, and T. Jauk, "Investigations on Combustion and Heat Transfer in a Large Gaseous Fuelled Engine," in *SAE Technical Paper*. SAE International, Mar 2003, SAE Technical Paper 2003-01-0562. [Online]. Available: https://doi.org/10.4271/2003-01-0562

[310] E. Toulson, H. C. Watson, and W. P. Attard, "Modeling Alternative Prechamber Fuels in Jet Assisted Ignition of Gasoline and LPG," in *SAE World Congress & Exhibition*. SAE International, Apr 2009, SAE Technical Paper 2009-01-0721. [Online]. Available: https://doi.org/10.4271/2009-01-0721

[311] B. Hoepke, S. Jannsen, E. Kasseris, and W. K. Cheng, "Egr effects on boosted si engine operation and knock integral correlation," *SAE International Journal of Engines*, vol. 5, no. 2, pp. 547–559, 2012. [Online]. Available: https://doi.org/10.4271/2012-01-0707

[312] T. Alger, B. Mangold, C. Roberts, and J. Gingrich, "The interaction of fuel anti-knock index and cooled EGR on engine performance and efficiency," *SAE International Journal of Engines*, vol. 5, no. 3, pp. 1229–1241, 2012. [Online]. Available: https://doi.org/10.4271/2012-01-1149

[313] P. Roberts and C. Sheppard, "The influence of residual gas NO content on knock onset of iso-octane, PRF, TRF and ULG mixtures in SI engines," *SAE International Journal of Engines*, vol. 6, no. 4, pp. 2028–2043, 2013. [Online]. Available: https://doi.org/10.4271/2013-01-9046

[314] T. Alger, M. Walls, C. Chadwell, S. Joo, B. Denton, K. Kleinow, and D. Robertson, "The interaction between fuel anti-knock index and reformation ratio in an engine equipped with dedicated EGR," *SAE International Journal of Engines*, vol. 9, no. 2, pp. 786–795, 2016. [Online]. Available: https://doi.org/10.4271/2016-01-0712

[315] S. W. Wagnon, W. J. Pitz, M. Mehl, J. P. Szybist, and D. Splitter, "The reduced effectiveness of egr to mitigate knock at high loads in boosted si engines," *SAE International Journal of Engines*, vol. 10, no. 5, pp. 2305–2318, 2017. [Online]. Available: https://doi.org/10.4271/2017-24-0061

[316] N. Yokoo, T. Tomoda, K. Nakata, M. Sjöberg, D. Vuilleumier, and N. Kim, "On the role of nitric oxide for the knock-mitigation effectiveness of egr in a disi engine operated with various gasoline fuels," *SAE International Journal of Advances and Current Practices in Mobility*, vol. 2, no. 1, pp. 272–291, 2019. [Online]. Available: https://doi.org/10.4271/2019-01-2150

[317] A. Lewis, S. Akehurst, C. Brace, C. Copeland, S. Bredda, J. Fernandes, J. Turner, A. Popplewell, R. Patel, T. Johnson, N. Darnton, S. Richardson, R. Martinez-Botas, A. Romagnoli, R. Tudor, C. Bithell, R. Jackson, A. Burluka, S. Remmert, and R. Cracknell, "Ultra boost for economy: Extending the limits of extreme engine downsizing," *SAE International Journal of Engines*, vol. 7, no. 1, pp. 387–417, 2014. [Online]. Available: https://doi.org/10.4271/2014-01-1185

[318] P. Adomeit, M. Jakob, S. Pischinger, A. Brunn, and J. Ewald, "Effect of Intake Port Design on the Flow Field Stability of a Gasoline DI Engine," in *SAE Technical Paper*. SAE International, Apr 2011, SAE Technical Paper 2011-01-1284. [Online]. Available: https://doi.org/10.4271/2011-01-1284

[319] E. Baum, B. Peterson, C. Surmann, D. Michaelis, B. Böhm, and A. Dreizler, "Investigation of the 3D flow field in an IC engine using tomographic PIV," *Proceedings of the Combustion Institute*, vol. 34, no. 2, pp. 2903–2910, 2013. [Online]. Available: https://www.sciencedirect.com/science/article/pii/S1540748912002313

[320] Y. Yoshihara, K. Nakata, D. Takahashi, T. Omura, and A. Ota, "Development of high tumble intake-port for high thermal efficiency engines," in *SAE Technical Paper*. SAE International, Apr 2016, SAE Technical Paper 2016-01-0692. [Online]. Available: https://doi.org/10.4271/2016-01-0692

[321] S. Itabashi, E. Murase, H. Tanaka, M. Yamaguchi, and T. Muraguchi, "New Combustion and Powertrain Control Technologies for Fun-to-Drive Dynamic Performance and Better Fuel Economy," in *SAE Technical Paper*. SAE International, Mar 2017, SAE Technical Paper 2017-01-0589. [Online]. Available: https://doi.org/10.4271/2017-01-0589

[322] K. Suzuki, K. Uehera, E. Murase, and S. Nogawa, "Study of ignitability in strong flow field," in *Ignition Systems for Gasoline Engines*, S. M. Günther M., Ed. Cham: Springer, 2016, ch. 4, pp. 69–84. [Online]. Available: https://doi.org/10.1007/978-3-319-45504-4_4

[323] N. Hayashi, A. Sugiura, Y. Abe, and K. Suzuki, "Development of Ignition Technology for Dilute Combustion Engines," *SAE Int. J. Engines*, vol. 10, pp. 984–995, Mar 2017. [Online]. Available: https://doi.org/10.4271/2017-01-0676

[324] D. J. Corrigan, E. Pascolini, D. Zecchetti, and F. Titus, "Ignition System Development for High Speed, High Load, Lean Boosted Engines," in *Ignition Systems for Gasoline Engines*, S. M. Günther M., Ed. Cham: Springer, 2016, ch. 13, pp. 217–242. [Online]. Available: https://doi.org/10.1007/978-3-319-45504-4_13

[325] C. A. Idicheria and P. M. Najt, "Potential of Advanced Corona Ignition System (ACIS) for Future Engine Applications," in *Ignition Systems for Gasoline Engines*, S. M. Günther M., Ed. Cham: Springer, 2016, ch. 19, pp. 315–331. [Online]. Available: https://doi.org/10.1007/978-3-319-45504-4_19

[326] D. Singleton, J. M. Sanders, M. A. Thomas, M. S. Jr., J. Sevik, M. Pamminger, and T. Wallner, "Demonstration of Improved Dilution Tolerance Using a Production-Intent Compact Nanosecond Pulse Ignition System," in *Ignition Systems for Gasoline Engines*, S. M. Günther M., Ed. Cham: Springer, 2016, ch. 3, pp. 315–331. [Online]. Available: https://doi.org/10.1007/978-3-319-45504-4_3

[327] A. d'Adamo, F. Berni, S. Breda, M. Lugli, S. Fontanesi, and G. Cantore, "A Numerical Investigation on the Potentials of Water Injection as a Fuel Efficiency Enhancer in Highly Downsized GDI Engines," in *SAE Technical Paper*. SAE International, Apr 2015, SAE Technical Paper 2015-01-0393. [Online]. Available: https://doi.org/10.4271/2015-01-0393

[328] I. Hermann, C. Glahn, M. Kluin, M. Paroll, and W. Gumprich, "Water Injection for Gasoline Engines - Quo Vadis?" in *Knocking in Gasoline Engines*. Springer, Cham, Nov 2017, pp. 299–321. [Online]. Available: https://doi.org/10.1007/978-3-319-69760-4_18

[329] C. Heinrich, H. Dörksen, A. Esch, and K. Krämer, "Gasoline water direct injection (GWDI) as a key feature for future gasoline engines," in *Knocking in Gasoline Engines*, M. Günther and M. Sens, Eds. Springer International Publishing, 2018, pp. 322–337.

[330] M. Hunger, T. Böcking, U. Walther, M. Günther, N. Freisinger, and G. Karl, "Potential of direct water injection to reduce knocking and increase the efficiency of gasoline engines," in *Knocking in Gasoline Engines*, M. Günther and M. Sens, Eds. Springer International Publishing, 2018, pp. 338–359.

[331] S. Paltrinieri, F. Mortellaro, N. Silvestri, L. Rolando, M. Medda, and D. Corrigan, "Water Injection Contribution to Enabling Stoichiometric Air-to-Fuel Ratio Operation at Rated Power Conditions of a High-Performance DISI Single Cylinder Engine," in *SAE Technical Paper*. SAE International, Sep 2019, SAE Technical Paper 2019-01-0173. [Online]. Available: https://doi.org/10.4271/2019-24-0173

[332] A. Vacca, M. Bargende, M. Chiodi, T. Franken, C. Netzer, M. S. Gern, M. Kauf, and A. C. Kulzer, "Analysis of Water Injection Strategies to Exploit the Thermodynamic Effects of Water in Gasoline Engines by Means of a 3D-CFD Virtual Test Bench," in *SAE Technical Paper*. SAE International, Sep 2019, SAE Technical Paper 2019-24-0102. [Online]. Available: https://doi.org/10.4271/2019-24-0102

[333] L. Seidel, T. Franken, F. Mauss, A. Matrisciano, A. C. Kulzer, and F. Schuerg, "Analysis of the water addition efficiency on knock suppression for different octane ratings," *SAE International Journal of Advances and Current Practices in Mobility*, vol. 2, no. 5, pp. 2531–2552, 2020. [Online]. Available: https://doi.org/10.4271/2020-01-0551

[334] ANSYS, "CHEMKIN Pro Homepage," accessed: 12/04/2021. [Online]. Available: https://www.ansys.com/products/fluids/ansys-chemkin-pro

[335] Convergent Science, "Converge homepage," accessed: 12/04/2021. [Online]. Available: https://convergecfd.com

[336] SIEMENS, "Simcenter STAR-CCM+ Homepage," accessed: 12/04/2021. [Online]. Available: https://www.plm.automation.siemens.com/global/en/products/simcenter/STAR-CCM.html

[337] N. Atef, G. Kukkadapu, S. Y. Mohamed, M. A. Rashidi, C. Banyon, M. Mehl, K. A. Heufer, E. F. Nasir, A. Alfazazi, A. K. Das, C. K. Westbrook, W. J. Pitz, T. Lu, A. Farooq, C.-J. Sung, H. J. Curran, and S. M. Sarathy, "A comprehensive iso-octane combustion model with improved thermochemistry and chemical kinetics," *Combustion and Flame*, vol. 178, pp. 111–134, 2017. [Online]. Available: https://www.sciencedirect.com/science/article/pii/S0010218016304059

[338] J. A. Miller, R. Sivaramakrishnan, Y. Tao, C. F. Goldsmith, M. P. Burke, A. W. Jasper, N. Hansen, N. J. Labbe, P. Glarborg, and J. Zádor, "Combustion Chemistry in the Twenty-first Century: Developing Theory-informed Chemical Kinetics Models," *Progress in Energy and Combustion Science*, vol. 83, p. 100886, 2021. [Online]. Available: https://www.sciencedirect.com/science/article/pii/S0360128520300964

[339] S. Luisi, V. Doria, A. Stroppiana, F. Millo, and M. Mirzaeian, "Experimental Investigation on Early and Late Intake Valve Closures for Knock Mitigation through Miller Cycle in a Downsized Turbocharged Engine," in *SAE 2015 World Congress & Exhibition*. SAE International, Apr 2015, SAE Technical Paper 2015-01-0760. [Online]. Available: https://doi.org/10.4271/2015-01-0760

[340] J. E. Ketterer, E. Gautier, and E. J. Keating, "The Development and Evaluation of Robust Combustion Systems for Miller Cycle Engines," in *WCX World Congress Experience*. SAE International, Apr 2018, SAE Technical Paper 2018-01-1416. [Online]. Available: https://doi.org/10.4271/2018-01-1416

[341] G. P. Blair, *Design and Simulation of Four-Stroke Engines*. Warrendale: SAE International, Aug 1999, ISBN: 978-0-7680-0440-3.

[342] J. Taylor, D. Gurney, P. Freeland, R. Dingelstadt, J. Stehlig, and V. Bruggesser, "Intake Manifold Length Effects on Turbocharged Gasoline Downsizing Engine Performance and Fuel Economy," in *SAE 2012 World Congress & Exhibition*. SAE International, Apr 2012, SAE Technical Paper 2012-01-0714. [Online]. Available: https://doi.org/10.4271/2012-01-0714

[343] E. Toulson, H. J. Schock, and W. P. Attard, "A review of pre-chamber initiated jet ignition combustion systems," in *SAE 2010 Powertrains Fuels & Lubricants Meeting*. SAE International, 2010. [Online]. Available: https://doi.org/10.4271/2010-01-2263

[344] W. P. Attard and P. Parsons, "Flame kernel development for a spark initiated pre-chamber combustion system capable of high load, high efficiency and near zero NOx emissions," *SAE International Journal of Engines*, vol. 3, no. 2, pp. 408–427, 2010. [Online]. Available: https://doi.org/10.4271/2010-01-2260

[345] W. P. Attard and H. Blaxill, "A single fuel pre-chamber jet ignition powertrain achieving high load, high efficiency and near zero nox emissions," *SAE International Journal of Engines*, vol. 5, no. 3, pp. 734–746, 2011. [Online]. Available: https://doi.org/10.4271/2011-01-2023

[346] W. P. Attard, M. Bassett, P. Parsons, and H. Blaxill, "A New Combustion System Achieving High Drive Cycle Fuel Economy Improvements in a Modern Vehicle Powertrain," in *SAE 2011 World Congress& Exhibition*. SAE International, Apr 2011, SAE Technical Paper 2011-01-0664. [Online]. Available: https://doi.org/10.4271/2011-01-0664

[347] W. P. Attard and H. Blaxill, "A Lean Burn Gasoline Fueled Pre-Chamber Jet Ignition Combustion System Achieving High Efficiency and Low NOx at Part Load," in *SAE 2012 World Congress& Exhibition*. SAE International, Apr 2012, SAE Technical Paper 2012-01-1146. [Online]. Available: https://doi.org/10.4271/2012-01-1146

[348] P. Litke, W. P. Attard, H. Blaxill, and E. K. Anderson, "Knock limit extension with a gasoline fueled pre-chamber jet igniter in a modern vehicle powertrain," *SAE International Journal of Engines*, vol. 5, no. 3, pp. 1201–1215, 2012. [Online]. Available: https://doi.org/10.4271/2012-01-1143

[349] D. Mazzoni, E. Musu, F. Bedogni, G. Pivetti, P. Zolesi, and S. Magistrali, "European patent ep17190088a: Gasoline internal combustion engine having precombustion chamber and two spark plugs," March 2019, JP2019049258A. [Online]. Available: https://worldwide.espacenet.com/patent/search?q=pn%3DJP2019049258A

[350] Maserati, "Maserati presents Nettuno: the new 100% Maserati engine that adopts F1 technology for a road car," 2020, Accessed Jan 2021. [Online]. Available: https://www.media.maserati.com/en-ww/releases/1575

[351] D. J. Corrigan, M. Di Sacco, M. Medda, S. Paltrinieri, and V. Rossi, "European patent ep3561255a1: High-performance internal combustion engine with improved handling of emissions and method for controlling such engine," October 2019, EP3561255A1. [Online]. Available: https://worldwide.espacenet.com/patent/search?q=pn%3DEP3561255A1

[352] H. Yun, N. Wermuth, and P. Najt, "Extending the High Load Operating Limit of a Naturally-Aspirated Gasoline HCCI Combustion Engine," *SAE Int. J. Engines*, vol. 3, pp. 681–699, Apr 2010. [Online]. Available: https://doi.org/10.4271/2010-01-0847

[353] L. Manofsky, J. Vavra, D. N. Assanis, and A. Babajimopoulos, "Bridging the Gap between HCCI and SI: Spark-Assisted Compression Ignition," in *SAE Technical Paper*. SAE International, Apr 2011, SAE Technical Paper 2011-01-1179. [Online]. Available: https://doi.org/10.4271/2011-01-1179

[354] J. E. Dec and Y. Yang, "Boosted HCCI for high power without engine knock and with ultra-low nox emissions - using conventional gasoline," *SAE International Journal of Engines*, vol. 3, no. 1, pp. 750–767, 2010. [Online]. Available: https://doi.org/10.4271/2010-01-1086

[355] A. Maria, W. K. Cheng, K. Kar, and W. Cannella, "Understanding knock metric for controlled auto-ignition engines," *SAE International Journal of Engines*, vol. 6, no. 1, pp. 533–540, 2013. [Online]. Available: https://doi.org/10.4271/2013-01-1658

[356] A. Iijima, N. Ito, T. Shimada, M. Yamada, and H. Shoji, "A study of HCCI knocking accompanied by pressure oscillations based on visualization of the entire bore area," *SAE International Journal of Engines*, vol. 7, no. 4, pp. 1863–1874, 2014. [Online]. Available: https://doi.org/10.4271/2014-01-2664

[357] A. Iijima, H. Shoji, Y. Yoshida, C. Rin, M. Yamada, T. Shimada, and N. Ito, "A study of the behavior of in-cylinder pressure waves under HCCI knocking by using an optically accessible engine," *SAE International Journal of Engines*, vol. 9, no. 1, pp. 1–10, 2015. [Online]. Available: https://doi.org/10.4271/2015-01-1795

[358] E. Nakai, T. Goto, K. Ezumi, Y. Tsumura, K. Endou, Y. Kanda, T. Urushihara, M. Sueoka, and M. Hitomi, "Mazda SKYACTIV-X 2.0L Gasoline Engine," in *28th Aachen Colloquium Automobile and Engine Technology*, 2019.

[359] E. Kasseris and J. B. Heywood, "Charge cooling effects on knock limits in SI DI engines using gasoline/ethanol blends: Part 2-effective octane numbers," *SAE International Journal of Fuels and Lubricants*, vol. 5, no. 2, pp. 844–854, 2012. [Online]. Available: https://doi.org/10.4271/2012-01-1284

[360] K. Steurs, C. Blomberg, and K. Boulouchos, "Formulation of a knock model for ethanol and iso-octane under specific consideration of the thermal boundary layer within the end-gas," *SAE International Journal of Engines*, vol. 7, no. 4, pp. 1752–1772, 2014. [Online]. Available: https://doi.org/10.4271/2014-01-2607

[361] K. Steurs, C. K. Blomberg, and K. Boulouchos, "Knock in an ethanol fueled spark ignition engine: Detection methods with cycle-statistical analysis and predictions using different auto-ignition models," *SAE International Journal of Engines*, vol. 7, no. 2, pp. 568–583, 2014. [Online]. Available: https://doi.org/10.4271/2014-01-1215

[362] T. G. Leone, E. D. Olin, J. E. Anderson, H. H. Jung, M. H. Shelby, and R. A. Stein, "Effects of fuel octane rating and ethanol content on knock, fuel economy, and co2 for a turbocharged di engine," *SAE International Journal of Fuels and Lubricants*, vol. 7, no. 1, pp. 9–28, 2014. [Online]. Available: https://doi.org/10.4271/2014-01-1228

[363] G. M. Chupka, E. Christensen, L. Fouts, T. L. Alleman, M. A. Ratcliff, and R. L. McCormick, "Heat of vaporization measurements for ethanol blends up to 50 volume percent in several hydrocarbon blendstocks and implications for knock in si engines," *SAE International Journal of Fuels and Lubricants*, vol. 8, no. 2, pp. 251–263, 2015. [Online]. Available: https://doi.org/10.4271/2015-01-0763

[364] E. Binder, P. Grigoriadis, M. Sens, J. Kitte, A. Schwindt, J. Trepohl, and L. Böttcher, "A Clean Methane ICE Concept with >45% Efficiency for Hybrid Powertrains," in *29th Aachen Colloquium Sustainable Mobility*, 2020.

[365] H. Stoffels, C. Weber, F. Graf, S. Lauer, J. Ehrhard, M. Moretti, and M. Neveling, "The Methane Fuel Based Turbocharged Direct Injection Engine in a Hybrid Powertrain - An Efficient Synergy," in *SAE Technical Paper*. SAE International, Sep 2019, SAE Technical Paper 2019-24-0201. [Online]. Available: https://doi.org/10.4271/2019-24-0201

[366] K. Johnson, M. J. Veenstra, D. Gotthold, K. Simmons, K. Alvine, B. Hobein, D. Houston, N. Newhouse, B. Yeggy, A. Vaipan, T. Steinhausler, and A. Rau, "Advancements and Opportunities for On-Board 700 Bar Compressed Hydrogen Tanks in the Progression Towards the Commercialization of Fuel Cell Vehicles," *SAE Int. J. Alt. Power.*, vol. 6, pp. 201–218, Mar 2017. [Online]. Available: https://doi.org/10.4271/2017-01-1183

[367] N. S. Matthias, T. Wallner, and R. Scarcelli, "A Hydrogen Direct Injection Engine Concept that Exceeds U.S. DOE Light-Duty Efficiency Targets," *SAE Int. J. Engines*, vol. 5, pp. 838–849, Apr 2012. [Online]. Available: https://doi.org/10.4271/2012-01-0653

[368] B. Heuser, "Closed carbon cycle mobility," November 2020. [Online]. Available: http://www.c3-mobility.de/wp-content/uploads/2020/11/2020_08_C3_Mobility_Projektvorstellung_Englisch.pdf

[369] J. Williams and H. Hamje, "Testing and Modelling the Effect of High Octane Petrols on an Adapted Vehicle," Concawe, Tech. Rep., May 2020, ISBN: 978-2-87567-119-6. [Online]. Available: https://www.concawe.eu/wp-content/uploads/Rpt_20-8.pdf

[370] D. Valdenaire and S. Mennecier, "High Octane Petrol Study," Concawe, Tech. Rep., Sep 2020, ISBN: 978-2-87567-125-5. [Online]. Available: https://www.concawe.eu/wp-content/uploads/Rpt_20-17.pdf

[371] P. Adomeit, A. Brassat, M. Günther, A. Amer, H. Babiker, J. Chang, and G. Kalghatgi, "Fuel effects on knock in a highly boosted direct injection spark ignition engine," *SAE International Journal of Fuels and Lubricants*, vol. 5, no. 3, pp. 1048–1065, 2012. [Online]. Available: https://doi.org/10.4271/2012-01-1634

[372] G. Kalghatgi, R. Head, J. Chang, Y. Viollet, H. Babiker, and A. Amer, "An alternative method based on toluene/n-heptane surrogate fuels for rating the anti-knock quality of practical gasolines," *SAE International Journal of Fuels and Lubricants*, vol. 7, no. 3, pp. 663–672, 2014. [Online]. Available: https://doi.org/10.4271/2014-01-2609

[373] G. Kalghatgi, H. Babiker, and J. Badra, "A simple method to predict knock using toluene, n-heptane and iso-octane blends (TPRF) as gasoline surrogates," *SAE International Journal of Engines*, vol. 8, no. 2, pp. 505–519, 2015. [Online]. Available: https://doi.org/10.4271/2015-01-0757

[374] S. Gail, R. F. Cracknell, D. Corrigan, A. Festa, V. Shankar, B. Poulet, G. Lovett, R. D. Büttgen, K. A. Heufer, R. Mariconti, M. Cucchi, and F. Mortellaro, "Evaluating a novel gasoline surrogate containing isopentane using a rapid compression machine and an engine," *Proceedings of the Combustion Institute*, vol. 38, no. 4, pp. 5643–5653, 2021. [Online]. Available: https://www.sciencedirect.com/science/article/pii/S1540748920305538

[375] M. Mehl, W. J. Pitz, C. K. Westbrook, and H. J. Curran, "Kinetic modeling of gasoline surrogate components and mixtures under engine conditions," *Proceedings of the Combustion Institute*, vol. 33, no. 1, pp. 193–200, 2011. [Online]. Available: https://www.sciencedirect.com/science/article/pii/S1540748910000787

[376] T. Kitada, M. Kuchita, S. Hayashi, T. Shirota, Y. Sakai, and H. Kawazoe, "A study on knocking prediction improvement using chemical reaction calculation," *SAE International Journal of Engines*, vol. 9, no. 1, pp. 201–209, 2015. [Online]. Available: https://doi.org/10.4271/2015-01-1905

[377] A. Fandakov, M. Bargende, A. C. Kulzer, and M. Grill, "Two-stage ignition occurrence in the end gas and modeling its influence on engine knock," *SAE International Journal of Engines*, vol. 10, no. 4, pp. 2109–2128, 2017. [Online]. Available: https://doi.org/10.4271/2017-24-0001

[378] N. Yokoo, T. Tomoda, K. Nakata, N. Kim, D. Vuilleumier, and M. Sjöberg, "Using chemical kinetics to understand effects of fuel type and compression ratio on knock-mitigation effectiveness of various egr constituents," *SAE International Journal of Advances and Current Practices in Mobility*, vol. 1, no. 4, pp. 1560–1580, 2019. [Online]. Available: https://doi.org/10.4271/2019-01-1140

[379] S. Fontanesi, S. Paltrinieri, A. D'Adamo, G. Cantore, and C. Rutland, "Knock tendency prediction in a high performance engine using LES and tabulated chemistry," *SAE International Journal of Fuels and Lubricants*, vol. 6, no. 1, pp. 98–118, 2013. [Online]. Available: https://doi.org/10.4271/2013-01-1082

[380] A. Robert, S. Richard, O. Colin, and T. Poinsot, "LES study of deflagration to detonation mechanisms in a downsized spark ignition engine," *Combustion and Flame*, vol. 162, no. 7, pp. 2788–2807, 2015. [Online]. Available: https://www.sciencedirect.com/science/article/pii/S0010218015001212

[381] M. Ritter, L.-M. Malbec, and O. Laget, "Assessment and Validation of Internal Aerodynamics and Mixture Preparation in Spark-Ignition Engine Using LES Approach," *SAE International Journal of Advances and Current Practices in Mobility*, vol. 3, no. 1, pp. 95–112, Sep 2020. [Online]. Available: https://doi.org/10.4271/2020-01-2009

[382] E. Corti, C. Forte, G. M. Bianchi, and D. Moro, "Relating knocking combustions effects to measurable data," *SAE International Journal of Engines*, vol. 8, no. 5, pp. 2133–2144, 2015. [Online]. Available: https://doi.org/10.4271/2015-24-2429

[383] A. D'Adamo, S. Breda, S. Fontanesi, and G. Cantore, "A RANS-based CFD model to predict the statistical occurrence of knock in spark-ignition engines," *SAE International Journal of Engines*, vol. 9, no. 1, pp. 618–630, 2016. [Online]. Available: https://doi.org/10.4271/2016-01-0581

[384] A. D'Adamo, S. Breda, S. Iaccarino, F. Berni, S. Fontanesi, B. Zardin, M. Borghi, A. Irimescu, and S. Merola, "Development of a RANS-based knock model to infer the knock probability in a research spark-ignition engine," *SAE International Journal of Engines*, vol. 10, no. 3, pp. 722–739, 2017. [Online]. Available: https://doi.org/10.4271/2017-01-0551

[385] G. Valentino, S. Breda, A. D'Adamo, S. Fontanesi, N. Giovannoni, F. Testa, A. Irimescu, S. Merola, and C. Tornatore, "CFD analysis of combustion and knock in an optically accessible GDI engine," *SAE International Journal of Engines*, vol. 9, no. 1, pp. 641–656, 2016. [Online]. Available: https://doi.org/10.4271/2016-01-0601

[386] F. Mauss, S. Bjerkborn, K. Frojd, and C. Perlman, "A Monte Carlo based turbulent flame propagation model for predictive SI in-cylinder engine simulations employing detailed chemistry for accurate knock prediction," *SAE International Journal of Engines*, vol. 5, no. 4, pp. 1637–1647, 2012. [Online]. Available: https://doi.org/10.4271/2012-01-1680

[387] D. Kozarac, R. Tomic, I. Taritas, J.-Y. Chen, and R. W. Dibble, "A model for prediction of knock in the cycle simulation by detail characterization of fuel and temperature stratification," *SAE International Journal of Engines*, vol. 8, no. 4, pp. 1520–1534, 2015. [Online]. Available: https://doi.org/10.4271/2015-01-1245

[388] F. Minarelli, D. Cacciatore, D. Siano, V. De Bellis, and L. Teodosio, "Knock and cycle by cycle analysis of a high performance V12 spark ignition engine. part 1: Experimental data and correlations assessment," *SAE International Journal of Engines*, vol. 8, no. 5, pp. 1993–2001, 2015. [Online]. Available: https://doi.org/10.4271/2015-24-2392

[389] F. Bozza, F. Minarelli, D. Cacciatore, and V. De Bellis, "Knock and cycle by cycle analysis of a high performance V12 spark ignition engine. part 2: 1D combustion and knock modeling," *SAE International Journal of Engines*, vol. 8, no. 5, pp. 2002–2011, 2015. [Online]. Available: https://doi.org/10.4271/2015-24-2393

[390] S. Fontanesi, E. Severi, F. Bozza, V. De Bellis, and D. Siano, "Analysis of knock tendency in a small VVA turbocharged engine based on integrated 1D-3D simulations and auto-regressive technique," *SAE International Journal of Engines*, vol. 7, no. 1, pp. 72–86, 2014. [Online]. Available: https://doi.org/10.4271/2014-01-1065

[391] A. Kikusato, K. Jin, and Y. Daisho, "A numerical simulation study on improving the thermal efficiency of a spark ignited engine — part 1: Modeling of a spark ignited engine combustion to predict engine performance considering flame propagation, knock, and combustion chamber wall —," *SAE International Journal of Engines*, vol. 7, no. 1, pp. 96–105, 2014. [Online]. Available: https://doi.org/10.4271/2014-01-1073

[392] A. Kikusato, K. Terahata, K. Jin, and Y. Daisho, "A numerical simulation study on improving the thermal efficiency of a spark ignited engine — part 2: Predicting instantaneous combustion chamber wall temperatures, heat losses and knock —," *SAE International Journal of Engines*, vol. 7, no. 1, pp. 87–95, 2014. [Online]. Available: https://doi.org/10.4271/2014-01-1066

[393] N. Peters, B. Kerschgens, and G. Paczko, "Super-knock prediction using a refined theory of turbulence," *SAE International Journal of Engines*, vol. 6, no. 2, pp. 953–967, 2013. [Online]. Available: https://doi.org/10.4271/2013-01-1109

[394] T. Lauer, M. Heiss, N. Bobicic, and S. Pritze, "Model Approach for Pre-Ignition Mechanisms," *MTZ Worldwide*, vol. 75, pp. 44 – 49, 2014. [Online]. Available: https://doi.org/10.1007/s38313-014-0010-6

[395] Z. Jia, M. Wang, H. Liu, Z. Wang, Y. Qi, X. He, J.-X. Wang, M. Wooldridge, and M. Fatouraie, "Highly turbocharged gasoline engine and rapid compression machine studies of super-knock," *SAE International Journal of Engines*, vol. 9, no. 3, pp. 1475–1485, 2016. [Online]. Available: https://doi.org/10.4271/2016-01-0686

[396] G. Kalghatgi, I. Algunaibet, and K. Morganti, "On knock intensity and superknock in SI engines," *SAE International Journal of Engines*, vol. 10, no. 3, pp. 1051–1063, 2017. [Online]. Available: https://doi.org/10.4271/2017-01-0689

[397] M. Ohtomo, T. Suzuoki, S. Yamamoto, H. Miyagawa, M. Ohtomo, T. Suzuoki, S. Yamamoto, and H. Miyagawa, "Effect of fuel-air mixture dilution on knock intensity in an SI engine," *SAE International Journal of Engines*, vol. 11, no. 6, pp. 757–768, 2018. [Online]. Available: https://doi.org/10.4271/2018-01-0211

[398] J. Cho and H. H. Song, "Understanding the effect of inhomogeneous mixing on knocking characteristics of iso-octane by using rapid compression machine," *SAE International Journal of Engines*, vol. 11, no. 6, pp. 769–781, 2018. [Online]. Available: https://doi.org/10.4271/2018-01-0212

[399] F. Catapano, M. Costa, G. Marseglia, P. Sementa, U. Sorge, and B. M. Vaglieco, "Experimental and numerical investigation in a turbocharged GDI engine under knock condition by means of conventional and non-conventional methods," *SAE International Journal of Engines*, vol. 8, no. 2, pp. 437–446, 2015. [Online]. Available: https://doi.org/10.4271/2015-01-0397

[400] F. Catapano, P. Sementa, and B. M. Vaglieco, "Characterization of knock tendency and onset in a GDI engine by means of conventional measurements and a non-conventional flame dynamics optical analysis," *SAE International Journal of Engines*, vol. 10, no. 5, pp. 2439–2450, 2017. [Online]. Available: https://doi.org/10.4271/2017-24-0099

[401] Y. Imaoka, K. Shouji, T. Inoue, and T. Noda, "A study of combustion technology for a high compression ratio engine: The influence of combustion chamber wall temperature on knocking," *SAE International Journal of Engines*, vol. 9, no. 2, pp. 768–776, 2016. [Online]. Available: https://doi.org/10.4271/2016-01-0703

[402] A. Iijima, T. Izako, T. Ishikawa, T. Yamashita, S. Takahata, H. Kudo, K. Shimizu, M. Tanabe, and H. Shoji, "Analysis of Interaction between Autoignition and Strong Pressure Wave Formation during Knock in a Supercharged SI Engine Based on High Speed Photography of the End Gas," *SAE International Journal of Engines*, vol. 10, no. 5, pp. 2616–2623, Nov 2017.

[403] K. Huber and J. Hauber, "Cylinder pressure-based knock detection - challenges in cylinder pressure indication and application in a new engine-based fuel test method," in *Knocking in Gasoline Engines*. Springer, Cham, Nov 2013, pp. 119–141.

[404] A. Broatch, J. Gomez-Soriano, Y. Wu, T. Lu, P. Pal, C. P. Kolodziej, S. Choi, S. Som, and Y. C. See, "Development of a virtual CFR engine model for knocking combustion analysis," *SAE International Journal of Engines*, vol. 11, no. 6, pp. 1069–1082, 2018. [Online]. Available: https://doi.org/10.4271/2018-01-0187

[405] M. C. Jespersen, T. Rockstroh, C. P. Kolodziej, S. S. Goldsborough, and T. Wallner, "Insights into engine knock: Comparison of knock metrics across ranges of intake temperature and pressure in the CFR engine," *SAE International Journal of Fuels and Lubricants*, vol. 11, no. 4, pp. 545–561, 2018. [Online]. Available: https://doi.org/10.4271/2018-01-0210

[406] A. Hoth, J. Pulpeiro Gonzalez, C. P. Kolodziej, and T. Rockstroh, "Effects of lambda on knocking characteristics and RON rating," *SAE International Journal of Advances and Current Practices in Mobility*, vol. 1, no. 3, pp. 1188–1201, 2019. [Online]. Available: https://doi.org/10.4271/2019-01-0627

[407] B. Xiao, S. Wang, and R. G. Prucka, "Virtual combustion phasing target correction in the knock region for model-based control of multi-fuel SI engines," *SAE International Journal of Engines*, vol. 6, no. 1, pp. 228–236, 2013. [Online]. Available: https://doi.org/10.4271/2013-01-0307

[408] E. Corti, C. Forte, G. M. Bianchi, and L. Zoffoli, "A control-oriented knock intensity estimator," *SAE International Journal of Engines*, vol. 10, no. 4, pp. 2219–2229, 2017. [Online]. Available: https://doi.org/10.4271/2017-24-0055

[409] J. M. Spelina, J. C. Peyton Jones, and J. Frey, "Recent advances in knock analysis, simulation, and control," *SAE International Journal of Engines*, vol. 7, no. 2, pp. 947–955, 2014. [Online]. Available: https://doi.org/10.4271/2014-01-1349

[410] J. C. Peyton Jones and J. Frey, "Threshold optimization and performance evaluation of a classical knock controller," *SAE International Journal of Engines*, vol. 8, no. 3, pp. 1021–1028, 2015. [Online]. Available: https://doi.org/10.4271/2015-01-0871

[411] J. Peyton Jones, J. M. Spelina, and J. Frey, "Control-oriented knock simulation," *SAE International Journal of Engines*, vol. 9, no. 2, pp. 1201–1209, 2016. [Online]. Available: https://doi.org/10.4271/2016-01-0821

[412] M. A. Panza, D. D'Agostino, and D. Siano, "Knock detection based on MAPO analysis, AR model and discrete wavelet transform applied to the in-cylinder pressure data: Results and comparison," *SAE International Journal of Engines*, vol. 8, no. 1, pp. 1–13, 2014. [Online]. Available: https://doi.org/10.4271/2014-01-2547

[413] A. Rosetti, C. Iotti, and G. Cantore, "Intake Manifold Primary Trumpet Tuning Options for Fuel Flow Limited High Performance I.C.E." in *14th International Conference on Engines & Vehicles*. SAE International, Sep 2019, SAE Technical Paper 2019-24-0005. [Online]. Available: https://doi.org/10.4271/2019-24-0005

[414] K. H. Clasen and L. Koopmans, "Investigation of Homogeneous Lean SI Combustion in High Load Operating Conditions," *SAE Int. J. Adv. & Curr. Prac. in Mobility*, vol. 2, pp. 2051–2066, Apr 2020. [Online]. Available: https://doi.org/10.4271/2020-01-0959

[415] P. Symonds, "Future Powertrains in F1," Presented at the IMechE High Performance Powertrains Conference, Online, 2020.

[416] U. Burke, R. Cracknell, M. Evans, B. Poulet, S. Gail, I. Kitsopanidis, D. Salters, and K. Heufer, "Use of a rapid compression machine to characterize the anti-knock properties of high octane fuels," Presented at the 36th International Symposium on Combustion , Seoul, 2016.

[417] "FIA Formula 1 Regulations 2021," 2021. [Online]. Available: https://www.fia.com/regulation/category/110

[418] "Mercedes AMG F1 INSIGHT: Five Examples Why F1 Is Accelerating the Future," 2018, Accessed Jan 2021. [Online]. Available: https://www.mercedesamgf1.com/en/news/2018/10/insight-five-examples-why-f1-is-accelerating-the-future/

[419] G. Zhang, Q. Wang, G. Chen, D. de Oliveira, J. Park, M. Wei, S. Zhang, W. Lu, F. Zhao, and I. Scholten, "Geely hybrid engine: World class efficiency for hybrid vehicles," in *29th Aachen Colloquium Sustainable Mobility*, 2020.

[420] M. Cimini, "Garrett E-Turbo Technology Accelerating Global Powertrain Electrification Trends Beginning with Mercedes-AMG," July 2020. [Online]. Available: https://www.garrettmotion.com/news/media-materials/press-releases/

[421] D. Splitter, A. Pawlowski, and R. Wagner, "A historical analysis of the co-evolution of gasoline octane number and spark-ignition engines," *Frontiers in Mechanical Engineering*, vol. 1, p. 16, 2016. [Online]. Available: https://www.frontiersin.org/article/10.3389/fmech.2015.00016

[422] V. Mittal, "Distribution of knock frequencies in modern engines compared to historical data," in *International Powertrains, Fuels & Lubricants Meeting*. SAE International, Sep 2018, sAE Technical Paper 2018-01-1666. [Online]. Available: https://doi.org/10.4271/2018-01-1666

[423] A. Swarts and V. Kalaskar, "Bridging the knock severity gap to CFR octane rating engines," *SAE International Journal of Advances and Current Practices in Mobility*, vol. 3, no. 1, pp. 240–249, 2021. [Online]. Available: https://doi.org/10.4271/2020-01-2050

[424] M. Khosravi and H. Pitsch, "Investigation of knock and resonance under heavy knocking conditions in gasoline engines using continuous wavelet transform," *SAE International Journal of Engines*, vol. 14, no. 4, pp. 595–608, 2021. [Online]. Available: https://doi.org/10.4271/03-14-04-0036

[425] B. Pla, J. D. L. Morena, P. Bares, and I. Jiménez, "Knock analysis in the crank angle domain for low-knocking cycles detection," in *WCX SAE World Congress Experience*. SAE International, 2020, SAE Technical Paper 2020-01-0549. [Online]. Available: https://doi.org/10.4271/2020-01-0549

[426] K. Senecal and F. Leach, *Racing Toward Zero: The Untold Story of Driving Green*. Warrendale: SAE International, 2021.

[427] D. J. Corrigan and S. Fontanesi, "Knock: A century of research," *SAE International Journal of Engines*, vol. 15, no. 1, 2022. [Online]. Available: https://doi.org/10.4271/03-15-01-0004

[428] C. R. Pond and J. Biundo, "Gasoline engine knock analysis using cylinder pressure data," in *International Congress and Exposition*. SAE International, 1998, SAE Technical Paper 980896. [Online]. Available: https://doi.org/10.4271/980896

[429] D. J. Corrigan, S. Breda, and S. Fontanesi, "A simple CFD model for knocking cylinder pressure data interpretation: Part 1," in *15th International Conference on Engines and Vehicles*. SAE International, 2021. [Online]. Available: https://doi.org/10.4271/2021-24-0051

[430] A. D. Pierce, *Acoustics: An Introduction to Its Physical Principles and Applications*, 3rd ed. Springer, Cham, 2019.

[431] SIEMENS, "STAR-CD Methodology, Version 4.30."

[432] R. D. Reitz and R. Diwakar, "Effect of drop breakup on fuel sprays," in *SAE International Congress and Exposition*. SAE International, 1986. [Online]. Available: https://doi.org/10.4271/860469

[433] J. H. Gary and G. E. Handwerk, *Petroleum Refining Technology and Economics*, 4th ed. Dekker, Basel, 2001.

[434] A. Lewis, K. Giles, S. Akehurst, J. Turner, A. Popplewell, R. Patel, S. Remmert, S. Campbell, R. Cracknell, and A. Schuetze, "Octane appetite: The relevance of a lower limit to the MON specification in a downsized, highly boosted DISI engine," *SAE International Journal of Fuels and Lubricants*, vol. 7, no. 3, pp. 743–755, 2014. [Online]. Available: https://doi.org/10.4271/2014-01-2718

[435] D. J. Corrigan, "Prechamber ignition literature survey," Internal Report, Ferrari Gestione Sportiva, 2011.

[436] D. J. Corrigan, D. Carpentiero, E. Pascolini, M. Maffioletti, and D. Salters, "Mono engine: First TJI (prechamber) engine analysis," Internal Report, Ferrari Gestione Sportiva, 2015.

[437] F. Titus, F. Rauber, and K. Beck, "Interim report on mono optical investigations," Internal Report to Ferrari Gestione Sportiva, MOT (APL Group), 2015.

[438] D. J. Corrigan, "106 prechamber direct injection," Internal Report, Ferrari Gestione Sportiva, 2015.

[439] D. Corrigan, "107 ICOS analysis," Internal Report, Ferrari Gestione Sportiva, 2016.

[440] I. Whelan, "F154BD - spark sweep pre-camera," Internal Report, Ferrari SpA, 2015.

[441] D. J. Corrigan, M. Medda, S. Paltrinieri, V. Rossi, and M. Cucchi, "Prechamber investigations - summary of activity to date in Ferrari GT," Internal Report, Ferrari SpA, 2018.

[442] N. Silvestri, S. Paltrinieri, M. D. Sacco, M. Cozzolino, and D. J. Corrigan, "Sviluppo patrizia," Internal Report, Ferrari SpA, 2020.

[443] N. Silvestri, R. Tonelli, and D. J. Corrigan, "Mono patrizia: Indagine su condotti aspirazione," Internal Report, Ferrari SpA, 2020.

[444] European Commission, Directorate-General for Climate Action, "Proposal for a REGULATION OF THE EUROPEAN PARLIAMENT AND OF THE COUNCIL amending Regulation (EU) 2019/631 as regards strengthening the CO2 emission performance standards for new passenger cars and new light commercial vehicles in line with the Union's increased climate ambition," *Procedure 2021/0197/COD*, 2021.

[445] ACEA. Fuel types of new cars, 2020. Accessed: 25/10/2021. [Online]. Available: https://www.acea.auto/fuel-pc/fuel-types-of-new-cars-electric-10-5-hybrid-11-9-petrol-47-5-market-share-full-year-2020/

[446] M. Rothbart, "e-fuel production via renewables and the impact on the in-use CO2 performance," in *SAE Powertrains, Fuels and Lubricants Meeting*. SAE International, 2020. [Online]. Available: https://doi.org/10.4271/2020-01-2139

[447] E. Rossi, S. Hummel, F. Cupo, A. Vacca, M. Chiodi, M. Bargende, J. Villforth, A. C. Kulzer, and H.-P. Deeg, "Experimental and numerical investigation for improved mixture formation of an efuel compared to standard gasoline," in *15th International Conference on Engines and Vehicles*. SAE International, 2021. [Online]. Available: https://doi.org/10.4271/2021-24-0019

[448] L. Rouleau, F. Duffour, B. Walter, R. Kumar, and L. Nowak, "Experimental and numerical investigation on hydrogen internal combustion engine," in *15th International Conference on Engines and Vehicles*. SAE International, 2021. [Online]. Available: https://doi.org/10.4271/2021-24-0060

[449] Q. Tang, R. Sampath, M. E. Marquez, P. Sharma, P. Hlaing, M. B. Houidi, E. Cenker, J. Chang, G. Magnotti, and B. Johansson, "Optical diagnostics on the pre-chamber jet and main chamber ignition in the active pre-chamber combustion," *Combustion and Flame*, vol. 228, pp. 218–235, 2021. [Online]. Available: https://www.sciencedirect.com/science/article/pii/S0010218021000638

[450] M. F. Palakunnummal, S. Priyadarshi, M. Ellis, and M. Nazha, "A cylinder pressure-based knock detection method for pre-chamber ignition gasoline engine." [Online]. Available: https://doi.org/10.4271/03-14-03-0024

[451] L. A. Gussak, V. P. Karpov, and Y. V. Tikhonov, "The application of lag-process in prechamber engines," in *Passenger Car Meeting and Exposition*. SAE International, 1979. [Online]. Available: https://doi.org/10.4271/790692

[452] S. Mallat, "A theory for multiresolution signal decomposition: the wavelet representation," *IEEE Transactions on Pattern Analysis and Machine Intelligence*, vol. 11, no. 7, pp. 674–693, 1989.

[453] J. Ghojel, "Review of the development and applications of the Wiebe function: A tribute to the contribution of Ivan Wiebe to engine research," *International Journal of Engine Research*, vol. 11, p. 297, 2010.

[454] D. J. Corrigan, "Second study of the effects of transients on knock," Internal Report, Ferrari Gestione Sportiva, 2013.

[455] D. J. Corrigan and E. Pascolini, "Knock thermal model update," Internal Report, Ferrari Gestione Sportiva, 2014.

[456] D. J. Corrigan, "Race weekend knock analysis - monaco," Internal Report, Ferrari Gestione Sportiva, 2014.

[457] A. Borelli and D. Corrigan, "Introduzione e calibrazione thermal model," Internal Report, Ferrari SpA, 2021.

APPENDIX $\mathcal{A}$

List of Outputs

Appendix A. List of Outputs

Table A.1: Outputs during PhD

Title	Type (Status)	Contribution
Water Injection Contribution to Enabling Stoichiometric Air-to-Fuel Ratio Operation at Rated Power Conditions of a High-Performance DISI Single Cylinder Engine	Technical Paper (Published [331])	Responsible for the experimental activity, co-author
Evaluating a novel gasoline surrogate containing isopentane using a rapid compression machine and an engine	Journal Article (Published [374])	Responsible for the engine activity, co-author
High Performance Internal Combustion Engine with Improved Handling of Emissions and Method for Controlling Such Engine	European Patent (Granted [351])	Lead author, inventor
Knock: A Century of Research	Journal Article (Published [427])	Lead author
Procedimento ed apparato per regolare la fasatura di accensione di un motore a combustione interna	Italian Patent (Awaiting Feedback)	Author, inventor
A Simple CFD Model for Knocking Cylinder Pressure Data Interpretation: Part 1	Technical Paper (Published [429])	Lead author
Knocking Cylinder Pressure Data Interpretation for Modern High Performance Engines - A Computational Fluid Dynamics Informed Approach	Journal Article (Accepted)	Lead author
Engine Knock Detection Methods for Spark Ignition and Prechamber Combustion Systems in a High Performance Engine	Journal Article (Accepted)	Lead author

APPENDIX B

Annual Reports

B.1 Year 1

Dáire James Corrigan, PhD student (Dottorato Industriale con Ferrari SpA)

03/11/19

Report about the first year:

Ferrari is a manufacturer of both high performance road cars and Formula 1 single-seaters. During my PhD, I will contrast these two areas of activity and in particular identify where road-car powertrain development can adopt approaches and technology seen in the racing world.

It is important to realise that the applications of powertrain for on-road and on-track use are fundamentally different. Figure 1 shows the relative importance of various powertrain objectives in order to realize a successful product. (This figure is illustrative and based on the author's experience of both these environments rather than representing an official Ferrari company view). It shows that the most important common objective is full load performance.

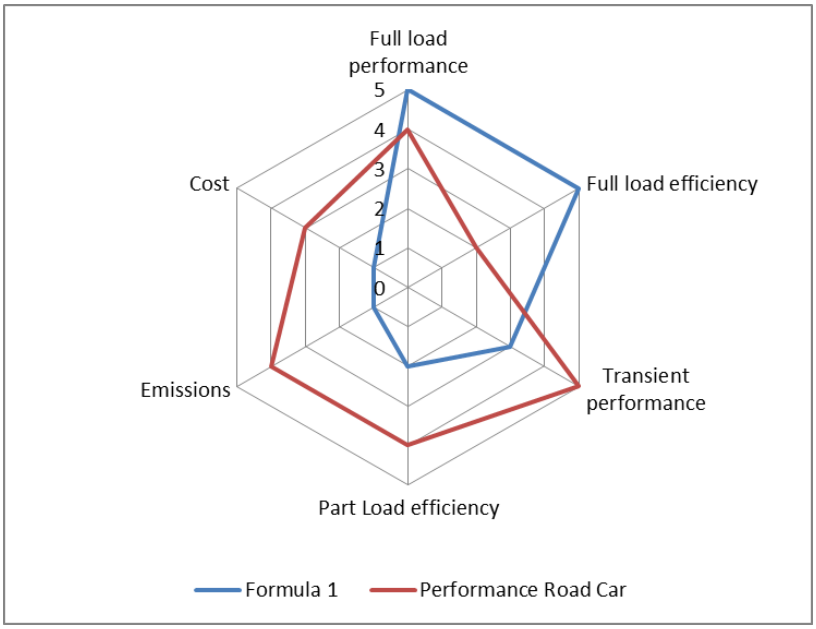

Fig.1 – Comparison between Development Objectives between Performance Road Car and Formula 1 Powertrain Development

Engineers have been endeavouring to improve full-load performance of the Internal Combustion Engine (ICE) since its inception. For a normally aspirated engine, the main driver is airflow – the more air that can be induced into the combustion chamber, the more fuel can be oxidized releasing more heat which is ultimately converted to kinetic energy in order to accelerate a vehicle. In recent years, both Formula 1 and the majority of performance road cars have moved to turbocharging however.

A turbocharged engine is typically not airflow limited, or at least is not inherently so. Much greater charge can be trapped in the combustion chamber each cycle than is conventionally the case for a normally aspirated engine but this increases the risk of another significant performance limitation – knock.

Knock may also occur on normally aspirated engines but it is much more prevalent with turbocharging. Many statements of what knock actually is have been made over the years. The accepted interpretation currently, is that knock occurs due to an auto-ignition event in the end-gas of the combustion chamber causing a rapid localized release of heat leading to pressure waves propagating across the combustion chamber. The localized heat release may melt the nearby region of the combustion chamber. The pressure

waves also tend to set up oscillations in the combustion chamber and can lead to piston ring or other mechanical damage. The pressure waves are how knock is normally identified and quantified experimentally.

Knock is effectively a race between the controlled combustion of the charge by the flame front and the normally uncontrolled end gas auto ignition chemistry. If the flame front arrives before the induction time of the end gas has expired, no knock will occur. On the other hand, if the flame front is rather slow, or the end gas temperature and pressure are very high, knock is much more likely. The end gas temperature can be lowered either by using a lower compression ratio or retarding the ignition timing. Both of these will lower efficiency however, hence are undesirable.

A number of technologies can be applied to combat knock without losing efficiency. Table 1 reassumes five major areas which are relevant both in road and race car applications. In this first year, I have worked on two of these in the road car environment having already experience from Formula 1 – Dilution and Prechambers.

Tab.1 – Key Technologies for Knock Mitigation

Technology	Flame Front Propagation	End Gas Reactivity	Cyclic Variation	Notes
High tumble ports	:-)	:-|	:-)	Increases boost requirement
Prechamber	:-)	:-|	:-)	Issues with part load
Dilution	:-(	:-)	:-(	F1: lean, road car: EGR or water injection
Miller	:-(	:-)	:-(	Increases boost requirement
Fuel development	:-)	:-)	:-)	Most relevant for F1

Dilution improves the knock limit by making the end gas less reactive. It may be achieved simply by running lean and this approach is applied in Formula 1. A three way catalyst only works in a narrow band around stoichiometry however and hence running lean is rarely applied with spark ignition road car engines. An analogous approach is to add an inert gas or liquid whilst maintaining the ratio of air to fuel at stoichiometry. Exhaust gas circulation is one such approach but another, which is gaining popularity, is water injection. Water injection has a second knock mitigation effect beyond that of the introduction of an inert substance as the heat of vaporisation of the water reduces the charge temperature.

The two approaches to dilution between the road car and racing applications are different, but similar issues are observed with combustion stability. This is because lowering the reactivity of the mixture not only affects the auto-ignition delay but also the laminar, and hence turbulent, flame speed. At a certain point this may become too low to have repeatable combustion and hence cyclic variability, commonly characterised as the Coefficient of Variation of Indicated Mean Effective Pressure (CoV of IMEP), suffers. Figure 2 shows this effect when a Formula 1 single-cylinder engine is run too lean and Figure 3 the effect of increasing water content together with Millerisation on a road car single-cylinder. These data are from a paper where I was a co-author.

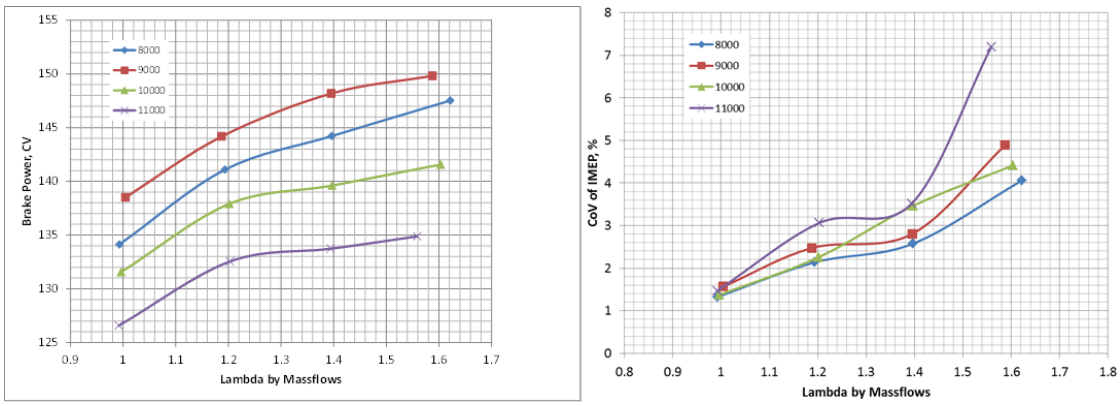

Fig.2 – Lambda Sweep to Instability Limit on Formula 1 Single-Cylinder Engine

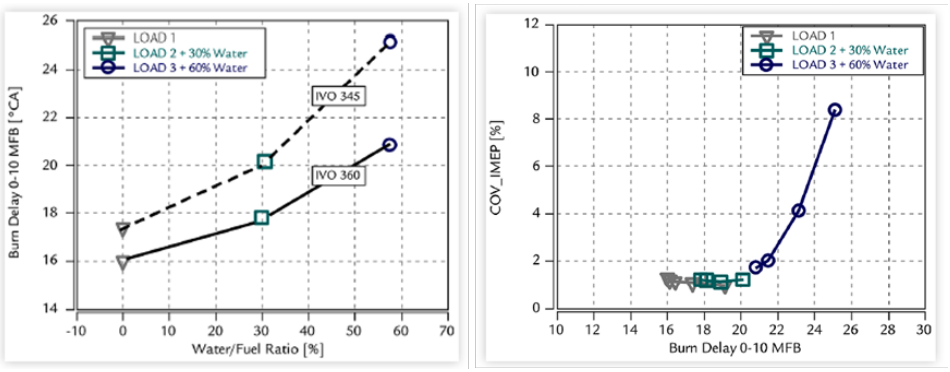

Fig.3 – Water/Miller Sweep until Instability Limit on Road Car Single-Cylinder Engine from SAE 2019-24-0173: "*Water Injection Contribution to Enabling Stoichiometric Air-to-Fuel Ratio Operation at Rated Power Conditions of a High-Performance DISI Single Cylinder Engine*"

A second interesting technology for improving full-load performance is the prechamber. These are in common use in Formula 1 at present and there is also interest in the road-car community. A prechamber is an enhanced ignition device. The combustion begins in a small volume, typically 2% of the main chamber volume, normally initiated by a conventional spark plug. The consumption of charge within the prechamber increases the pressure therein, resulting in hot reacting gas mixture being forced into the main chamber through a number of orifices. This has the potential to consume the main-chamber mixture in a faster and more stable manner than can be achieved with a conventional spark ignition system. This means there is less time available for autoignition, and hence knock, to occur in the end gas. The combustion stability is also much improved when such a system is operating well allowing the Knock-Limited Spark Advance (KLSA) to be moved earlier hence improving efficiency. Figure 4 shows how the combustion stability was improved through application of a prechamber on a Formula 1 single-cylinder engine. Single cycles of data are plotted in terms of IMEPH (Indicated Mean Effective Pressure during compression and expansion strokes) and MFB50 (Mass Fraction Burned 50% - the mid-point of combustion phasing based on analysis of apparent heat release from pressure indication).

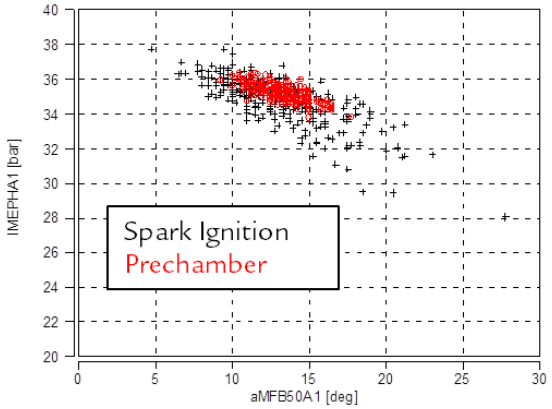

Fig.4 – Improvement of Cyclic Variability of IMEP and MFB50 on a Formula 1 Single-Cylinder Engine through Application of a Prechamber

Similar improvements are seen in high load conditions on a road car engine. Problems however, are observed with low load and especially highly retarded running. This is an engine use case which is not required on a racing engine but which is necessary for effective catalyst heating on a road car engine. Experimental activity I followed in the last year showed that it was not possible to match the stability of a standard spark igniter on a single-cylinder engine with a prechamber as is shown in Figure 5.

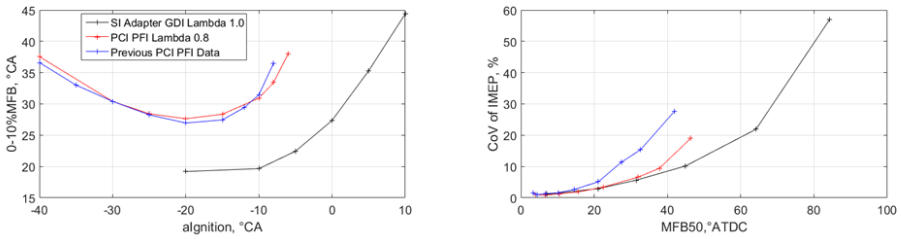

Figure 5: Retardability Limit of Prechamber (PCI) in Comparison to Conventional Spark Ignition (SI) on a Road-Car Single-Cylinder Engine

We discussed these results with a number of consultancies including FEV, AVL, IAV and Mahle Powertrain. It emerged that poor combustion stability during extremely retarded running using a prechamber is a commonly observed problem. Furthermore, actions which can be taken to improve retardability risk to render the prechamber less effective in full load performance.

A secondary spark plug is a potential solution but most arrangements of the components in the combustion chamber would prohibit the effective coupling of a direct injector and conventional spark plug (a technique known as spark coupled injection, which can greatly improve combustion stability in catalyst heating) if it is also desired to position the prechamber at the centre of the combustion chamber. We came up with a new arrangement which features an exhaust side direct injector, central prechamber and conventional spark plug located between these other two components. I was the lead author of the patent application. A European patent was achieved in April of this year and a US patent in October as shown in Figure 6.

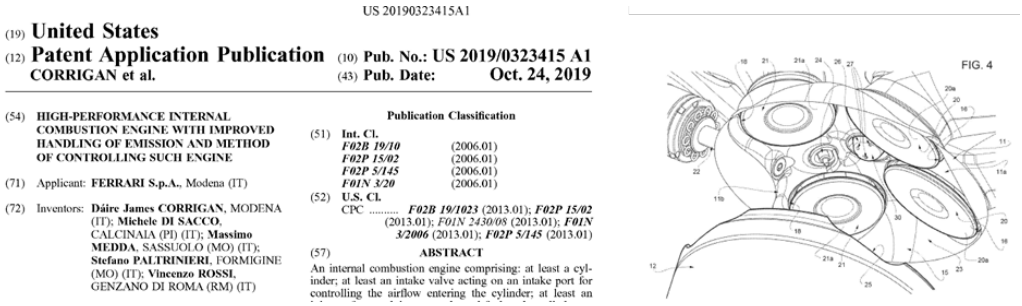

US 20190323415A1

(19) **United States**

(12) **Patent Application Publication** (10) **Pub. No.: US 2019/0323415 A1**

CORRIGAN et al. (43) **Pub. Date: Oct. 24, 2019**

(54) **HIGH-PERFORMANCE INTERNAL COMBUSTION ENGINE WITH IMPROVED HANDLING OF EMISSION AND METHOD OF CONTROLLING SUCH ENGINE**

(71) Applicant: **FERRARI S.p.A.**, Modena (IT)

(72) Inventors: **Dáire James CORRIGAN**, MODENA (IT); **Michele DI SACCO**, CALCINAIA (PI) (IT); **Massimo MEDDA**, SASSUOLO (MO) (IT); **Stefano PALTRINIERI**, FORMIGINE (MO) (IT); **Vincenzo ROSSI**, GENZANO DI ROMA (RM) (IT)

Publication Classification

(51) **Int. Cl.**

F02B 19/10	(2006.01)
F02P 15/02	(2006.01)
F02P 5/145	(2006.01)
F01N 3/20	(2006.01)

(52) **U.S. Cl.**

CPC ***F02B 19/1023*** (2013.01); ***F02P 15/02*** (2013.01); *F01N 2430/08* (2013.01); ***F01N 3/2006*** (2013.01); ***F02P 5/145*** (2013.01)

(57) **ABSTRACT**

An internal combustion engine comprising: at least a cylinder; at least an intake valve acting on an intake port for controlling the airflow entering the cylinder; at least an

FIG. 4

Fig.6 – Ferrari US Patent of New Combustion Chamber Layout with Prechamber and Secondary Igniter

Initial results have shown good catalyst heating combustion stability with this new arrangement as was hoped. Full load testing is underway at present.

Together with work on engine performance, I have also been working on improving experimental methodology particularly with regard to emissions. Whilst there are no emissions limits for Formula 1 cars, the general approach of bringing vehicle simulation into the engine test cell is more mature in racing than road-car environments. This is known as “road to rig”. The end goal of my thesis would be to demonstrate an emissions cycle on a single-cylinder test bench. This was not realistic in the first year. What I have been able to implement, assisted by colleagues, was a WLTC cycle of a Plug-in Hybrid Electric Vehicle (PHEV) on a conventional engine test bench. Vehicle parameters, gearbox and P4 electric motors are modelled in a hardware in the loop simulation. An overlay of some key telemetry channels is shown in Figure 7. There is still some work to do to exactly match the real vehicle but good progress has already been made.

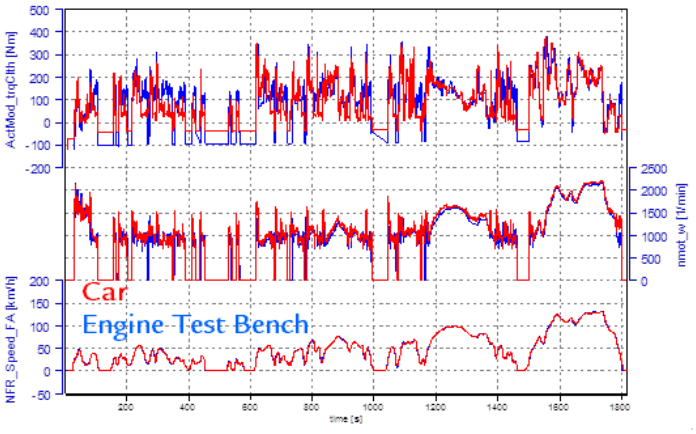

Fig.7 – WLTC Implementation on an Engine Test bench with vehicle and hybrid parameter modelling. Channels from Top to bottom: Torque at engine clutch, Engine Speed, Vehicle Speed

A significant new challenge in road car development is Real Driving Emissions (RDE). Here there is no prescribed test cycle and hence is an area where the racing world is simpler than that of road cars. Every manufacturer needs to therefore decide the worst case for their particular application and ensure the emissions are robust against this. It is difficult to study single manoeuvres in a repeatable manner on the road or on a conventional emissions roller chassis dyno. I therefore decided to perform such testing on a high dynamic four wheel drive chassis dyno. As this facility did not have dedicated emissions measurements, I used a Portable Emissions Measurement System (PEMS) which is normally used for on-road testing. The installation of the car in the chassis dyno is shown in Figure 8. Testing was performed without a driver in order to have perfectly repeatable actuations and to perform sweeps of single parameters. Rapid cooling of the aftertreatment system was also implemented for more rapid testing iterations.

Both of these new techniques proved highly efficient and I will further develop them in the remaining years of my PhD, together with aiming to bring dynamic and emissions testing still earlier in the development process.

Fig.8 – RDE Testing on Chassis Dyno on Plugin Hybrid Electric Vehicle (PHEV)

Technical Exchanges in which I participated:

- AVL
- FEV
- IAV
- Hyundai

Congresses:

- AVL Development Methodology November 2019

B.2 Year 2

Efficient Development of High Performance Engines: Technology and Methodology Transfer from Race to Road.

Second Year Report

Dáire James Corrigan - XXXIV Cycle
PhD Programme "Enzo Ferrari" in
Industrial and Environmental Engineering
Supervisor: Prof. Stefano Fontanesi

November 5, 2021

Abstract

This report briefly resumes the key activities of the second year of my PhD. Key topics covered include further development of the novel prechamber combustion system introduced in my first year, fuel development activity leading to a publication, the beginning of a new approach to understanding of engine knock, and initial development of a rapid injection calibration system.

1 Introduction

The aim of my PhD is to critically examine technologies and methodologies from Formula 1 which can be applied or as they are, or with suitable modifications, to high performance road car engine development. In my first year report, I showed that maximum engine performance was a target in common for both and that on boosted engines this is largely limited by knock. In the past year, I have focused on three knock-related topics: prechamber development, fuel understanding and knock understanding. I have taken inspiration both from my past in racing and also historical activity. I am also continuing to evaluate opportunities to apply rapid calibration techniques from the racing world to road-car engineering.

2 Fuel Understanding

In the early part of the 20th century, fuel development was not only performed by fuel suppliers but also automotive manufacturers [1],[2],[3]. There were also large scale collaborations between car companies and fuel companies, the most notable being the Cooperative Fuels Research group of the 1930s. A large number of participants worked together to define the standard fuel testing methods which are still known to this day as the RON (Research Octane Number) and MON (Motor Octane Number) tests [4],[5],[6],[7]. Ironically, although these early researchers were very critical of their own method, and carried out large activities on a biannual basis to continually check if the approach should change [8],[9],[10],[11], it has remained largely unaltered to this day.

It has become relatively rare to have a deep collaboration between fuel and engine developers in the modern period. A notable exception to this is Formula 1 where engine and fuel suppliers work hand in hand to improve performance [12]. Modern Formula 1 fuels are effectively laboratory blends consisting of a limited number of components (at least seven for regulatory reasons but typically not more than this [13]). The challenge is to find the best components in order to create the best fuel for a particular engine. Testing of a Formula 1 engine is very expensive and hence as much work is done upstream as possible making use of the traditional RON and MON tests, but also facilities for studying chemical kinetics - principally a Rapid Compression Machine (RCM) and/or a Shock Tube (ST) [14]. These facilities allow direct measurement of ignition delay times at a controlled pressure and temperature. They can be used to search for new fuel components, by tuning the facilities to operate at pressure and temperature conditions corresponding to the end-gas in an internal combustion engine. They are also routinely used to validate chemical kinetics mechanisms.

In the road car world in contrast, the automotive manufacturer has very little control over the fuel and hence the engine must be designed to tolerate what is available on the market. Understanding and replicating that fuel in a calculation environment is challenging however. I discussed with Ferrari's official fuel supplier, Shell, the possibility to make use of some of the Formula 1 methodology with a goal to improving the accuracy of knock calculations. Instead of producing a surrogate in a calculation environment with the aim to replicate a complex refinery blend, I suggested to produce and validate a physical surrogate to match the knock behaviour of RON98 fuel in a Ferrari road car engine. I requested to not only match RON and MON but also to validate the surrogate in the research facilities of the University of Aachen, as performed for Formula 1. Shell furthermore proposed to attempt to match some volatility parameters of the fuel as well. The result was effectively a three component surrogate fuel (Toluene, Heptane, Isopentane). Shell produced and verified the fuel using their blending tools

and lab facilities, Aachen University characterised the ignition delay across the full range of temperatures of interest and I directed the engine testing and analysed the data. The RCM data is shown in Figure 1 and ignition timing sweeps on a Ferrari F154FA engine in Figure 2.

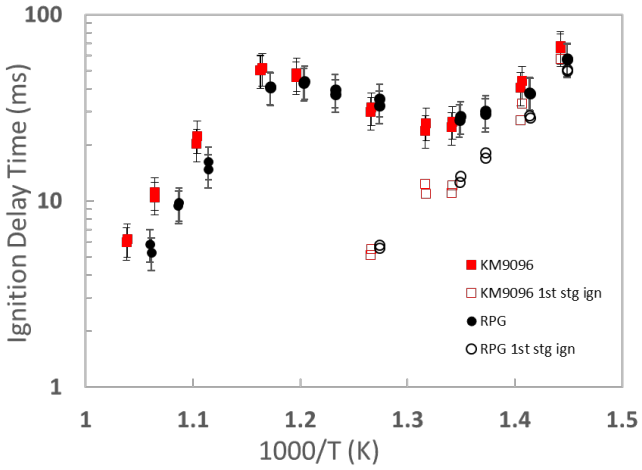

Figure 1: Rapid Compression Machine Ignition Delay Characterisation of **Reference Premium Gasoline (RPG)** and **Surrogate Blend** [15]

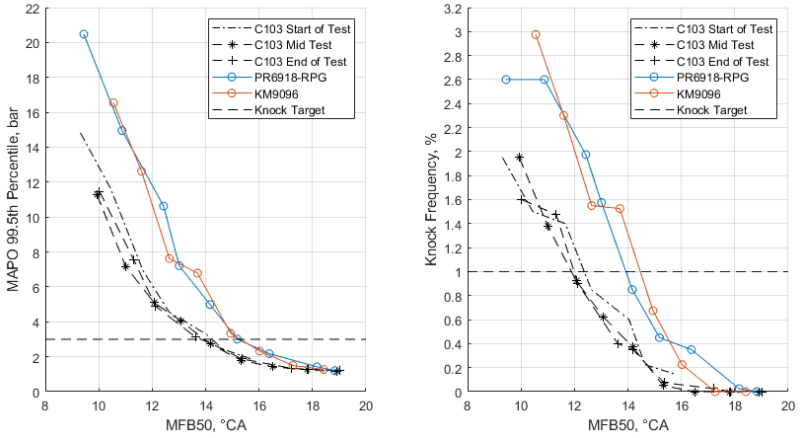

Figure 2: Ignition Timings Sweeps of **Reference Premium Gasoline** and **Surrogate Blend** [15]

Together we wrote a report which was published in the *"Proceedings of the Combustion Institute"* in September [15]. I demonstrated that the knock limit of this fuel was comparable to that of a reference RON98 refinery blend to within experimental repeatability on our engine. The value of this

work is that we can now use a chemical kinetics mechanism with just three components and if this can be well matched to the validation data from the Aachen facility, we know it will also perform similarly to a market fuel in our engine.

I also applied in this activity a cylinder pressure based knock severity index that I had developed in my Formula 1 career to the road car engine data. The results were generally satisfactory but more tuning of the approach was required than on the Formula 1 engine. This opened up a new line of inquiry which i will discuss below.

I stated above that road car manufacturers generally have very little influence on fuel development but occasionally an opportunity presents itself. Fuel suppliers are currently examining how to introduce fuel with 20% ethanol content (E20). This could potentially be used to give a RON increase. There is also some evidence that at matched RON an E20 fuel should perform better from a knock perspective than an E5 blend. I am therefore collaborating again with Shell to test some E20 blends at different octane levels in the next weeks. An RCM facility will again be employed, this time to separate chemical from physical knock effects. This may again lead to a new co-publication.

3 Knock Understanding

In the past, I was responsible for engine performance development of Ferrari Gestione Sportiva. As modern Formula 1 engines are significantly knock limited, it was very important to have a reliable knock index in order to perform engine and fuel comparison tests at matched knocking intensity. I created an index with a threshold based on the base noise in the dataset, characterised by the median of the Maximum Amplitude Pressure Oscillation (MAPO) values. This is shown in Figure 3. This worked very well on Formula 1 engines and a single parameterisation was adequate for a range of speeds, sensor types and locations at full load. I have since found that this index cannot be straightforwardly applied to the wider range of speeds, loads and engine geometries found in road car engines and hence I decided to begin work on a new index.

I am performing an extensive literature survey going back over a century, as much of the fundamental understanding in the field of knock comes from the 1920s and 1930s [16], [17], [18], [19], [2], [20], [3], [21], [22], [23], [24], [25], [26], [27], [11], [28], [29], [30], [31]. A work which stands out is that of Draper at the Massachusetts Institute of Technology in 1934 [32]. In this work, Draper showed that the frequencies measured by a pressure transducer when knock occurs can be explained by simple acoustic theory. This simple theory is not straightforward to apply to a running engine, and this was particularly the case in the 1930s. Draper took a very innovative

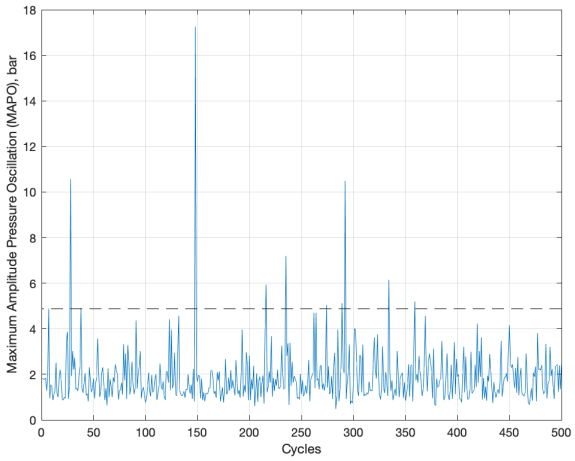

Figure 3: Median based Knock Threshold

approach to this problem - he complimented the running engine testing with measurements taken whilst the engine was stationary by setting of a small explosive charge in the periphery of the combustion chamber to simulate a knocking event. This greatly simplified the analysis as the geometry of the combustion chamber was fixed during the measurement and the engine was filled with air at standard conditions. The acoustic velocity was therefore well known. He furthermore showed that the main mode excited by this explosion was also found on the running engine when knock occurred but at a higher frequency corresponding to the higher temperature and hence acoustic velocity in the fired engine.

The work of Draper has been frequently cited and often applied to this day in interpreting frequency information on knocking cylinder pressure traces. He himself underlined however, that it should only be directly applied to an engine with a simple cylindrical combustion chamber, as for the Cooperative Fuels Research (CFR) engine he used in his experiment. Taking inspiration from Draper's publication, I proposed to my supervisor Professor Fontanesi to reproduce his approach in Computational Fluid Dynamics (CFD) software. If we could validate it, we could then modify the simple CFD experiment one step at a time, moving gradually towards a modern running engine and tracking the frequencies of the modes as we went. It would also be possible to perform detailed studies of the impact of sensor mounting location with respect to autoignition event location.

The mesh of the basic cylindrical model is shown in Figure 4. A local heat source is introduced at one side of the cylinder with very high power for a short time to represent the explosive charge used by Draper. This produces an incident wave which travels through the combustion chamber

as shown in Figure 5. Draper calculated ten different possible modes of vibration but the experimental results suggested the strongest was the first transversal mode. If we examine the pressures in the the model close to the end of the calculation time, we can indeed see this mode very clearly as shown in Figure 6.

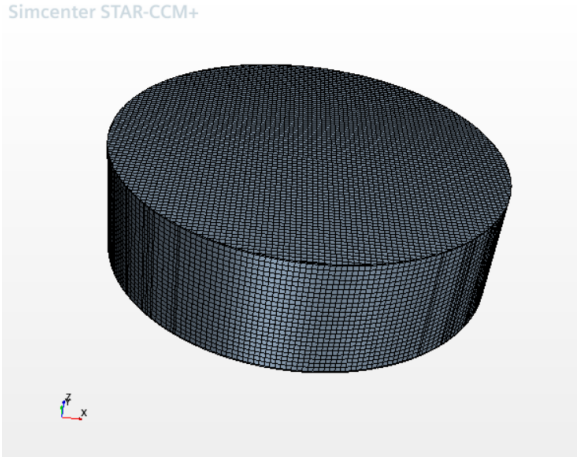

Figure 4: Cylindrical Mesh Representing Draper Experiment

Draper of course could not see these pressure waves in his engine and hence had to rely on a pressure transducer, which was mounted diametrically opposite the explosion device. This pressure measurements has been replicated in the model to allow validation with the Draper paper. I have reproduced the frequency/amplitude characteristics of the electronic equipment available to Draper and shown that the pressure measurement from the model qualitatively matches the figure from the paper very well as shown in Figure 7.

Further pressure measurements have been added with a view to gradually

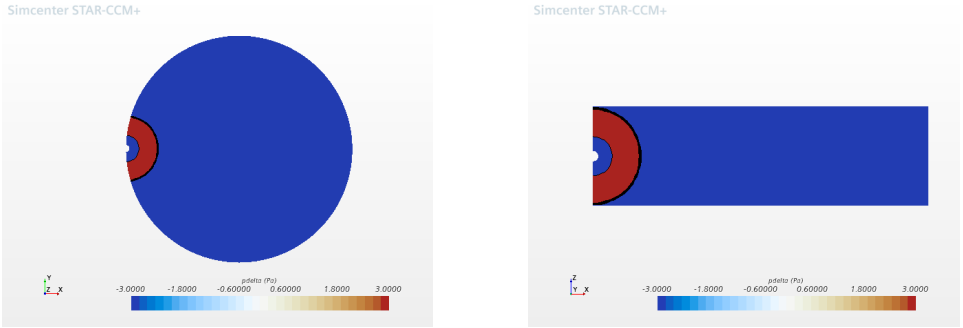

(a) Above View (b) Side View

Figure 5: Initial Pressure Wave from “Detonation Event”

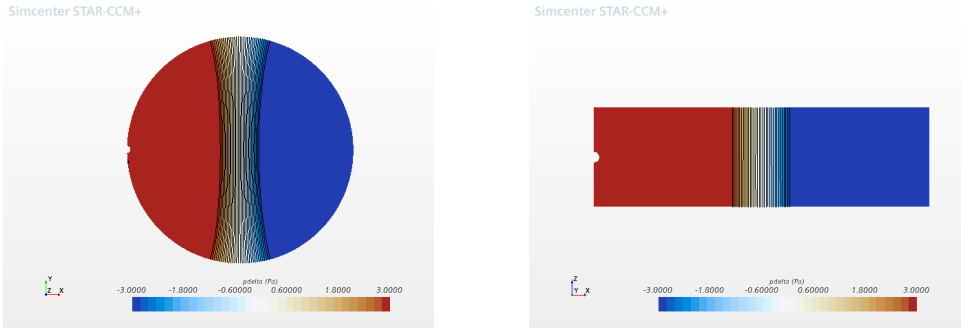

(a) Above View (b) Side View

Figure 6: First Transversal Mode after almost 10ms

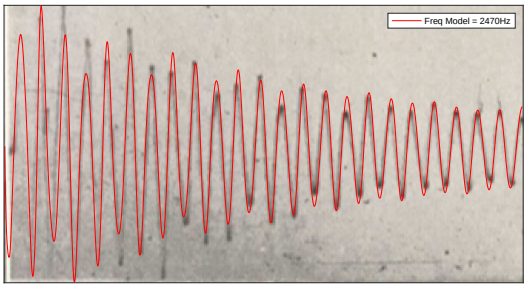

Figure 7: Comparison of **Model Output** and **Photographic record from 1934 Draper Paper**

migrating the model towards a modern combustion chamber geometry and comparisons with experimental data.

The initial model was constructed following my suggestion by a CFD specialist (Sebastiano Breda of R&D CFD) in Star CCM+. I am learning to use this software to perform geometry and heat source modifications to the model. I have also constructed an extensive analysis routine making use of both traditional Fast Fourier Transforms (FFT) and more modern Continous Wavelet Transforms (CWT) and Wavelet Synchro-Squeezed Transforms (WSST) in Matlab software. The latter two allow deeper interrogation of data in the Time/Frequency domain. This is particularly important for the case of a fired engine where the acoustic velocity, and hence the mode frequencies, are not constant. I am applying this in a similar way to data from virtual pressures sensors in the CFD model and real data from the engine. An example is shown in Figure 8.

A key output of the analysis routine is automatic recognition of modes excited on a per cycle (real engine data) or per sensor (model) basis. An example is shown in Figure 9. This work will lead to at least one and perhaps

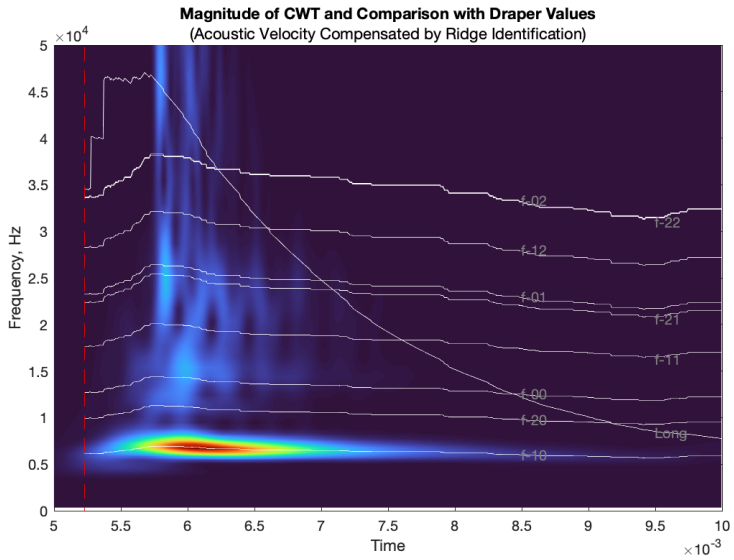

Figure 8: Average of Multiple Cycles' Continous Wavelet Transforms on F154FA Engine with Theoretical Combustion Chamber Frequencies Calculated as per Draper

several publications.

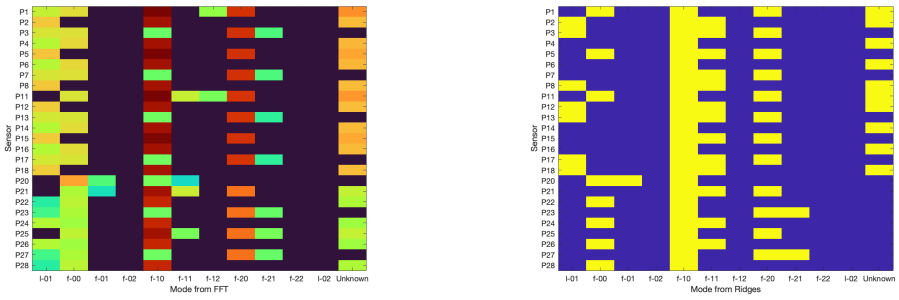

(a) FFT Based Mode Finder

(b) WSST Based Mode Finder

Figure 9: Mode Identification from 25 Different Pressure Sensors from Simulation Model of Draper Experiment using Two Different Approaches

4 Prechamber

In my first year report I showed a novel combustion system featuring a prechamber, an exhaust side injector and a secondary spark plug. I was the lead author of the patent application for this concept which takes inspiration from both Formula 1 and road car approaches. At the end of my first year

we showed that it performed well in a catalyst heating condition. This was the largest open point of the concept as to our knowledge no-one had proven an exhaust side injector spark-coupled concept could work well before. We have since found that the new combustion concept is exceeding our expectations also from a performance point of view. I lead the team of engineers responsible for the experimental activity on the research engine where we are studying this novel system. One of the innovations I introduced was the possibility to swap intake ports on the engine test bed without dismounting the head. This has allowed us to perform a sweep of tumble level in a greatly reduced time and at significantly lower cost in comparison to producing a series of full cylinder heads. It also leads to more reliable data as there are fewer operations of mounting and dismounting of the engine which can have an impact on results stability. Figure 10 shows some of the inserts which were created in order to sweep the tumble level.

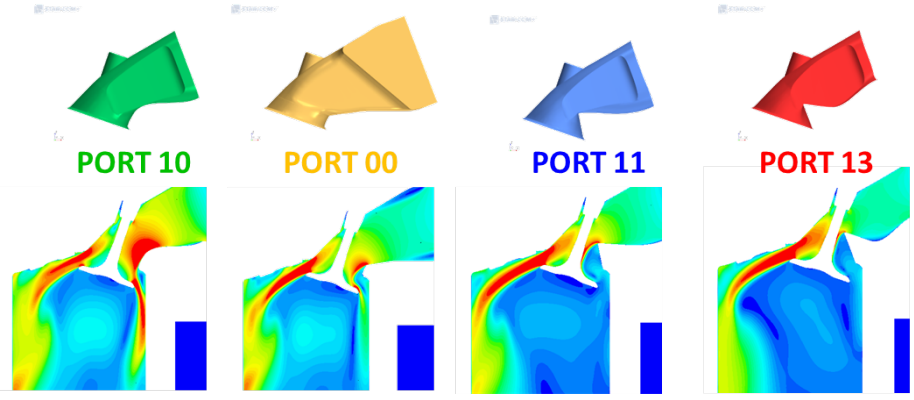

Figure 10: Intake Port Designs and CFD Results for Sweeping of Tumble Level on Novel Prechamber Engine

A number of techniques for reducing knock propensity in an engine, such as running lean, water injection, EGR, Millerisation and Anti-tuning, also reduce flame speeds. The standard way to combat this is to increase tumble through sending more flow over the top of the intake valve head. This tumble is converted into turbulence late in the compression stroke and accelerates and hence stabilises the combustion process. The tumble comes with a disadvantage however: the ports required to create it generally have a lower volumetric efficiency as not all the valve curtain area is used during inflow into the cylinder. The prechamber, like a high tumble port, also creates fast and stable early combustion. We found in Formula 1 that this allowed increasing of Millerisation and antituning together with lowering of intake port tumble. This allowed to compensate somewhat the boost increases required for Miller and antituning without sacrificing combustion stability.

Our road car prechamber engine is confirming that high tumble is not required when a prechamber is present. It can be seen in Figure 11 that the knock limit is improved for the lower tumble variants and that these significantly outperform the current production engine concept. This is even more clear in Figure 12 where the correlation between knock limited combustion phasing and tumble level for the prechamber engine is shown in Figure 12.

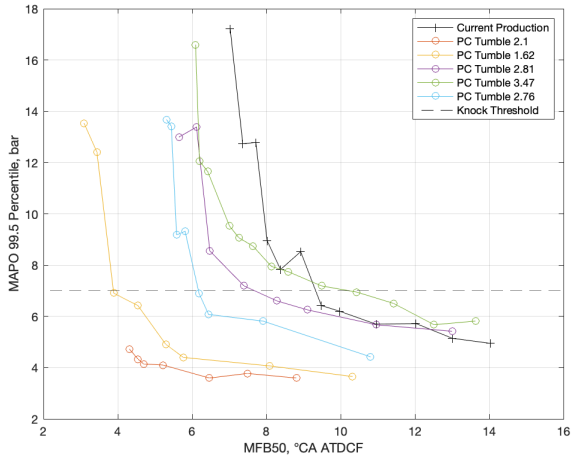

Figure 11: Combustion Phasing Sweeps on Various Intake Ports

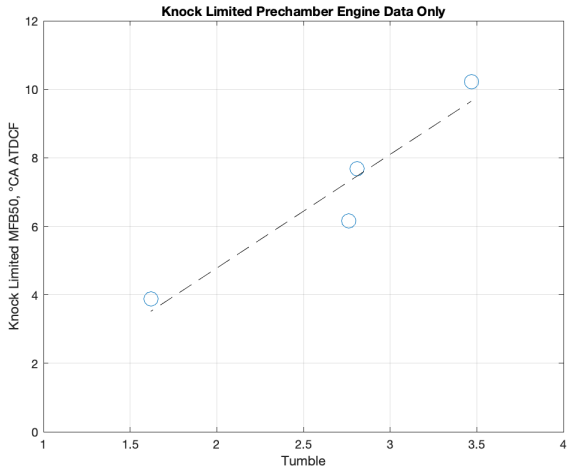

Figure 12: Knock Limit Against Tumble on Prechamber Engine

5 Rapid Development

One of the key requirements in Formula 1 is extremely rapid development. One of the bottlenecks is how quickly a standard performance test can be performed. Part of this is the calibration activity necessary to achieve the target knock level. Another potentially time consuming task is mapping of the fuel injection timing. To improve this, when I worked in Formula 1, I created a new ECU (Engine Control Unit) strategy. The injection timing was varied on a cyclic basis and results were also analysed cyclically to select the injection timing for best ignition delay, combustion stability and IMEP (Indicated Mean Effective Pressure). An example is shown in Figure 13.

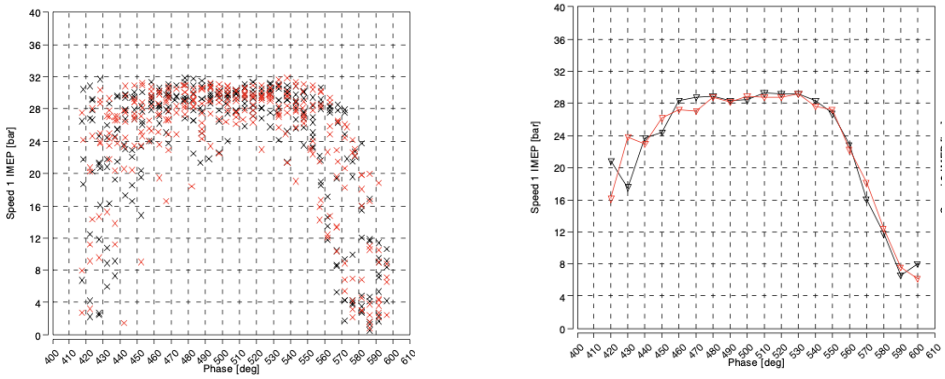

(a) Raw Cyclic Results of IMEP against Start of Injection (SOI) Timing

(b) Binned Cyclic Results of IMEP against Start of Injection (SOI) Timing

Figure 13: Automatic Injection Sequencer Data on Formula 1 Engine

I didn't initially attempt to reproduce this system when I moved to road car development as here it is fundamental to consider particulate emissions when mapping the injection timing. Traditional instruments for particulate measurement are too slow to respond to cyclic variations. In the meantime, for an unrelated activity, I suggested use of an optically based technique for in-cylinder particulate investigations on a Ferrari road car engine. The custom optical spark plug for this activity is shown in Figure 14. This worked well and hence I realised it could be the missing link in order to map injection timing cyclically also on a road car engine. I therefore wrote a specification document to recreate the Formula 1 ECU strategy (which I named the Automatic Injection Sequencer) but considering also multiple injection events in a single cycle. This software has since been debugged in bench testing and will be applied in a feasibility study of the approach during November together with optical measurements for particulate estimation and a fast hydrocarbon measurement system. If it performs as hoped it could become a game-changer for injection calibration both from a time point of

view (particularly considering that we may need to map up to six injection events in a single cycle in the near future) but also to permit investigation on injection timing sensitivity during engine warmup. If successful this would lead to a further publication.

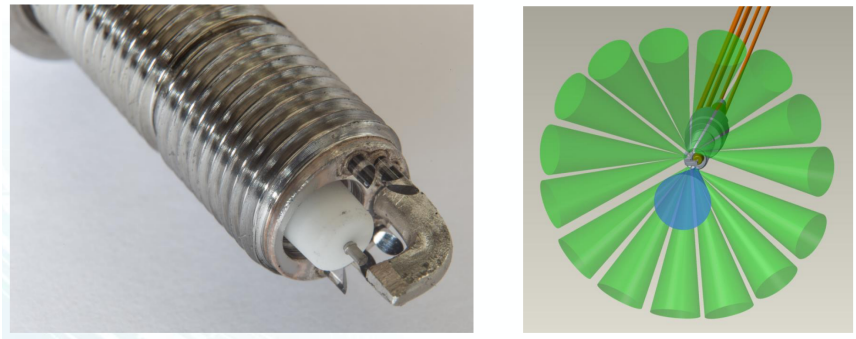

Figure 14: Fibre Optical Spark Plug for Ultrafast Particulate Measurement

6 Publications during Second Year

- Evaluating a novel gasoline surrogate containing isopentane using a rapid compression machine and an engine [15]

7 Conferences Attended during Second Year

I had planned to attend a greater number of conferences this year but unfortunately due to COVID19 this has not been possible. I have been able to follow some online conferences however.

- 32nd International AVL Conference "Engine and Environment"
- 14th International AVL Symposium on Propulsion Diagnostics

References

[1] C. F. KETTERING, "Fuel research developments," in *Pre-1964 SAE Technical Papers*, SAE International, jan 1921.

[2] T. MIDGLEY and T. A. BOYD, "Methods of measuring detonation in engines," in *Pre-1964 SAE Technical Papers*, SAE International, jan 1922.

[3] T. MIDGLEY and R. JANEWAY, "Laws governing gaseous detonation," in *Pre-1964 SAE Technical Papers*, SAE International, jan 1923.

[4] E. Graham, "Jacket and cylinder-head temperature effects upon relative knock-ratings," in *Pre-1964 SAE Technical Papers*, SAE International, jan 1931.

[5] J. M. Campbell, W. G. Lovell, and T. A. Boyd, "Influence of carbureter setting and spark timing on knock ratings - annual meeting paper," in *Pre-1964 SAE Technical Papers*, SAE International, jan 1931.

[6] H. F. Huf, J. R. Sabina, and J. B. Hill, "Effect of sound intensity on knock ratings," in *Pre-1964 SAE Technical Papers*, SAE International, jan 1931.

[7] C. B. Veal, H. W. Best, J. M. Campbell, and W. M. Holaday, "Antiknock research coordinates laboratory and road tests," in *Pre-1964 SAE Technical Papers*, SAE International, jan 1933.

[8] C. B. Veal, "C. f. r. committee report on 1934 detonation road tests," in *Pre-1964 SAE Technical Papers*, SAE International, jan 1935.

[9] T. A. Boyd, "1937 road knock tests," in *Pre-1964 SAE Technical Papers*, SAE International, jan 1938.

[10] J. M. Campbell and W. G. Lovell, "Application of statistical concepts to the knock-rating problem," in *Pre-1964 SAE Technical Papers*, SAE International, jan 1938.

[11] D. B. Brooks and R. B. Cleaton, "The precision of knock rating - 1936-1938 - report from cooperative fuel research committee," in *Pre-1964 SAE Technical Papers*, SAE International, jan 1939.

[12] L. Sassi, I. Kitsopanidis, and G. Lovett, "Evolutions in f1 engine technology: Pursuing performance from today's power unit through efficiency," *37th Vienna Engine Symposium*, 2016.

[13] Federation Internationale de l'Automobile, "2020 formula 1 technical regulations," 2020.

[14] U. Burke, R. F. Cracknell, M. T. Evans, B. Poulet, S. Gail, I. Kitsopanidis, D. Salters, and K. A. Heufer, "Use of a rapid compression machine to characterize the anti-knock properties of high octane fuels," *36th International Symposium on Combustion Seoul, Korea*, 2016.

[15] S. Gail, R. F. Cracknell, D. Corrigan, A. Festa, V. Shankar, B. Poulet, G. Lovett, R. D. Büttgen, K. A. Heufer, R. Mariconti, M. Cucchi, and F. Mortellaro, "Evaluating a novel gasoline surrogate containing isopentane using a rapid compression machine and an engine," *Proceedings of the Combustion Institute*, 2020.

[16] D. MACKENZIE and R. K. HONAMAN, "The velocity of flame propagation in engine cylinders," in *Pre-1964 SAE Technical Papers*, SAE International, jan 1920.

[17] H. C. DICKINSON, "Resume of bureau of standards fuel study," in *Pre-1964 SAE Technical Papers*, SAE International, jan 1921.

[18] D. CLERK, "Cylinder actions in gas and gasoline engines," in *Pre-1964 SAE Technical Papers*, SAE International, jan 1921.

[19] H. R. RICARDO, "Recent research work on the internal-combustion engine," in *Pre-1964 SAE Technical Papers*, SAE International, jan 1922.

[20] A. TROWBRIDGE, "Photographic recording of engine data," in *Pre-1964 SAE Technical Papers*, SAE International, jan 1922.

[21] H. L. HORNING, "Effect of compression on detonation and its control," in *Pre-1964 SAE Technical Papers*, SAE International, jan 1923.

[22] G. L. CLARK and A. L. HENNE, "Ultraviolet spectroscopy of engine-fuel flames," in *Pre-1964 SAE Technical Papers*, SAE International, jan 1927.

[23] E. GRAHAM, "Detonation specifications for automotive fuels," in *Pre-1964 SAE Technical Papers*, SAE International, jan 1927.

[24] H. K. CUMMINGS, "Methods of measuring the antiknock value of fuels," in *Pre-1964 SAE Technical Papers*, SAE International, jan 1927.

[25] E. J. MARTIN and D. F. CARIS, "A new electrical engine-indicator," in *Pre-1964 SAE Technical Papers*, SAE International, jan 1928.

[26] R. N. Janeway, "Combustion control by cylinder-head design," in *Pre-1964 SAE Technical Papers*, SAE International, jan 1929.

[27] E. Beale and R. Stansfield, "The sunbury knock indicator," in *Pre-1964 SAE Technical Papers*, SAE International, jan 1937.

[28] C. F. Marvin, "Observations of flame in an engine," in *Pre-1964 SAE Technical Papers*, SAE International, jan 1934.

[29] G. M. Rassweiler and L. Withrow, "Flame temperatures vary with knock and combustion-chamber position," in *Pre-1964 SAE Technical Papers*, SAE International, jan 1935.

[30] L. Withrow and G. M. Rassweiler, "Slow motion shows knocking and non-knocking explosions," in *Pre-1964 SAE Technical Papers*, SAE International, jan 1936.

[31] N. MacCoull and G. T. Stanton, "The measurement of engine knock by electro-acoustic instruments," in *Pre-1964 SAE Technical Papers*, SAE International, jan 1936.

[32] C. S. Draper, "The physical effects of detonation in a closed cylindrical chamber," in *NACA Technical Reports*, National Advisory Committee for Aeronautics, jan 1935.

B.3 Year 3

Efficient Development of High Performance Engines: Technology and Methodology Transfer from Race to Road.

Third Year Report

Dáire James Corrigan - XXXIV Cycle
PhD Programme "Enzo Ferrari" in
Industrial and Environmental Engineering
Supervisor: Prof. Stefano Fontanesi

November 6, 2021

Abstract

This report briefly resumes the key activities of the third year of my PhD. The majority of activity in my final year has focused on knock. This has already led to both a journal paper and a conference publication. I will also present at a dedicated conference on knock in December. A new methodology using CFD to map the acoustic response of combustion chambers has been demonstrated and used to infer information on knock location in the chamber. New techniques for interpreting knocking experimental datasets have also been applied. The final activity in my PhD will be to further develop these techniques for engines with multiple pressure transducers and prechamber ignition systems.

1 Introduction

The aim of my PhD is to critically examine technologies and methodologies from Formula 1 which can be applied or as they are, or with suitable modifications, to high performance road car engine development. In my first year report, I showed that maximum engine performance was a target in common for both and that on boosted engines this is largely limited by knock. In

the second year, I focused on three knock-related topics: prechamber development, fuel understanding and knock understanding. In my final year I have gone into to significantly more detail on knock and developed a new methodology to aid in the interpretation of cylinder pressure data.

2 Knock Literature Survey

Knock has been studied by automotive researchers since the very beginning of the automobile. This means there is a rich vein of historic literature. I decided to perform a review of 100 years of knocking research. This turned into a massive undertaking leading to a journal paper with over 400 references [1]. This was still one of the most popular journal papers on the SAE website some months after it was published, as shown in Figure 1.

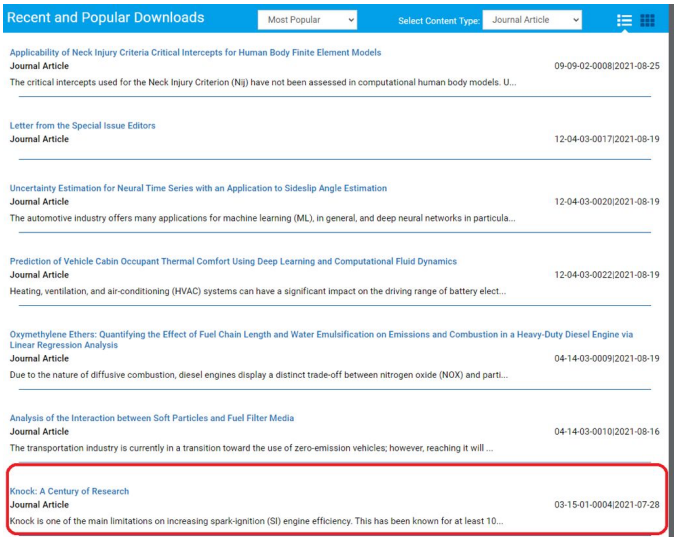

Figure 1: Knock literature review still among the most popular Journal downloads two months after publication

Some of the most interesting articles cited in the survey were those that described work on knock understanding by C.S. Draper [2],[3]. This became the inspiration for the following activity in my research.

3 Knock Understanding: Historic Experiment Recreation

As described in the second year report, CFD was used to recreate the original experiment of Draper. This lead to the publication of an SAE Technical Paper at the Internal Combustion Engines conference in Capri, 2021. The title of the paper was "A Simple CFD Model for Knocking Cylinder Pressure Data Interpretation: Part 1". In addition to recreating Draper's experiment, the response of a simple combustion chamber geometry to ignition location was mapped over a range of conditions. A sophisticated post processing routine was created in MATLAB to analyze data from 61 virtual pressure transducers in the model. This allowed mode shapes to be directly confirmed, as shown in Figure 2

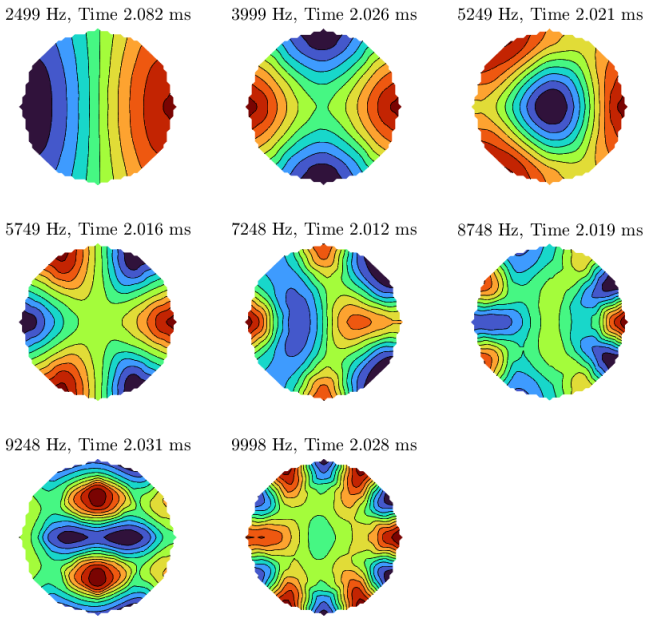

Figure 2: Modes of vibration of a cylindrical combustion chamber, isolated through band pass filtering of multiple pressure transducers

FFT analysis and band pass filtering work well for stationary cases. To analyse a moving piston run, wavelet synchrosqueezing and ridge identification were used, as shown in in Figure 3. The high frequency data from the model can be seen to follow the theoretical mode frequencies from analytic calculations, as used by Draper.

The paper demonstrated the accuracy and utility of using CFD modeling for this purpose and was once again very well received. In the period after the

conference, it was the fourth highest ranked download on the SAE website.

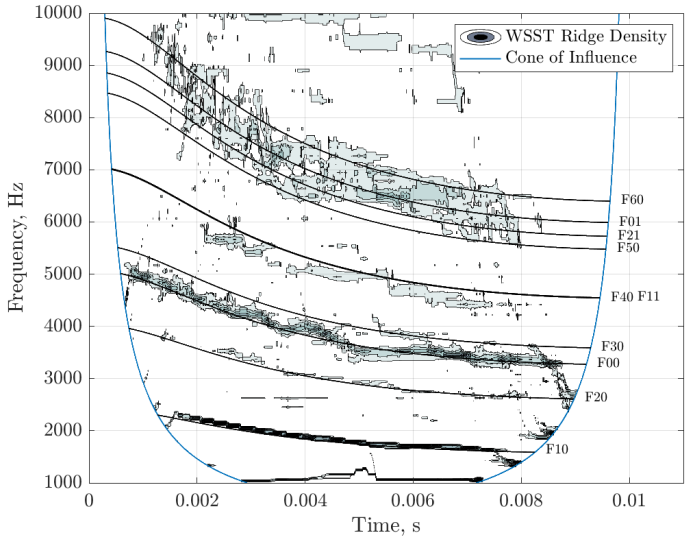

Figure 3: Wavelet Synchrosqueezed transform ridge density comparison with theoretical modal frequencies for moving piston case

The follow on activity was to apply the same methodology to modern combustion chambers and compare it to experimental data. This will be described in the next section.

4 Knock Understanding: Comparison of CFD Model with Modern Data

Having validated the CFD approach to mapping combustion chamber acoustic modes, the logical next step was to perform the same analysis on modern engines and to compare to experimental data. Two Ferrari engine types were considered for this activity, as shown in Table 1. These feature quite different combustion chamber geometries. One engine is turbocharged and the other is naturally aspirated and thus has a much higher compression ratio.

The CFD analysis performed for the simple cylindrical chamber was repeated for these modern engines. Of particular interest was a sweep of the ignition site, representing the knock location, around the circumference of the combustion chamber. Due to asymmetries in the design of the V8 engine combustion chamber, both modal frequencies and amplitudes change with ignition site location. This is shown in Figure 4.

Table 1: Technical Specifications of Test Engines

Name	F140HB	F154FA
Type	V12 NA	V8 Turbo
Bore (mm)	94	88
Swept Volume	6500 cc	3990 cc
Injection System	Direct, Inlet Side	Direct, Central
Compression Ratio	13.6:1	9.5:1
Maximum Speed (rpm)	9500	8000
Specific Output (CV/L)	1208	195

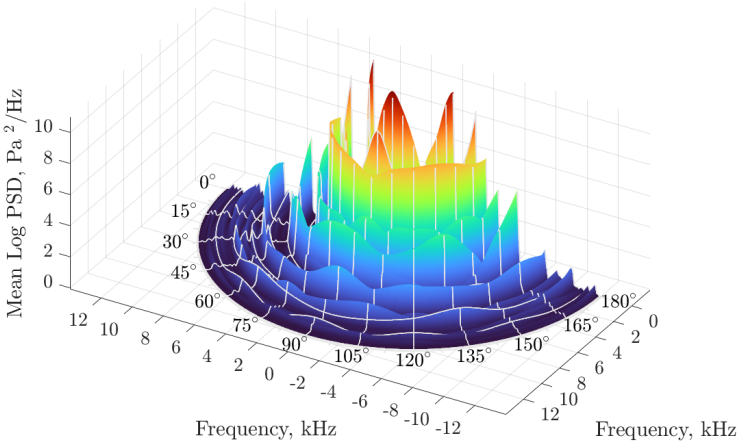

Figure 4: Power spectral density of CFD model cylinder pressure signals for various heat source locations

In the experimental activity, a technique for separating knocking from non-knocking cycles proposed in the 1980's was applied [4]. This method had been discovered in the knock literature review and does not seem to be frequently cited. It is based on the deviation from a lognormal fit, as shown in Figure 5. Once the cycles had been divided into knocking and non-knocking, their frequency information was analyzed to infer the knock location. This is supported by the CFD model output. The results are shown in Figure 6.

With a single pressure transducer, knock can only be narrowed down to one of four locations. A second transducer gives the possibility to narrow down the location still further and to apply both frequency based and wave arrival time techniques. Experimental activity with a second transducer has just been completed and will be the object of study in the third and final

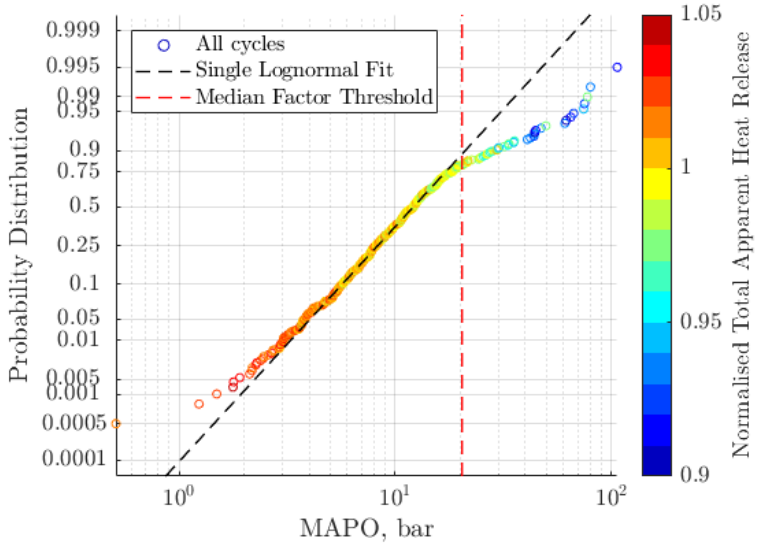

Figure 5: Frequency derived estimation of knock location from experimental cylinder pressure data

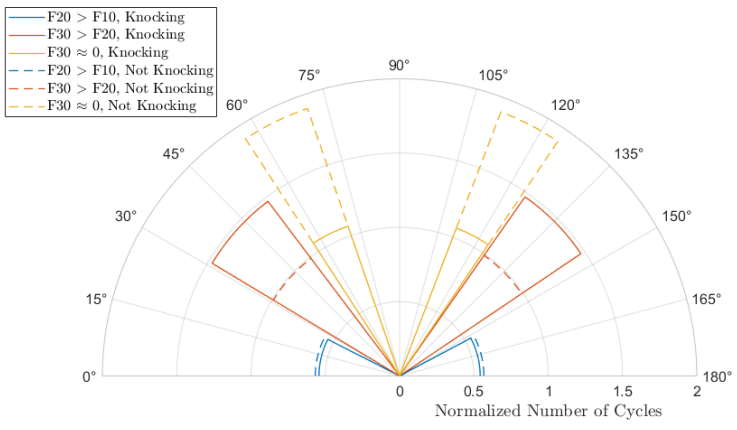

Figure 6: Frequency derived estimation of knock location from experimental cylinder pressure data supported by CFD model

paper in this series. I am also applying methods developed in this paper to aid in analysis of prechamber knocking data and especially to separate "true knock" from background noise. This is also planned to lead to a publication.

5 Publications during Third Year

- "Knock: A Century of Research" [1]
- "A Simple CFD Model for Knocking Cylinder Pressure Data Interpretation: Part 1" [5]
- "A Simple CFD Model for Knocking Cylinder Pressure Data Interpretation: Part 2" - to be published at the 6th International Conference on Knocking in Gasoline Engines, Berlin, December 2021

6 Conferences Attended during Third Year

- 15th International Conference on Engines & Vehicles Capri, September 2021
- 6th International Conference on Knocking in Gasoline Engines, Berlin, December 2021

References

[1] D. J. Corrigan and S. Fontanesi, "Knock: A century of research," *SAE International Journal of Engines*, 2021.

[2] C. S. Draper, "The Physical Effects of Detonation in a Closed Cylindrical Chamber," Tech. Rep. NACA-TR-493, National Advisory Committee for Aeronautics, Jan 1935.

[3] C. Draper, "Pressure Waves Accompanying Detonation in the Internal Combustion Engine," in *Power Plants and Propellers Session, Sixth Annual Meeting, I. Ae. S.*, Institute of Aeronautical Sciences, Jan 1938.

[4] T. Iwata, K. Sakakibara, and H. Haragucti, "A New Method to Automatically Optimize the Knock Detection Level in the Knock Control System," Sep 1989. SAE Technical Paper 891964.

[5] D. J. Corrigan, S. Breda, and S. Fontanesi, "A simple cfd model for knocking cylinder pressure data interpretation: Part 1," in *15th International Conference on Engines Vehicles*, SAE International, 2021.